A study of engine fuel efficiency and oiliness additives

by

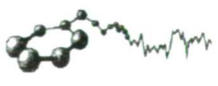
Valeria Anghel

A thesis submitted for the degree of Doctor of Philosophy
of the University of London

January 1998

Tribology Section
Department of Mechanical Engineering
Imperial College of Science, Technology and Medicine
London SW7 2BX





BIBL.
LONDIN.
UNIV

ABSTRACT

The thesis examines the behaviour of friction modifier additives and their influence on engine fuel efficiency. Such additives are used in the development of new, fuel efficient engine oils which are designed to reduce friction losses in automotive engines.

The thesis is in two parts. In the first part, a means was sought for predicting engine test performance using simple and cheap bench tests. Lubricant properties relevant to fuel economy performance were measured on laboratory test rigs. The ultrathin interferometry technique was applied to study the film forming capacities of lubricants and a "Stribeck curve" for concentrated contact conditions (EHD/boundary) was obtained. The measured data were correlated with efficiency data from engine tests using statistical models. This enabled the importance of boundary lubrication to be quantified in each engine test.

The second part of the thesis is a fundamental study of oiliness additives and their effect on friction. The basic question of whether these additives form thick or thin boundary films was explored using ultrathin film interferometry. Initially, classical additives such as long chain fatty acids were blended in hexadecane and their film forming and friction properties were assessed. More practically relevant compounds such as fatty acids salts (copper oleate) and commercial additives (C_{36} dimer acid ester) were than studied. Using thin-film interferometry it was possible to demonstrate that carboxylic acid salts and, occasionally, fatty acids themselves form thick boundary films of the order of tens of nanometers thickness in concentrated contacts under low speed conditions which were able to survive not just rolling but also sliding conditions. It appears that these thick films can make a significant contribution to friction reduction in the mixed/boundary regime, decreasing friction down to levels reminiscent of full film EHD lubrication.

ACKNOWLEDGEMENTS

I would like to express my gratitude to Prof. H. Spikes for his helpful supervision, useful ideas and suggestions and also to Dr. P. Cann for her kind advice and encouragement during the time in which this work was carried out.

Many thanks to all the members of the Tribology Laboratory for providing such a relaxed and cheerful environment in which to work (and play) and especially to Dr. Takero Makino for his valuable help with Fortran programming.

I am also much indebted to Dr. C. Bovington from Exxon Chemical Ltd. for his kindly interest in my work and to Exxon Chemical Ltd. itself for the provision of the necessary funding which made this study possible.

And finally, I am grateful to my sister for offering the moral support, encouragement and confidence when I mostly needed it.

TABLE of CONTENTS

Page

ABSTRACT 2

ACKNOWLEDGEMENTS 3

CONTENTS 4

LIST of FIGURES 10

LIST of TABLES 16

NOMENCLATURE 18

CHAP. 1. INTRODUCTION 20

1.1. PROJECT AIMS 21

1.2. LAYOUT OF THE THESIS 22

CHAP. 2. BACKGROUND TO FRICTION 24

2.1. DRY FRICTION 24

2.2. SURFACE ROUGHNESS 26

2.3. LUBRICATED FRICTION 27

2.3.1. Lambda ratio 28

2.3.2. Lubrication regimes 29

2.3.2.1. Hydrodynamic (HD) regime 29

Friction in HD regime 31

2.3.2.2. Elastohydrodynamic (EHD) regime 31

Origins of EHD friction or "traction 36

2.3.2.3. Boundary regime 39

2.3.2.4. Mixed regime 43

2.3.3. Stribeck Curve 44

REFERENCES 47

CHAP. 3. LUBRICANT-RELATED ENGINE FRICTION 51
3.1. ENGINE LOSSES 51
3.1.1. Engine mechanical losses 54
3.2. LUBRICATION OF MAIN ENGINE TRIBOLOGICAL COMPONENTS 56
3.2.1. Piston assembly 58
3.2.2. Bearings 61
3.2.3. Valve train 62
3.3. ENGINE FUEL EFFICIENCY 64
3.3.1. General 64
3.3.1.1. Influence of lubricant viscosity 65
3.3.1.2. Influence of boundary friction 67
3.3.1.3. Other relevant lubricant properties 68
3.3.2. Engine tests for fuel efficiency 68
3.3.2.1. ASTM Sequence VI test 69
3.3.2.2. ASTM Sequence VI A test 72
3.4. ENGINE FUEL EFFICIENCY PREDICTION 73
3.4.1. Strategy of approach 73
3.4.2. Previous regression work 75
REFERENCES 79

CHAP. 4. MEASUREMENT TECHNIQUES 91
4.1. MEASUREMENT OF EHD PROPERTIES 91
4.1.1. Film thickness measurement 91
4.1.1.1. Techniques 92
4.1.1.2. Basic principles of optical interferometry 93
4.1.1.3. Ultra-thin film technique 98
4.1.1.4. Test rig description 100
4.1.2. Traction measurement 102
4.2. MEASUREMENT OF BOUNDARY FRICTION PROPERTIES 104
4.3. MEASUREMENT OF HYDRODYNAMIC PROPERTIES 105
REFERENCES 106

CHAP. 5. BENCH TEST RESULTS **109**
5.1. RESULTS FOR SEQUENCE VI OILS 109
5.1.1. Lubricants used in the study 109
5.1.2. EHD film thickness results 110
5.1.3. Traction results 113
5.1.4. Boundary friction results 117
5.1.5. Viscometric results 121
5.2. RESULTS FOR SEQUENCE VI A OILS 122
5.2.1. Lubricants employed 122
5.2.2. Test results 123
REFERENCES 125

CHAP. 6. FUEL EFFICIENCY PREDICTION WORK **127**
6.1. REGRESSION ANALYSIS 127
6.1.1. Sequence VI correlation results 128
6.1.1.1. Single parameter correlations *128*
6.1.1.2. Multiple parameter correlation *130*
(a) "Arbitrary" correlation 131
(b) Weighting regimes of lubrication 134
6.1.2. Sequence VI A correlation results 135
6.1.3. Comparison of Sequence VI and VI A tests 137
6.2. DISCRIMINANT FUNCTION ANALYSIS 138
6.2.1. Data sample employed 140
6.2.2. Results 142
6.2.3. The influence of the number of parameters 143
6.2.4. Discussion 146
6.3. CONCLUSIONS 147
REFERENCES 149

CHAP. 7. OILINESS ADDITIVES: A REVIEW **150**
7.1. GENERAL INTRODUCTION 150

7.2. TYPES OF BOUNDARY ADDITIVES 151
7.2.1. Anti-wear additives 152
7.2.2. Extreme-pressure additives 152
7.2.3. Oiliness additives 153
7.3. OILINESS ADDITIVES-MONOLAYER OR MULTILAYER ? 154
7.3.1. Monolayer issue 155
7.3.2. Multimolecular films 159
REFERENCES 162

CHAP. 8. FATTY ACID STUDY 169
8.1. MATERIALS EMPLOYED 169
8.2. CLEANING AND TESTING PROCEDURES 171
8.2.1. Cleaning techniques 171
8.2.2. Measurement techniques 172
8.3. FILM THICKNESS RESULTS 172
8.3.1. Film thickness of purified hexadecane 172
8.3.2. Film thickness of surfactant solutions 174
Toluene/acetone cleaning 174
Presoaking 177
Chloroform/IPA cleaning 177
Test time effect 177
Acid cleaning 178
Effect of adsorbed moisture 179
8.3.3. Concentration influence 180
8.4. DISCUSSION 181
REFERENCES 183

CHAP. 9. COPPER OLEATE AND C_{36} DIMER STUDY 185
9.1. MATERIALS EMPLOYED 185
9.2. FILM THICKNESS RESULTS 187
9.2.1. Film thickness of hexadecane and 100SN mineral oil 187
9.2.2. Film thickness results for additive-containing solutions

at 25°C 188
With hexadecane as solvent *188*
With 100SN as solvent *191*
9.2.3. Film thickness results for additive-containing solutions at 60°C 192
Time effect *193*
9.2.4. Film thickness results for additive-containing solutions in mixed sliding/rolling conditions 195
Influence of test time *198*
Visual evidence *201*
Negative sliding *202*
9.2.5. Traction results 204
Traction results for surfactant solutions in hexadecane *205*
Traction results for surfactant solutions in mineral oil *207*
9.2.6. Discussion 211
REFERENCES 216

CHAP. 10. ADDITIONAL TECHNIQUES APPLIED TO BOUNDARY FILM STUDY 219
10.1. VIDEO IMAGE ANALYSIS 219
10.1.1. 2-D profiling 222
10.1.2. 3-D profiling 226
10.2. INFRARED SPECTROSCOPY 229
10.2.1. General 229
10.2.2. Infrared spectra of carboxylic acid salts 230
10.2.3. Description of the system employed 230
10.2.4. Spectra results for copper oleate 232
Transmission tests *232*
Reflection tests *234*
Room temperature results 234

Results at 60°C 238
10.3. DISCUSSION 240
10.3.1. Physico-chemical characteristics 240
10.3.2. Low and high shear rate behaviour 241
10.3.3. Possible structure of thick boundary films 243
REFERENCES 246
CHAP. 11. CONCLUSIONS AND FUTURE WORK RECOMMENDATIONS 250
11.1. CONCLUSIONS 250
11.2. FUTURE WORK RECOMMENDATIONS 252
REFERENCES 255
APPENDIX A 256
APPENDIX B 259
APPENDIX C 262
APPENDIX D 265
APPENDIX E 273
APPENDIX F 275
APPENDIX G 282
APPENDIX H 284

LIST OF FIGURES

Page

Fig.2.1.	*Relative fatigue life vs. λ ratio*	*29*
Fig.2.2	*Hydrodynamic lubrication*	*29*
Fig.2.3.	*Contour map of EHD contact*	*33*
Fig.2.4.	*Regime chart for circular contact*	*35*
Fig.2.5.	*Traction coefficient vs. slide roll ratio*	*37*
Fig.2.6.	*Boundary lubrication*	*39*
Fig.2.7.	*Contact region according to Hardy*	*40*
Fig.2.8.	*Contact region according to Bowden and Tabor*	*41*
Fig.2.9.	*Pressurised film model for boundary lubrication*	*41*
Fig.2.10.	*Stribeck curve - Hydrodynamic regime*	*45*
Fig.2.11.	*Stribeck curve - Elastohydrodynamic regime*	*46*
Fig.3.1.	*Typical energy distribution in an automotive engine*	*53*
Fig.3.2.	*Schematic of major energy consumers in an IC engine*	*55*
Fig.3.3.	*Breakdown of total engine friction*	*55*
Fig.3.4.	*Stribeck diagram for various engine components lubrication*	*57*
Fig.3.5.	*Sequence VI fuel economy test method*	*71*
Fig.4.1.	*Basic interferometric system*	*94*
Fig.4.2.	*Schematic of ultra-thin film technique*	*98*
Fig.4.3.	*Schematic representation of spectrometer set-up*	*99*
Fig.4.4.	*EHD rig*	*100*
Fig.4.5.	*Traction rig*	*103*
Fig.4.6.	*Layout of HFRR rig*	*104*
Fig.5.1.	*Film thickness vs.speed for R 517 (a) and R 519 (b) oils, for four temperatures*	*111*
Fig.5.2.	*Traction coefficient vs. S/R for R 502 and R 513 at five temperatures*	*113*
Fig.5.3.	*Traction coefficient vs.rolling speed for R502*	*115*
Fig.5.4.	*Traction coefficient vs.rolling speed for R516 and R519*	*116*
Fig.5.5.	*Traction vs.specific film thickness for R502*	*117*

Fig.5.6.	*Friction coefficient variation with time for R502*	*118*
Fig.5.7.	*Oil R502 - Friction coefficient variation with stroke length*	*119*
Fig.5.8.	*Oil R518 - Friction coefficient variation with stroke length*	*119*
Fig.5.9.	*Oil R517 - Friction coefficient variation with stroke length*	*120*
Fig.6.1.	*Single correlation with R150 and R275: importance of parameters*	*129*
Fig.6.2.	*R150 and R275-comparison between measured and predicted values*	*133*
Fig.6.3.	*EFEI-comparison between measured and predicted values*	*134*
Fig.6.4.	*Contribution of lubrication regimes to each Sequence VI phase*	*135*
Fig.6.5.	*Contribution of lubrication regimes to all Sequence VI A stages*	*136*
Fig.6.6.	*Contribution of lubrication regimes to overall Sequence VI and VI A performance*	*138*
Fig.6.7.	*Discriminant functions distribution for the best three parameters for 14 oils*	*142*
Fig.6.8.	*Discriminant functions distribution for the best three parameters for 13 oils*	*143*
Fig.6.9.	*Discrimination plots for the best combination of 4, 3 and 2 parameters*	*144*
Fig.6.10.	*Parameter choice-comparison for two variable case*	*145*
	a) discrimination given by a bad choice of parameters	*145*
	b) good choice discrimination	*146*
Fig.7.1.	*Key interactions between adsorbate molecules*	*135*
Fig.8.1.	*Film thickness vs. speed for hexadecane @ 25°C*	*173*
Fig.8.2.	*Film thickness vs. speed for 0.1% wt. palmitic acid @ 25°C*	*174*
Fig.8.3.	*Film thickness vs. speed for stearic acid solutions @ 25°C*	*175*
Fig.8.4.	*Thin films of palmitic and oleic acids - forward plots @ 25°C*	*176*
Fig.8.5.	*Boundary film reformation in the second stage of the test for 0.1% palmitic acid @ 25°C*	*176*
Fig.8.6.	*Two stage film thickness vs. speed results for palmitic acid solution @ 25°C (chloroform/IPA cleaning)*	*177*
Fig.8.7.	*Three stage film thickness vs speed results for oleic acid solution @ 25°C (toluene/acetone cleaning)*	*178*

Fig.8.8. *Film thickness vs. speed for oleic acid solution in hexadecane-concentration influence @ 25°C* *180*

Fig.8.9. *Film thickness vs. speed for palmitic acid solution in hexadecane-concentration influence @ 25°C* *180*

Fig. 9.1. *Chemical formula for C_{36} dimer acid / ethylene glycol* *187*

Fig.9.2. *Film thickness vs. speed for 100SN mineral oil at three temperatures* *188*

Fig.9.3. *Film thickness vs. speed for 0.1% Cu Oleate in hexadecane @ 25°C* *189*

Fig.9.4. *Reformation of thicker film at slow speeds for 0.1% Cu Oleate in hexadecane @ 25°C* *189*

Fig.9.5. *Film thickness vs. speed for 0.01% Cu Oleate in hexadecane @ 25°C* *190*

Fig.9.6. *Film thickness vs. speed for 0.1% C_{36} dimer acid ester in hexadecane @ 25°C* *191*

Fig.9.7. *Film thickness vs. speed for 0.1% Cu Oleate in 100SN @ 25°C* *192*

Fig.9.8. *Film thickness vs. speed for 0.1%C_{36} dimer acid ester in 100SN @ 25°C* *192*

Fig.9.9. *Film thickness vs. speed for 0.1% Cu oleate in 100SN @ 60°C* *193*

Fig.9.10. *Film thickness vs. speed for 0.1% C_{36} dimer acid ester in 100SN @ 60°C* *193*

Fig.9.11. *Film thickness vs. speed for 0.1%Cu oleate in 100SN @ 60°C, pure rolling, time effect* *194*

Fig.9.12. *Film thickness growth with time for 0.1% Cu oleate in 100SN solution @ 60°C, pure rolling* *195*

Fig.9.13. *Film thickness vs. speed for 0.1% Cu oleate in 100SN @ 25°C, 50% SRR* *196*

Fig.9.14. *Film thickness vs. speed for 0.1% Cu oleate in 100SN @ 60°C, 50% SRR* *196*

Fig.9.15. *Film thickness vs. speed for 0.1% C_{36} dimer acid ester in 100SN @ 60°C, 50% SRR* *197*

Fig.9.16. *Film thickness vs. speed for 0.1% Cu oleate in 100SN @ 100°C, 50% SRR* *197*

Fig.9.17. *Film thickness vs. speed for 0.1% C_{36} dimer acid ester in 100SN @ 100°C, 50% SRR* 198

Fig.9.18. *Film thickness vs. speed for 0.1%Cu oleate in 100SN @ 60°C, 50% SRR, time effect* 198

Fig.9.19. *Film thickness growth with time for 0.1% Cu oleate in 100SN solution @ 60°C, 50% SRR* 199

Fig.9.20. *Film thickness vs. speed for 0.1%C_{36} dimer acid ester in 100SN @ 60°C, 50% SRR, time effect* 199

Fig.9.21. *Film thickness growth with time for 0.1% C_{36} dimer acid ester in 100SN solution @ 60°C, 50% SRR* 200

Fig.9.22. *Film thickness vs. speed for 0.1% Cu oleate in 100SN @ 100°C, 50% SRR, time effect* 200

Fig.9.23. *Film thickness growth with time for two solutions of 0.1% Cu oleate in 100SN @ 100°C, 50% SRR* 201

Fig.9.24. *Photographs of the monitor screen showing the dispersed contact images* 202

Fig.9.25. *Film thickness vs. speed for 0.1%Cu oleate in 100SN @ 60°C, 50% negative SRR, time effect* 203

Fig.9.26. *Film thickness growth with time for two solutions of 0.1% Cu oleate in 100SN @ 60°C, 50% negative SRR* 204

Fig.9.27. *Traction coefficient vs. speed for pure hexadecane @ 50% SRR, 25°C* 205

Fig.9.28. *Traction coefficient vs. speed for pure hexadecane @ 50% SRR, 60°C* 205

Fig.9.29. *Traction coefficient vs. speed for 0.1% wt. Cu oleate in hexadecane @ 50% SRR, 25°C* 206

Fig.9.30. *Traction coefficient vs. speed for 0.1% wt. Cu oleate in hexadecane @ 50% SRR, 60°C* 206

Fig.9.31. *Traction coefficient vs. speed for 0.1% wt. C_{36} dimer acid ester in hexadecane @ 50% SRR, 25°C* 207

Fig.9.32. *Traction coefficient vs. speed for 0.1% wt. C_{36} dimer acid ester in hexadecane @ 50% SRR, 60°C* 207

Fig.9.33. *Traction coefficient vs. slide/roll ratio for 100SN at three*

	temperatures	*208*
Fig.9.34.	*Traction coefficient vs. speed for 100SN @ 50% SRR and three temperatures*	*208*
Fig.9.35.	*Traction coefficient vs. slide/roll ratio for 0.1% wt. Cu oleate in 100SN at three temperatures*	*209*
Fig.9.36.	*Traction coefficient vs. speed for 0.1% wt. Cu oleate in 100SN @ 25°C*	*209*
Fig.9.37.	*Traction coefficient vs. speed for 0.1% wt. Cu oleate in 100SN @ 60°C*	*210*
Fig.9.38.	*Traction coefficient vs. speed for 0.1% wt. Cu oleate in 100SN @ 100°C*	*210*
Fig.9.39.	*Traction coefficient vs. speed for 0.1% wt. C_{36} dimer acid ester in 100SN @ 25°C*	*211*
Fig.9.40.	*Traction coefficient vs. speed for 0.1% wt. C_{36} dimer acid ester in 100SN @ 60°C*	*211*
Fig.9.41.	*Shifted Stribeck curve for viscous films*	*214*
Fig.9.42.	*Friction reduction mechanism of thick boundary films*	*215*
Fig.10.1.	*Photographs of the Hertzian contact*	*220*
Fig.10.2.	*Video images of the contact during a time dependence test*	*221*
Fig.10.3.	*Schematic of the procedure for film thickness profiling*	*223*
Fig.10.4.	*Film profile and central film thickness for 0.1% wt. Cu oleate in hexadecane @ 25°C, pure rolling*	*224*
Fig.10.5.	*Film profile and central film thickness for 0.1% wt. Cu oleate in 100SN, 50% SRR, 60°C*	*225*
Fig.10.6.	*Schematic of the spacer layer imaging system*	*226*
Fig.10.7.	*3-D film thickness map for a strip area across the contact*	*228*
Fig.10.8.	*Diagram of carbon-oxygen bonds in a fatty acid salt*	*230*
Fig.10.9.	*Sliding optical EHD device*	*231*
Fig.10.10.	*Transmission spectra for pure hexadecane and copper oleate*	*233*
Fig.10.11.	*Spectra comparison for pure Cu oleate, hexadecane and their 0.1% wt. solution*	*234*
Fig.10.12.	*IR spectra around 1500 cm^{-1}, inlet region for 0.1% wt. Cu oleate in hexadecane at 3 speeds and 25°C*	*235*

Fig.10.13. *IR spectra from 0.1% Cu oleate in hexadecane at 25°C, 0.0034 m/s, for two test stages* 236

Fig.10.14. *IR spectra from the inlet region for 0.1% wt. Cu oleate in hexadecane at 0.0034 m/s, 25°C - time dependence* 237

Fig.10.15. *Comparison between IR spectra taken in the beginning and at the end of test for 0.1% wt. Cu oleate solution in hexadecane at 25°C* 237

Fig.10.16. *IR spectra from the inlet region for Cu oleate solution in hexadecane at 4 speeds, 60°C* 238

Fig.10.17. *IR spectra for Cu oleate solution in hexadecane taken in the inlet and further out regions at 0.0034 m/s and 60°C* 239

Fig.10.18. *IR spectra for Cu oleate solution in hexadecane taken in the inlet and outlet regions at 0.005 m/s and 60°C* 239

Fig.10.19. *Contact inlet zone for slow speeds/small clearances* 241

LIST of TABLES

Page

Table 2.1.	Typical α values for base oils	92
Table 3.1.	Energy flows in engines	52
Table 3.2.	Variables affecting road fuel economy tests	69
Table 3.3.	Reference oils for Sequence VI test	70
Table 3.4.	Test parameters for Sequence VI	70
Table 3.5.	Test parameters for Sequence VI A test	72
Table 4.1.	Test conditions for EHD film thickness measurement	101
Table 4.2.	Test conditions for traction measurements	102
Table 4.3.	HFR test conditions	105
Table 5.1.	Reference lubricants for Sequence VI test	110
Table 5.2.	EHD film thickness results at 1 m/s (mm)	112
Table 5.3.	Traction data for Sequence VI test oils	114
Table 5.4.	Traction coefficients at mixed EHD/boundary conditions at 135°C	116
Table 5.5.	Boundary friction data for Sequence VI oils	121
Table 5.6.	Viscometric data for Sequence VI test oils	121
Table 5.7.	Other rheological parameters for Sequence VI test oils	122
Table 5.8.	Sequence VI A reference oils, test performance data	123
Table 5.9.	Sequence VI A oils: EHD film thickness at 1m/s entrainment speed	123

Table 5.10. Sequence VI A oils: limiting traction coefficient 124

Table 5.11. Sequence VI A oils: boundary friction results 124

Table 5.12. Sequence VI A oils: viscometric properties 124

Table 6.1. Sequence VI A tests: correlation equations 135

Table 6.2. Two group separation based on efficiency data 140

Table 6.3. Viscometric data for additional 5 oils 141

Table 6.4. Film thickness data for the 5 added oils at 1m/s (μm) 141

Table 6.5. Limiting traction coefficient and traction at 50% sliding for the 5 additional oils 141

Table 6.6. Boundary friction coefficient for the 5 additional oils 141

Table 8.1. Carboxylic acid additives 170

Table 9.1. Physical properties for 100SN base oil 186

Table 10.1. Test conditions for the sliding rig 232

NOMENCLATURE

R_a	centre line average (CLA) roughness
R_q	root-mean-square (RMS) roughness
HD	hydrodynamic
EHD	elastohydrodynamic
B	boundary
h	film thickness (m)
U	velocity (m/s) or mean surface speed (see text)
	$U = (U_1 + U_2)/2$
U_n	surface speed of component n
W	normal load (N)
p	pressure or Hertzian pressure (Pa)
h_c	central film thickness in EHD contact
h_0	minimum film thickness in EHD contact
R_{11}, R_{12}	principal radii of contact (m)
R'_x	reduced radius perpendicular to the rolling direction
	$1/R'_x = 1/R_{11} + 1/R_{21}$
R'y	reduced radius parallel to the rolling direction
	$1/R'_y = 1/R_{12} + 1/R_{22}$
E'	reduced Young's modulus (N/m^2)
	$\frac{1}{E} = \frac{1}{2}\left[\left(\frac{1-\sigma_1^2}{E_1}\right) + \left(\frac{1-\sigma_2^2}{E_2}\right)\right]$
E	Young's modulus
	E = stress / longitudinal strain
k	ellipticity parameter
$\overline{U}$	speed parameter
$\overline{G}$	materials parameter
$\overline{W}$	load parameter

g_v	dimensionless viscosity parameter
g_E	dimensionless elasticity parameter
S/R	slide-roll ratio
G	elastic shear modulus
D	Deborah number
HFRR	high frequency reciprocating rig
N	fringe order
n	refractive index
c	velocity of light

$\dot{\gamma}$	strain rate (s^{-1})
α	pressure viscosity coefficient (Pa^{-1})
ϕ	phase change due to reflection
η	dynamic viscosity (Pa s)
λ	specific film thickness or "lambda ratio"
λ	wavelength (m)
μ	friction coefficient
ν	kinematic viscosity (m^2/s)
ρ	density (kg/m^3)
σ_n	Poisson's ratio
τ	shear stress (N/m^2)
τ_c	limiting shear stress (N/m^2)
τ_e	Eyring stress (N/m^2)
$\bar{\nu}$	wave number (cm^{-1})

CHAPTER 1

INTRODUCTION

In the second half of this century, engine and lubricant technologies have been increasingly influenced by two key factors. One is concern over environmental protection. In the US and Japan the acceptable level of exhaust emissions, for example, has been reduced by more than a factor of ten over the last two decades and in the near future the Californian ULEV (ultra low emission vehicle) standards will impose a further reduction in hydrocarbon emission levels down to 0.055 g/mile over 100,000 miles.

At the same time, requirements have been introduced for reductions in fuel consumption, both to conserve natural resources and to reduce CO_2 emissions. Improvements in fuel economy by carefully formulated oils represent a major preoccupation of both engine and lubricant manufacturers and engine oil has become an important engine design parameter for improved fuel efficiency. The international lubricant standardisation and approval committee (ILSAC) has recently developed a new standard for engine oils, ILSAC GF-2, which amongst other changes in lubricant quality, establishes a set of compulsory fuel efficiency targets linked to SAE viscosity grade. This has led to the development of a new engine test for measuring lubricant-related fuel economy, the ASTM Sequence VIA which has become part of the new ILSAC GF-2 standard. Based on results of Sequence VIA testing, SAE 5W-30 GF-2 oils should provide an improvement in fuel economy of 0.8% as compared to average

5W-30 GF-1 oils. Oils with even higher fuel efficiency are planned to be in use for the next millennium which would have to show better and also durable fuel economy in a new test Sequence VIB. This test is in development in the USA and is planned for introduction in the years 2000-2001.

As a result of these stringent requirements, increasing fuel efficiency (FE) through engine oil formulation has become an important task for engine and lubricant manufacturers. However, the estimation of FE benefits gained through improved engine oils using ASTM engine test procedures is expensive and time consuming and any means of reducing the need for such tests is highly desirable.

1.1. Project aims

This project addresses this problem in two ways. One is to find a way of predicting engine test performance by using simple and cheaper laboratory bench tests. The second is to understand better the influence of lubricant additives on friction, so that lubricant formulators are able to more reliably blend efficient lubricants. Thus the main goals of the proposed work are as follows:

(a) to determine contributions of different types of friction to engine oil fuel efficiency

(b) to understand and quantify the contribution of oiliness additives to engine oil fuel efficiency

(c) to identify the mechanism of action of oiliness additives

In the first part, lubricant properties which are considered to influence fuel economy performance such as high shear rate viscosity, boundary friction coefficient, EHD traction coefficient and EHD film thickness were measured on laboratory test rigs. The data were then correlated with the FE performance from Sequence VI and VIA engine tests and a study of the behaviour of lubricants in such test conditions was carried out.

The second part of this project is concerned with the study of friction modifier additives as a way of achieving and maintaining low boundary friction. Fatty acid solutions in hexadecane were initially employed. More practically relevant compounds such as

copper oleate and C_{36} dimer acid ester which are employed as additives in marketed lubricants, were then studied. Investigations of their film forming capacities and their mechanism of action in ensuring the anti-friction protection for the surfaces in motion were carried out.

1.2. Layout of the thesis

The work presented in this thesis is organised as follows. Chapter 2 contains a brief description of the laws governing friction phenomena. Dry, solid friction and lubricated friction are discussed in turn, with emphasis on lubrication regimes. Film thickness dependence on parameters such as velocity, load, viscosity predicted by the hydrodynamic and elastohydrodynamic theories together with friction calculation are also discussed. The dissertation upon friction is further expanded in chapter 3 by considering engine frictional losses. Short literature reviews on friction and lubrication of main tribological engine components with a discussion about means of reducing friction losses through engine oil formulation are then presented. ASTM engine tests and the strategy of fuel efficiency prediction approach are then outlined in order to create the background for experimental and modelling work.

Chapter 4 describes the main experimental techniques used in this study to measure lubricant properties relevant to friction in each lubrication regime. In chapter 5 the full set of results obtained from laboratory bench tests are presented for both Sequence VI and VIA reference oils. Subsequently these measured properties are correlated with fuel efficiency data from ASTM Sequence VI and VIA tests, work described in chapter 6. The statistical techniques of multiparametric regression and discriminant function analysis were employed for fuel efficiency prediction. Discussions and conclusions drawn from the fuel economy results are also outlined in chapter 6.

Chapter 7 moves into the second part of this thesis, the study of oiliness additives with the goal of engine friction reduction through better engine oil formulation. The chapter contains a review of previous work carried out on oiliness-type boundary additives as an attempt to examine the mechanisms by which they work. Experimental work employing long-chain fatty acids is described in chapter 8. The influence of several

factors such as chain length, concentration, rolling time and cleaning methods upon their film forming capabilities was investigated.

Chapter 9 is dedicated to the study of commercial friction modifying additives. A similar approach to fatty acids study was used for film thickness measurements with emphasis on time dependence and temperature effects. The influence of shear on film formation was studied by varying the slide/roll ratio in the EHD film test and EHD friction variation with mean entrainment speed was also determined.

Chapter 10 describes the work carried out using additional techniques in order to characterise the boundary films detected in optical tests. Video recording techniques were used to take images straight from the EHD contact and two mapping methods were employed to create 2-D and 3-D maps of the film distribution over the Hertzian contact area. In order to obtain information about the chemistry of lubricant films, another in-contact technique was employed: reflection-absorption Fourier transform infra-red (FTIR) microspectroscopy. A discussion on properties and possible mechanisms of boundary films formation is outlined at the end of the chapter.

The last chapter, 11 summarises the conclusions and future work recommendations that could be conducted in this area of research.

CHAPTER 2

BACKGROUND TO FRICTION

This chapter, as the title shows, is concerned with friction phenomena. In the begining, a short description of dry solid friction and the basic laws which govern it are presented. This is then followed by a discussion of lubricated friction between solid bodies and the concept of lubrication regimes. Each lubrication regime is then described in turn and the dependence of film thickness on parameters such as velocity, load, viscosity, predicted by hydrodynamic and elastohydrodynamic theory, is shown. Friction in the HD and EHD lubrication regimes is also discussed. Finally, a modified version of the classical Stribeck curve is presented.

2.1. Dry friction

As it is well known, when one solid body slides over another there is a resistance to the motion which is called *friction*. Friction between objects is a matter of everyday experience and from earliest times man has made ingenious attempts to eliminate it or to diminish it to as small a value as possible. A relationship between the resistive force and the load applied between the bodies was first observed by Leonardo da Vinci at the end of the fifteenth century [2.1], but only later, in 1699 was published a real study of the phenomenon by the French army engineer, Guillaume Amonton [2.2]. He formulated the two basic laws of friction which state that :

1) friction force is directly proportional to the load between the surfaces
2) friction is independent of the apparent area of contact between the sliding surfaces.

The magnitude of the frictional force depends greatly on the nature of both surfaces in contact. This is described by the *coefficient of friction*, μ which is given by the ratio between the frictional force, F and the load, W.

$$\mu = \frac{F}{W} \qquad (E2.1)$$

Amonton's observations were verified in 1785 by Coulomb who made a clear distinction between *static friction*, the force required to start sliding, and *kinetic friction*, the force required to maintain it.

He showed that kinetic friction could be appreciably lower than static friction and made the observation, which is sometimes quoted as the third law, that the kinetic friction is nearly independent of the speed of sliding [**2.1**]. The distinction between static and kinetic friction yields a variable coefficient of friction, particularly at slow sliding speeds when sliding is not a continuous process and the phenomenon often leads to a "stick-slip" motion.

Most current theories of sliding friction stem from the important work of Bowden and Tabor. In their model they assume that frictional force arises from two distinct surface interactions: adhesion of contacting asperities and interlocking or ploughing of opposing asperities during sliding. So the resultant frictional force F is taken to be the sum of the contributing terms, F_{adh} due to adhesion and F_{def} due to deformation [**2.1**]

$$F = F_{adh} + F_{def} \qquad (E2.2)$$

In recent years, more complicated models of friction have been developed [**2.4**] which take into account

- the increase in real area of contact which results from sliding
- ploughing effects

- the geometry of rough surfaces .

Recently, an impressive amount of work has been carried out by Israelachvili and his co-workers on studying tribological phenomena at atomic scale. His recently developed model of friction suggests that the static friction force F_S is directly related to the equilibrium or reversible part of adhesion or interaction energy during a loading-unloading cycle and that kinetic friction force F_K is correlated more with the irreversible component [2.5]. Thus, for two molecularly smooth surfaces the total dry friction can be described by a general equation of the form

$$F = C_1 A + C_2 L \qquad \text{(E2.3)}$$

with C_1, C_2, constants. The first term A, may be considered as the intrinsic "adhesion" contribution to the friction force, the second L, as the load-dependent "structural" contribution, though both terms depend on the structure of the two surface lattices. In the case of rough or worn surfaces, their area of true molecular contact is very small and the adhesion contribution to the total friction force is usually negligibly small. This leaves only the load-dependent structural term in the expression above, which for rough surfaces takes the form known as Amonton's law, $F = \mu L$ [2.5].

2.2. Surface roughness

In understanding the origins of solid friction it is important to realise that there will always be a roughness on real engineering surfaces which will become apparent when surfaces are examined at a sufficiently high magnification. A simple and most widely used way of describing the surface geometry is by using the two roughness parameters: R_a or centre line average (CLA) and R_q or root mean square (RMS). The first of these is defined by the equation :

$$R_a = \frac{1}{L} \int_0^L |z| \, dx \qquad \text{(E2.4)}$$

where z is the height of the surface measured above the mean level, x is the coordinate in the surface and L is the measured length. However the R_a surface parameter fails to differentiate between a relatively gently undulating surface and one with a much spikier profile. The RMS roughness parameter overcomes this difficulty since the squared term gives greater significance to large surface variations from the mean. R_q is defined by the equation :

$$R_q = \sqrt{\frac{1}{L}\int_0^L z^2 dx} \qquad \text{(E2.5)}$$

Many more complex descriptions of roughness exist (such as fractal models) and for a more detailed view, reference [2.3] can be consulted.

Traditionally, surface roughness is measured by a profilometer which draws a stylus over a sample length of the surface of the component and reproduces a magnified trace of the surface profile. Modern developments in image capturing and processing techniques have made feasible alternative optical methods of obtaining three-dimensional topographical information. These rely on storing digitally the image of the surface formed in a conventional interference microscope illuminated with either white or monochromatic light. The imaging software is capable of providing contour maps, profiles and oblique views for the captured data with vertical resolution down to a few tens of nanometers and horizontal resolution of better than a micron [2.2].

2.3. Lubricated friction

If solid surfaces are clean, free from oxides and other surface films and from adsorbed gases (in ultra-high vacuum conditions, at pressures typically $< 10^{-8}$ Pa), then large-scale adhesion is observed between metals during sliding. With soft and ductile metals such as lead and indium, the adhesion forces at the junctions may be even stronger than the cohesive strength of the metal itself. In such conditions, the coefficient of friction has extremely high values, typically 2 to 10 or even more and gross seizure frequently follows when sliding is attempted. In practical conditions, however, the metal surfaces are usually contaminated by oxides so that an interface of lower shear strength is

interposed between them which reduces friction substantially (μ = 0.4 to 0.8) [2.2]. Even so, friction is still unacceptably high for most engineering applications and would lead to extremely high frictional forces and energy losses.

In dry lubrication, all of the applied load is borne by the asperity contacts. When liquid or gaseous lubricants are present in high speed contacts, however, the fluid can be dragged between the surfaces to form a "hydrodynamic lubricating film". In such cases the applied load is borne by the pressurised fluid film. Therefore, *lubricants* are used to reduce friction by introducing between the sliding surfaces a layer of material with lower shear strength than the surfaces themselves. To a greater or lesser extent, the use of a lubricant will always reduce the rate of sliding wear. Other beneficial effects of some lubricants are: cooling of the surfaces both by the reduction of frictional heat dissipation and by bulk convection; protection of surfaces from water thus reducing corrosion; removal of the debris generated by wear process and protection of metal surfaces from acid combustion products in engines.

2.3.1. Lambda ratio

In fluid film lubrication, the extent to which the total load carried is shared between the fluid and the larger surface asperities depends upon the relative height of the asperities and the oil film thickness which is often described in terms of the "specific film thickness" or *lambda ratio* (λ). This relates the minimum oil film thickness in the contact, h_0 to the composite surface roughness, R_{qc}, as in the following formula

$$\lambda = \frac{h_0}{R_{qc}} \qquad (E2.6)$$

with

$$R_{qc} = \sqrt{R^2_{q1} + R^2_{q2}} \qquad (E2.7)$$

where R_{q1} and R_{q2} are the RMS roughness of the two solid surfaces. The concept was first outlined by Tallian [2.6] in 1979 who used it to simplify lubricant design procedures and to produce a plot of relative fatigue life vs. λ (figure 2.1., taken from reference [2.6]).

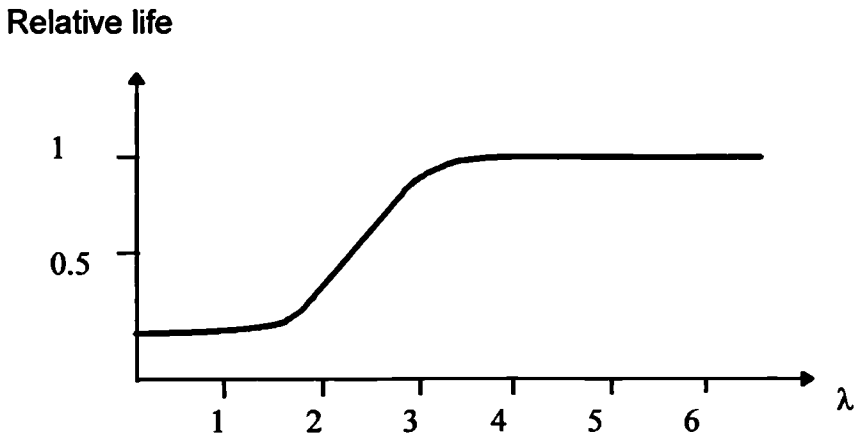


Fig.2.1. Relative fatigue life vs. λ ratio

The lambda value has been found to correlate with wear, scuffing and rolling contact fatigue [2.37]. For λ ratios of 1 or less, considerable solid-solid contact is likely to take place between the asperities of opposing surfaces. This may result in surface damage and reduced life.

2.3.2. Lubrication regimes

Depending upon how the load is carried (by fluid film or asperities), a number of lubrication regimes can be distinguished. The most important are hydrodynamic (HD), elastohydrodynamic (EHD) and boundary (B) regimes.

2.3.2.1. Hydrodynamic (HD) regime

In the hydrodynamic lubrication regime the surfaces are separated by a fluid film which is usually thick in comparison with the surfaces asperity heights.

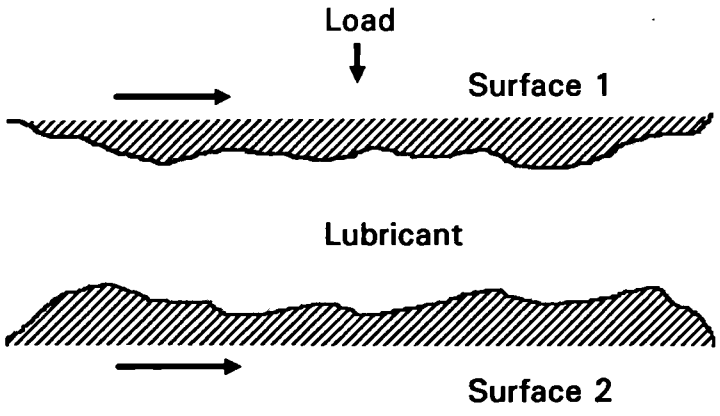


Fig. 2.2 Hydrodynamic lubrication

This is the most frequently occurring liquid lubrication regime and operates in plain journal bearings, thrust pad bearings, piston rings/liners except at top and bottom dead centres, etc.

Normally the pressures are less than 2 MPa and can cause only small elastic distortions of the solid surfaces which, to a first approximation, can be treated as rigid, although in impulsively loaded systems such as internal combustion engine crankshaft bearings, the pressures can reach a transient maximum of ~ 50 MPa [**2.7**]. The generation of the interposing fluid layer relies on the geometry and motion of the surfaces together with the viscous properties of the fluid. The surfaces in contact are conformal (i.e. they must be so closely matched in dimensions that they are separated only by a small gap over a relatively large area) and the speeds are moderate to high. The entry into the load zone is tapered and the oil pressure increases as it is forced into the wedge. The thickness of the generated film is often in the range of 1 to 100 μm and the friction coefficient is of the order of 0.007 to 0.03. Ideally no asperity interaction occurs (lambda ratio is normally higher than 10), so wear and other forms of surface damage are greatly reduced.

The classical problem in HD theory is the establishment of a relation between the velocity of sliding, the geometry of the surfaces, the properties of the lubricant, the magnitude of the normal load that the lubricant supports and the film thickness. The distribution of pressure within a HD lubricant film was first described by Reynolds [**2.8**] who developed an equation which relates the variation of pressure with distance with the following parameters: viscosity of the fluid (η), sliding velocity (U) and film thickness (h). The dependence of film thickness on the shown parameters is given by a relation of the form:

$$h \sim [(\eta U) / W]^{0.5} \qquad (E2.8)$$

The expression is not entirely accurate because the effect of frictional heating has been neglected, which is inadmissible except for very lightly load bearings. The viscosity of the lubricant is exceedingly temperature-dependent and thus the film thickness will also depend strongly on temperature .

Friction in HD regime

It can be shown that friction in HD lubrication has similar dependency to film thickness for Newtonian fluids. By definition, friction coefficient is given by the relation (E2.1). The friction force is the product of shear stress and the contact area, A

$$F = \tau A \qquad (E2.9)$$

For Newtonian fluids, shear stress τ is directly proportional to the rate of shear $\dot{\gamma}$, so it can be expressed as

$$\tau = \eta\dot{\gamma} \qquad (E2.10)$$

If $\dot{\gamma}$ is further expressed in terms of speed and film thickness h, than we have:

$$\dot{\gamma} = \frac{U}{h} \qquad (E2.11)$$

By substituting all the above in equation (E2.1) and taking film thickness as in relation (E2.8) the final expression for μ is of the form

$$\mu \sim [(\eta U) / W]^{0.5} \qquad (E2.12)$$

This shows that friction and film thickness in HD regime are both determined by the effective viscosity of the lubricant within the contact. The thicker the film between surfaces in motion, the higher the friction from fluid shear.

2.3.2.2. Elastohydrodynamic (EHD) regime

If the contacting surfaces are counterformal, involving nominally point or line contact, then the local pressures in the contact zone will generally be much higher than those encountered in HD lubrication. The contact between gear teeth, between a cam and its follower, or between a ball and its track in a ball bearing, all involve concentrated contacts of very small area (~ 300 μm width). In such conditions, the local pressures between steel components can reach up to several GPa (typically 1 to 3.5). The film thickness ranges between 0.1 to 1 μm and the lambda value is generally between 3 and 10 so there is little chance of asperities interaction. The coefficient of friction is between 0.03 and 0.1. In such contacts, the conditions experienced by the lubricant are extreme, involving both very high pressures and high shear rates (10^6 - 10^8 s^{-1}).

If the hydrodynamic theory is applied to these conditions, it predicts negligible film thickness which is not found in practice. This indicates that there must be other

phenomena which help to increase the separation between surfaces in motion and the HD theory has to be modified accordingly.

(a) The first phenomenon is an increase in fluid viscosity by several orders of magnitude due to very high local pressures, mentioned by Everett in 1937 [**2.9**]. This can be taken into account by using the relation developed by Barus [**2.10**] for moderate pressures (< 0.14 GPa) :

$$\eta_p = \eta_0 e^{\alpha p} \qquad (E2.13)$$

where the subscripts *0* and *p* refer to atmospheric pressure and any pressure P; α is the *pressure-viscosity coefficient*, defined as in expression :

$$\alpha = \frac{1}{\eta}\left(\frac{\partial \eta}{\partial p}\right)_T \qquad (E2.14)$$

The pressure-viscosity coefficient or α-value for most lubricants lies between 5 and 35 GPa^{-1}. Typical values for different base stocks are listed below [**2.11**] :

Lubricant	α value (GPa^{-1})
mineral oil (naphthenic)	27(25°C), 15(100°C)
poly-α-olefin	11(20°C)
traction fluid	39(20°C), 12(100°C)

Table 2.1. Typical α values for base oils

The higher the α value, the better the film-forming capacity of the lubricant. To some degree, the value of α is dependent on the flexibility of the molecules in the lubricant (the more flexible molecules, the lower the α value) and in consequence, the pressure-viscosity coefficient drops for all fluids with increasing temperature [**2.4**].

At higher pressures the variation of viscosity with pressure is better described by the relation developed by Cameron [**2.12**]:

$$\eta_p = \eta_0 (1 + cp)^n \qquad (E2.15)$$

with c, n constants, n = 16

(b) The second phenomenon is the local elastic deformation of the surfaces in contact which increases the area over which the load is carried. This can be taken into account by using Hertz's theory (1886) [**2.13**].

Thus theoretical solutions of EHD lubrication involve solving Reynolds equation together with a viscosity-pressure equation and an elastic deformation equation. The film predicted by this theory for a point contact of a ball on a flat, has a central plateau of nearly constant separation (h_c) bounded by a horseshoe-shaped constriction around the sides and towards the outlet (h_0), in which the film is reduced typically by about one quarter (figure 2.3)

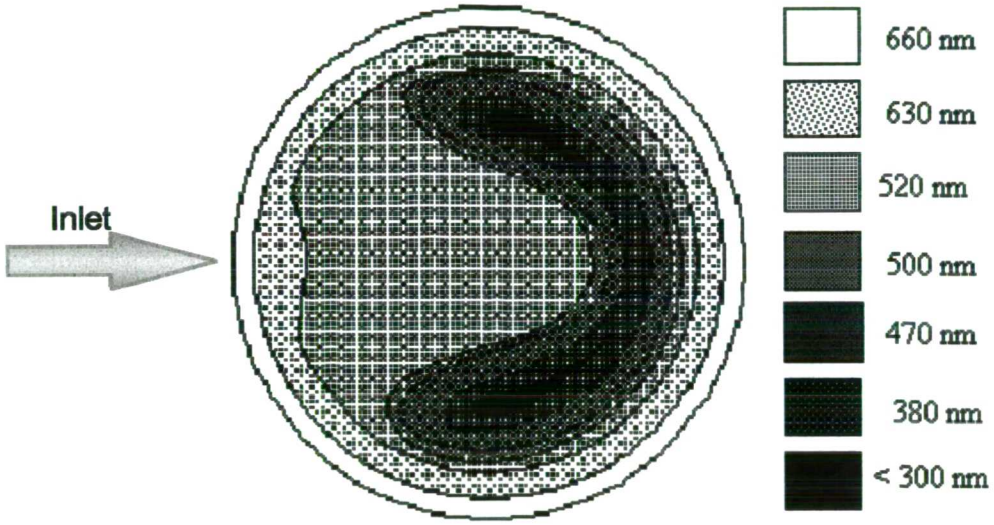


Fig.2.3. Contour map of EHD contact

The constriction in the exit occurs as a result of a rapid pressure drop followed by the viscosity drop that occurs at the outlet, and so the separation decreases to maintain the continuity of flow.

Unless drastic simplifications are introduced, numerical methods are necessary to solve EHD problems. Several different power-law expressions have been published, but the most widely used are the regression equations derived by Dowson and Hamrock [**2.14**] to predict the EHD film thickness for Newtonian oils under isothermal conditions for any contact geometry. The equations for central and minimum film thickness respectively, are given below :

$$\frac{h_c}{R'_x} = 2.69\left(\frac{U\eta_0}{E'R'_x}\right)^{0.67}(\alpha E')^{0.53}\left(\frac{W}{E'R'^2_x}\right)^{-0.067}\left(1-0.61e^{-0.73k}\right) \qquad \text{(E2.16)}$$

$$\frac{h_o}{R'_x} = 3.63\left(\frac{U\eta_0}{E'R'_x}\right)^{0.68}(\alpha E')^{0.49}\left(\frac{W}{E'R'^2_x}\right)^{-0.073}\left(1-e^{-0.68k}\right) \qquad \text{(E2.17)}$$

where $$k = 1.03\left(\frac{R'_y}{R'_x}\right)^{0.64} \qquad \text{(E2.18)}$$

K is the ellipticity parameter and is equal to 1.03 for point contact and ∞ for line contact. The other parameters are U, the mean entrainment speed of the two surfaces, η_0 the dynamic viscosity of the lubricant at atmospheric pressure, α the pressure-viscosity coefficient of the lubricant, E' the reduced elastic modulus of the two surfaces, R' the reduced radius in the direction of entrainment and W the applied load.

The minimum film thickness (h_0) in combination with surface roughness, controls the amount of metal-metal contact and thus fatigue life.

Film thickness is usually defined in terms of three dimensionless groups (the first three terms in brackets from equations E2.16, E2.17) which are the speed parameter ($\overline{U}$), the materials parameter ($\overline{G}$) and the load parameter ($\overline{W}$). Depending on the response of contacting surfaces and fluid viscosity towards the pressures encountered in the EHD contact, four separate regimes can be established [**2.15**]. They are plotted in a regime chart which, for point (circular) contacts depicts a dimensionless viscosity parameter g_v against a dimensionless elasticity parameter g_E. The g_v and g_E parameters are defined in terms of the three dimensionless parameters from EHD equations, E2.16 and E2.17, as follows:

$$g_V = \frac{\overline{G}\,\overline{W}^3}{\overline{U}^2} \qquad \text{(E2.19)}$$

$$g_E = \frac{\overline{W}^{8/3}}{\overline{U}^2} \qquad \text{(E2.20)}$$

With the values for g_V and g_E introduced in the chart below, the actual lubrication regime can be determined and hence the appropriate regression equations for film thickness calculation

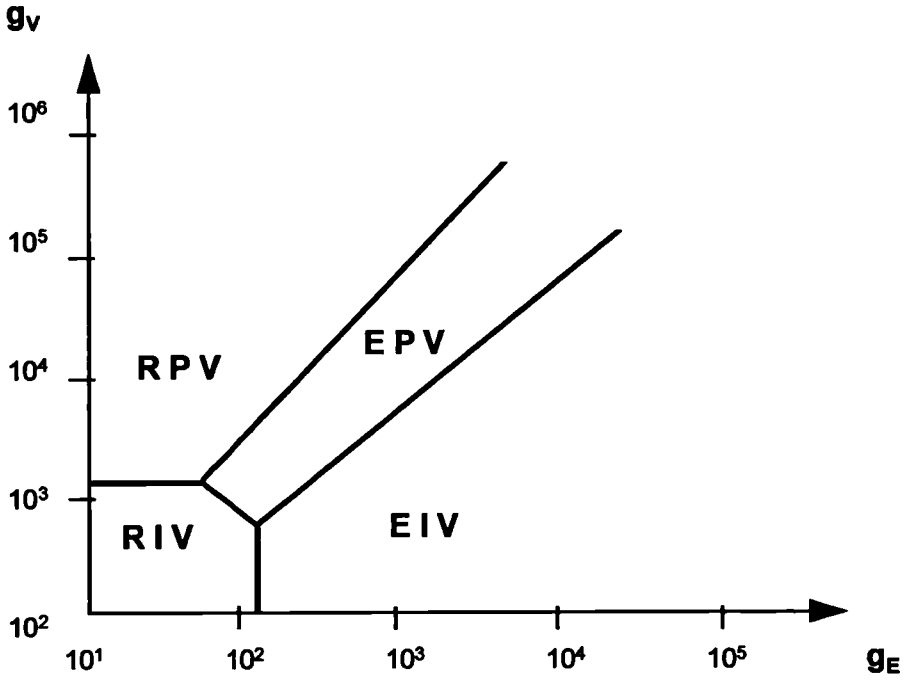


Fig.2.4. Regime chart for circular contact

The four regions are characterised as follows :

RIV - *rigid isoviscous* - low variation of viscosity and elasticity parameters; typically most well lubricated contacts where classical HD equations apply,

EIV - *elastic isoviscous* - only the elasticity parameter is large, the lubricant viscosity is not significantly influenced by pressure; frequently in contacts where at least one surface has a low elastic modulus, e.g. in seals,

RPV - *rigid piezoviscous* - large increase of lubricant viscosity with pressure, while the solid surfaces keep their geometry undeformed; typically for contacts lubricated with high pressure sensitive fluid,

EPV - *elastic piezoviscous* - both the elasticity and viscosity parameters are appropriately large; mainly the contacts formed between non-conforming surfaces where EHD equations apply, e.g. gears, metal rolling element bearings.

A more detailed description can be found in ref.[**2.16**].

Origins of EHD friction or "traction"

Traction is basically the name given to *friction* in an EHD contact i.e. the tangential force in the direction of rolling or sliding. The friction force in EHD usually has two components: one from solid, solid contact at asperities, F_S, and the other transmitted by the fluid, F_L. Total traction force is given by:

$$F = F_S + F_L \qquad (E2.21)$$

If the λ ratio is high, than F_S will be negligible and friction will have only the component due to fluid shear, F_L.

Just as in hydrodynamics, the friction or traction is determined by the integral of the shear stress in the lubricant film over the contact area.

$$\mu = \frac{F}{W} = \frac{\int_A \tau \, dA}{\int_A p dA} \qquad (E2.22)$$

The shear properties of a lubricant are generally studied by using a disc machine. Typical results of EHD traction curves at high λ ratios where F_s is negligible are shown in figure 2.5. which depicts the traction coefficient versus slide roll ratio S/R, where

$$S/R = 2\frac{|U_1 - U_2|}{(U_1 + U_2)} * 100\% \qquad (E2.23)$$

The mean rolling or "entrainment" speed $U=(U_1+U_2)/2$ draws the lubricant in the contact and generates the film thickness whilst the sliding speed $\Delta U=U_1-U_2$ (in modulus) shears this film and gives rise to the traction force.

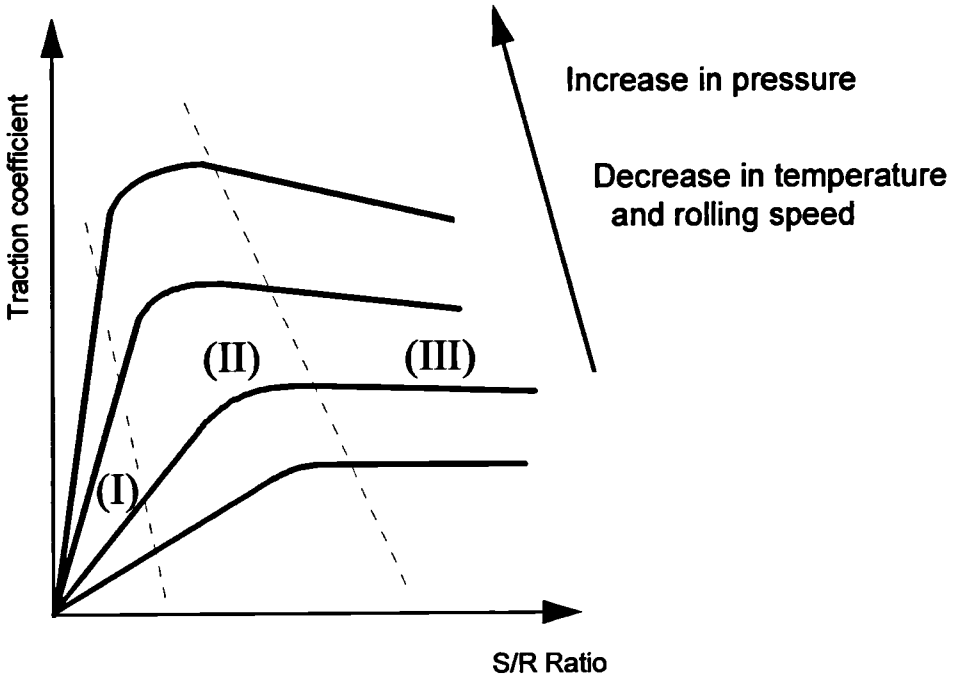


Fig.2.5. Traction coefficient vs. slide roll ratio

Traction curves can be used to investigate the rheology of lubricants as shear stress τ can be obtained from traction force over the contact area and the rate of shear is also available by knowing the film thickness data corresponding to the test speeds.

In general traction curves display three regions:

(I) Newtonian viscous - a linear region where shear stress τ is proportional to shear rate $\dot{\gamma}$ which is normally the case for low viscosity fluids (Newtonian). At high pressures this region is restricted to extremely low sliding speeds; traction is dominated by the non-linear behaviour.

(II) Non-linear region - where shear-thinning and viscoelastic response of the lubricant to the high shear stresses is predominant. Here the dependence of shear stress to shear rate is no longer proportional.

(III) Plastic region - as the pressure increases, the shear stress of the film reaches the limiting plastic yield stress. At high pressures and high sliding speeds encountered

in an EHD contact, the stress may fall with increasing shear rate, mainly because of thermal heating.

Many different models have been proposed to explain the rheological behaviour of the lubricants in EHD conditions, i.e. to relate the shear stress to the strain rate. Based on experimental evidence, most of them incorporate Newtonian behaviour at low pressures and shear rates; a shear thinning relationship with increasing shear rate or shear stress; a viscoelastic component at high shear rates and pressures and plastic yield at constant stress at a limiting shear stress, τ_c [**2.18**]. The most widely known and investigated is the model developed by Johnson et al. [**2.17**] which uses four fluid properties to define the rheology at a given temperature and pressure: G, η_0, τ_c and τ_e. The symbols represent: G is the elastic shear modulus, η_0 is the viscosity of the lubricant at room temperature and atmospheric pressure, τ_e is the so-called "Eyring stress" and represents the stress above which the fluid becomes appreciably non-linear and finally, τ_c , the limiting shear stress. In their relationship the fluid strain rate has two components, a viscous and an elastic one. Because it is similar to the Maxwell equation, except for the non-Newtonian nature of the viscous term, it is known as " non-linear Maxwell" model.

$$\dot{\gamma} = \frac{\tau_e}{\eta_0} sinh\left(\frac{\tau}{\tau_e}\right) + \frac{\dot{\tau}}{G} \qquad (E2.24)$$

The viscous term tends to Newtonian behaviour (τ/η_0) at low shear stresses, but shears thin rapidly above the Eyring stress. The elastic term is dependent upon the relaxation time of the fluid (η/G) compared to the transit time in the contact, the ratio called Deborah number, D

$$D = \frac{\eta_0 U}{Gb} \qquad (E2.25)$$

where b represents the contact width. When D increases close to unity, i.e. the elastic response of the fluid to the applied stress is comparable to the duration of the event, the viscoelastic effects are predominant. As G ~ 10^9 Pa and the transit time in EHD contacts b/U is generally less than about 10^{-3} sec, D exceeds unity when the viscosity η exceeds 10^6 Pa s, which is commonly the case for the pressures in an EHD contact. At high shear stresses the fluid yields at a limiting shear stress, τ_c, like a plastic solid.

Strong evidence for the existence of a critical or limiting shear stress as a property of the fluid has been provided by the experiments of Bair and Winer [**2.19, 2.20**] who compressed a sample of the fluid in a high pressure cell and carried out a shear stress-shear strain experiment at a rate at which shear heating effects were negligible. Disc machine experiments reported by Evans and Johnson [**2.21**] that were also carried out under truly isothermal conditions revealed a limiting shear stress τ_c which was consistent with the data obtained by Bair and Winer. Recently Bair and Winer have found evidence of slip planes or shear bands [**2.22**] within a pressurised liquid film at about 20° to the surfaces as might be expected from the yield of a bulk solid.

It is important to note that in EHD contacts the film thickness and friction (traction) are decoupled. The film thickness is determined by the effective viscosity of the lubricant in the contact inlet, whilst traction comes from the shear stress of the lubricant in the central region of the contact and is determined by the rheological response of the film material to the very severe conditions in the contact (high pressure, high strain rate and short transit time, 10^{-3} sec).

2.3.2.3. Boundary regime

Boundary lubrication is encountered in systems which operate at low speeds and viscosities under excessive loading and heating, continual stopping and starting or under starvation conditions. Thus the separating film between the surfaces in motion is no longer continuous and most or all of the load is borne at asperity contacts.

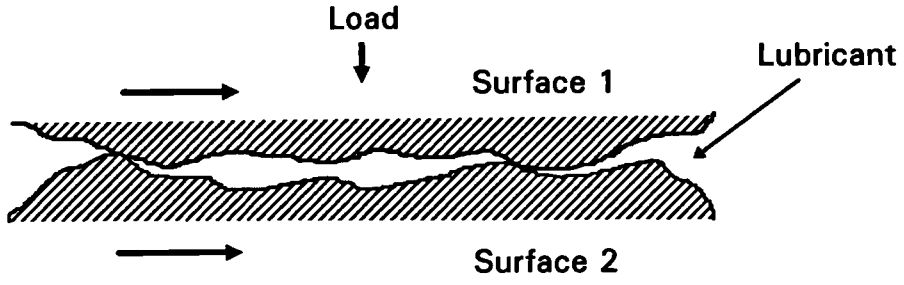


Fig. 2.6. Boundary lubrication

The specific film thickness λ is less than 1, the separation goes down to few nanometers (0.05 to 0.001 μm) and the coefficient of friction is approximately between 0.08 and 0.3.

In such conditions, the friction is essentially independent of the bulk fluid viscosity and is governed by the physical and chemical properties of the surface film (so called *boundary film*). These films are formed as a result of the chemical and physical interactions between the metal and the fluid during use and their structure and properties are different from the bulk fluid and the rubbing surfaces. The term "boundary lubrication" was first introduced by Sir William Hardy in 1922 [**2.23**], a pioneer in the development of surface science. His monolayer concept of oiliness became the basis of the well-known monolayer adsorption model of boundary lubrication (figure 2.7).

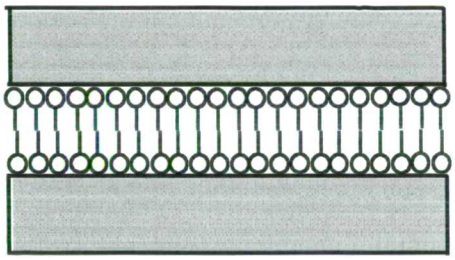


Fig. 2.7. Contact region according to Hardy

However later work proved that his model can not be correct for at least two reasons. First, it is generally found that with very light loads, the coefficient of friction under boundary lubrication conditions, *rises* to near normal values [**2.1**] and that boundary lubrication fails under very high loads and with repeated traverses of the same track. Second, it is found that metal-metal contacts are still present even under normal boundary lubrication conditions where μ is small [**2.24**].

Thus the concept need to be modified and this was mainly due to the work of Bowden and Tabor who considered that the load is supported by the lubricant film as well as by minute metallic junctions formed where the asperities penetrate the lubricant (figure 2.8).

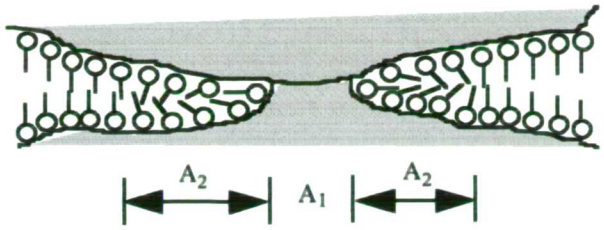


Fig.2.8. Contact region according to Bowden and Tabor

A third model was proposed later by Adamson [**2.25**] in 1960 and is shown in figure 2.9.

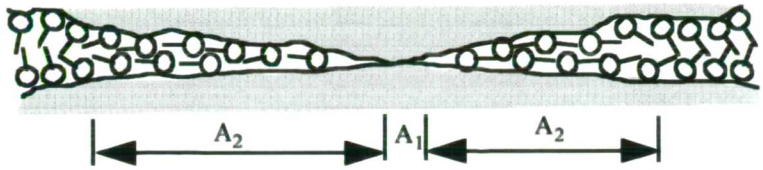


Fig.2.9. Pressurised film model for boundary lubrication

The situation represents the more general case of high loads when the surfaces are pressed together under increased load; it is assumed that the model of Bowden and Tabor is valid only for the particular case of very light loads. That is, with small loads, there will be regions of slight metal-metal contact with a surrounding fringe of essentially normal monolayer. For normal loads most of the load is being supported by the boundary film and that therefore the film itself is under mechanical pressure. As a result, the molecules of the film are lying flat and the coefficient of shear for the film fraction would be much smaller than for the metal-metal areas and for the vertical oriented molecules [**2.25**]. This corresponds to the observed low μ values under boundary lubrication conditions with normal loads.

It is unlikely that many moving systems solely operate in the boundary regime, but for most of them, the time spent in this regime is quite considerable: for example in journal bearings, boundary friction may develop whenever the shaft passes through zero speed during starting or stopping.

Boundary regime is currently the least understood of the lubrication regimes and no generally mathematical model has yet been accepted, partly because it is dependent on a

number of factors which are difficult to control (nature of metal surface, minor amounts of impurity in oils, humidity, oxygen availability, etc.) and also because it is difficult to measure and study such thin, molecular surface layer - a more detailed explanation of the current theories can be found in [**2.26**]. The simple friction model developed by Bowden and Tabor [**2.1**] and explained earlier, suggests that successful boundary lubrication depends upon minimising asperity adhesion and interlocking, that results in severe stick-slip. This implies an appropriate surface roughness and run-in time to avoid severe wear and seizure.

The mechanisms which generate the surface films in boundary lubrication are considered to be of three types:

(1) physical adsorption,

(2) chemical adsorption

(3) chemical reaction

These may operate separately, sequentially (in a limited temperature range) or in conjunction.

The strongest is the *chemical reaction* which takes place between the metal and components in the lubricant. This implies an exchange of valence electrons between the two substances and the formation of a new compound. The reaction is irreversible and the films formed are very stable. These films are formed at high temperatures and pressures and can withstand such critical conditions by continuously growing the film as long as the concentration of the reactants is maintained.

Chemical adsorption is the second strongest mechanism which forms the protective layer by ionic chemical bonds. Chemisorbed films are weaker than the chemical reacted ones and can not withstand high temperatures and loads. Failure of lubrication normally occurs when the melting point of the boundary film is reached, usually between 120-180°C.

The third interaction mechanism is *physical adsorption*. The protective films are held to the surface by weak physical Van der Waals forces. No exchange of electrons takes place between the fluid and the rubbing surfaces and the bond is reversible and weak.

The film is quite unstable, temperature sensitive and is desorbed from the surfaces when the thermal energy approaches the bond strength (or when the film dissolve in the bulk lubricant when its solubilization temperature is reached [2.27]). This type of bond is common with long chain polar surfactants which form dense layers of hydrophobic chains typically 2 to 3 nm long. They are called "oiliness" additives. In addition there may also be strong forces of lateral attraction between the chains which increase the strength of film.

2.3.2.4. Mixed regime

Between the regimes of hydrodynamic or elastohydrodynamic lubrication on one hand and boundary lubrication on the other is the regime known as *mixed* or *partial* lubrication. The transition from HD or EHD regime to boundary regime is relatively gradual and the regimes overlap each other. As the sliding speed is decreased (or the load increased) the wedge of lubricant separating the surfaces becomes thinner and thinner and the number of surface asperities penetrating the film becomes more and more numerous. At the tips of these asperities the lubrication is of boundary nature, so that the amount of boundary lubrication increases gradually whilst the amount of fluid lubrication decreases. To properly chart this region requires a detailed understanding of the influence of surface topography on fluid behaviour and of the influence of contact and fluid pressure on surface topography.

Most authors consider that the transition from hydrodynamic or EHD lubrication to mixed lubrication starts at about λ=2 to 3 and that most of load continues to be born by the fluid down to λ=1 [2.28]. However there is still little known about the transition from mixed to boundary lubrication. The use of lambda values in the context of very low lambda ratios is not sufficiently accurate since it embodies the roughness of the undeformed surfaces whereas in the very thin film region, considerable elastic and plastic deformation will have occurred. Although much valuable work has been carried out so far, we are not yet sure of the extent to which asperities contact each other or are elastically-flattened in real contacts. Recently, the rough surface problem has been solved computationally using a 3-D roughness model [2.29] but the situation where lambda is less than about 0.5 cannot be modelled yet [2.28]. This is unfortunate since

many practical components operate either continuously or transiently in mixed lubrication, including almost all systems which exhibit wear, such as pistons and cams. Considerable experimental work has been done in order to analyse the mixed lubrication regime. This has helped in clarifying and confirming the analytical and computational efforts. Thus the fact that electrical contact resistance (ECR) measurements demonstrates that asperities do contact has played an important role in subduing over-enthusiasm concerning early micro-EHD computations, where it initially appeared that almost all roughness flattens out. A recently-developed experimental technique [**2.30**] makes it possible to look directly at surface roughness itself in EHD/mixed contacts and determine the extent of elastic smoothing of real rough surfaces. This uses optical interferometry [**2.31**] coupled with interference colour analysis to produce 2-D maps of film thickness for very thin films in EHD contacts.

2.3.3. Stribeck Curve

The "Stribeck Curve" [**2.32**] was one of the earliest forms of lubrication chart distinguishing between fluid film, mixed and boundary lubrication. The first President of the ASME, Robert H Thurston [**2.33**] reported in 1885 that the friction in a journal bearing passed through a minimum as the load increased; a transition now associated with a change from fluid-film to mixed lubrication [**2.34**]. The curve was initially plotted for the case of a journal bearing working in the hydrodynamic lubrication regime and represents the relation between the friction coefficient in the bearing and the dimensionless parameter ($\eta U/W$), sometimes called the Hersey number [**2.35**], where η is the viscosity of the lubricant, U is the sliding speed and W is the normal load on the bearing. The diagram shows the lubrication regimes (boundary lubrication, mixed lubrication and hydrodynamic lubrication) for the corresponding values of μ and the other paramerers. Some authors [**2.7, 2.35, 2.36**] have published a modified Stribeck curve which shows the elasohydrodynamic regime on the same plot with the hydrodynamic regime. However, experiments have shown that friction in EHD has a different evolution at high speeds and hence high lambda values, from friction in hydrodynamic regime

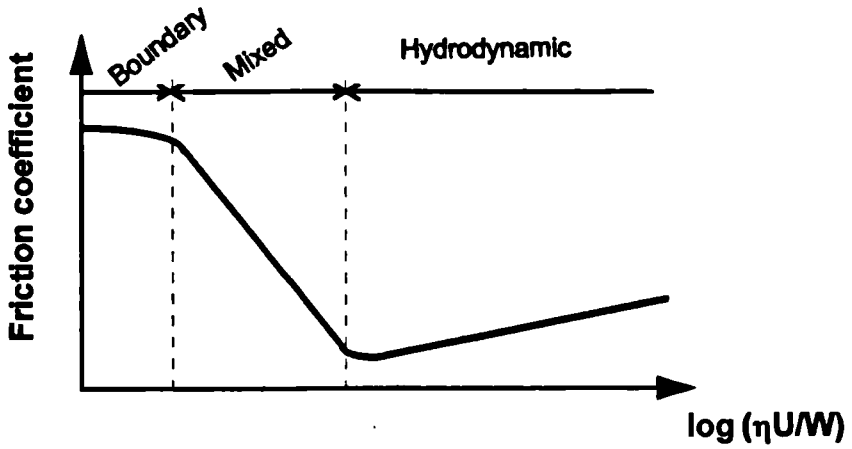


Fig.2.10. Stribeck curve - Hydrodynamic regime

In the boundary regime for low speeds and low lubricant viscosity, there is a considerable amount of solid-to-solid contact which increases the coefficient of friction up to values between 0.08 and 0.3. In this situation, the value of μ depends on the particular materials involved; it may vary from less than unity to the very large values characteristic of seizure and gross adhesion.

As the speed and thus the specific film thickness increases, there is a drop in friction as a result of less asperity interaction and more hydrodynamic support of the load. This means that friction will be more influenced by the shear strength of the bulk lubricant which is lower than the shear strength of the adsorbed boundary layer. The friction coefficient continues to drop until it reaches a minimum value (typically between 0.005 and 0.03) where the solid friction has fallen to a low value and yet the viscous shear losses have not grown large. Than μ starts to increase as an effect of viscous friction because more fluid is dragged into the contact as speed increases.

For slow speeds, the behaviour described by the Stribeck curve for the EHD regime (figure 2.11) is similar to that of the HD regime.

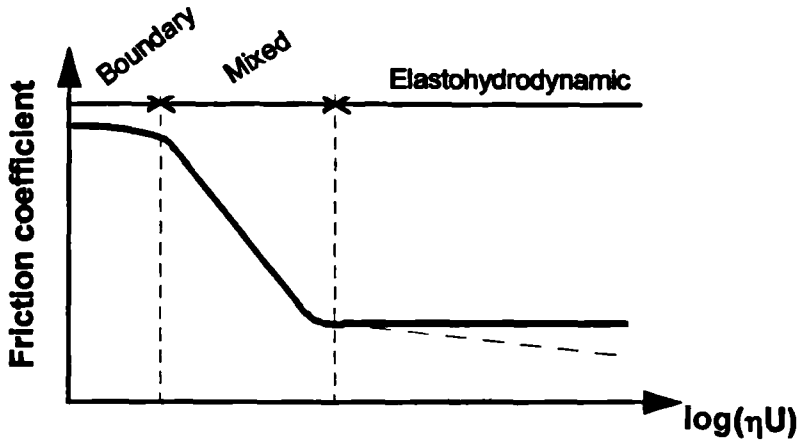


Fig.2.11. Stribeck curve - Elastohydrodynamic regime

The friction falls to a minimum value of about 0.05 then is practically independent of speed. A reason for this behaviour is that under high contact pressures encountered in EHD regime, as the speed is increased, the lubricant behaves more like a plastic solid by reaching a limiting shear stress at which it yields plastically. However, the friction coefficient will drop slightly because of shear heating effects which are inevitable at high speeds. The load W was excluded from the independent parameter because in EHD regime the film thickness varies only marginally with load so that ($\eta U/W$) is no longer an appropriate grouping.

REFERENCES

[2.1] Bowden F.P. and Tabor D., "Friction and Lubrication", Methuen & Co Ltd., London, 1967,

[2.2] Williams G. A., "Engineering Tribology", Oxford University Press, 1994,

[2.3] Sayles R. S., "Roughness and Debris in Machine Element Contacts: Some Current and Future Engineering Implications", 9th BP-IMechE Tribology lecture, Nov. 1994,

[2.4] Spikes H. A., "Lecture Notes", Imperial College, London, 1995,

[2.5] Israelachvili J.N., You-Lung Chen and Yoshizawa H., "Relationship between adhesion and friction forces", J. Adhesion Sci. Technol., Vol. 8, pp. 1231-1249, 1994,

[2.6] Tallian T., "EHD Effects in Rolling Contact Fatigue", Proc. 5th Leeds Lyon Symp. on Tribology (London MEP), p. 253, 1979,

[2.7] Hutchings I. M., "Tribology: Friction and Wear of Engineering Materials", Edward Arnold, 1992,

[2.8] Reynolds O., "On the Theory of Lubrication and its Application to Mr. Beauchamp Tower's Experiments, Including an Experimental Determination of the Viscosity of Olive Oil", Phil. Trans. Proc. Roy Soc. p. 157, pt. 1, 177, 1886,

[2.9] Everett H. A., SAE Journal 41, 531, 1937,

[2.10] Barus C, "Isothermals, Isopietics and Isometrics in Relation to Viscosity", Am. J. of Sci. 3rd Series, 45, pp. 87-96, 1893,

[2.11] Cann P.M., "An Introduction to Lubrication", internal paper, Imperial College, Tribology Section, London,

[2.12] Chu P.S.Y. and Cameron A., "Pressure Viscosity Characteristics of Lubricating Oils", J. Inst. Pet., 48, pp. 147-55, 1962,

[2.13] Hertz H., "On the Contact of Elastic Solids" published in English in "Miscellaneous Papers by Heinrich Hertz", Macmillian, 1896,

[2.14] Dowson D. and Hamrock B. J., "Elastohydrodynamic Lubrication, the Fundamentals of Roller and Gear Lubrication", Pergamon Press, Oxford, 1966,

[2.15] Johnson K.L., "Regimes of EHD Lubrication", J. Mech. Eng. Sci. 12, 1, pp. 9-16, 1970,

[2.16] Hamrock B. J. and Dowson D., "Ball Bearing Lubrication", Wiley, 1981,

[2.17] Johnson K.L. and Tevaarwerk J.L., "Shear Behaviour of EHD Oil Films", Proc. Roy. Soc. London. A356, pp. 215-236, 1977,

[2.18] Spikes H.A., "Non-Newtonian Aspects of Lubricant Rheology", Lecture Notes, Imperial College, London, 1995,

[2.19] Bair S. and Winer W.O., "Shear Strength Measurements of Lubricants at High Pressure", Trans. ASME, J. Lubric. Technol., Series F, 101, pp. 251-257, 1979,

[2.20] Bair S. and Winer W.O., "Some Observation in High Pressure Rheology of Lubricants", Trans. ASME, J. Lubric. Technol., Ser. F, 104, pp. 357-364, 1982,

[2.21] Evans C.R. and Johnson K.L., "The Rheological Properties of EHD Lubricants", Proc. IMechE, Vol. 200 no C_5, 1986,

[2.22] Bair S., Winer W.O. and Distin K.W., "Experimental Investigation into Shear Localization in an Operating Contact", *Thin Films in Tribology,* Proc. 19th Leeds-Lyon Symposium, ed. D. Dowson et al. publ. Elsevier, 1993,

[2.23] Hardy H. B. and Doubleday I., "Boundary Lubrication - The Paraffin Series", Proc. Roy. Soc. Lond. A100, pp. 550-757, 1922,

[2.24] Bowden F. B. and Tabor D., "The Friction and Lubrication of Solids", Oxford University Press, 1964,

[2.25] Adamson A.W., "The Physical Chemistry of Surfaces", Interscience, New York, 1960,

[2.26] Spikes H. A., "The behaviour of Lubricants in Contacts: Current Understanding and Future Possibilities", Proc. IMechE Vol. 208, 1994,

[2.27] Kreuz K.L., Fein R.S. and Rand S.J., "Solubilization Effects in Boundary Lubrication", Symposium on Deposit, Wear and Emission Control by Lubricant and Fuel Additives, Am. Chem. Soc., Sept. 1969,

[2.28] Spikes H.A., "Mixed Lubrication - an Overview", Symposium "Tribology - Solving Friction and Wear Problems", published in Lubrication Science 9, pp. 221-253, 1997,

BIBL. LONDIN. UNIV

[2.29] Chang L., Jackson A. and Webster M.N., "Effects of 3-D Surface Topography on the EHL film Thickness and Film Behaviour", Trib. Trans.37, pp. 435-444, 1994,

[2.30] Cann P.H., Hutchinson J. and Spikes H.A., "The Development of a Spacer Layer Imaging Method (SLIM) for Mapping EHD Contacts", Trib. Trans. 39, pp. 915-921, 1996,

[2.31] Johnson G.H., Wayte R. and Spikes H.A., "The Measurement and Study of Very Thin Lubricant Films in Concentrated Contacts", Trib. Trans. 34, pp. 187-94, 1991,

[2.32] Stribeck R., "Die Wesentlichen Eigenschaften der Gleit und Rollenlager", Z. Ver. dt. Ing., 46, No. 38, 1341-8; No. 39, 1463-70, 1902,

[2.33] Thurston R.H., "A Treatise on Friction and Lost Work in Machinery and Millwork", Wiley, New York, 1885,

[2.34] Dowson D., "Thin Films in Tribology", *Thin Films in Tribology,* Proc. 19th Leeds-Lyon Symposium, ed. D. Dowson et al. publ. Elsevier, 1993,

[2.35] Stepina V. and Vesely V., "Lubricants and Special Fluids", Tribology Series, 23, Elsevier, 1992,

[2.36] Mortier R.M. & Orszulik S.T., "Chemistry and Technology of Lubricants", p. 4, Blackie and Son, 1992,

[2.37] "Life Adjustment Factor for Ball and Roller Bearings", ASME Engineering Design Guide, 1971

CHAPTER 3

LUBRICANT-RELATED ENGINE FRICTION

This chapter first examines engine losses with emphasis on mechanical (mainly frictional) losses. A discussion of the friction and lubrication of the main tribological engine components (piston-rings, bearings, valve train) follows, each accompanied by a short literature review. Attention then shifts towards the engine fuel efficiency and the possible ways to reduce fuel consumption through lubricant formulation. The last part of the chapter is concerned with fuel efficiency engine tests in particular ASTM Sequence VI and VI A, which provide efficiency data used for correlations in subsequent chapters. The strategy of the fuel economy prediction approach is outlined together with a discussion of previous prediction work.

3.1. Engine losses

Engine friction is a subject of continuous interest among engine manufacturers. Higher friction invariably means the generation of higher surface temperatures which generally exacerbates the rates of surface damage and wear. Just as importantly, higher friction means poorer fuel economy and the initial impetus for the research in engine friction reduction stemmed from the so called "energy crisis" of the 1970s [3.1] which resulted in a rapid increase in crude oil costs and a higher concern about the remaining life of the world's petroleum reserves.

Often the difference between a good and an average engine design is the difference in their frictional losses. To understand the significance of friction in relation to the output of useful work in an engine, and hence to fuel economy, it is helpful to consider how the total energy provided by fuel combustion in the engine becomes subdivided. Some passes out as useful work, but the reminder is lost by various mechanisms and leaves the engine via the exhaust gasses, cooling water, heat losses from the engine itself and as noise.

Fundamental thermodynamic principles mean that thermal efficiency of an internal combustion engine is theoretically limited to a value substantially less than unity by the temperatures of the reservoirs which experience the heat transfer interactions [3.2]. Thermal energy losses derive also from incomplete combustion of the fuel which makes the combustion efficiency less than unity. Consequently conventional internal combustion engines have inherently low thermal efficiencies, generally between 20% and 30% [3.3, 3.4]. This means that, of the energy released from the combustion process some 70-80% is not transferred as work but is lost as energy carried away in the hot exhaust gases, in the heat transfer losses directly from the engine walls and sump or in the heat transfer to the coolant. The proportion which is transferred to each depends upon the design of the engine and the conditions under which it is running. Milton [3.4] has published a rough distribution of energy flow at wide-open throttle and medium speed for a spark-ignition (SI), a compression-ignition (CI) engine and gas turbine which is reproduced in table 3.1. It should be noticed that the table specifies the indicated power, but an additional portion of this, possibly one-fifth (say 7% of the fuel energy for SI engine) [3.4] is also lost as friction.

	SI	CI	Gas turbine
Energy to indicated horse power	36%	50%	45%
Energy to coolant (water or air)	24%	20%	
Energy to exhaust	30%	20%	45%
Remainder (through walls or sump)	10%	10%	10%

Table 3.1. Energy flows in engines

Since heat losses represent the major part of the energy losses, considerable research and development attention has been given to their reduction. For example studies of the

combustion process have been widespread and the "low heat rejection" (initially called "adiabatic") engine has attracted attention [**3.3**].

The losses due to mechanical aspects of the engine (mainly friction) are small compared to their thermal losses. The general distribution of the energy of the fuel and the contribution of the friction losses of the major machine elements to the mechanical component of this dissipation has been analysed by a number of authors [**3.5, 3.6, 3.7**]. It is evident that the dissipation of the power produced by the fuel will depend upon many factors, including the type of engine and the load and speed conditions; however certain generalisations are of value in an overall appreciation. In terms of energy distribution in a typical engine, the analysis made by Martin [**3.6**] showed that 30% of available energy within the fuel is lost to the exhaust, 30% to cylinder cooling and only 40% provides the indicated power (figure 3.1a), in which he includes pumping losses. Of the indicated power, less than half is available as useful mechanical output.

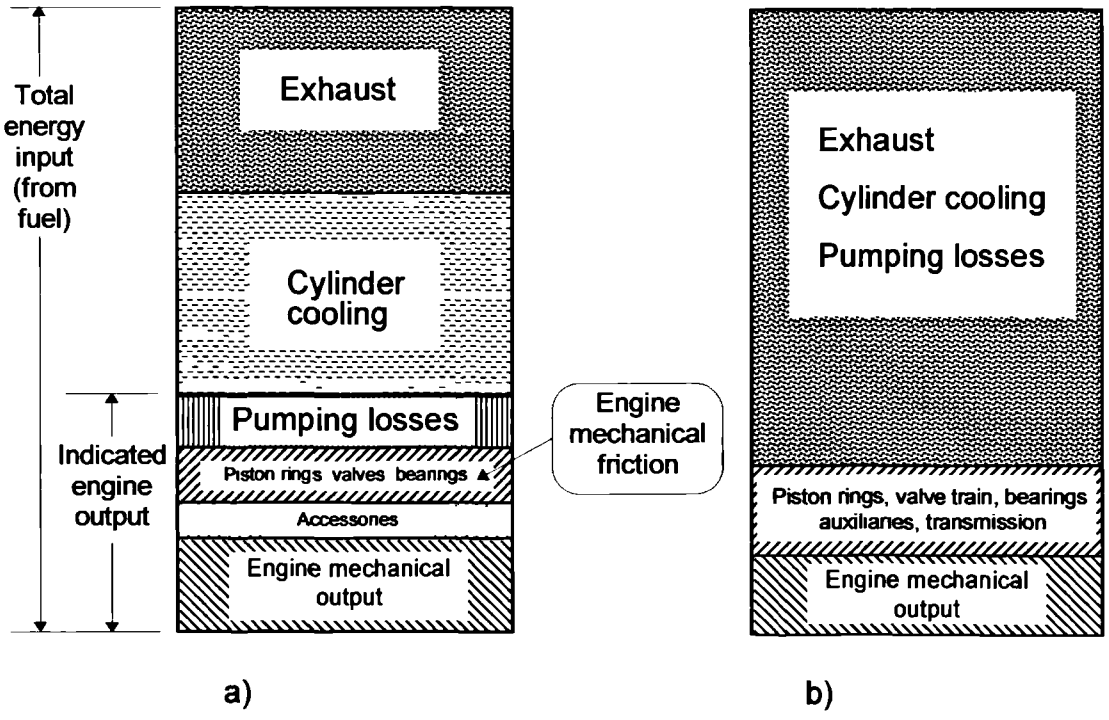


Fig.3.1. Typical energy distribution in an automotive engine

In a similar way, Andersson [**3.8**] has analysed the power distribution in a particular car during city driving (figure 3.1b). He concluded that about 73% of the energy input is lost due to cooling by heat transfer from engine surfaces, the exhaust of hot gases and pumping losses. Thus of the reminder, some 15% of the energy may be consumed as

mechanical losses by the piston assembly, bearings, valve train, auxiliaries and transmission. This leaves 12% of the total power transmitted to the wheels to accelerate the vehicle and overcoming rolling and air resistance.

Initially it appears from figures 3.1a and b that by comparison with thermal losses, mechanical losses due to friction are small. However, it must be appreciated that these losses certainly form a large proportion of the total available work output [3.5]. Thus from the total energy available from fuel, only 40% provides the indicated power. From this, about 45-50% is lost as friction and the rest provides the useful work. This shows that the ratio of friction losses to useful work is approximately equal and a 10% reduction in friction losses would theoretically lead to a similar increase in engine mechanical output.

3.1.1. Engine mechanical losses

As can be seen from the above power distributions, mechanical friction losses due to piston rings, valve train and bearings account for about 15% of the total power [3.8] or if referred to the indicated power, they could amount up to 25% (or more) of this [3.9]. The useful mechanical output figures vary from one author to another, for example Andersson [3.8] states that about 12% of the total power is transmitted to the wheels whereas Parker [3.5] suggests that the mechanical output is 18%. Precise figures depend upon many factors including engine type and operating conditions as can be seen from the analysis made for four engines in table 1 in reference [3.5].

The engine components known to be mainly responsible for the mechanical losses are the piston assembly which is the greatest loss source, followed by the crankshaft bearings, auxiliaries, transmission and valve train. The auxiliaries include oil and cooling pumps, fan, alternator, etc. A schematic of major energy consumers in the internal combustion engine is presented in figure 3.2.

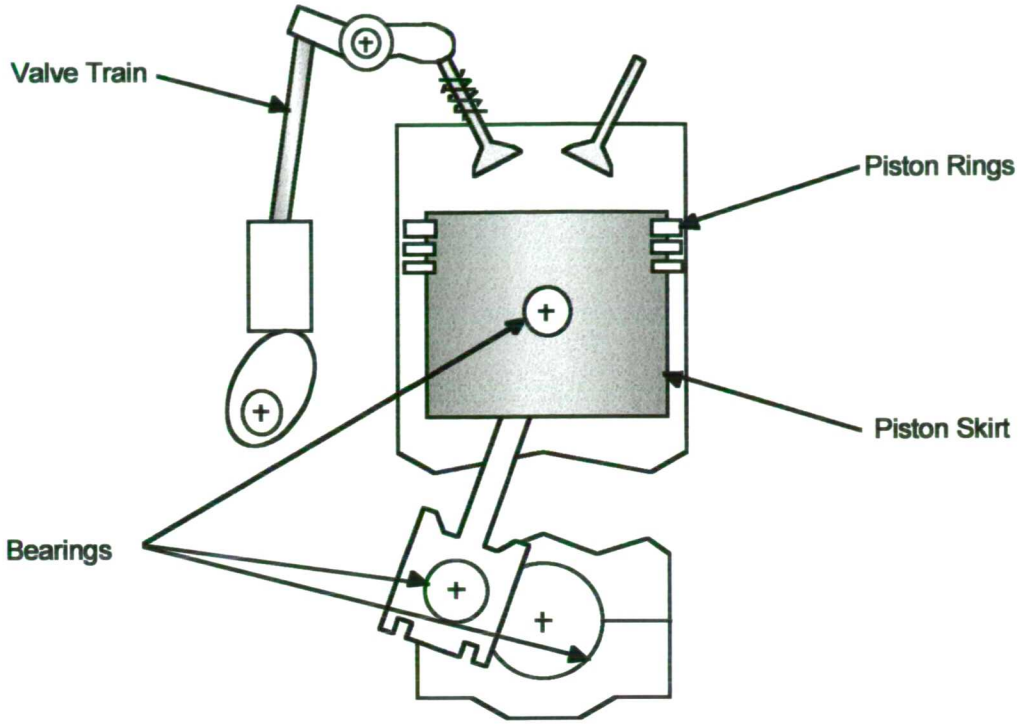


Fig.3.2. Schematic of major energy consumers in an IC engine

Motored engine tests where the engine is disassembled or broken down to stages, can be used to determine the friction associated with each major engine assembly. These tests show the large contribution to the total friction from the piston assembly, valve train, crankshaft bearings and water and oil pumps. Lang and Kernen [**3.11**] have presented a general pie chart outlining the proportion of total engine friction due to the different components.

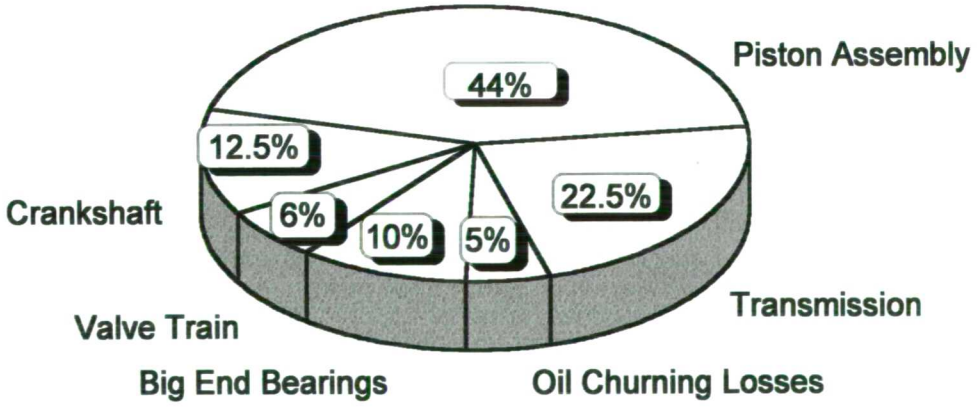


Fig.3.3. Breakdown of total engine friction

It can be seen that out of the 72.5% of the engine mechanical losses that are of tribological origin, about 54% are due to the piston assembly (piston, piston rings and connecting rod bearings), 6% due to the valve train and 12.5% to main bearings. Recent estimates of valve train losses suggest that the 6% figure quoted above seriously underestimates their current importance [**3.12**]. Calculated values for V6 and V8 engines range from 12% to 34%, depending mainly on engine speed. A number of authors have found quite similar results for piston assembly friction losses: Li around 60% [**3.13**], Cleveland and Bishop 67% [**3.14**], Nakada 50-60% [**3.15**], for petrol applications and Ricardo and Hempson, 58% for diesel applications [**3.16**]. Heywood [**3.2**] suggests that friction losses are divided between the main engine components in the following proportions : piston assembly 50%, valve train 25%, crankshaft bearings 10%, accessories 15%.

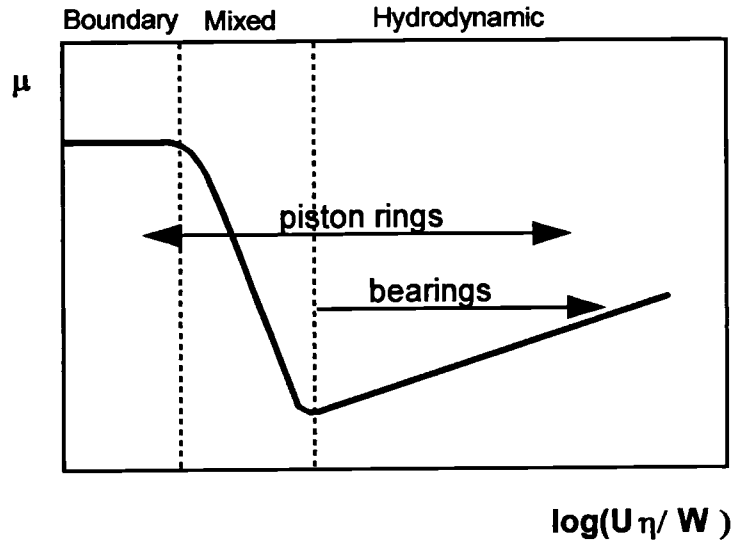
It should be borne in mind, however, that the values given above tend to be obtained from motoring tests and under real firing conditions some differences can occur, as it was demonstrated by Ball et al. [**3.17**]. Motoring losses are different from firing losses for several reasons amongst which is the fact that only the compression pressure and not the firing pressure acts in the piston, piston rings and bearings which lowers the rubbing friction. On the other hand, the piston and cylinder bore temperatures are lower in motored operations which results in higher viscosity of the lubricant and therefore increased viscous friction.

Studies of engine friction as a function of speed and load have shown that the percentage of mechanical losses arising from both piston assembly and crankshaft friction increase consistently with speed and are much larger at low load than at full load [**3.5**].

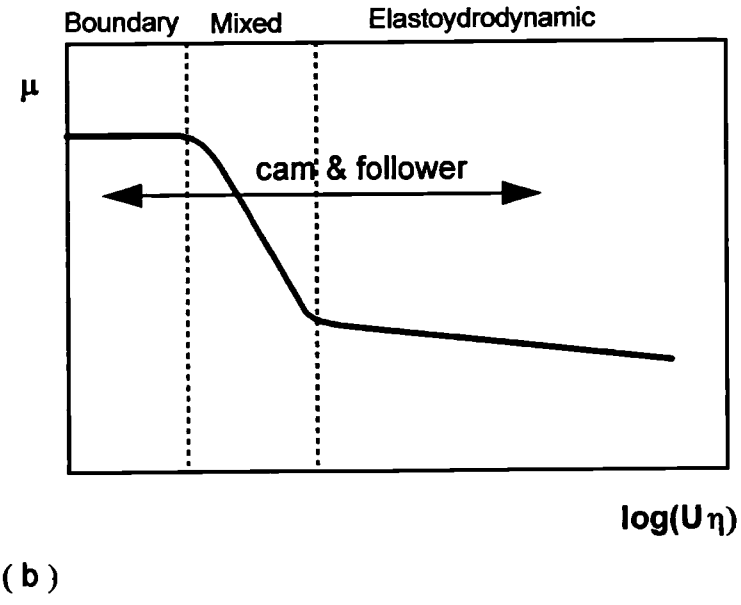
3.2. Lubrication of main engine tribological components

In general, moving components of an engine operate under specific lubrication regimes depending upon design, operating conditions and the rheology and chemistry of the lubricant. From the lubrication point of view, it has been suggested that about two

thirds of the friction losses come from hydrodynamic lubrication and one third from mixed lubrication [3.9]. It is interesting to place the major frictional components of the internal combustion engine on the Stribeck diagram described in the previous chapter. Figure 3.4.(a and b) shows such an attempt. It can be seen that they cover the range from boundary lubrication to fluid film hydrodynamic lubrication.



(a)



(b)

Fig.3.4. Stribeck diagram for various engine components lubrication

The non-dimensional parameter ηU/W can be substituted by the lambda ratio of the minimum film thickness over the r.m.s. of the surface asperities in order to relate the

lubrication to the separation in the contact. Thus the piston rings enjoy full film lubrication and probably operate mainly in the medium shear rate, HD regime except for the top and bottom dead centres where boundary friction prevails. In the main journal bearings, the lubrication regime is also hydrodynamic, but at start up and shut down of the engine boundary lubrication occurs. The shear rates experienced by the lubricant in the bearings are probably considerably higher than in the pistons, shear rates of 10^7 s^{-1} may be present, however [**3.18**]. The cam and follower is the most difficult component to lubricate because the contact pressures are much higher than in the pistons and bearings and both EHD and boundary lubrication occur at different parts of the lift cycle. In general, EHD lubrication occurs *during* top lift, whereas boundary lubrication prevails *near* top lift [**3.9**].

In the following paragraphs a brief discussion about the friction and lubrication of the main engine components will be presented. A more detailed analysis is beyond the scope of this work.

3.2.1. Piston assembly

As it was shown previously, the piston assembly is the dominant source of rubbing friction (it accounts for almost 50% of mechanical losses). The components that contribute to friction are: piston rings (compression and oil control rings), piston skirt and piston pin. In the literature is suggested that piston skirt is normally the largest contributor, about 25% of piston assembly friction, whilst the rings account for only 19% [**3.11, 3.19**]. However there is also a large amount of evidence to indicate that the rings can account for some three quarters of the total piston friction [**3.21**]. The discrepancies among the above literature sources are due to the fact that different test methods, engines and test conditions were used to generate the data. Also authors tend to define piston and ring friction differently (in some cases piston and connecting rod friction are summed, while in others they are presented separately).

Lubrication of piston skirts is normally hydrodynamic [**3.22, 3.23**]. The measurements of piston skirt friction performed by Thring [**3.24**] also concluded that friction was predominantly due to viscous drag at mid-stroke and that friction at the ends of the

piston stroke due to boundary or mixed lubrication had little impact on friction horsepower (although it was important with respect to wear and scuffing). The "floating liner" method was first reported by Furuhama and Sasaki [3.25] and has been widely used for measuring piston friction by a numerous number of researchers [3.26, 3.27, 3.28]. Parker [3.28] also showed the benefit to be gained by reducing the area of action of the viscous shear stresses in the oil film between the cylinder wall and the piston skirt. As a result of experimental studies, major design changes followed in the piston skirt geometry and skirt-bore clearance, on one hand, and in reducing lubricant viscosity on the other, in order to reduce total engine friction and thus lower fuel consumption.

Piston rings probably are the most complex tribological component in a vehicle. Power, fuel consumption, hydrocarbon emissions, oil consumption, blow-by, wear noise are all affected by the design of the ring-liner interface. Most piston rings experience effective hydrodynamic lubrication over much of the engine cycle, with surface interactions and boundary lubrication dominating the situation at the dead centre positions, although there has been a suggestion that EHD effects may not be insignificant [3.29]. The barrel profile of the piston rings provides a mechanism for the build up of an oil film by hydrodynamic action provided that the piston velocity is relatively high. The rings are loaded against the cylinder liner by a combination of elastic and gas pressure forces which can be quite significant especially near the top dead centre of compression stroke when the gas loads acting behind the rings are at their maximum.

The film thicknesses generated between the rings and liner have been measured experimentally. Furuhama et al. [3.30] was the first to report lubricant film thickness measurements in a piston assembly. Later on, Hamilton and Moore [3.31] successfully applied a capacity gauge in a running engine for the film thickness measurements. The measured thickness values were in the range of 0.4 - 2.5 μm which was somewhat lower than would have been expected if the rings were flooded with oil. These findings indicated that in practice, piston rings operate under starved conditions so that only a narrow band of the ring near the part of the barrel surface which is outermost at any moment is actually involved in hydrodynamic action [3.32]. It is worth mentioning that the fluorescence method was also used to measure the film thickness in the piston assembly. Smart and Ford [3.33] were the first to use fluorescence for measuring the

thickness of films in 1974 and the method was further developed by introducing the laser as the source of ultraviolet light [3.34]. Since than a large number of researchers have applied it to studies of film thickness in engines [3.35, 3.36, 3.46].

The experimental evidence supports the hypothesis that full fluid film lubrication occurs in the mid-stroke and this raised the possibility of applying HD lubrication theory to study the piston-ring lubrication. Theoretical analysis has been carried out by a large number of researchers during the past 60 years. Initial steady-state analyses [3.37, 3.38] assumed typical loads and sliding speeds for the mid-stroke position and confirmed that a piston ring with a convex profile could generate an adequate film between itself and cylinder liner. Later Furuhama [3.39] recognised that the squeeze term in the Reynolds equation had to be included in the analysis in order to calculate the load bearing capacity of the lubricant film. The ring profile, the interactions between the rings and their grooves and the inter-rings pressures have been shown to have a profound effect upon film thickness, lubricant flow and friction. The early studies were restricted to the performance of a single ring but in due course it became possible to analyse a complete ring pack by imposing a condition of lubricant flow continuity and account for lubricant starvation [3.40]. The influence of asperity interaction was taken into account in the mixed lubrication model proposed by Rhode in 1980 [3.41], by Richez et al. in 1982 [3.42] and followed by many other studies later. The hydrodynamic aspect of the model was based on the average Reynolds equation developed by Patir and Cheng [3.43] and the asperity interaction model employed was that developed by Greenwood and Tripp [3.44]. The contribution of EHD lubrication to the tribological performance of piston rings was first investigated by Dowson et al. in 1983 [3.29]. More recently Hwu and Weng [3.45] applied the EHD theory to calculate the minimum oil film thickness and film pressures in the lubricant. The influence of engine oils was also studied by accounting for temperature and pressure effects upon shear viscosity [3.29] and the increase in viscosity due to evaporation of the lubricant as a result of the high temperatures encountered in an engine (the lubricant temperature may reach 200-260°C in the top ring area [3.3]). Non-Newtonian, viscoelastic effects and also surface tension were analysed by Hoult et al. [3.46] for the case of high molecular weight additives in the base stock oil.

The complexity of the piston ring/cylinder liner system and the task of developing high-performance engines has caused many automotive companies to design their products using computer models. These models obtain simultaneous solutions to the highly inter-related phenomena of ring dynamics, blow-by and ring pack lubrication [3.47]. The General Motors laboratories have developed an integrated software package, FLARE for lubrication analysis of engine bearings, valve train, piston skirt and rings [3.12].

3.2.2. Bearings

World-wide, more tribological research has been committed to the development of engine bearings (design, material, lubricant) than, perhaps, to all other vehicle tribological areas combined. Engine bearings, which may absorb about 25% of the mechanical losses, normally operate under hydrodynamic lubrication although the importance of elastic deflections is clearly recognised in some cases [3.20].

Under normal operating conditions, large loads can be carried by journal bearings with low energy losses due to complete separation of the two surfaces in relative motion by the lubricant film. For the crankshaft bearings, however, loads vary in magnitude and direction [3.23] because they result primarily from the inertial loads of the piston/connecting rod mechanism and the cylinder gas loads. The journal eccentricity determines the minimum film thickness between the journal and bearing surfaces and is thus a critical design parameter. If the film thickness is too low, asperities will break through the lubricant film and substantially increase friction and wear. Typically a minimum film thickness of 2 μm is considered suitable in journal bearing design [3.10].

One of the most challenging tasks in bearing-related experiments has been the measurement of minimum film thickness in an operating engine. The capacitance technique has proved to be the most appropriate method [3.48, 3.49] although it has some drawbacks. The difficulty with this method is that the instantaneous shape of the bearing clearance space and the cavitation extent have to be known in order to convert the measured capacitance to minimum film thickness [3.10].

Nowadays, bearing and engine manufacturers have access to an array of computer models to analyse engine bearings and predict their performances e.g. oil film thickness, oil film pressure, friction losses etc. However engine bearing tribology is still not fully understood. Film thickness cannot be predicted in an absolute sense and it is still not possible to relate it to the surface roughness of the crankshaft [**3.10**]. Good correlation between measured and predicted film thickness has, however, been reported when EHD effects were included in the analysis [**3.50**]. Recently elastohydrodynamic lubrication theory has been used to study the stiffness of the bearing housing in order to optimise bearing performance [**3.51**].

Most of the analyses currently used are based on Newtonian oil behaviour, whereas the oils used in engines are multigrade non-Newtonian fluids. New analysis methods have been developed which take into account thermal and non-Newtonian effects of the lubricants in engine bearings [**3.52, 3.53**], but these effects are still barely understood as are the effects of oil additives on bearing wear and the factors influencing the oil pressure at the big end bearing feed hole [**3.54**].

In spite of the availability of fairly comprehensive analytical models and good film thickness and friction measurements for journal bearings operating under engine-like conditions, comparisons between analytical and measured data are scarce [**3.10**].

3.2.3. Valve train

The valve train carries loads over the entire speed range of the engine. The contact between cam and follower is a highly-loaded one with Hertzian stresses comparable to those found in gears. At low speeds, the loads acting on the valve train are due primarily to the spring forces, while at higher speeds the inertia forces of the component masses dominate [**3.2**]. While the valve train is generally taken to consume about 10% of the mechanical losses (although this may be quite a bit higher for low engine speeds and large capacity engines), because of "surface interactions" the cam and follower has been the most prominent machine element in the automobile engine from the perspective of failures. Until a quarter of a century ago, boundary lubrication was considered to be the effective mode of operation for the cam and follower [**3.20**] although there were some

exceptions that dealt with the possibility of thin film lubrication due to elastohydrodynamic mechanism [**3.55, 3.562, 3.57**]. The idea of a thicker lubricant film that would help explaining contradictory results as those found by Müller [**3.55**] was missed by valve train designers until recent years. In the last fifteen years many researchers have studied and predicted the tribological performance of automotive cams and followers from the perspective of fluid film lubrication as opposed to boundary lubrication [**3.58, 3.59, 3.60**]. In his analysis Dowson [**3.58**] showed that the calculated lambda ratios for the flank areas were in the range of 4 and 6.5 for the position and speed range examined which implied that the surfaces were essentially separated and EHD lubrication would be operative. At the nose area, however, the λ ratios obtained were about 0.3, suggesting boundary lubrication.

The predictions of theoretical analysis have been validated experimentally. Williamson et al. [**3.61**] used a capacitance technique to measure the film thickness between a cam and a follower and recorded that the magnitude of the variation of oil film thickness with viscosity is strongly dependent upon the position within the cam cycle. The response was greatest in the flank regions and least in the zero film and the cam nose positions. Harrison [**3.62**] or Dowson et al. [**3.63**] used an electrical resistivity technique to measure the film state. The electrical resistivity method has also provided a remarkable good correlation of film thickness variation in the portions of the cycle where the entraining velocity of lubricant into the contact was small or even zero and where squeeze film EHD lubrication effects were thought to be important [**3.64**]. As the quasi-static analysis predicts zero film thickness at the position of zero entraining velocity, the idea of including squeeze film effects in the lubrication analysis was considered by Zhu [**3.64**] who undertook a transient EHD lubrication analysis. The assumption that the lubricant film thickness at the zero entraining condition on the rising flank should be marginally higher than at the corresponding location of the falling flank was successfully validated by electrical potential measurements. Transient EHD lubrication analysis has received a lot of attention from quite a number of researchers [**3.57, 3.59, 3.65**].

Lubrication analysis has clearly revealed the prospect of poor tribological performance in the vicinity of the cam nose and at two specific points between the flank shoulders

and nose region. Thus it is important to recognise that boundary lubrication has a role to play in addition to thin film elastohydrodynamics and that the role of lubricant additives in forming protective reaction films on the surfaces is vital to satisfactory operation. Significant progress has been made in the analysis of deterioration and failure of cams and followers by including the influence of EHD films in valve train wear modelling [**3.66**].

3.3. Engine fuel efficiency

3.3.1. General

Friction losses, fuel consumption and exhaust emissions are strongly related to engine performance and also to each other. Thus reduction in friction losses will increase fuel efficiency and will also lead to a reduction of exhaust emissions thus fulfilling requirements for both environmental protection and fuel economy. Recently, requirements for improved automobile fuel economy have been emphasised because of global environmental problems resulting from the increase in CO_2 emissions. In the USA, CAFE (Corporate Average Fuel Economy) regulations have been strengthened and in Japan new fuel economy goals have been established recently [**3.67**]. Thus the CAFE fuel consumption regulations up to 1996 were established at 27.5 mpg for passenger cars and in Japan the average improvement by year 2000 must be 8.5% based on 1990 data [**3.68**]. These requirements represent great challenges for oil and automotive manufacturers because many gains have already been achieved in the past and only small improvements remained possible.

From the point of view of engine tribology, reducing fuel consumption means decreasing engine friction. This can be achieved both through engine design changes and energy-conserving crankcase oils. Carefully formulated lubricants can make significant contributions to reduced fuel consumption by reducing

(i) boundary friction

(ii) viscous friction

Both types of frictional loss directly affect engine fuel economy. Rubbing losses occur when engine components run in boundary or mixed lubrication regimes where asperity contact prevails (as it has previously discussed in section 3.2). Lubricant resistance to the movement of surfaces in contact, or viscous drag, is directly influenced by the oil viscosity; the higher the viscosity, the larger the viscous drag. As a result, the component of viscous friction is more important for engine components working mainly under hydrodynamic lubrication conditions where the separating oil film is thick enough to induce a resistance to motion.

Following the above discussion, it has been suggested that there are two main possibilities for increasing engine fuel efficiency through lubricant formulation:

(i) balance of viscometric proportions

(ii) control of surface chemical process.

The first and most easiest way to gain fuel savings is to reduce the viscosity of the lubricants. However, the use of lower viscosity oils can lead to higher oil consumption, lower film thickness and even rupture of the fluid film [3.70]. This leads to poor engine performance due to excessive wear of engine parts and bearing failure which could be controlled by the use of friction modifiers. This topic will be discussed as part of the surface chemical process.

3.3.1.1. Influence of lubricant viscosity

In the 1950s, the only property of engine oils considered to significantly influence fuel economy was kinematic viscosity and many authors investigated the influence of oil viscosity upon engine friction and fuel efficiency [3.69]. With the development of multigrade lubricants it was necessary to analyse and compare their behaviour with regard to fuel saving. Chamberlin and Sheahnan [3.71] showed in 1975 that 2.3% fuel economy benefit could be achieved for SAE 10W-40 oils over an SAE 40 base line oil in steady state (60 mph road load) engine dynamometer fuel consumption tests. The same conclusion, that multigrade oils give lower fuel consumption than single grade oils was reported by Hamaguchi et al. [3.72] and Bell et al. [3.73] and explained in terms of the temporary viscosity loss of the VI improver polymer under conditions of high shear stress.

The effect of kinematic oil viscosity on fuel economy under partially (43.3°C oil temperature) and fully warmed-up (93.3°C oil temperature) engine conditions was studied among others, by Passut and Kollman [**3.74**], Goodwin and Haviland [**3.75**] , Broman et al. [**3.72**]. Their studies showed that benefits of the reduction in viscosity due to warm-up could range between 1.1% and 2.8% [**3.76**]. However, Ghirla and Smith [**3.77**] showed that simply reducing the viscosity of multigrade engine oils by as much as 50% did not produce consistent, statistically significant fuel economy benefits in cyclic EPA tests, although constant speed tests showed larger fuel economy differences. Overall, studies relating changes in oil kinematic viscosity to fuel economy under warmed-up engine conditions have shown that the benefits are greatest under constant (steady state), medium speed (40-60 mph) operation. Under cyclic, warmed-up operation, when boundary friction effects become increasingly more important, fuel economy benefits resulting from a lower kinematic viscosity are significantly reduced. There can even be a reversal in fuel economy effects, i.e. in hot running engines, under cyclic operation (highway cycle), a lower viscosity oil can give poorer fuel economy than an oil with higher viscosity [**3.75**].

Studies performed in the 1980s suggested that engine friction and fuel economy correlated better with oil viscosity measured at higher shear rates ($10^6 s^{-1}$) than with the low-shear kinematic viscosity [**3.78**]. In 1980, Dancy et al. [**3.79**] measured engine motoring torque in order to determine friction variations due to both oil viscosity and additive differences. Only by using high shear rate viscosity as a reference could they place the studied oils on an equal viscosity basis. Cassiani et al. [**3.80**] also used high shear viscosity to correlate power loss measurements in fired and motored engines for a series of 7 oils. In 1981, Galluccio and Koller [**3.81**] showed that the relative fuel efficiency of multigrade engine oils correlated well with their high temperature (100°C), high shear rate (10^6 s^{-1}) viscosities. Dobson [**3.82**] also found similar results, but he referred them only to "some-engined" cars run under certain driving modes. Much of the work carried out to relate fuel efficiency to engine oil viscosity has proved that some engines (cars) and driving conditions are more responsive to engine oil viscosity than others, which makes it difficult to find a specific measure of oil rheology able to correlate with all aspects of engine operation [**3.78**].

By the mid 1980s it was clear that high temperature, high shear rate (HTHS) viscosity was an important parameter in terms of fuel consumption [**3.83**]. Therefore many suggestions were made for HTHS to be standardised and as a result, the SAE J Engine Oil Viscosity Classification was changed in March 1993 [**3.68**]. The HTHS viscosity was standardised at 150°C and 10^6 s^{-1} shear rate, at a value of 2.6 mPa s, but the task for the future is to introduce advanced low viscosity oils with HTHS viscosity of 2.4-2.6 mPa s such as SAE 0W-20 or SAE 5W-20, on the market [**3.84**]. This may be possible by using extra high viscosity index (125-150) base oils [**3.84**] and also synthetic or partially synthetic base oils with lower volatility [**3.72**] in order to obtain both low viscosity and also low oil volatility (and thus low emissions).

3.3.1.2. Influence of boundary friction

The second key approach to reducing fuel consumption through engine oil formulation is related to surface chemistry. Friction modifiers help maintain a certain degree of lubrication and of low friction even in critical situations when engine components operate under boundary lubrication regime and oil viscosity alone is no longer capable to keep surfaces apart by hydrodynamic effect. Friction reduction engine technology developed in 1970s was directed towards reducing rubbing losses via new oil chemistry [**3.78**]. Measurements of average fuel economy improvement have shown the benefit that can be obtained by using formulated oils with added friction modifiers [**3.71, 3.76, 3.85**]. For example, Broman [**3.76**] showed that SAE 10W-40 oil containing colloidal graphite produced an average of 5.1% improvement in fuel economy under cycling conditions and 3% under steady state conditions when compared against a conventional SAE 10W-40 motor oil. The influence of molybdenum disulphide to both the rear axle and engine lubricant performance was studied by Haviland and Goodwin [**3.86**] who showed that fuel economy improvements provided by the additive averaged 1.2% in road tests and 4.6% in Environmental Protection Agency City/ Highway (EPA 55/45) fuel economy test. The superiority of friction modified oils over non-friction modified ones in fuel economy performances was also stated by Roberts et al. [**3.87**] with the mention that the results were very dependent on test mode and conditions and varied considerably from vehicle-to-vehicle, even within models. Another friction modifier, an organic molybdenum compound, was tested by Hamaguchi et al. [**3.72**] and an

improvement in fuel efficiency up to 5% was reported. More recently [3.88], studies on friction reduction capabilities of a MoDTC/ZnDTP additive combinaton used in the formulation of advanced low friction/low viscosity engine oils, have shown the importance of interactions of additives between themselves and with base oil during the aging process.

3.3.1.3. Other relevant lubricant properties

Besides HTHS viscosity and boundary friction, the elastohyroydnamic properties of engine oils are also relevant to fuel economy. The pressure-viscosity coefficient and EHD traction coefficient tend to be overlooked because of the scarcity of relevant data [3.89]. However, evidence suggests that about 0.5% fuel economy improvement is obtained in the ASTM Sequence VI engine test when pressure-viscosity properties are improved by changing from a solvent refined base stock to a hydrocracked oil [3.89].

It has also been shown using traction tests performed with Sequence VI oils that lubricants with a higher rate of increase of traction coefficient with decreasing speed also show poorer fuel efficiency (see chapter 5, section 5.1.3).

3.3.2. Engine tests for fuel efficiency

The influence of the engine lubricant upon fuel economy is generally evaluated by engine tests. In order to find the improvement in fuel consumption achieved by advances in engine oil formulation, lubricant and additive companies have developed a series of engine tests in which lubricants are tested in an engine under a complex combination of conditions representative of an engine in use. These tests can be divided in two main types: in-house (bench) tests and road tests. The first category includes engine dynamometer and chassis-dynamometer tests [3.72]. Chassis dynamometer tests are usually performed at constant speed and fuel economy is measured at that particular speed (e.g. 60 and 80 km/h) [3.72]. Another type of vehicle chassis-dynamometer test is the EPA Metro/Highway Cycle test where the real driving conditions are better simulated. In Japan an equivalent test is 10-Mode Cycle test [3.72]. ASTM Sequence VIA is already the third fuel efficiency test introduced in the US since 1979 after the 5 Car and Sequence VI tests. In Europe, the first such test M111, recently developed by

CEC (Co-ordinating European Council) for ACEA (Association of European Car Constructors, in French) is being introduced at the present time [3.91].

Road tests are fleet-type tests where a number of cars are run under similar conditions and the fuel economy is compared using both test engine oils and reference oils. Examples of such tests are ASTM 5 Car (which uses a five car fleet), Highway Fleet Test, Racing Circuit Fleet Test (with seven car fleet), etc. [3.72].

One problem with these tests is that they give quite a lot of scatter because the results are dependent on many variables. The following table is showing some of the factors influencing road fuel economy road tests [from 3.87].

Ambient conditions	Temperature, barometric pressure, humidity, wind, precipitation
Driving conditions	Traffic-acceleration/ deceleration/ stop, visibility, terrain
Vehicle configuration	Gross weight, tyres type and pressure, windows, lights, other ancillaries
Engine condition	Age, servicing - ignition timing and plugs
Engine operation conditions	Speed and load, temperatures - oil/ water/ air
Other variables	Fuel and fuel measurement method, driver, motor oil and motor oil carry over effect.

Table 3.2. Variables affecting road fuel economy tests

In consequence, in order to obtain reliable results, it is necessary to run the tests several times and one measurement represents the average of sometimes, more than 20 tests [3.92]. As a result, accurate measurements of lubricant related engine fuel efficiency are difficult, time consuming and very expensive.

As part of the work performed in this study is related to ASTM Sequence VI and VI A engine tests, a few more details about these will be given in the next paragraphs.

3.3.2.1. ASTM Sequence VI test

ASTM Sequence VI determines the mean fuel saving (the average "Equivalent Fuel Economy Improvement" or EFEI) of an engine crankcase oil over that of a 20W30 reference oil. The method involves comparing fuel consumption using the test oil in a

1982 Buick 3.8 litre V6 engine operating at both 65°C and 135°C oil temperature with that of reference oils. The measurements at the two temperatures are then combined to produce a mean EFEI value. The reference oils are as follows [3.92]:

Reference oils	FEEO 100 (HR) (high viscosity reference oil)	FEEO 201 (FO) (detergent flush oil)	FEEO 103 (FM) (friction modified high reference oil)	FEEO 102 (LR) (low viscosity reference oil)
SAE grade	20W-30	20W-30	20W-30	50

Table 3.3. Reference oils for Sequence VI test

The test conditions are given below [3.93]:

Stages	1	2
Test duration, hr	65	20
Engine speed, rpm	1500	1500
Load, kW (BHP)	5.96 (8)	5.96 (8)
Fuel type	Amoco Indolene Clear (unleaded)	Amoco Indolene Clear (unleaded)
Air-to-fuel ratio	14.1	14.1
Oil temperature, °F	150	275
Coolant temperature,°F	130	230

Table 3.4. Test parameters for Sequence VI

The fuel consumption is measured gravimetrically and the parameter for evaluation of fuel economy is % EFEI. The expression used to determine EFEI is as follows:

$$\%EFEI = \frac{0.66 * R150 + 0.34 * R275 - 0.34 * FMR + 2.76}{1.45} \times 100 \qquad (E3.1)$$

where R150, R275 and FMR are determined by:

$$R150 = \frac{HR150avg - Cand150avg}{HR150avg} \qquad (E3.2)$$

$$R275 = \frac{HR150avg - Cand275avg}{HR150avg} \qquad (E3.3)$$

$$FMR = \frac{HR150 - FM275}{HR150} \qquad (E3.4)$$

Each of the parameters on the right hand side of equations E3.2 to E3.4 are engine fuel consumption measured from tests using the lubricants and conditions shown below:

Cand= candidate oil
HR= calibration oil
FM= calibration oil

R150 = fuel efficiency at 65°C (150°F)
R275 = fuel efficiency at 135°C 275°F)

The overall sequence VI test thus involves testing the fuel consumption of the engine using two calibration oils (HR and FM), one at 150°F and one at 275°F oil temperature and the fuel consumption of the candidate test oil at both of these temperatures. As equation E3.1 shows, the EFEI weights fuel saving performance towards that of the lower temperature stage.

The following schematic, courtesy of Exxon Chemical Ltd, shows the overall Sequence VI test procedure.

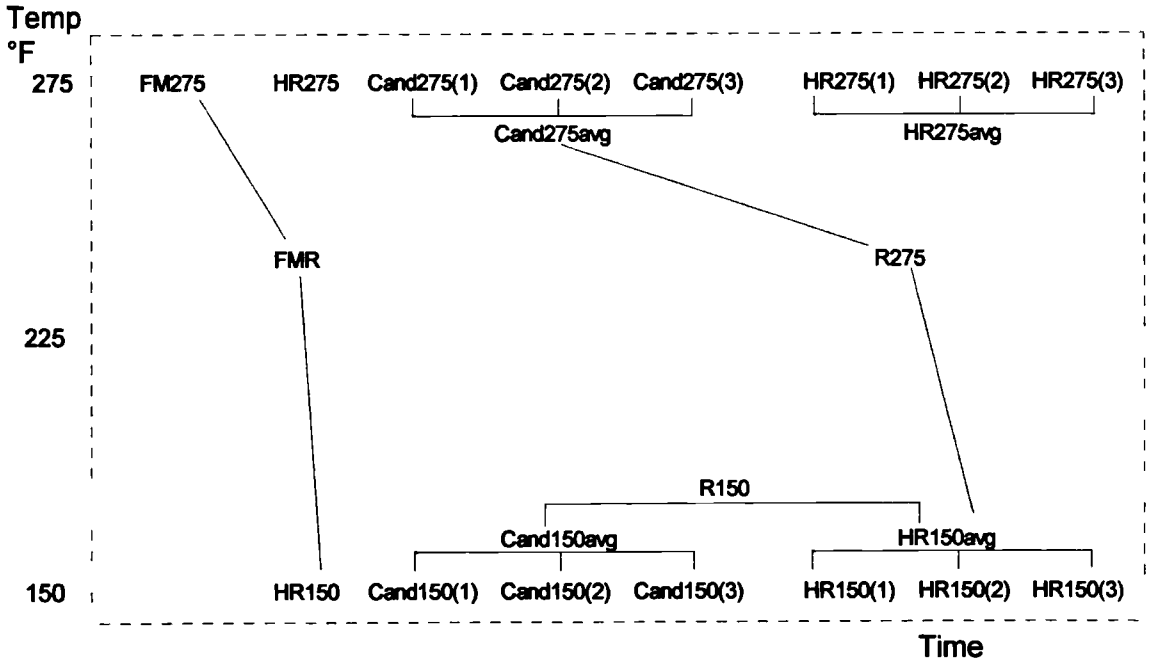


Fig.3.5. Sequence VI fuel economy test method

3.3.2.2. ASTM Sequence VIA test

Claims that Sequence VI test conditions were not representative of the performance of modern engines and low viscosity oils led to the development of the new Sequence VIA test [**3.94**] which was introduced in 1997. The procedure measures the effects of engine oil on fuel economy of gasoline cars and light duty (8500 lb. gross vehicle weight or less) trucks equipped with a "low friction" engine, 4.6L 8V Ford "Modular" [**3.92**] using a roller-type valve. The reference oil is SAE 5W-30 and fuel consumption is again measured gravimetrically. This is a dynamometer engine test and consists of 6 stages in which temperature, speed and load conditions are varied in order to cover most possible situations typically encountered in a running engine. The parameters for all the stages are given below [**3.92**]:

Stages	1	2	3	4	5	6
Test duration, hr	40-51	40-51	40-51	40-51	40-51	40-51
Load, Nm	26	26	37	98	98	26
Power, kW	2.18	2.18	5.81	15.4	15.4	2.18
Speed, rpm	800	800	1500	1500	1500	800
Oil temperature, °C	105	70	70	70	45	45
Cooling temperature, °C	95	60	60	60	45	45

Table 3.5. Test parameters for Sequence VI A test

Thus stage 1 is representative of mixed and boundary lubrication whereas stage 4 for example, of hydrodynamic lubrication conditions.

The overall fuel efficiency in Sequence VIA is calculated from results of all six stages, taking into account weighting factors for individual stages. The calculation of %FEI follows the pattern below:

Test stage	Actual (kg/kW hr)		Nominal power (kW)		Time factor (hours)		Fuel consumed (kg)
1	BSFC	×	2.18	×	0.077472	=	
2	BSFC	×	2.18	×	0.082500	=	
3	BSFC	×	5.81	×	0.035417	=	
4	BSFC	×	15.39	×	0.078250	=	
5	BSFC	×	15.39	×	0.033139	=	
6	BSFC	×	2.18	×	0.045444	=	
Total mass fuel consumption for all 6 stages						=	
Instead of original stage 7 which has been deleted						add	0.2540 kg

The average brake specific fuel consumption (BSFC) is multiplied by the shown nominal power and time factor and the result is recorded as fuel consumed up to six decimal places. This provides fuel consumption factors for equivalent power consumption as in the EPA Metro/Highway fuel economy test. The amount of 0.2540 kg is added to the sum of fuel consumption from all 6 stages. This is a constant for a test stage which is not run, but which gives an appropriate magnitude to the fuel economy improvement result. The above calculations are made for the reference oil BC immediately preceding the candidate, for the candidate oil and the reference oil BC immediately after the candidate. Then the average BC fuel consumption $BC_{average}$ is calculated with $BC_{preceding}$ and BC_{after}. Finally, the candidate oil fuel economy improvement (%FEI) is computed as follows:

$$\%FEI = \frac{BC_{average} - Candidate}{BC_{average}} \times 100 \qquad (E3.5)$$

Engine friction modelling shows that further improvements in fuel efficiency of engine oils are possible. These improvements are now being considered in the development of the next generation fuel economy test, Sequence VIB, and the future ILSAC engine oil category GF-3, both to be introduced in the years 2000-2001 [**3.91**]. The new test will incorporate oil aging conditions equivalent to 4,000-6,000 miles which would better reflect customer operation.

As mentioned previously, engine tests are extremely expensive to run and also give considerable scatter. Because of this, lubricant and additive companies have considerable interest in developing simple and cheap bench tests which are able to predict lubricant-related friction losses in a typical internal combustion engine.

3.4. Engine fuel efficiency prediction

3.4.1. Strategy of approach

Any means of predicting the influence of a lubricant on the overall engine friction and thus fuel economy must take account of the behaviour of the lubricant in each of the

lubrication regime experienced by the engine moving parts. Thus prediction of engine fuel efficiency using bench tests requires :

(i) bench tests able to simulate all the lubrication regimes in an engine (hydrodynamic, EHD and boundary) under realistic conditions and produce measures of friction in each

(ii) some method of relating the results of these bench tests to engine efficiency.

These are, broadly, three possible ways of relating bench tests to engine efficiency test performance.

The first is simply to use general tribological common-sense and in particular, the principle that the lower the friction in all lubrication regimes, the better. However, this approach is unable to yield any quantitative predictions; nor can it cope with the problem that low friction in one regime may result in high friction in another; thus requiring quantitative compromises to be reached. Thus a decrease in viscosity might well reduce friction in hydrodynamic bearings, but increase friction in cams by resulting in a higher proportion of boundary lubrication.

The second approach, which has been used in this study, is parametric regression analysis which implies that the relationship between engine fuel efficiency and the parameters chosen to characterise lubricant behaviour is described satisfactorily by a simple linear expression of the form:

$$F = a_0 - a_1 * X_1 - a_2 * X_2 - a_3 * X_3 \qquad \text{(E3.6)}$$

where F is the fuel economy performance of the lubricant, X_1 is a bench test measure of hydrodynamic friction, X_2 is a bench test measure of EHD friction, X_3 is a bench test measure of boundary friction and a_0, a_1, a_2, a_3 are constants. The three friction-related terms are negative because high friction implies low fuel economy and thus a low value of F.

The main limitation of the regression approach is that it can only be practically used to correlate fuel efficiency with two or three measured bench test parameters. This is because the number of lubricants needed in the data set rises very rapidly with the number of parameters to be fitted. However, in practice, the lubricant data set, i.e. the number of oils for which EFEI data is available, is always very limited simply because of the high cost of the engine tests. In reality, however, the engine "sees" and responds to a much larger range of lubricant properties than just three values; including the whole function of hydrodynamic friction, EHD traction and boundary friction with temperature.

To allow for this, the most sophisticated approach to the problem of relating bench test measurements to engine results is to computationally model each component in the engine; the valve train, pistons and bearings, in such a manner that frictional and other performance data can be used to quantify the likely overall friction in each engine component over one engine cycle. This approach can take account of the variation of factors such as viscosity and friction with temperature and shear rate and the individual component values can than be combined and correlated with overall engine efficiency. Some of this type of modelling work was described briefly in the section 3.2.1. of this chapter.

The problem with this approach is that it is considerably more complex than other methods and also may be critically dependent upon the modelling assumptions made. It is also difficult, in practice, to measure lubricant properties over a wide range of temperatures and shear rates and to adequately take account of factors such as oil-ageing. Also it should be noted that some aspects of tribology, such as friction in mixed lubrication is not yet well enough understood for reliable models to be produced.

3.4.2. Previous regression work

As engine fuel efficiency tests were only relatively recently introduced, few authors have published work on engine fuel efficiency prediction. The linear regression technique was first used by Benchaita and Lockwood [3.9] who developed a first order linear model able to predict the lubricant fuel economy performance measured by two industry tests, ASTM Five Car and Sequence VI. Their model was based on three measured lubricant

bench test properties at 100°C, high shear rate dynamic viscosity (HTHS), EHD film thickness at 1 m/s and boundary friction coefficient μ. Equation E3.7 shows one of the equations produced.

$$\%FE = 9.52 - 0.48*(HTHS) - 29*(EHDfilm) - 15.9*(\mu) \qquad (E3.7)$$

Benchaita and Lockwood obtained very good correlation with engine test data using a set of eight reference oils, the correlation coefficient squared R^2 lying between 0.705 and 0.99 depending on the number of data used. Their model suggested that 5 to 6% fuel economy improvement (over the industry high reference oil HR-4, 20W-40 SAE grade) could be attained in principle. It also showed that HD friction losses contribute the most to the lubricant-related engine friction (ca. 41%), followed by boundary friction losses (ca. 37%) and EHD friction losses (ca. 22%) [**3.9**]. The authors concluded that fuel economy improvement is increased by using low viscosity oils; an observation which is confirmed by the general trend towards lower viscosity grades.

A similar approach has been used by Moore [**3.95**] who tried to correlate fuel efficiency with boundary friction properties. He measured boundary friction using two laboratory test techniques i.e. pin-on-disc and reciprocating rig. Both yield data which showed promising correlation with fuel savings measured in engine tests, especially with Sequence VI test .The optimum correlation with Sequence VI was achieved when screening test temperatures were in the range 100°C-120°C; the correlation became weaker as temperature was increased [**3.95**]. Under the most appropriate test conditions, the regression equation produced was as follows:

$$\%FE = 13.37 - 0.742*(HTHS) - 62.5(\mu) \qquad (E3.8)$$

Moore also mentioned the posibilility that pressure-viscosity effects could be significant on the basis that recent estimates for the valve train losses in modern types of engine might range from 12% to 34%. He concluded that an additional term might be needed in the correlation to take into account the variation of viscosity with pressure.

If the average values for each lubricant parameter are calculated and used in equations E3.7 and E3.8, an estimate of boundary and hydrodynamic friction can be made. For HTHS viscosity a mean value (at 150°C and 10^6 s^{-1}) would be around 3.5 cP and for the friction coefficient μ, about 0.1. Multiplying these values by their coefficients, the values for HTHS term and μ term in Benchaita & Lockwood equation would give 1.7 and 1.6 respectively and in Moore's equation, 2.6 and 6.25. Thus we can estimate that the model developed by Benchaita and Lockwood shows similar proportions of boundary and hydrodynamic friction (50:50) whereas in Moore's model the amount of boundary friction is much higher, the proportion being about 30:70. Certainly the results are strongly dependent on the oils tested.

Although Benchaita and Lockwood obtained a very good correlation their work had a number of important limitations.

One is that the model used bench test data at 100°C. However EHD film thickness could be measured only at temperatures temperatures up to 75°C and values for 100°C were obtained by extrapolation.

A second limitation was that both EHD film thickness and HTHS viscosity were used in the correlation. However EHD film thickness is itself highly dependent upon viscosity **[3.96]**. Thus the variables employed were not fully independent. The authors justified their choice of EHD film thickness on the basis that as well as depending upon viscosity, this value depends upon lubricant pressure-viscosity coefficient or α-value. The higher the α-value, the thicker the EHD film. They suggested that friction or traction coefficient in EHD correlates with α-value, so that their EHD film thickness was, ultimately, a method of comparing EHD friction properties of lubricant. However, this reasoning contains an inherent contradiction in that, whilst a low friction oil should be one with low EHD traction coefficient it should be one with high pressure-viscosity coefficient so as to maximise EHD film formation.

A third important limitation of Benchaita and Lockwood study was that subsequent, independent measurement of the rheologic properties of the reference oils used, made during the current programme, indicated that the authors accidentally interchanged the

data between two of the tested oils (R516 and R517 in table 5.1 from chapter 5). This gave a very good correlation coefficient $R^2 = 0.963$ (with 8 reference oils) which was largely fortuitous. If the regression is repeated with the corrected data, a coefficient of 0.560 is obtained.

Although the work carried out by Benchaita and Lockwood has the above mentioned limitations, it was used in the current study as a starting point in engine fuel economy prediction. After analysing this previous work results and determining its limitations, an attempt was made to develop a correlation between EFEI and bench test measurements which can provide useful results for fuel efficiency calculations.

REFERENCES

[3.1] Dowson D., Taylor C. M., Zhu G., "An Experimental Study of the Tribology of a Cam and Flat Faced Follower", Paper C375/025, IMechE, 1989,

[3.2] Heywood J.B., "Internal Combustion Engine Fundamentals", McGraw-Hill International Editors, 1988,

[3.3] Lansdown A.R., "High Temperature Lubrication", Mechanical Engineering Publications, 1994,

[3.4] Milton B.E., "Thermodynamics, Combustion and Engines", Chapman and Hall, first edition, 1995,

[3.5] Parker D. A., Adams D. R., "Friction Losses in the Reciprocating Internal Combustion Engine", Paper C5/82, IMechE, 1982, pp. 31-39,

[3.6] Martin F. A., "Friction in Internal Combustion Engines - Reduction of Friction and Wear", Paper C67/85, IMechE International Tribology Conference, London, 1985,

[3.7] Hoshi M., "Reducing Friction Losses in Automobile Engines", Tribology International, vol. 17, 4, pp. 185-189, 1984,

[3.8] Andersson B.S., "Company Perspective in Vehicle Tribology - Volvo", Vehicle Tribology / D.Dowson et al. (editors), Elsevier Publ., 1991,

[3.9] Benchaita M. T.& Lockwood F. E., "Reliable Model of Lubricant-Related Friction in Internal Combustion Engines", Lubrication Science 5-4, July 1993, pp. 259-281,

[3.10] Goenka P. K., "Role of Tribology in Vehicle Design-General Motors Perspective", Vehicle Tribology/ D.Dowson et al.(editors), Elsevier Publ., 1991,

[3.11] Lang O. R. and Kernen R., "Reibungsverluste in Verbrennungsmotoren" (Friction Losses in Combustion Engines), Schmiertechnik u Tribologie, 3/1982,

[3.12] Goenka P.K., Paranjpe R.S. and Jeng Y.R., "FLARE: an Integrated Software Package for Friction and Lubrication Analysis of Automotive Engines, Part 1-Overview and Applications", SAE paper 920487, 1992,

[3.13] Li C. H., "Piston Thermal Deformation and Friction Considerations", SAE Paper 820086, 1982,

[3.14] Cleveland A. E. and Bishop I. N., "Several Possible Paths to Improved Part-Load Economy of Part-Ignition Engines", SAE Paper 150A, 1960,

[3.15] Masahido Nakada, "Trends in Engine Technology and Tribology", Tribology International, vol. 27, number 1, pp. 3-8, 1994,

[3.16] Ricardo H. and Hempson J.G.G., "The High Speed Internal Combustion Engine", Blackie, London, Fifth edition, 1968,

[3.17] Ball W.F., Jackson N.S., Pilley A.D. and Porter B.C., "The Friction of a 1.6 litre Automotive Engine - Gasoline and Diesel", SAE paper 860418, 1986,

[3.18] Bates T.W. and Vickars M.A., "Measurement of Oil Film Thickness in Big-End Bearings and its Relevance to Engine Oil Classifications", Lub. Sci. 3, pp. 233-256, 1991,

[3.19] Holt J.W.and Heisell O., "Design and Development of a Two Ring Piston Assembly", paper 29, AE Group Symposium, 1986,

[3.20] Taylor C.M., "Fluid Film Lubrication in Automobile Valve Trains", Proc. IMechE , vol. 208, 1994,

[3.21] Furuhama S., Kojima M., Enomoto Y. and Yamaguchi Y., "Some Studies on Two Ring Pistons in Automobile Turbocharged Gasolene Engine", SAE paper 870183, 1987,

[3.22] Parker D.A., "Tribology of Automotive Components", IMechE Proc., Part D: Transport Engineering , vol. 204, No.1, pp. 1-19, 1990,

[3.23] Taylor C.F., "The Internal Combustion Engine in Theory and Practice", vol. 1, MIT Press, 1966,

[3.24] Thring R.H., "Piston Skirt Friction in Internal Combustion Engines", IMechE C375/002, 1989,

[3.25] Furuhama S. and Sasaki S., "Effect of Oil Properties on Piston Frictional Force", JSAE Review, Nov. 1984,

[3.26] Takiguchi M., Machida K. and Furuhama S., "Piston Friction Force of a Small High Speed Gasolene Engine", Trans. ASME, vol. 110, pp 112-118, 1988,

[3.27] Thring R.H., "Piston Ring Friction in Internal Combustion Engines", ASME 87-ICE-20,

[3.28] Parker D.A., Adams D.R. and Donnison G., "The Measurement and Reduction of Piston Assembly Friction ", 2nd International Conference

on Combustion Engines - Reduction of Friction and Wear, London, 1989,

[3.29] Dowson D., Ruddy B.L. and Economou P.N., "The EHD Lubrication of Piston Rings", Proc. Royal Soc. London , A 386, pp 409-430, 1983,

[3.30] Furuhama S. and Sumi T., "A Dynamic Theory of Piston Lubrication (3rd report, Measurement of Oil Film Thickness)", Bulletin of the JSME, vol. 4, No 16, pp. 744-752, 1961,

[3.31] Hamilton G.M. and Moore S.L., "The Behaviour of Piston Rings, Measurement of the Oil Film Thickness between the Piston Rings and Liner of a Small Diesel Engine" - first paper, Proc. IMechE, vol. 188, no. 20, pp. 253-261, 1974,

[3.32] Neale M.J. and Eyre T.S., "Piston Ring and Cylinder Liner Problems", IMechE, C7/82, pp. 55-63, 1982,

[3.33] Smart A.E. and Ford R.A.J., "Measurement of Thin Liquid Films by a Fluorescence Technique", Wear 29, p. 41, 1974,

[3.34] Ford R.A.J., "Laser Based Fluorescence Technique for Measuring Thin Films", Wear 51, p. 289, 1979,

[3.35] Ting L.L., "Development of a Laser Fluorescence Technique for Measuring Piston Ring Oil Film Thickness", Journal of Lubrication Technology, 102, p. 165, 1980,

[3.36] Richardson D.E. and Borman G.L., "Using Fibre Optics and Laser Fluorescence for Measuring Thin Oil Films with Application to Engines", SAE paper 912388, 1991,

[3.37] Castelman R.A., "A Hydrodynamic Theory of Piston Ring Lubrication", Physics, vol. 7, pp. 364-367, 1936,

[3.38] Eilon S. and Saunders O.A., "A Study of Piston Ring Lubrication", Proc. IMechE, vol. 171, no. 11, pp. 427-433, 1957,

[3.39] Furuhama S., "A Dynamic Theory of Piston Lubrication (first report, Calculation)", Bulletin of the JSME, vol. 2, no 7, pp. 423-428, 1959,

[3.40] Dowson D., Economou P.N., Ruddy B.L. et al., "Piston Ring Lubrication Part 2. Theoretical Analysis of a Single Ring and a Complete Ring Pack" in "Energy Conservation through Fluid Film Lubrication Technology: Frontiers in Research and Design", ASME, pp. 53-52, 1979,

[3.41] Rhode S.M., "A Mixed Friction Model for Dynamically Loaded Contacts with Application to Piston Ring Lubrication", Friction and Traction, Proc. of the 7th Leeds-Lyon Symposium on Tribology, editors D. Dowson, C.M. Taylor, M. Godet and D. Berthe, pp. 262-278, Westbury House ,1980,

[3.42] Richez M.F., Constanz B. and Winquist K., "Theoretical and Experimental Study of Ring Liner Friction", Tribology of Reciprocating Engines, Proc. of the 9th Leeds-Lyon Symposium on Tribology, editors D. Dowson, C.M. Taylor, M. Godet and D. Berthe, pp. 122-131, Butterworths, 1982,

[3.43] Patir N. and Cheng H.S., "An Average Flow Model for Determining Effects of Three Dimensional Roughness on Partial Hydrodynamic Lubrication", Trans. ASME, Journal of Lubrication Technology, vol. 100, pp. 12-17, 1978,

[3.44] Greenwood J.A. and Tripp J.H., "The Contact of Two Nominally Flat Surfaces", Proc. IMechE, vol. 185, no. 48, pp. 625-633, 1971,

[3.45] Hwu C.J. and Weng C.I., "EHD Lubrication of Piston Rings", Wear, vol. 151, pp. 203-215, 1991,

[3.46] Hoult D. P., Wong V.W. and Azzola G.H., "Direct Observation of the Friction Reducing of Multigrade Lubricants", SAE paper 910742, 1991,

[3.47] Keribar R., Dursunkaya L. and Flemming M.F., "An Integrated Model of Ring Pack Performance", ASME Trans., Journal of Engineering for Gas Turbines and Power, vol. 113, pp. 382-389, 1991,

[3.48] Craig R.C., King W.H. and Appeldoorn J.K., "Oil Film Thickness in Engine Bearings - The Bearing as a Capacitor", SAE Paper 821250, 1982,

[3.49] Pratt G.C. and Whitney W.J., "Progress with Aluminium-Lead Crankshaft Bearing Alloys", SAE Paper 890552, 1989,

[3.50] Bates T.W., Fantino B., Frene J. and Launay L., "Oil Film Thickness in an Elastic Connecting Rod Bearing - Comparison between Theory and Experiment", paper presented at the 1989 STLE Annual Meeting, Atlanta, Georgia, May 1-4, 1989,

[3.51] Torii H. et al., "EHD Lubrication of a Connecting Rod Journal Bearing in Consideration of Shapes of the Bearings", SAE Paper 920485, 1992,

[3.52] Gecim B.A., "Non Newtonian Effects of Multigrade Oils on Journal Bearing Performance", STLE, Trib. Trans. 33, 3, pp. 384-394, 1990,

[3.53] Han T. and Paranjpe R.S., "A Finite Volume Analysis of the Thermohydrodynamic Performance of Finite Journal Bearings", ASME Journal of Tribology, vol. 112, pp. 557-566, July 1990,

[3.54] Meernik P.R., "Lubricant Flow to Connecting Rod Bearings through a Rotating Crankshaft", SAE Paper 860229, 1986,

[3.55] Müller R., "the effect of Lubrication on Cam and Tappet Performance", Motortechnische Z., 27, 58, 1966,

[3.56] Dyson A., "EHD Lubrication and Ewar of Cam Bearing against Cylindrical Tappets", SAE Paper 770018, 1977,

[3.57] Vichard J.P. and Godet M., "Simultaneous Measurement of Load, Friction and Film Thickness in a Cam and Tappet System", Proc. IMechE, vol. 182, Pt. 3G, pp. 109-113, 1967-68,

[3.58] Dowson D., Harrison P. and Taylor C.M., "The Lubrication of Automotive Cams and Followers", 12th Leeds-Lyon Symposium on Tribology-Mechanisms and Surface Distress, pp. 305-322, Butterworths (Oxford), 1986,

[3.59] Bedewi M.A., Dowson D. and Taylor C.M., "EHD Lubrication of Line Contacts Subjected to Time Depending Loading with Particular Reference to Roller Bearings and Cams and Followers", 12th Leeds-Lyon Symposium on Tribology-Mechanisms and Surface Distress, pp. 189-304, Butterworths (Oxford), 1986,

[3.60] Ball A., Dowson D., Taylor C.M., "Cam and Follower Design", 15th Leeds-Lyon Symposium on Tribology-Tribological Design of Machine Elements, Trib. Series 14, pp. 111-130, Elsevier, 1989,

[3.61] Williamson B.P., Galliard I.R. and Benwell S., "Measurement of Oil Film Thickness between a Cam and a Bucket Follower in a Motored Cylinder Head. Part 1: Newtonian Oils. ", International Fuels and Lubricants Meeting and Exposition, Baltimore, Maryland, Sept. 1989, SAE 892150,

[3.62] Harrison P., "A Study of the Lubrication of Automotive Cams", PhD Thesis, Univ. of Leeds, 1985,

[3.63] Dowson D., Harrison P., Taylor C.M. and Zhu G., "Experimental Observations of Lubricant Film State between a Cam and Bucket Follower Using the Electrical Resistivity Technique", Proceedings of International Tribology Conference, Nagoya, Japan, vol. 1, pp. 119-124, 1990,

[3.64] Zhu G., " A Theoretical and Experimental Study of the Tribology of a Cam and Follower", PhD Thesis, Univ. of Leeds, 1988,

[3.65] Dowson D., Taylor C.M. and Zhu G., "A Transient EHD Lubrication of a Cam and Follower", J. Phys. D, Appl. Phys., 25 (1A), A313-A320, 1992,

[3.66] Colgan T., Bell J.C., "Modelling Valve Train Wear for Cycling Conditions", Proceedings of International Tribology Conference, Nagoya, Japan, vol. 2, pp. 1231-1235, 1990,

[3.67] Naitoh Y., "Gasolene Engine Oils", J. Journal of Trib. 38, no. 2, 1993,

[3.68] Hisamoto Aihara , "Gasolene Engine Oil for Better Air Quality and Fuel Economy", J. Journal of Trib., vol. 39, no. 10, pp.1145-1152, 1994,

[3.69] Georgi C.W., "Some Effects of Motor Oils and Additives on Engine Fuel Consumption", SAE paper no. 238, 1954,

[3.70] Orrin O.S. and Coles B.W., "Effects of Engine Oil Composition on Oil Consumption", SAE paper 710141, 1971,

[3.71] Chamberlin W.B. and SheahnanT.J., "Automotive Fuel Savings through Selected Lubricants", SAE paper 750377, SAE Meeting, Detroit, Feb. 24-28, 1975,

[3.72] Hamaguchi H., Maeda Y. and Maeda T., "Fuel Efficient Motor Oils for Japanese Passenger Cars", SAE paper 810316, 1981,

[3.73] Bell J.C. and Vosiey M.A., "Some Relationship between the Viscometric Properties of Motor Oil and Performance in European Engines ", SAE paper 770378, 1977,

[3.74] Passut C.A. and Kollman R.E., "Laboratory Techniques for Evaluation of Engine Oil Effects on Fuel Economy", SAE paper 780601, 1978,

[3.75] Goodwin M.C. and Haviland M.L., "Fuel Economy Improvements in EPA and Road Tests and Engine Oil and Rear Axle Lubricant Viscosity Reduction", SAE paper 780596, 1978,

[3.76] Broman V.E., DeJovine J, DeVries D.L. and Keller G.H., "Testing of Friction Modified Crankcase Oils for Improved Fuel Economy", SAE paper 780597, 1978,

[3.77] Ghirla P. J. and Smith R.K., "Automotive Engine Friction and Fuel Efficiency-Viscous versus Non-Viscous Effects", SAE paper 780984, 1978,

[3.78] "The Relationship between High-Temperature Oil Rheology and Engine Operation "-a status report prepared by ASTM Task Force D02.07.0B TF/EC, Dec 1984,

[3.79] Dancy J.H., Marshall H.T. and Oliver R.C., "Determining Frictional Characteristics of Engine Oils by Engine Friction and Viscosity Measurements", SAE paper 800364, 1980,

[3.80] Cassiani-Ingoni A., Dilelio G.F., VanOs N. and Vickars M., "European Activity Concerning Oil Viscosity Classification-Part 2", SAE paper 800546, 1980,

[3.81] Galluccio R.A.and Koller R.D., "The Relationship between Engine Multigrade Oil Characteristics and Fuel Consumption in Engine-Dynamometer Tests", SAE paper 811188, 1981,

[3.82] Dobson G.R., "Analysis of High-Shear Rate Viscosity Data for Engine Oils", Tribology International, 14, pp. 195-198, 1981,

[3.83] Clevenger J.E., Carlson D.C. and Kleiser W.M., "The Effects of Engine Oil Viscosity and Composition on Fuel Efficiency", SAE paper 841389, Fuels and Lubricants Meeting and Exposition, Baltimore, Maryland, Oct. 8-11, 1984,

[3.84] Korcek S., "Engine Oils 2000", J. Journal of Tribology, vol. 38, no.3, 1993,

[3.85] Bennington J.E., Cole D.E., Ghirla P.J. and Smith R.K., "Stable Colloid Additives for Engine Oils -Potential Improvement in Fuel Economy", SAE paper 750677, 1975,

[3.86] Haviland M.L. and Goodwin M.C., "Fuel Economy Improvements with Friction Modified Engine Oils in Environmental Protection Agency and Road Tests", SAE paper 790945, 1979,

[3.87] Roberts D.C., Gaskill G.P. and Richard G.P., "The Influence of Motor Oil Viscosity and Friction Modification on Automotive Fuel Economy", IMechE C6/82, 1982,

[3.88] Johnson M.D., Clausing E.M., Jensen R. K. Schriewer K. and Korcek S., "Effects on Aging on Frictional Properties of Fuel Efficient Engine Oils", SAE paper 952532, 1995,

[3.89] Moore A.J., "The Behaviour of Lubricants in EHD Contacts", IMechE Proc., J. of Tribology, vol. 211, No. 2, pp. 91-106, 1997,

[3.90] Igarashi J, Kagaya M, Satoh T and Nagashima T, "High Viscosity Index Petroleum Base Stocks-the High Potential Base Stocks for Fuel Economy Automotive Lubricants", SAE paper 920659, 1992,

[3.91] Korcek S., "Engine Oil Fuel Efficiency-Practical Issues", submitted for publication in the Proceedings of 24th Leeds-Lyon Symp.on Trib., London, Sept. 1997. "Tribology for Energy Conservation", ed. Dowson D. et al., Elsevier Science,

[3.92] ASTM Sequence VI and VI A conditions and calculations, courtesy of Exxon Chemical Co., Paramins Technology Division

[3.93] Reference for Lubricant and Fuel Performance , courtesy of Lubrizol Co.

[3.94] Murakawa H. and Ohira H., "Automotive Engine Oil Quality . Overview: Japan, USA and Europe", J. Journal of Tribology , vol. 38, no. 3, 1993,

[3.95] Moore A.J., Fuel Efficiency Screening Tests for Automotive Engine Oils", SAE paper, 932689, 1993,

[3.96] Dowson D. and Hamrock B. J., "Elastohydrodynamic Lubrication, the Fundamentals of Roller and Gear Lubrication", Pergamon Press, Oxford, 1966

CHAPTER 4

MEASUREMENT TECHNIQUES

This chapter describes the main experimental techniques used in this study for determining lubricant properties relevant to friction in each lubrication regime (hydrodynamic, EHD and boundary). These values are required for the prediction of fuel economy as will be described in chapter five.

4.1. Measurement of EHD properties

Two different types of elastohydrodynamic property were measured, EHD film thickness and traction.

4.1.1. Film thickness measurement

In this study, the method used for measuring the separation between lubricated surfaces in motion was ultra-thin film optical interferometry. This is a relatively simple way to determine the film thickness directly from within the contact under realistic conditions of pressure and shear. The technique was developed in the 1960s in order to study the newly recognised regime of EHD lubrication **[4.1]** and will be described in detail later in this chapter.

Many other techniques have also been used for film thickness measurement and a brief description for the most common ones will be given in the next section.

4.1.1.1. Techniques

The main techniques for measuring film thickness can be divided into two broad categories: electrical and radiation-based techniques.

Electrical methods are based on the use of lubricant as a dielectric separating the surfaces in contact. As the measurement is carried out using the rubbing surfaces as electrodes, it is obvious that both should be good electricity conductors i.e. they should be metals and that they should be electrically isolated from one another. Two extensively used electrical methods are resistance and capacitance techniques. Both measure the average of the film thickness across the contact area. Only with the micro transducer method where a small electrode is deposited on one surface, it is possible to obtain film profiles across the contact. This method was described by Safa [**4.2**]. The main problem with this method is the production of the micro transducers that are able to resist being worn off by abrasive wear due to the conditions found in EHD contacts. Generally the minimum film thickness measurable with these techniques is in the range of 150-200 nm which makes them unsuitable for boundary films determinations where the separation between the surfaces is comparable to their roughness. This would produce occasionally touching of the asperities, short-circuiting the contact. The electrical resistance method is based on measuring the resistance across the contact when a low voltage of 10 to 25 mV is applied [**4.3**], which gives a useful indication of the existence or absence of oil film. However, the measurement of resistance gives only qualitative results as it is not possible to calibrate resistance in terms of oil film thickness [**4.3**]. The capacitance method measures the electrical capacity between the contact surfaces with the lubricant as a dielectric. In this case, the limitation is the dielectric constant of the oil which is not always easy to determine especially if the lubricant contains additives that form chemically reacted films with different properties from the bulk oil. In spite of their problems, the electrical methods have been widely used for film thickness measurements mainly because they use metal surfaces which well reproduce the conditions found in real life systems. Thus a large number of authors have used electrical techniques for film measurements in automotive engine components such as piston rings, bearings and valve trains [**4.4, 4.5, 4.6, 4.7**].

Amongst radiation techniques, the X-ray method, the fluorescence method and optical interferometry are discussed below.

The first of these measures the X-ray flux transmitted through the lubricant-filled gap between rubbing surfaces, relying on the property that the lubricant is transparent to radiation whereas the bounding metal surfaces absorb it entirely [**4.3**]. The technique was developed as a way of measuring an absolute value of film thickness. The main limitation is the calculation of the absorption coefficient as a function of the density of the lubricant in the contact which depends on the local temperature conditions. Also the two contacting bodies must have similar geometry to form a contact without interpenetration, thus offering a clear line of sight through the contact.

The fluorescence method is based on the ability of mineral oils to emit radiation when irradiated with ultra-violet light. The wavelength of the fluorescent light is always longer than that of the incident light [**4.8**]. From the intensity of the fluorescent light, the volume of oil in the focus area can be calculated and thus the film thickness. In early work the ultra-violet light was obtained by filtering a mercury arc. Subsequently a laser was used. When a blue laser source was used it was found that most oils gave better fluorescence with less absorption of the light and less degradation of the oil [**4.18**]. The method has the limitation, as with most of the optical techniques, that at least one surface must be transparent to light which means that real life conditions cannot be well reproduced. Despite this, fluorescence techniques have been extensively applied to studies of oil film thickness in engines [**4.9, 4.10**].

The optical interference method will be discussed in more detail in the following section.

4.1.1.2. Basic principles of optical interferometry

The basic principle of interferometry is shown in figure 4.1. By superposition of two or more waves, optical interference will occur only if the wave trains are emitted simultaneously by a single point of the wave source i.e. they are coherent. The description of the phenomenon is well documented in many text books such as those by Tolansky [**4.11**] and Francon [**4.12**]. In order to fulfil the interference condition, two

methods can be used to obtain coherent beams. One is by division of wave front in which the wave is divided by two slits and than recombined to form interference fringes (known as Young's experiment). The second, which has been employed in this work, is by division of amplitude of the incident wave and uses a semi-reflecting surface for obtaining two coherent beams (figure 4.1). A semi-reflective coating (usually chromium) was first used in lubrication work by Foord et. al. in 1967 [**4.13**] in order to improve the fringe visibility by obtaining two reflecting beams with equal intensities. A condition for high visibility fringes is that the reflectivity of the transparent medium should be comparable to that of the metal surface (the metal ball was found to have about 60% reflectance and 40% absorbance). One way of increasing the reflectivity is by coating the transparent material with thin metal or dielectric films. Thus Foord replaced high refractive index glass, which gave only 1.3% reflection, with standard glass coated on one side with a 20 nm thick chromium layer. The layer has about 18% reflectance, 25% absorbance and 53% transmitance and the resulting intensities of the interfering rays were 0.15 and 0.176 which gave a very good visibility of 0.996 [**4.14**].

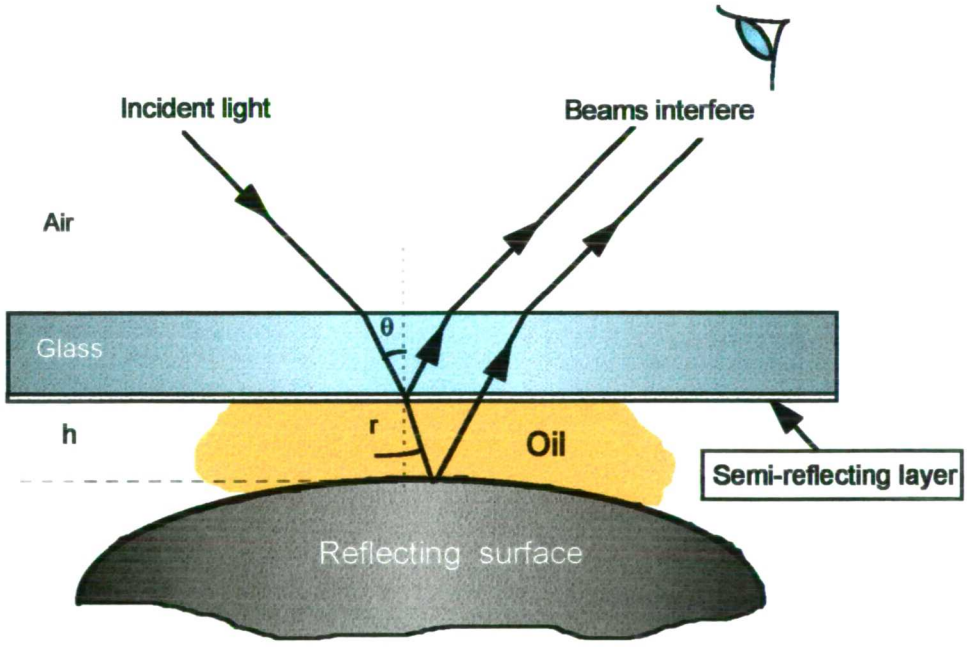


Fig.4.1. Basic interferometric system

The figure shows the separation gap between a glass disc and a reflecting metal surface. The incident wave from the light source passes through the glass and reaches the semi-reflecting layer deposited on the lower surface of the glass. Here is divided by partial

reflection into two waves: one wave is transmitted further through the gap and will be reflected by the reflecting metal surface. The second is reflected directly by the semi-reflecting layer. The resulting wave front maintains its original width but has reduced amplitude. On recombining, the resulting intensity depends on the phase difference which in its turn is a function of the actual path difference between the two waves since they have travelled different distances. For oblique incidence the path difference *d*, depends on the refraction angle *r* and on the "optical "path difference *2nh*, by the formula:

$$d = 2nh\ \cos r + \phi \qquad \text{(E4.1)}$$

where n - is the refractive index of the separation medium

h - is the physical gap thickness

ϕ - is a phase change due to reflection and is taken to be 0.28 for film thickness calculations [**4.15**]

For reflection on dielectric surfaces, the phase change ϕ is equal to π from a rare to dense medium and zero from dense to rare. With metal reflections the situation is more complex and the phase change lies somewhere between 0 and π [**4.16**].

If the two waves are in phase, they will constructively interfere and the phase difference will be an integral number of wavelengths, $N\lambda$. Thus, the condition for constructive interference will be:

$$N\lambda = 2nh\ \cos r + \phi \qquad N = 1,2,3,... \qquad \text{(E4.2)}$$

N is called the fringe order.

When the phase difference is not an integral number of wavelengths, the beams will destructively interfere and dark fringes of minimum intensity will be produced. For maximum destructive interference,

$$\left(N + 1/2\lambda\right) = 2nh\ \cos r + \phi \qquad N = 0,1,2,3,... \qquad \text{(E4.3)}$$

For normal incidence (collimated light) the refraction angle is approximately the same to the incident one and for small values the cosine can be approximated to 1. Wedeven [**4.16**] showed that a typical commercial source has a deviation from normal (θ) of 8° which produced an increase in the observed film of less than 0.4% (thus the error can be

ignored). The formulae for determining the separation between the two surfaces and thus the thickness of the oil film, have become:

$$h = \frac{(N - \phi)}{2n}\lambda \qquad N = 1,2,3... \qquad (E4.4)$$

$$h = \frac{(N + 1/2 - \phi)}{2n}\lambda \qquad N = 0,1,2,3... \qquad (E4.5)$$

for constructive and destructive interference respectively.

Depending on the light source used, the interferometric system can be monochromatic, duochromatic and chromatic (white light).

When a monochromatic (single colour) source is used, the interference pattern is a succession of bright and dark fringes corresponding to constructive and destructive interference, respectively. If the light were perfectly monochromatic, the fringes would extend from the centre of the contact out to infinity. But since there is no such light the contrast becomes less farther away from the centre. Still, due to the narrow band width of monochromatic light the visibility remains good for considerable separations and the fringes are equally spaced by $\Delta = \lambda/4n$ (determined from subtracting eq. E4.4 from eq. E4.5). However, particularly for longer wavelengths, this fringe spacing is a coarse unit for measuring the separation in the contact. There is also difficult in determining the fringe order since there are only bright and dark fringes, equally spaced and there is no indication as to whether the order is increasing or decreasing. The only way to determine the fringe order is to count the fringes, which can be quite misleading.

Duochromatic interferometry uses two discrete wavebands from coloured sources (for example green and red [**4.16**]). This gives an increase in the number of points obtainable from a given order in comparison with monochromatic light (the number is doubled). The fringes are also closely spaced, have good colour contrast and the colour sequence provides a convenient means for determining the fringe order.

Chromatic interferometry uses white light which is a combination of different monochromatic waves with wavelengths between 400 nm for violet and 700 nm for dark red. Each of these forms an interference pattern. The fringe separation depends on wavelength; thus, for a given colour, the fringes are more widely spaced the greater the wavelength. As the separation is increased, different wavelengths will constructively interfere and the series of colours will repeat every order with a reduced relative spacing i.e. there are more data points per order. The fixed sequence of coloured fringes provides a good method to determine the fringe order. At higher separations the fringes become closer and the colours overlap each other. After 8 or 10 fringes **[4.8]**, so many colours are present at a given point that the resultant colour appears essentially white even though the interference is still taking place. This decrease in visibility limits the maximum separation that can be measured to about 1 μm, but since the lubricant film thickness generated in EHD contacts is of the same order as the wavelength of visible light (400-700 nm), the chromatic interferometry has been applied very successfully to film thickness measurement.

There are two major limitations of classical optical interferometry for studying lubricant films. One is the minimum film thickness that can be measured. For the minimum film thickness, the fringe order N is equal to 1 and the smallest wavelength detectable by human eye is violet (approx. 400 nm). For a refractive index of 1.4 (for standard mineral oil), a normal incident light and a phase change upon reflection of 0.28, the equation E4.4 would give a film thickness of approximate 100 nm. Thus films less than one-quarter of the wavelength of visible light cannot be measured using the classical technique. However, many films of practical importance tend to be thinner than this, especially at high temperatures, as are found in crankcase engines.

The second limitation of conventional interferometry is the resolution of the technique which is relying on human eye to distinguish the interferometric fringes. Thus on one hand the measurable thicknesses are only possible in steps of 50 nm and on the other, the resolution depends on the ability of human eye to distinguish colours accurately, typically 1/8 of the wavelength of light , i.e. approximately 50 to 90 nm.

4.1.1.3. Ultra-thin film technique

In order to overcome these limitations, two main improvements have been made.

One is a "spacer layer" (see figure 4.2.), initially introduced by Westlake [**4.14**] in 1970.

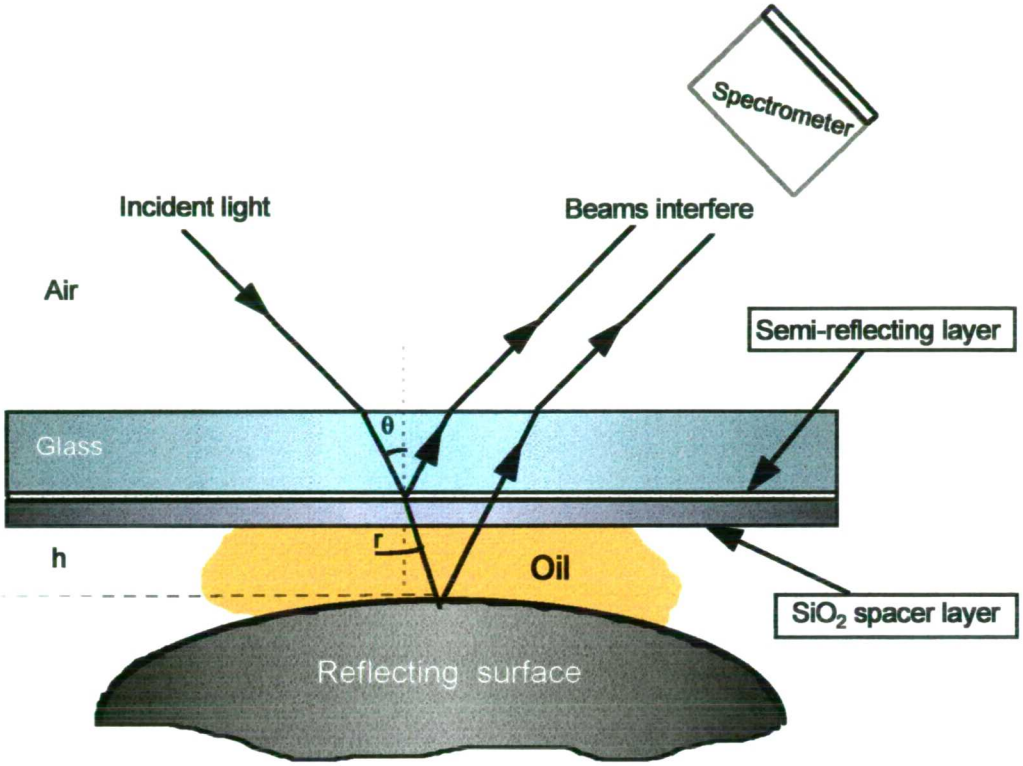


Fig.4.2. Schematic of ultra-thin film technique

A transparent layer of silicon dioxide (SiO_2) is deposited on top of the chromium semi-reflecting layer on one side of the glass disc. SiO_2 was found to have suitable qualities for an efficient spacer layer since it has a refractive index very close to that of most lubricants, has a negligible absorption and gives a durable coating. This added layer with a thickness comparable to the wavelength of light, acts like a solid layer of oil which gives a measurable film thickness even in static contact. This is measured at the beginning of the test on a dry contact and the value is then subtracted from each reading to give the real film thickness. Thus when constructive interference takes place, the film thickness is calculated from

$$h_{oil} = \frac{(N_{sp+oil} - \phi)\lambda_{sp+oil} - (N_{sp} - \phi)\lambda_{sp}}{2n_{oil}} \qquad N = 1,2,3,.. \qquad (E4.6)$$

since n_{oil} and n_{sp} are very similar in practice.

A major advance was made in 1985 by Johnson [**4.15**] when a spectrometer was introduced to accurately determine which particular wavelengths have constructively interfered and, consequently, calculate the film thickness value. The spectrometer contains a grating that can pivot about an axis. The interfered light reflected from the centre of the contact is directed into the spectrometer where the fine grating grooves disperse the light into its component wavelengths. Figure 4.3. shows a schematic representation of the spectral analysis set-up. The spectrometer is connected to a 50 images/second black and white video camera and a monitor which displays part of the the spectrum (typically over a wavelength range of 80 to 100 nm). The spectrometer grating can be rotated by the use of a micrometer to scan the whole spectrum. The spectral intensity is displayed in terms of wavelength λ as a band across the TV screen.

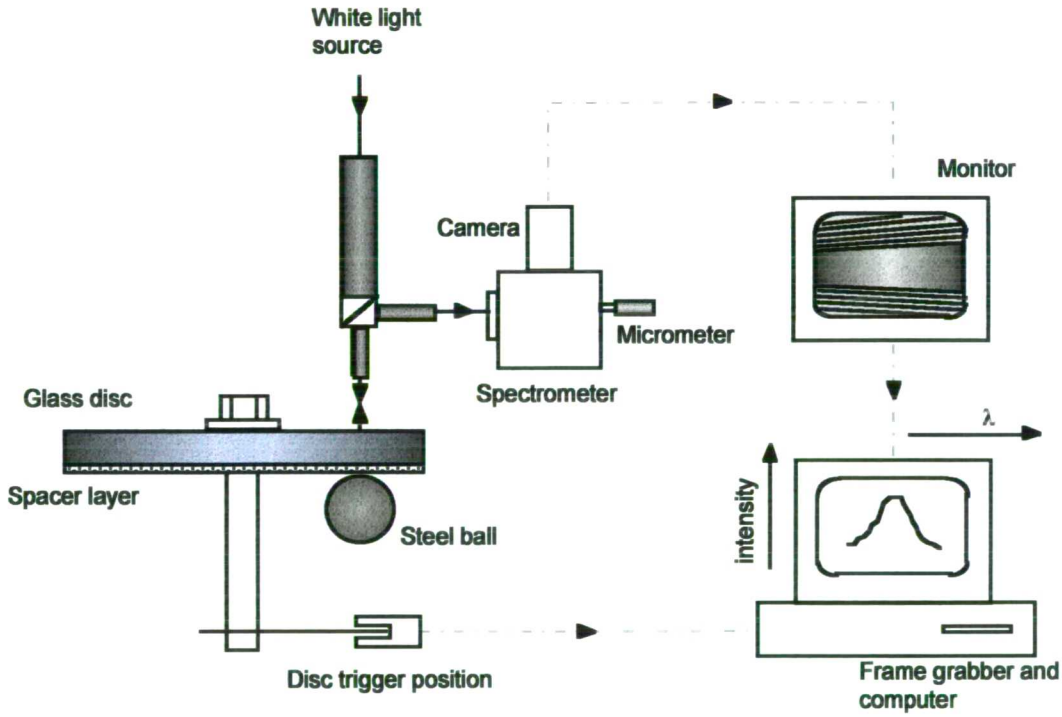


Fig.4.3. Schematic representation of spectrometer set-up

By identifying the wavelength at which maximum constructive interference occurs it is possible to determine the separation. In order to enable this, the system incorporates a frame grabber and a computer. Two calibrations are necessary. One is of the spectrometer with respect to micrometer reading by using the light from a mercury lamp, with known wavelength emission. The second calibration is of the spectrometer

with respect to screen position which is made by noting the variation in screen position for each spectral line, as a function of micrometer setting.

With these improvements the ultra-thin film technique enables films down to less than 5 nm thick to be measured with an accuracy of ± 2 nm [**4.17**].

4.1.1.4. Test rig description

The test rig employed is shown in figure 4.4.

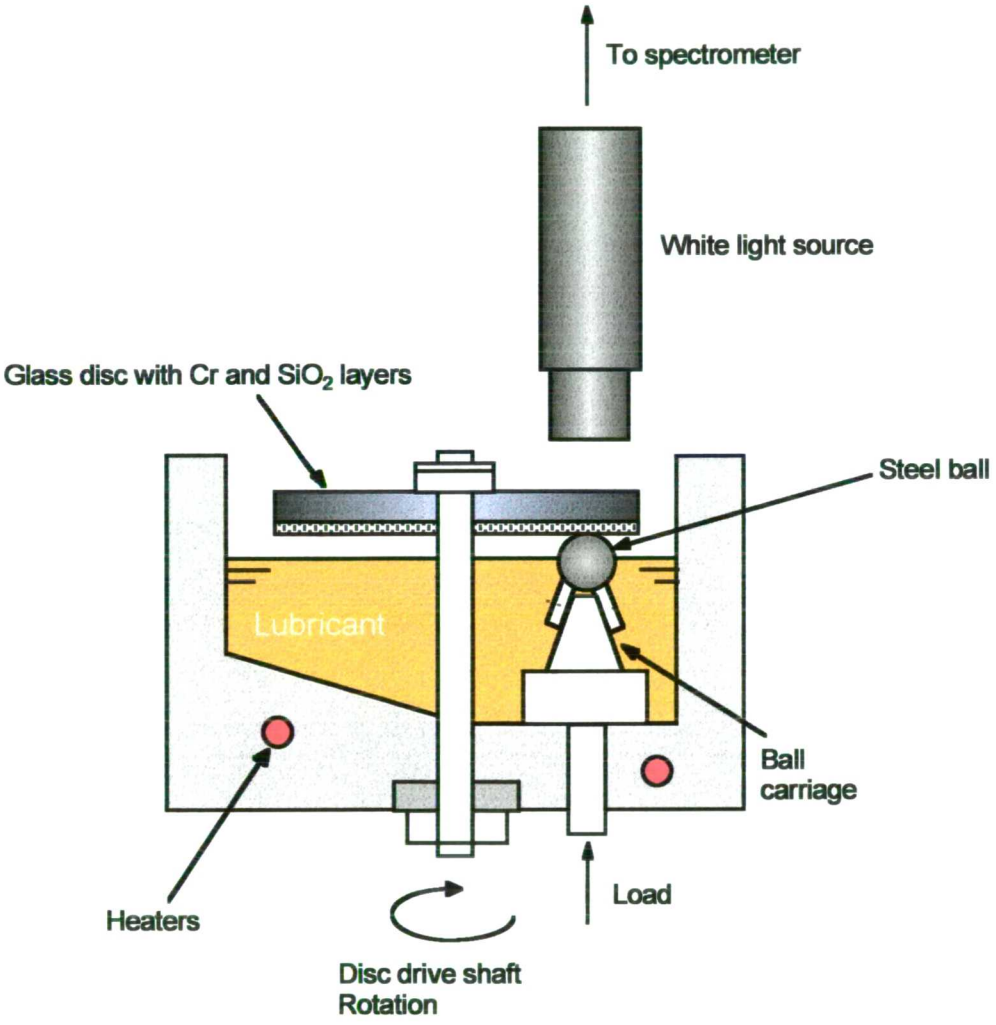


Fig.4.4. EHD rig

A 19.0 mm diameter, AISI 52100 steel ball is loaded against the flat surface of a glass disc to form a Hertzian-type contact. The disc is driven by a DC motor and, in turn, drives the ball usually in nominally pure rolling. A two speed gear box allows a speed variation from 10^{-3} to 5 ms^{-1}. The ball is half-immersed in test lubricant and ball, disc and lubricant are contained in a stainless steel chamber which is provided with electric

heaters so that the temperature can be maintained within ± 1°C. The bulk lubricant temperature as well as the temperature close to the contact inlet which is controlled by a local thermocouple, are measured during the test. Film thickness is measured using ultra-thin film interferometry and to enable this, the disc surface is coated with a 20 nm thick chromium layer covered by a 600 nm thick silica layer (as described in the previous paragraph). Both ball and glass have a roughness of approximately 11 nm rms and the Young's moduli of the two surfaces is 210 and 75 GPa for steel and glass respectively. The load applied is 20 N, corresponding to a maximum Hertz contact pressure of 0.54 GPa.

The test conditions employed in most of the current work are summarised in the following table:

Temperature range	25 to 120 °C
Speed range	0.001 to 1 m/s
Load	20 N
Hertzian pressure	0.54 GPa
Ball properties	AISI 52100 steel, 11 nm rms
	Young's modulus 210 GPa
Disc properties	glass, 11 nm rms
	Young's modulus 75 GPa

Table 4.1. Test conditions for EHD film thickness measurement

The experimental protocol was as follows. A new steel ball was used for each test. The test rig, glass disc and steel ball were cleaned thoroughly using toluene and analar acetone and the rig assembled. Before lubricant is added, the thickness of the spacer layer is measured in dry loaded contact. This value is subtracted from the overall film thickness measured when oil is present, in order to give the true value of the oil film. In a first stage, the software enabled the measurement of the spacer layer thickness in only one trigger point. In a later version, adapted for lower speed measurements in this study, it was possible to choose a number of points on the disc circumference in which the spacer layer was measured. As the shaft position is determined by an optical encoder, the software finds each recorded trigger point and the corresponding spacer layer value is subtracted from the total film measured, the reading showing the true oil thickness. This speeded up the measurements at slow speed by giving film values from averaging the readings from less than one disc rotation instead of at least three.

The lubricant was such added to half-cover the steel ball in order to ensure that the contact is fully flooded. The temperature was raised at its required value and film thickness measurements made at a range of rolling speeds mainly between 10^{-3} to 1 ms^{-1}.

4.1.2. Traction measurement

As well as EHD film thickness, EHD traction properties of lubricants were also measured in this study.

The rig used for traction measurements was the same as that employed for film thickness measurements, except that the glass disc was replaced by a smooth, hardened, polished steel disc, with a similar surface finish to that of the ball (measured disc surface roughness was in the range of 20 to 30 nm rms). For the traction tests, both the ball and the disc were driven by separate DC motors, enabling the slide/roll ratio to be controlled. Traction measurements were made between a 19.0 mm diameter, AISI 5200 steel ball in sliding contact with a steel disc. The Young's moduli of the two surfaces were 210 GPa for both. The load applied was 30 N which corresponds to a Hertzian pressure of 0.94 GPa. The test conditions are given in the following table:

Temperature range	40 to 135 °C
Speed range	0.001 to 2.5 m/s
Load	30 N
Hertzian pressure	0.94 GPa
Ball properties	AISI 52100 steel, 11-13 nm rms
	Young's modulus 210 GPa
	58-65 Rockwell C hardness
Disc properties	AISI 52100 steel, 20-30 nm rms
	Young's modulus 210 GPa
	63 Rockwell hardness

Table 4.2. Test conditions for traction measurements

The test rig is shown diagrammatically in figure 4.5.

The steel ball is mounted on a shaft, linked through a strain gauge beam to the ball drive motor to measure traction force. To obtain conventional EHD traction measurements,

the slide roll ratio is increased at a fixed ball speed to produce traction coefficient versus slide roll ratio plots. Slide roll ratio was previously defined in paragraph 2.3.2.2.1. as

$$S/R = \frac{sliding\ speed}{mean\ entrainment\ speed} = \frac{2|U1-U2|}{U1+U2} * 100\%$$

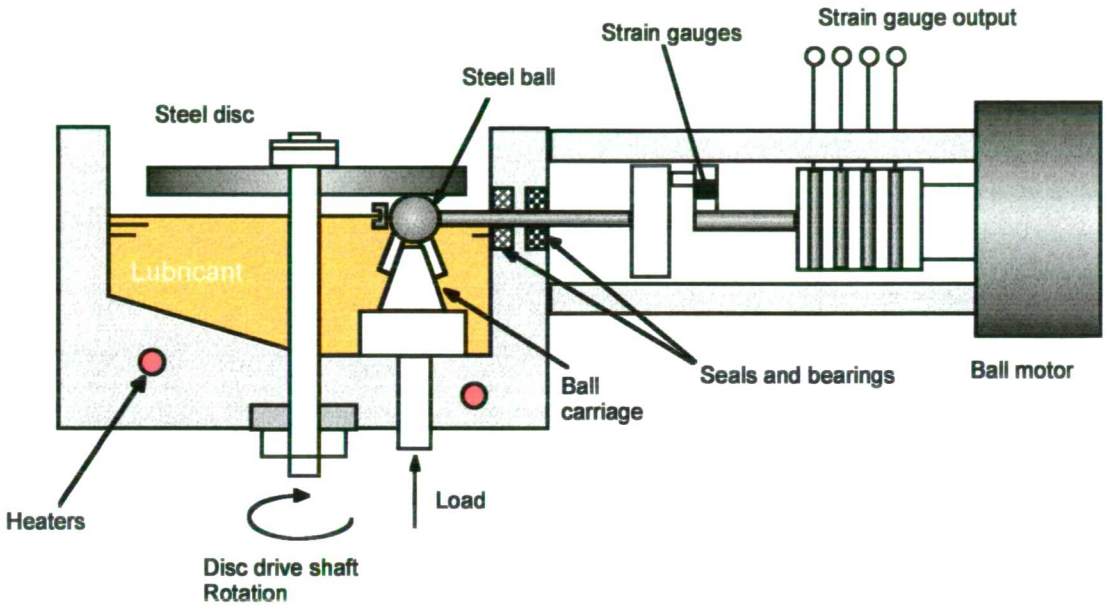


Fig. 4.5. Traction rig

To obtain friction values, two sets of measurements are taken for each SRR, one at negative SRR and one at the same but positive value. By keeping the ball speed constant at 1 m/s and making the disc run faster than the ball and then slower, the parasitic friction from seals, bearings, etc. is eliminated from traction value when the two readings are added and divided by 2.

Measurements were generally made at a series of set temperatures. The cleaning procedure was similar to film thickness tests.

4.2. Measurement of boundary friction properties

Coefficients of boundary friction were determined in this study using a high frequency reciprocating rig (HFRR) test rig at a range of different temperatures between 40 and 140°C. The HFRR lubricity test rig employed is shown schematically in figure 4.6.

A 6.0 mm diameter steel ball is held in a chuck and loaded downwards on the flat face of a 10.0 mm diameter steel disc. The disc is held in a bath which is two thirds filled with lubricant so that the contact between the ball and flat is fully immersed. The bath has heaters and a control system so that the temperature can be set at any value between room temperature and 200°C.

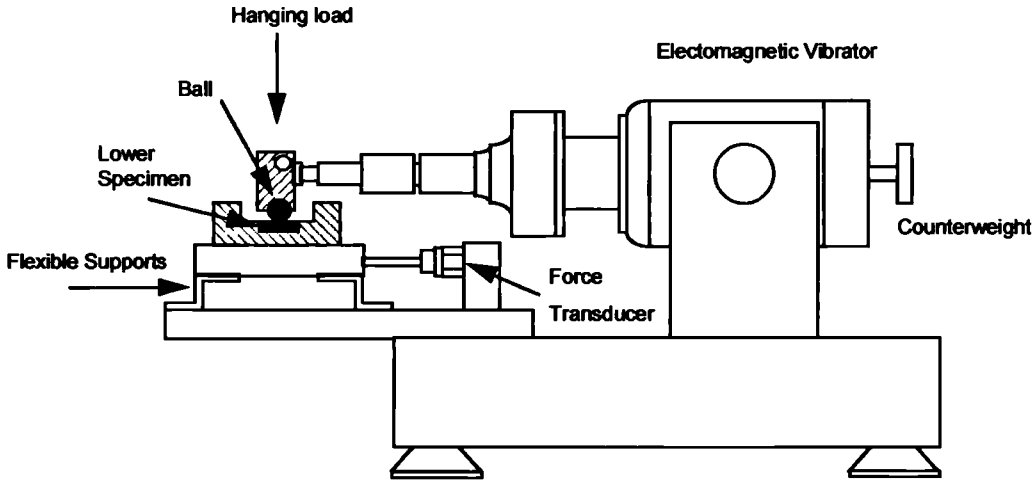


Fig. 4.6. Layout of HFRR rig

During a test, an electrical vibrator is employed to oscillate the ball backwards and forwards in contact with the flat at a stroke length and frequency that can be set by the user. A control circuit maintains constant stroke length regardless of the friction value. Friction between the ball and flat is measured using a load cell attached to the lower specimen holder.

Three values are continuously monitored throughout a test and logged by a microcomputer; the oil temperature, the friction coefficient and the electrical contact resistance. The last is measured by applying a small voltage of 15 mV across the contact

and provides an indication of the extent to which an insulating film is formed between the ball and flat.

The tests in this study were generally carried out under the conditions listed in table 4.3.

Stroke length	1000 µm
Stroke frequency	20 Hz
Load	400 g
Hertzian pressure	1.02 GPa
Temperature	stages of 40°C, 60°C, 80°C, 100°C, 120°C and 140°C
Test duration	10 minutes at each temperature
Ball properties	6 mm, AISI 52100 steel, 800 VPN
Disc properties	10 mm, AISI 52100 steel, 200 VPN

Table 4.3. HFR test conditions

A single ball and flat were used for each lubricant test. These were thoroughly cleaned in an ultrasonic bath using toluene and analar acetone and the rig assembled. Approximately 3 ml of lubricant were then applied. The temperature was generally raised in stages from 40 to 140°C in steps of 20°C with a ten minute reciprocating test at each temperature. Reciprocating motion was halted between stages, whilst the temperature was increasing.

The friction coefficient result for each stage was determined by averaging over the last 9.5 minutes of the stage, i.e. ignoring the first 30 seconds.

4.3. Measurement of hydrodynamic properties

Hydrodynamic properties were not measured directly but since hydrodynamic friction is directly dependent upon dynamic viscosity at the temperature and shear rate applied, lubricant viscosities were measured at a range of temperatures at both high and low shear rates. High shear rate viscosities in cP (HTHS) were measured by Exxon Chemical Co., Abingdon, using a Taper Bearing Simulator (TBS) (ASTM D4624) and low shear rate viscosities in cSt (Kvisc) using conventional capillary viscometry (ASTM D445).

REFERENCES

[4.1] Gohar R. and Cameron A., "The Mapping of Elastohydrodynamic Contacts", ASLE Trans. 10, pp. 215-225, 1967,

[4.2] Safa M.M.A., "Elastohydrodynamic Studies Using Thin Film Transducers", PhD Thesis, Imperial College, University of London, 1982,

[4.3] Cameron A., "The Principles of Lubrication", Longmans, 1966,

[4.4] Moore S.L and Hamilton G.M., "The Starved Lubrication of Piston Rings in a Diesel Engine", J. Mech. Eng. Science, 20, pp 345-352, 1978,

[4.5] Williamson B.P., Galliard I.R. and Benwell S., "Measurement of Oil Film Thickness in the Elastohydrodynamic Contact between a Cam and Bucket Follower in a Motored Cylinder Head. Part 1: Newtonian Oils", Int. Fuels and Lubricants Meeting and Exposition, Baltimore, Maryland, USA, Sept. 1989, SAE Pre-print 892150,

[4.6] Ninomiya N., Kawamura M. And Fujita K., "Electrical Observation of Lubricant Film between a Cam and a Lifter of an OHV Engine", SAE Paper 780930, 1978,

[4.7] Craig R.C., King W.H. and Appeldoorn J.K., "Oil Film Thickness in Engine Bearings - The Bearing as a Capacitor", SAE Paper 821250, 1982,

[4.8] Jenkins F.A. and White H.E., "Fundamentals of Optics", McGraw-Hill, fourth edition, 1967,

[4.9] Hoult D. P., Lux J.P., Wong V.W. and Billian S.A., "Calibration of Laser Fluorescence Measurement of Lubricant Film Thickness in Engines", SAE Paper 881587, 1988,

[4.10] Richardson D.E. and Borman G.L., "Using Fiber Optics and Laser Fluorescence for Measuring Thin Oil Films with Application to Engines", SAE paper 912388, 1991,

[4.11] Tolanski S., "An Introduction to Interferometry", Longmans, London, 1966,

[4.12] Francon M., "Optical Interferometry", Academic Press, New York, 1966,

[4.13] Foord C.A., Hammann W.C. and Cameron A., "Evaluation of Lubricants Using Optical Elastohydrodynamics", ASLE Trans 11, p. 31, 1968,

[4.14] Westlake F.J., "An Interferometric Study of Thin Fluid Films", PhD Thesis, Imperial College, University of London, 1970,

[4.15] Johnston G.J., "A Study of Lubricating Films Generated by Organo-Phosphorus Anti-Wear Additives", PhD Thesis, Imperial College, University of London, 1990,

[4.16] Wedeven L.D., "Optical Measurements in Elastohydrodynamic Rolling Contact Bearings", PhD Thesis, Imperial College, University of London, 1970,

[4.17] Gunsel S. And Spikes H.A., "In-situ Measurements of ZDDP Films in Concentrated Contacts", Trib. Trans. 36, 2, pp. 276-282, 1993,

[4.18] Aderin M.E., "Interferometric Studies of Thin Lubricant Films in Concentrated Contacts", PhD Thesis, Imperial College, University of London, 1994

CHAPTER 5

BENCH TEST RESULTS

This chapter presents the results obtained in bench test measurements for both Sequence VI and VI A reference oils. Lubricant properties considered to be relevant to engine fuel efficiency are measured using the methods described in chapter four. The correlation with fuel efficiency data available from engine tests is presented in the next chapter.

5.1. Results for Sequence VI oils

ASTM Sequence VI reference oils were tested as described in chapter 4 to assess their boundary, hydrodynamic and EHD friction properties. The selected bench tests were such that they focused separately on each lubrication regime. These measured properties were then correlated with fuel efficiency performance available from engine tests using linear regression techniques.

5.1.1. Lubricants used in the study

The ASTM reference lubricants were studied. The table below shows their SAE grades and the corresponding fuel efficiency. The overall EFEI is shown and also the separate efficiencies of the two stages of the test at 65°C (R150) and at 135°C (R275). The last column shows, where available, the number of engine tests from which the efficiency data were averaged. All Sequence VI data were supplied by Exxon Chemical Ltd.

Nr	Oils	SAE grade	R150	R275	EFEI	# Pts.
1	R 502	5 W 20	3.41	7.29	2.87	23
2	R 513	10 W 30	2.11	7.51	2.32	74
3	R 515	10 W 30	2.63	8.45	2.78	83
4	R 516	10 W 30	1.94	1.23	0.78	48
5	R 517	10 W 40	1.85	6.78	2.03	43
6	R 518	5 W 30	2.85	6.79	2.54	34
7	R 519	5 W 30	3.13	5.48	2.33	39
8	R 520	10 W 30	2.57	7.83	2.64	34
9	epv22d	5 W 30	4.46	11.75	4.26	
10	epv23-3	5 W 20	4.56	11.72	4.35	

Table 5.1. Reference lubricants for Sequence VI test

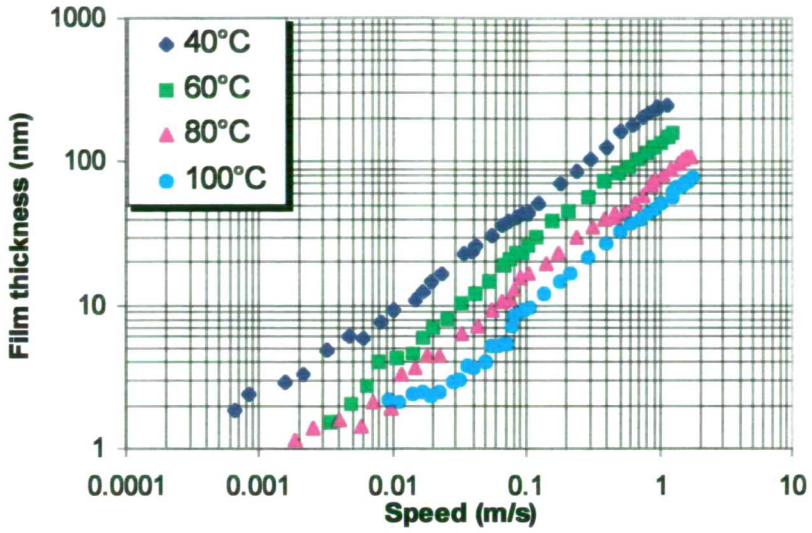
Initially the same eight ASTM reference oils were used as employed in earlier work by Benchaita [**5.1**]. Later in the programme, two more highly fuel efficient oils were added, to form a set of ten oils with a wide range of fuel economy improvement levels from low to high energy conserving oils. These are the last two oils listed in table 5.1.

5.1.2. EHD film thickness results

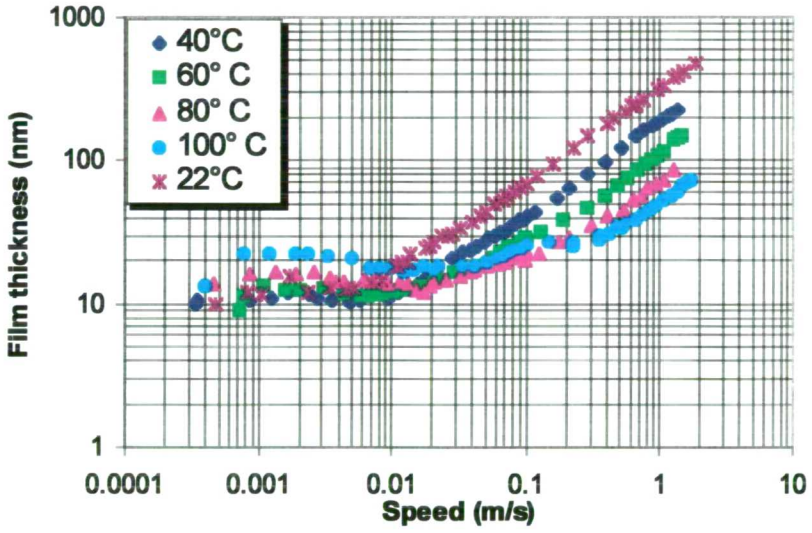
EHD film thickness was measured in the optical rig described in chapter 4. The results were plotted as the variation of logh i.e. log(central film thickness) against logU i.e. log(mean rolling speed). EHD theory [**5.2**] predicts that this variation should be linear, as shown in expression E5.1, with a slope between 0.6 and 0.7.

$$\log h = const + 0.67 \log U \qquad (E5.1)$$

Most lubricants showed a behaviour consistent with equation E5.1. A typical example is shown in figure 5.1a for oil R517. The plot is linear with a slope at 40°C of 0.68 as predicted by theory, although at 100°C the slope has increased at 0.76. Three sets of tests were performed and the repeatability was within ±5%.



(a) R 517 oil



(b) R 519 oil

Fig.5.1. Film thickness vs. speed for R 517 (a) and R 519 (b) oils, for four temperatures

Some fluids however, showed a non-linear behaviour at slow speeds with film thickness enhanced above that predicted by theory (figure 5.1b, oil R519). It can be seen that the film thickness is decreasing as the temperature increases due mainly to viscosity decrease. For both fluids, for speeds higher than 0.1 m/s the plots are linear as expected. However, as speed and thus the film thickness decreases, oil R519 forms a much higher film than R517, about 10 nm, which can give some indications about the additives present in the oils.

The behaviour at higher temperatures is consistent with the results obtained in recent work on ZDDP reaction films [5.3]. The increased film thickness is evident at lower temperatures as well and this might be due to the reaction of friction modifier additives or the presence of adsorbing VI Improvers [5.4].

The film thickness results in μm (EHD film) at 1 m/s (the speed value used by Benchaita and Lockwood) at four temperatures, are summarised in table 5.2.

Nr	Oils	EHD40 40°C	EHD60 60°C	EHD80 80°C	EHD100 100°C
1	R 502	0.190	0.109	0.080	0.053
2	R 513	0.285	0.165	0.089	0.055
3	R 515	0.276	0.152	0.088	0.055
4	R 516	0.265	0.141	0.086	0.058
5	R 517	0.247	0.137	0.082	0.025
6	R 518	0.204	0.108	0.064	0.049
7	R 519	0.194	0.116	0.073	0.052
8	R 520	0.269	0.138	0.073	0.055
9	epv22d	0.205	0.124	0.071	0.051
10	epv23-3	0.201	0.115	0.074	0.054

Table 5.2. EHD film thickness results at 1 m/s (μm)

A full set of film thickness plots is included in appendix A.

The influence of temperature, wavelength and pressure upon the refractive index need to be considered in calculation of the real film thickness. Measurements of the refractive index using the Abbe refractometer were made at a range of temperatures and showed a decrease of 2% over the whole range from 25 to 100°C. For films less than 5 nm this would result in a maximum increase of 0.1 nm which is insignificant. For higher films, 50 nm or more, the increase in thickness would be of the order of 1 nm which is less than the measurement precision.

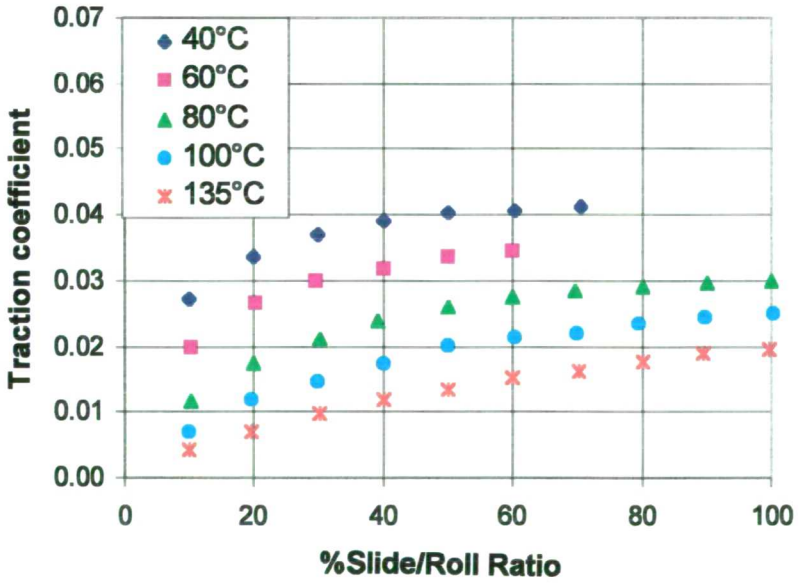
The refractive index *n* usually increases with pressure (details can be found in reference [5.5]) but in this study, the effect of contact pressure on the refractive index of the lubricant has been neglected. Since the predicted variation of *n* with pressure is small - an increase in pressure from atmospheric to 1 GPa has been shown to increase the refractive index by less than 10% [5.6] and this is unlikely to vary by much from oil to

oil - and thus be similar for all oils tested, the refractive index at atmospheric pressure was used. Neglecting the influence of pressure on refractive index is thus likely to result in a systematic overestimate of film thickness of about 4%.

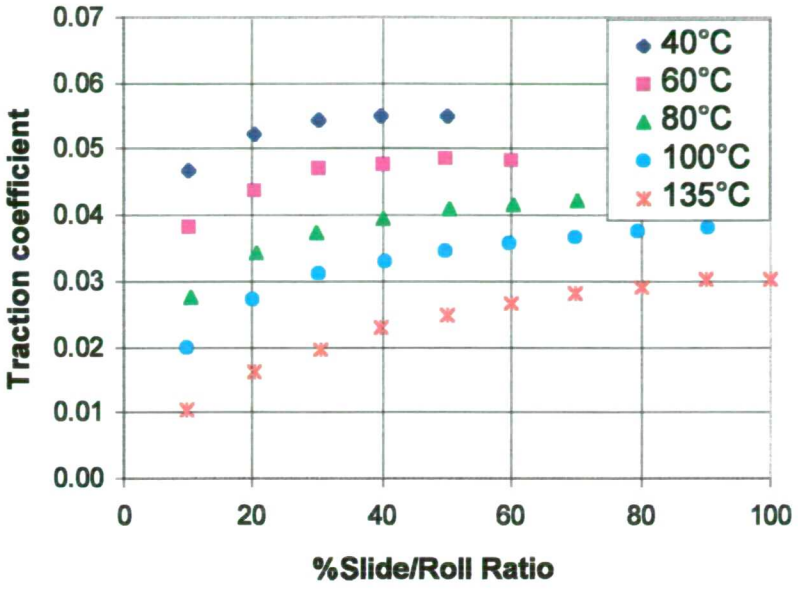
The software used to measure the film thickness takes into account the decrease of refractive index *n* with wavelength [**5.7**].

5.1.3. Traction results

The shear properties of the lubricants were measured using the traction rig described in section 4.1.2. Two types of measurements were made. In one, the mean rolling or entraining speed was held constant at 1 m/s and the friction coefficient measured as a function of slide/roll ratio. Since the film thickness at 1 m/s is generally greater than the composite surface roughness, this test usually measures the EHD film friction (traction) coefficient. The classical variation of traction coefficient with slide/roll ratio (S/R) results can be seen in figure 5.2, for two oils, R502 and R513.



(a) R502



(b) R513

Fig.5.2. Traction coefficient vs. S/R for R 502 and R 513 at five temperatures

It is worth noting that R502 is characterised by a lower limiting traction coefficient than R513 and, when compared to all other lubricants, was found to be the lowest of all (see the plots in appendix B). As the S/R ratio, i.e. the shear rate increases, traction coefficient rises to a limiting value. This limiting value is reached sooner at low than at high temperatures and falls with temperature. The traction coefficients for four temperatures are listed in table 5.3. These are the maximum, "limiting" traction coefficient or, when no maximum was reached, the value at 70% slide/roll ratio was taken. Three sets of tests were carried out and the repeatability was within ± 4%.

Nr	Oils	Trac40 40°C	Trac60 60°C	Trac80 80°C	Trac100 100°C
1	R 502	0.041	0.034	0.030	0.025
2	R 513	0.055	0.049	0.042	0.038
3	R 515	0.057	0.049	0.043	0.038
4	R 516	0.056	0.049	0.044	0.039
5	R 517	0.054	0.047	0.041	0.037
6	R 518	0.058	0.049	0.043	0.039
7	R 519	0.052	0.045	0.038	0.035
8	R 520	0.054	0.047	0.042	0.036
9	epv22d	0.056	0.048	0.043	0.037
10	epv23-3	0.057	0.050	0.047	0.047

Table 5.3. Traction data for Sequence VI test oils

The second type of traction experiment was made at 135°C when the slide/roll ratio was held constant and the rolling speed and thus entrainment speed was varied. By decreasing the mean rolling speed, this produces a corresponding reduction in film thickness, so that the variation of friction with film thickness can be analysed from EHD through mixed and boundary lubrication. Figure 5.3. shows the traction coefficient versus rolling speed plot for one fluid at three fixed slide roll ratios (20, 50 and 70%) at 135°C.

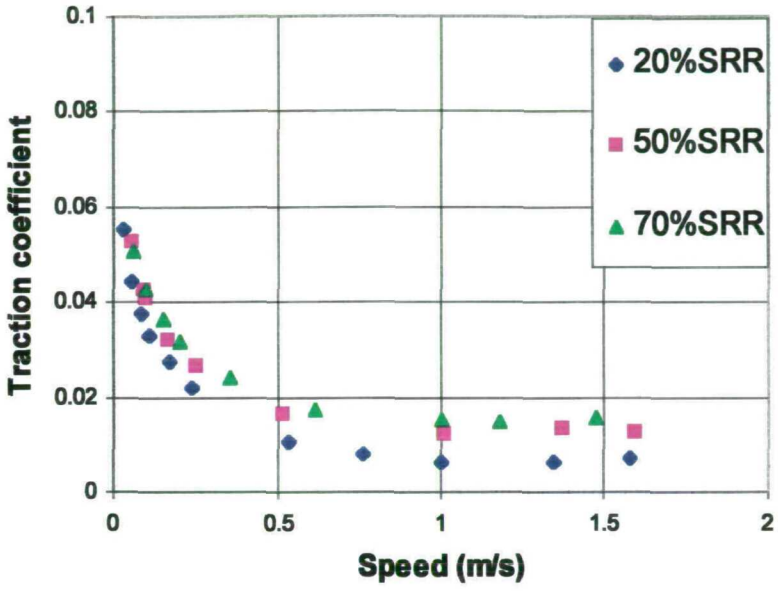


Fig.5.3. Traction coefficient vs. rolling speed for R502

The resulting curve can be explained in terms of the influence of film thickness on friction. At high rolling speeds and thus EHD film thickness, the friction coefficient is representative of that of the full EHD film. As the rolling speed is progressively lowered, however, the film thickness falls so that the friction is a mixture of elastohydrodynamic and boundary. At low speeds the friction coefficient continues to rise towards the boundary friction value, typically 0.1. The plot is thus effectively a "Stribeck curve" for a concentrated contact condition (EHD/boundary) rather than the more conventional HD/boundary condition. The behaviour of the various test lubricants measured in this way was very different. Figure 5.4 shows the test lubricants R516 and R519, which show much higher traction coefficient in the transitional EHD/boundary region than R502 oil. As the rolling speed and thus the film thickness is reduced, friction for these two lubricants rises from the EHD value at higher speeds than for the other

oils. This is believed, on the basis of recent work, to be due to the formation at the surface of an uneven ZDDP film which may effectively roughen the surfaces [**5.3**].

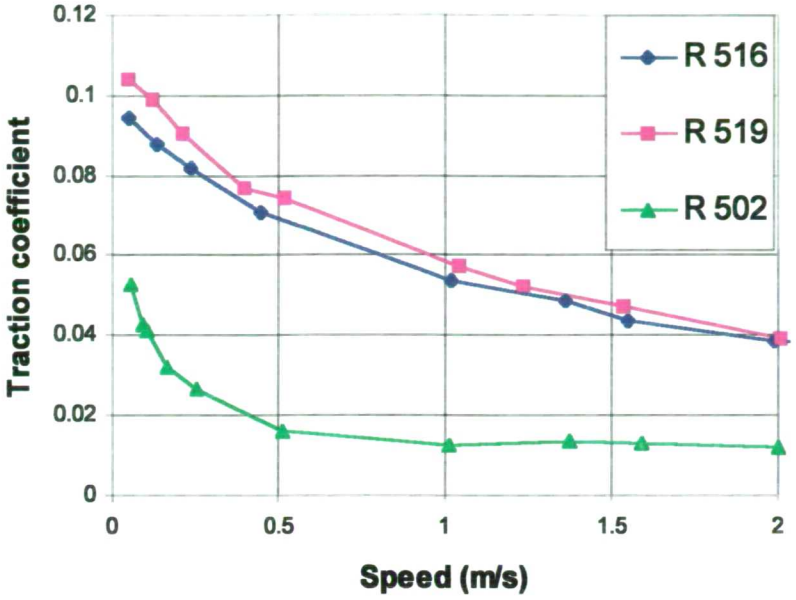


Fig.5.4. Traction coefficient vs. rolling speed for R516 and R519 at 50%SRR

Appendix C contains the friction/rolling speed plots for all fluids tested and table 5.4 summarises the values of intermediate traction coefficient at 1 m/s, 135°C and also the relative traction coefficient increase between 1 m/s and 0.1 m/s. This is calculated as:

$$Tr01Tr1 = \frac{(Tr.Coeff.\ at\ 0.1m/s - Tr.Coeff.\ at\ 1m/s)}{Tr.Coeff.\ at\ 1m/s} \qquad \text{(E5.2)}$$

Nr	Oils	Trac20SR 1m/s 20%SRR	Trac50SR 1m/s 50%SRR	Trac70SR 1m/s 70%SRR	20Tr01T1 at 20%SRR	50Tr01T1 at 50%SRR	70Tr01T1 at 70%SRR
1	R 502	0.011	0.016	0.017	3.71	2.58	1.87
2	R 513	0.018	0.026	0.027	2	1.05	0.76
3	R 515	0.021	0.028	0.031	1.35	1.65	0.79
4	R 516	0.061	0.071	0.070	0.65	0.67	0.69
5	R 517	0.020	0.026	0.030	1	0.60	0.64
6	R 518	0.030	0.034	0.038	1.5	1	0.79
7	R 519	0.072	0.074	0.071	0.75	0.74	0.71
8	R 520	0.015	0.023	0.025	1.13	0.64	0.60
9	epv22d	0.035	0.044	0.051	0.67	0.61	0.55
10	epv23-3	0.047	0.049	0.048	0.85	0.44	0.54

Table 5.4. Traction coefficients at mixed EHD/boundary conditions at 135°C

A better insight into the variation of traction coefficient in the lubrication regimes can be obtained if, instead of rolling speed, the corresponding specific film thickness values are represented on the abscissa axis in figure 5.5. Although the specific film thickness (λ ratio) is determined as the minimum film thickness over the composite surface roughness (as it was shown in paragraph 2.3.1), a good approximation is obtained if central film thickness measured with the optical rig, is used. The composite surface roughness is about 30 nm rms. Thus for λ ratios greater than 1, there is sufficient lubricant between the surfaces to support almost all of the load by a fluid film and friction has a constant value given by the shear strength of the EHD film. Decreasing the speed and thus the film thickness, the λ ratio falls below the film thickness becoming comparable to the surface roughness, so more load is borne by asperities. This results in a further increase of friction which, eventually, reaches the maximum value for boundary lubrication.

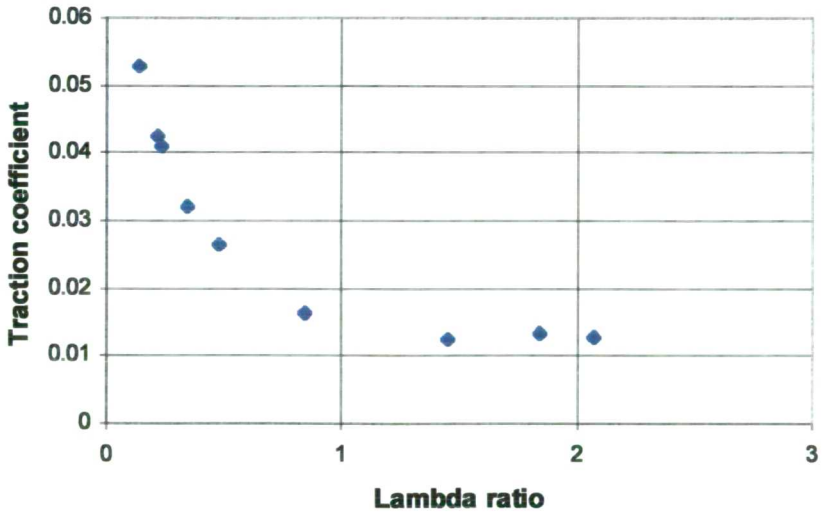


Fig.5.5. Traction vs. specific film thickness for R502

It should be born in mind that this is only an approximation since in the EHD rig, the film thickness is measured using different loads and materials from the traction rig (this results in about 10% overestimation) and in calculating the specific film thickness, the roughness values taken are those for undeformed surfaces.

5.1.4. Boundary friction results

Friction under boundary conditions was determined on the HFRR rig described in paragraph 4.2. Three types of parameters are recorded vs. time in such a test:

temperature, electrical resistance (as a quantitative measure of the separation in the contact) and the friction coefficient, μ. A typical result is shown in figure 5.6.

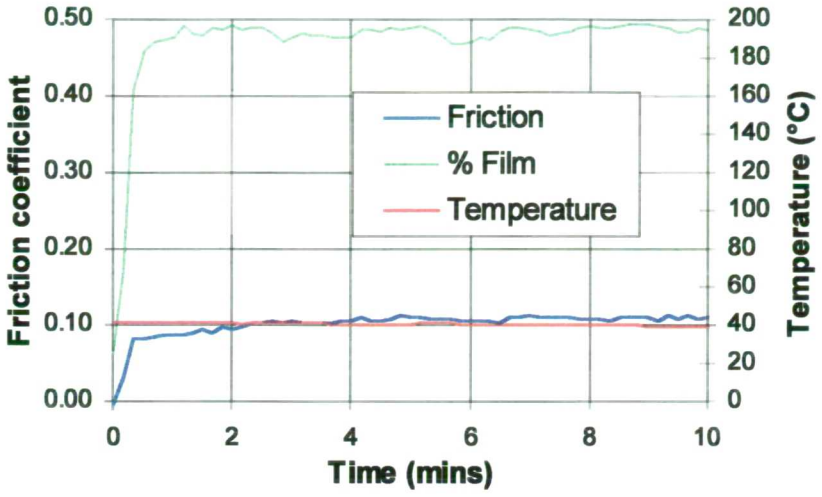


Fig.5.6. Friction coefficient variation with time for R502

In the attempt to better characterise the boundary conditions, three oils covering the viscosity range, were chosen to be tested at several different stroke lengths. Thus a low viscosity oil, R502, a medium viscous one, R518 and the most viscous one, R517 were tested at three extra stroke lengths apart from 1 mm i.e. 0.3 mm, 0.5 mm and 2 mm. The results are plotted in figures 5.7 to 5.9.

By varying the stroke length and keeping the load and frequency constant, the intention was to determine the change in friction with sliding speed. Since the effect of speed upon friction is influenced by many factors, it is very difficult to find a general trend for it. It was found by many authors that friction coefficient can decrease, remain constant and increase with speed [**5.8, 5.9**] and such a variable behaviour can be seen in the plots below. The simple hydrodynamic theory would predict that at high stroke length and thus increased speed, the amount of lubricant would be enough to separate the sliding surfaces and the friction would be lower. With temperature increase however, due to viscosity decrease, some solid interactions might occur which would shift the lubrication towards the mixed regime thus increasing friction. This seems to be the general behaviour with the low and high viscosity oils but not with the medium viscosity one. In this case, for temperatures higher than 80°C, the coefficient of friction is almost constant even dropping slightly. This might be explained by looking at the film thickness

results for oil R518 in Appendix A. This oil forms quite a thick boundary film which is present at high temperatures as well thus compensating for the decrease in viscosity and providing a low friction coefficient in the more severe conditions

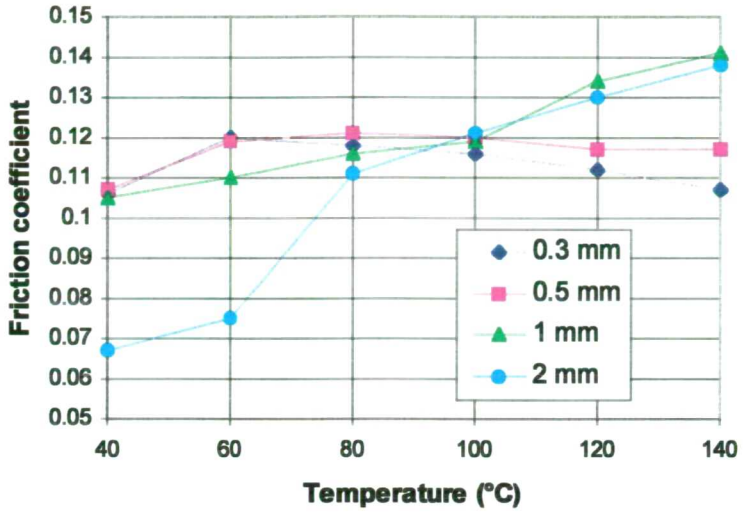


Fig.5.7. Oil R502 - Friction coefficient variation with stroke length

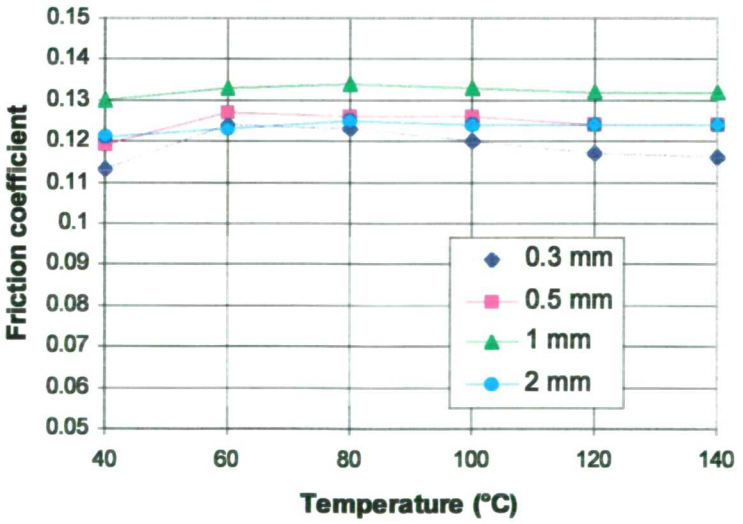


Fig.5.8. Oil R518 - Friction coefficient variation with stroke length

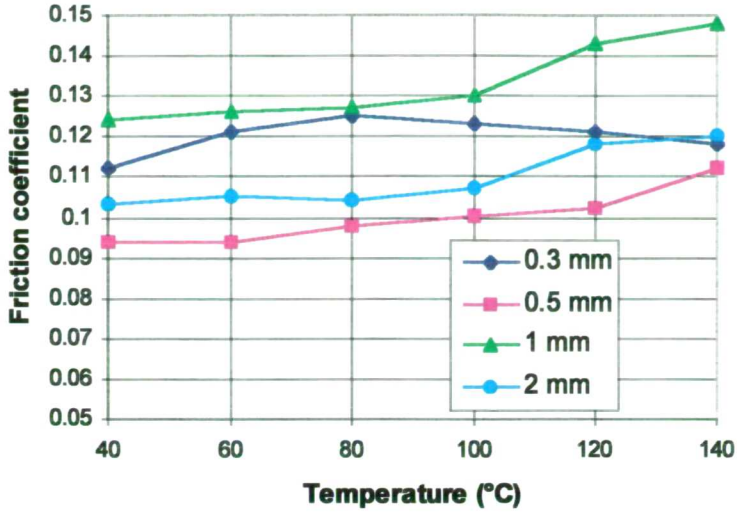


Fig.5.9. Oil R517 - Friction coefficient variation with stroke length

At lower sliding speeds, the hydrodynamic factor is less and one would expect higher values of friction than for higher speeds which is generally the case for lower temperatures. The general trend is an increase in friction up to 60 or 80°C followed by a decrease at higher temperatures which brings friction back to values close to the low temperature ones. All three oils follow this behaviour very closely apart from oil R517 that fails to at stroke 2. The decrease in friction with temperature may well be due to additive reaction or oil oxidation at temperatures higher than 80°C. Unlike the hydrodynamic regime, friction in boundary lubrication relies mainly on surface phenomena and the formation of a chemically reacted surface layer might well provide lower friction.

From the above discussion it can be seen that there is a considerable variation in boundary friction behaviour with speed. The test conditions chosen and shown in table 4.3 are considered to be the most appropriate for the friction tests. A 20 Hz frequency with 1 mm stroke gives a mean sliding speed of 0.02 m/s. At this speed, the film thickness value for R517 from figure 5.1a is about 19 nm at 40°C. The composite surface roughness for ball and flat is of the order of 50 nm and this would give a specific film thickness less than 0.4 which is less than 1, the value where boundary regime is considered to begin. This suggests that in the conditions chosen the system works, at least to a large extent, under the boundary regime. The analysed case should cover all the other situations since it was made for the most viscous oil at the lowest temperature.

Boundary friction coefficients for all test oils are listed in table 5.5 at 6 temperatures. The values represent the average value of μ over 9.5 minutes run, neglecting the first 30 seconds of the test. The friction coefficients tend to increase with temperature, probably because at low temperatures, the mixed lubrication component is reduced due to the higher viscosity of the lubricant under these conditions. The low friction coefficients for the two energy efficient oils can be clearly seen. At 100°C, friction coefficients in the range of 0.086 to 0.147 were found.

Nr	Oils	μ40 at 40°C	μ60 at 60°C	μ80 at 80°C	μ100 at 100°C	μ120 at 120°C	μ140 at 140°C
1	R 502	0.105	0.110	0.116	0.119	0.134	0.141
2	R 513	0.117	0.122	0.123	0.123	0.128	0.124
3	R 515	0.122	0.122	0.123	0.120	0.121	0.121
4	R 516	0.128	0.132	0.137	0.147	0.146	0.147
5	R 517	0.124	0.126	0.127	0.130	0.143	0.148
6	R 518	0.130	0.133	0.134	0.133	0.132	0.132
7	R 519	0.131	0.134	0.140	0.146	0.144	0.141
8	R 520	0.123	0.126	0.132	0.141	0.146	0.146
9	epv22d	0.109	0.099	0.098	0.086	0.094	0.110
10	epv23-3	0.101	0.094	0.086	0.088	0.092	0.100

Table 5.5. Boundary friction data for Sequence VI oils

5.1.5. Viscometric results

Table 5.6 lists the HTHS and low shear rate kinematic viscosity measurements made on all fluids tested. Viscosity was measured at 10^6 s^{-1} at 100°C and 150°C. It was not possible to attain these shear rates at lower temperature and high shear rate measurements at 60°C and 80°C were made at 10^5 s^{-1}.

Nr	Oils	HSvis 60°C cP	HSvis 80°C cP	HTHS 100°C cP	HTHS 150°C cP	Kvisc 40°C cSt	Kvisc 60°C cSt	Kvisc 80°C cSt	Kvisc 100°C cSt
1	R 502	15.08	8.56	5.49	2.33	36.57	18.17	10.48	6.73
2	R 513	22.23	11.22	7.40	3.04	73.08	32.86	17.56	10.62
3	R 515	19.48	10.47	6.70	2.96	62.04	30.10	16.93	10.63
4	R 516	20.84	11.03	7.00	3.01	77.18	34.97	18.74	11.35
5	R 517	23.81	12.90	8.40	3.64	93.79	43.10	23.22	14.07
6	R 518	14.44	8.19	5.38	2.51	55.25	27.23	15.50	9.82
7	R 519	17.90	9.85	6.53	2.93	61.88	29.74	16.63	10.39
8	R 520	20.32	10.82	6.92	2.95	68.68	31.69	17.23	10.55
9	epv22d	20.87	11.85	6.68	3.00	61.53	29.14	16.14	10.02
10	epv23-3	18.08	9.77	5.80	2.56	47.14	22.65	12.73	8.01

Table 5.6. Viscometric data for Sequence VI test oils
courtesy of Exxon Chemical

Other rheological parameters examined for consideration in correlation work, were (i) measures of shear thinning, i.e. the ratio of high shear rate viscosity to low shear rate viscosity and (ii) measures of viscosity-temperature sensitivity, i.e. the ratio of low shear rate viscosity at 40°C to that at 100°C. These properties are included in table 5.7. Also an equivalent measure of pressure-viscosity coefficient, 07FilmKv40 etc. was used, which represents the EHD film thickness at 1m/s divided by the kinematic viscosities raised to the power 1/0.7 at the same temperature.

Nr	Oils	Kvisc40°C/ Kvisc100°C	HTHS/Kvisc 60°C	HTHS/Kvisc 80°C	HTHS/Kvisc 100°C	HTHS/Kvisc 150°C
		K40K100	HTHSK60	HTHSK80	HTHSK100	HTHSK150
1	R 502	5.43	0.83	0.82	0.81	0.75
2	R 513	6.88	0.68	0.64	0.69	0.71
3	R 515	5.84	0.65	0.62	0.63	0.65
4	R 516	6.80	0.60	0.59	0.62	0.66
5	R 517	6.67	0.55	0.56	0.60	0.65
6	R 518	5.63	0.53	0.53	0.55	0.59
7	R 519	5.96	0.60	0.59	0.63	0.66
8	R 520	6.51	0.64	0.63	0.66	0.68
9	epv22d	6.14	0.71	0.73	0.66	0.71
10	epv23-3	5.89	0.79	0.76	0.72	0.74

Table 5.7. Other rheological parameters for Sequence VI test oils

5.2. Results for Sequence VI A oils

A similar approach was applied to the series of ASTM Sequence VI A reference lubricants. As described in section 3.3.2.2, with this test the oil performance is measured in 6 operating stages instead of two used for the Sequence VI test.

5.2.1. Lubricants employed

Data on Sequence VI A reference lubricants are shown in table 5.8

Nr	Oils	SAE grade	%EFEI	Stage 1	Stage 2	Stage 3	Stage 4	Stage 5	Stage 6
1	BO-2	5W30	0.01	0	0	0	0	0	0
2	R530	20W50	-1.699	-0.095	-2.166	-2.87	-2.096	-2.414	-3.382
3	R531	10W30	0.377	1.101	0.833	0.455	0.269	0.562	-0.336
4	R532	5W30	0.683	-1.06	0.975	1.431	0.975	1.456	0.64
5	R533	5W30	0.673	1.114	0.683	1.045	0.672	1.056	0.721
6	R534	5W30	0.599	-0.736	1.19	1.295	0.761	1.139	0.452
7	R535	5W20	1.411	0.488	2.442	2.332	1.7	1.976	1.405
8	R536	5W30	1.066	1.522	0.969	1.877	1.227	1.554	0.789
9	R1002	10W30	0.400	0.37	0.502	0.84	0.392	0.632	0.426

Table 5.8. Sequence VI A reference oils, test performance data

5.2.2. Test results

The results obtained on bench tests for Sequence VI A reference oils are outlined in this section. Film thickness, traction coefficient, boundary friction coefficient and viscometrics of the set of nine oils are shown in tables 5.9. to 5.12

Nr	Oils	EHD 40°C	EHD 60°C	EHD 80°C	EHD 100°C
1	BO-2	0.261	0.154	0.1	0.071
2	R530	0.465	0.23	0.137	0.097
3	R531	0.269	0.151	0.092	0.067
4	R532	0.205	0.128	0.077	0.056
5	R533	0.185	0.109	0.071	0.047
6	R534	0.197	0.115	0.074	0.049
7	R535	0.182	0.109	0.07	0.051
8	R536	0.178	0.104	0.068	0.046
9	R1002	0.224	0.135	0.089	0.061

Table 5.9. Sequence VI A oils: EHD film thickness at 1m/s entrainment speed (μm)

Nr	Oils	Trac40°C	Trac60°C	Trac80°C	Trac100°C
1	BO-2	0.043	0.036	0.028	0.028
2	R530	0.063	0.058	0.052	0.052
3	R531	0.063	0.053	0.045	0.045
4	R532	0.058	0.049	0.041	0.041
5	R533	0.056	0.048	0.041	0.041
6	R534	0.058	0.048	0.041	0.041
7	R535	0.048	0.04	0.031	0.031
8	R536	0.057	0.047	0.039	0.039
9	R1002	0.058	0.051	0.043	0.043

Table 5.10. Sequence VI A oils: limiting traction coefficient

Nr	Oils	μ 40°C	μ 60°C	μ 80°C	μ 100°C	μ 120°C	μ 140°C
1	BO-2	0.102	0.102	0.101	0.099	0.096	0.097
2	R530	0.112	0.114	0.117	0.121	0.126	0.126
3	R531	0.105	0.105	0.12	0.135	0.136	0.138
4	R532	0.11	0.127	0.126	0.128	0.13	0.13
5	R533	0.101	0.107	0.115	0.124	0.128	0.126
6	R534	0.11	0.112	0.113	0.112	0.112	0.114
7	R535	0.097	0.081	0.073	0.075	0.082	0.088
8	R536	0.109	0.107	0.104	0.101	0.099	0.098
9	R1002	0.111	0.11	0.113	0.113	0.114	0.116

Table 5.11. Sequence VI A oils: Boundary friction results

Nr	Oils	Kvisc40 cSt	Kvisc100 cSt	HTHS100 cP	HTHS150 cP
1	BO-2	59.95	10.28	8.12	3.37
2	R530	148.84	17.18	10.96	4.38
3	R531	72.99	10.83	7.31	3.15
4	R532	63.78	11.17	6.02	2.93
5	R533	63.32	11.25	5.99	2.91
6	R534	59.62	10.14	6.79	3.08
7	R535	42.43	8.4	5.71	2.59
8	R536	61.1	10.32	6.3	2.87
9	R1002	75.2	11.16	7.18	3.19

Table 5.12. Sequence VI A oils: Viscometric properties

These bench test results are used in the subsequent chapter for engine fuel efficiency prediction. They are correlated with fuel economy data available from ASTM engine tests by means of statistical analysis.

REFERENCES

[5.1] Benchaita M.T. and Lockwood F.E., "Reliable Model of Lubricant-Related Friction in Internal Combustion Engines", Lubrication Science 5-4, July 1993,

[5.2] Dowson D. and Hamrock B.J., "Elastohydrodynamic Lubrication, the Fundamentals of Roller and Gear Lubrication", Pergamon Press, Oxford, 1966,

[5.3] Tripaldi G., Vettor A. and Spikes H.A., "Friction behaviour of ZDDP Films in the Mixed Boundary/EHD Regime", SAE paper no. 962036, 1996,

[5.4] Smeeth M., Gunsel S. and Spikes H.A., "Boundary Film Formation by VI Improvers", Trib. Trans., 39, 3, pp. 726-734, 1996,

[5.5] Hamrock B.J., Jacobson B.O. and Bergstrom S.I., "Measurement of the Density of Base Fluids at Pressures to 2.2 GPa", ASLE Trans., 30, no. 2, pp. 196-202, 1987,

[5.6] Johnston G.J., "A Study of Lubricating Films Generated by Organo-Phosphorus Anti-Wear Additives", PhD Thesis, Imperial College, University of London, 1990,

[5.7] Aderin M.E., "Interferometric Studies of Thin Lubricant Films in Concentrated Contacts", PhD Thesis, Imperial College, University of London, 1994,

[5.8] Bowden F. P., Tabor D., "The Friction and Lubrication of Solids", Part I, 2nd edition, chap. 9, 11, Clarendon Press, 1954,

[5.9] Grunberg L. and Campbell R.B., "Metal Transfer in Boundary Lubrication and the Effect of Sliding Velocity and Surface Roughness", Proc. IMechE Conf. Lubrication and Wear, pp. 291-301, 1957,

CHAPTER 6

FUEL EFFICIENCY PREDICTION WORK

The bench test results from chapter 5 are correlated with fuel efficiency performance from Sequence VI and VI A engine tests using multiparametric regression. The work is carried out first for the reference lubricants used in ASTM Sequence VI fuel economy test and a similar approach is then used for the reference oils from ASTM Sequence VI A. Another statistical technique, discriminant function analysis, is used for oils on which Sequence VI A efficiency data were available.

6.1 Regression analysis

The lubricant performance data obtained from bench tests were analysed and correlated with engine test results using a linear regression technique. Initially, regression was made using the software package incorporated in Microsoft Excel (version 5.0), but as more parameters were obtained to characterise the lubricant behaviour, it was convenient to develop a computer program able to automatically calculate the regression equation and coefficient R^2 for all the possible combinations of the available bench test parameters. This program, written in Fortran 77, is listed in appendix D. The program also has the facilities to fit the data to a polynomial expression of the form :

$$Y = A + B*X_1^{p1} + C*X_2^{p2}.+ D*X_3^{p3} \qquad (E6.1)$$

where p1, p2 and p3 are powers not necessarily equal to unity. However, raising the data to different powers (0.5; 2; 3) showed no great difference from the results obtained with linear fitting, so this was not pursued further.

6.1.1. Sequence VI correlation results

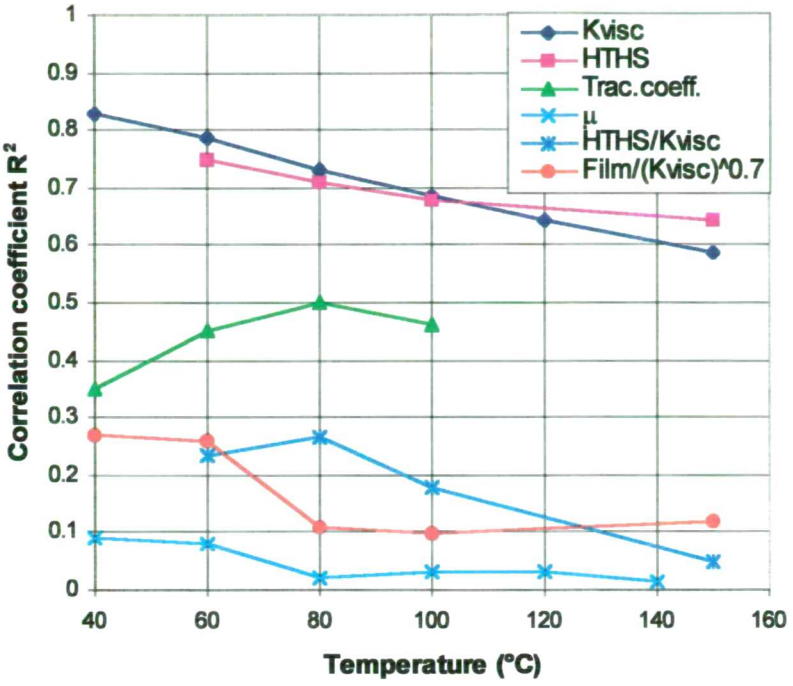
As it was indicated in paragraph 3.3.2.1, Sequence VI test consists of two separate phases, one R150 run at 65°C (150°F) and the second, R275 at 135°C (275°F). In this study, unlike previous ones, regression correlation was made to the two separate phases of the Sequence VI test and not directly to the composite %EFEI values. This was important since the two stages represent very different engine conditions and thus a quite different balance of regimes of lubrication. Fitting each phase separately to measured bench test parameters enabled a wider range of measured, relevant lubricant parameters to be correlated with engine performance data. The predicted fuel efficiencies from these two phases were then combined to generate the overall efficiency, %EFEI, according to equation 3.1.

Regression analysis was made with one, two and three bench test parameters.

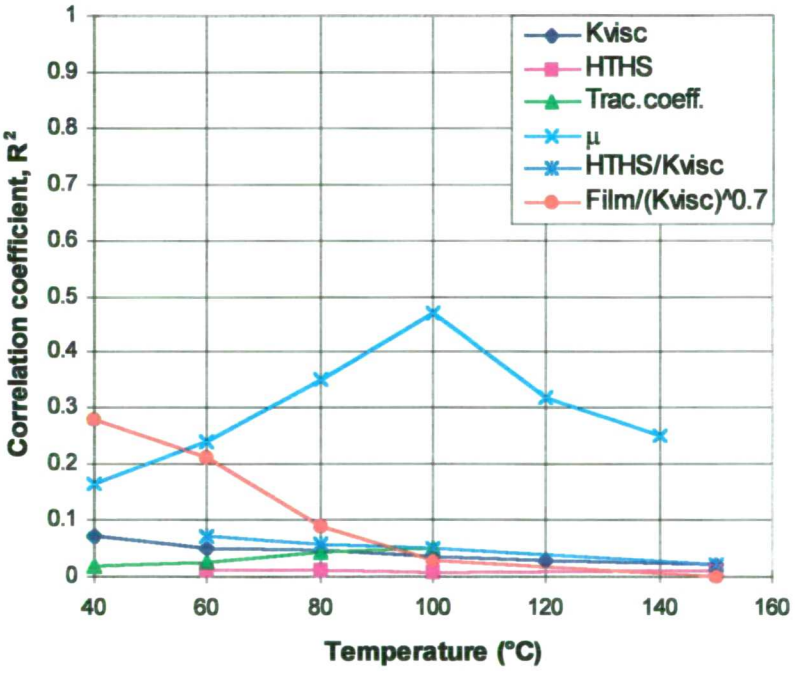
6.1.1.1. Single parameter correlations

Initially, single bench test parameters were correlated. This was helpful for evaluating the contribution to efficiency of each parameter taken on its own and showed the importance of viscometric terms for R150 but not for R275 (figure 6.1). The largest R^2 correlation coefficient is likely to be indicative of a significant effect of the parameter on engine fuel efficiency.

However, these single correlations were also somewhat misleading since they were strongly influenced by the particularities of the oil set used. For example, when the original eight oils alone were correlated, the R150 stage showed only slight correlation with boundary friction, whilst traction showed higher correlation (R^2 = 0.35 to 0.5, as shown in figure 6.1a), indicating the latter to be the most significant of all parameters except viscosity.



(a) correlation with R150 stage



(b) correlation with R275 stage

Fig.6.1. Single correlation with R150 and R275: importance of parameters

However, when the two fuel efficient oils were included, the correlation changed markedly. The correlation of R150 with boundary friction became much more important, with R^2 between 0.5 and 0.67, whilst that for traction became very small. The same trend was shown by the high temperature stage correlation; the two highly fuel-efficient oils changed the correlations to emphasise boundary friction coefficients (a maximum R^2 of 0.76 was obtained for μ at 100°C) and by decreasing the strength of traction. This is because these fuel efficient oils possessed low friction coefficients but not especially low traction coefficients.

Appendix E shows single parameter correlations with efficiencies from R150 and R275 stages for all ten oils (in this table, the properties 07FilmKv40 etc. were the EHD film thickness at 1m/s divided by the kinematic viscosities raised to the power 1/0.7 at the same temperature. According to EHD theory, these were equivalent to measures of pressure-viscosity coefficient). Note that in this appendix and also in appendices F and G (with three-parameter fits), the coefficients for each term are normalised, by dividing by the mean value of all ten measured values in the data set. This reduces the coefficients of all parameters to similar values; in effect giving each parameter similar-sized units.

As a further example of the vagaries of single parameter correlation it can be seen that for both R150 and R275, the correlation with the ratio of HTHS/Kvisc is positive; i.e. low shear thinning correlates with high fuel efficiency. This is contrary to normal belief and may reflect the fact that the two fuel efficient oils happen to show a low degree of shear thinning; possibly due to their having a synthetic base fluid component.

6.1.1.2. Multiple parameter correlation

Multiple parameter regression fitting allowed second parameters, which were swamped by more strongly correlating ones, to show their significance. In practice it was not useful to develop correlation equations with more than three bench test parameters, since the size of the engine test data set was not large enough to statistically accommodate more than this number. Correlation was carried out in two slightly different ways.

(a) "Arbitrary" correlation

Firstly, the fuel efficiency was arbitrarily correlated with all possible combinations of groups of two or three measured bench test properties. From the closeness of the correlation (the R-squared value), it was then possible to identify those combinations of lubricant properties which were most influential in determining the fuel efficiency. With two parameters, regression coefficients up to 0.8 were quite common and with three parameters coefficients up to 0.9 were easily attainable. In general, correlations with R150 showed that viscometrics are important for the model, whilst those with R275 emphasised the boundary and EHD friction parameters (μ and low speed traction).

Appendix F contains three parameter fits for R150 for which R^2 was greater than 0.88 and appendix G holds similar fits for R275 for $R^2 > 0.85$. There were far more high correlation fits for R150 than for R275 and only five R275 correlations had R^2 greater than 0.88. In this high temperature phase, two oils R516 and R519 showed anomalous behaviour in that their %EFEI was significantly worse than predicted from the correlation equations. Consideration of their mixed friction curves (see chapter 5, figure 5.4) shows that for these two fluids, as the rolling speed and thus the EHD film thickness is reduced, friction rises from the EHD value at higher speeds than for the other oils. This might be due to a poor ZDDP additive balance.

This approach yielded predictive FE equations. The preferred ones were not necessarily the ones with the highest correlation coefficients; it was considered that minor variations in R^2 at the high end were largely controlled by statistical scatter. Fits selected for use were those that gave high R^2 values, obeyed tribological common sense and also seemed robust, in that closely-related data, such as measurements of the same parameters at slightly different temperatures, also gave high correlations.

For R150, one promising expression was

$$R150 = 7.98 - 58.08*(EHD80) - 29.34*(\mu 120) + 4.94*(HTHSK100) \qquad (E6.2)$$

with the regression coefficient R^2 = 0.926. EHD80 is the film thickness in nm at 1 m/s and 80°C, μ120 is the friction coefficient at 120°C and HTHSK100 is the ratio of HTHS viscosity to kinematic viscosity, both at 100°C. The latter is effectively a measure of the of shear thinning, with a high value representing small amounts of shear thinning. At first this expression seems puzzling since whilst it predicts high efficiency with low values of EHD film thickness (effectively viscosity) and boundary friction, since both coefficients are negative, the third term is positive. This means that an oil which shows little shear thinning is highly efficient.

However, upon consideration this is as expected, since it must be remembered that the viscosity term, EHD film thickness, is already a very high shear rate measure. From this criterion, a high shear rate viscosity dependency would imply a high viscosity measured at low shear rate, which is clearly undesirable.

From the lubricant design point of view, rather than a fuel economy-predictive one, another convenient expression might be one containing low shear rate viscosity, such in:

$$R150 = 16.9 - 0.17*(Kvisc80) - 55.6*(\mu 60) - 6.8*(HTHSK100) \qquad (E6.3)$$

with the regression coefficient R^2 = 0.871. Kvisc80 is the kinematic viscosity in cSt at 80°C, μ60 is the friction coefficient at 60°C and HTHSK100 is, once again, the ratio of HTHS viscosity over kinematic viscosity, both at 100°C.

In this expression the shear thinning term is negative, i.e. the more shear thinning the better from the point of view of fuel economy. Again this is logical since, in this case, the viscosity term is a low shear rate value; a low value for HTHSK100 now implies an even lower viscosity at high shear rate.

A promising expression for the R275 phase was found to be:

$$R275 = 27.3 - 123*(\mu 120) - 77.4*(Trac70SRR) - 0.96*(50Tr01Tr1) \qquad (E6.4)$$

with regression coefficient R^2 = 0.864 and where μ120 is the friction coefficient at 120°C, Trac70SRR is the traction coefficient at 70% slide/roll ratio and 135°C and 50Tr01Tr1 is the relative traction coefficient increase between 1 m/s and 0.1 m/s at 50% slide/roll ratio and 135°C (as given by the expression E5.2).

An alternative, based on EHD film thickness is:

$$R275 = 35.22 - 312*(EHD100) - 139*(\mu 100) + 456*(07FilmKv80) \qquad (E6.5)$$

with regression coefficient R^2 = 0.905 and where 07FilmKv80 is the EHD film thickness at 1 m/s divided by the kinematic viscosity raised to the power 1/0.7, both at 80°C.

By combining the two equations E6.2 and E6.4 using equation E3.1, it was possible to predict overall fuel efficiency %EFEI which gave a regression coefficient R^2 = 0.884 when compared with the measured values (figure 6.3).

Figures 6.2 and 6.3 show the comparisons between efficiencies measured in engine tests and those predicted by the expressions selected

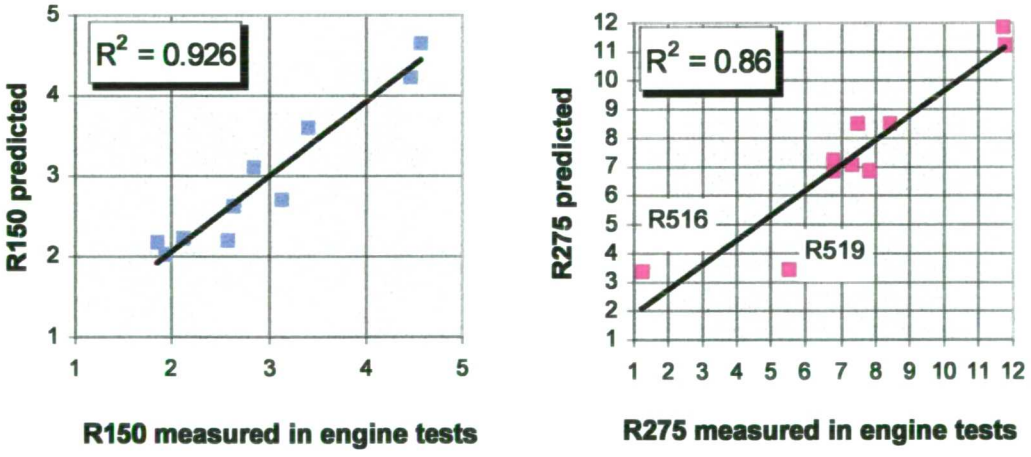


Fig.6.2. R150 and R275-comparison between measured and predicted values

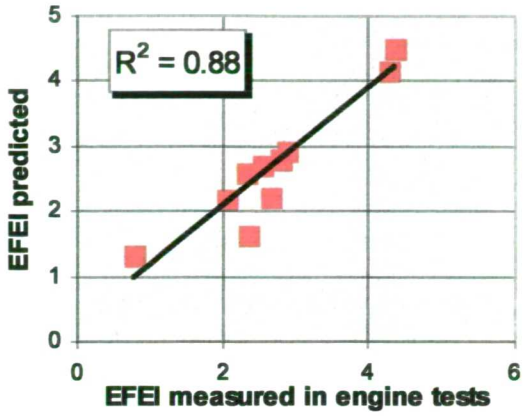


Fig.6.3. EFEI-comparison between measured and predicted values

(b) Weighting regimes of lubrication

The second approach for multiple parameter correlations was to deliberately correlate with fuel efficiency, three lubricant properties known to be related to the friction in the three regimes of lubrication, hydrodynamic, EHD and boundary. This enabled the relative importance of each lubrication regime to fuel efficiency in each engine test phase to be determined. Two of the strongest correlations thus found are shown below:

$R150 = 7.5 - 0.31*HTHS - 37.5*Trac$, with $R^2 = 0.92$

$R275 = 20.72 + 0.4*HTHS + 316*EHD - 163*\mu$, with $R^2 = 0.82$

For direct comparison of the relative importance of hydrodynamic, EHD and boundary lubricating properties of lubricants, the correlation coefficients were normalised by multiplying them by the average value of the appropriate property for the set of lubricants tested. Figure 6.4 shows the relative importance of different lubricant properties in the two phases of Sequence VI test. If the analysis is valid, then the changes in importance of the terms with changing operating conditions will be consistent with the theories of oil film behaviour.

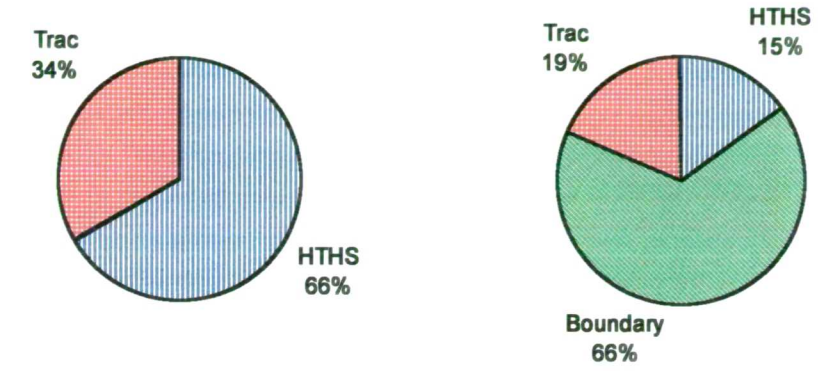


Fig.6.4. Contribution of lubrication regimes to each Sequence VI phase

It can be seen that the low temperature phase R150, is strongly dominated by the HTHS (hydrodynamic) viscosity with a significant contribution from EHD traction (mixed). Boundary friction contribution is insignificant. Phase two of the test differs only in that the oil temperature is increased from approximately 65°C to 135°C. This increase in temperature results in a decrease in oil viscosity and thus in film thickness. This would be expected to result in less hydrodynamic and more boundary lubrication in the engine. The analysis shows this to be the case and boundary friction is now the dominant term.

6.1.2. Sequence VI A correlation results

Regression analysis of the data on Sequence VI A oils was used to generate correlations between the various bench tests and fuel economy performance of the oils in all 6 phases of the test. These correlations also produced prediction equations which are shown in the table below.

Phase	A_0	HTHS	Trac	μ	R^2
1	12.36	0.128	95.68	64.21	0.93
2	7.91	0.30	29.52	21.43	0.94
3	7.19	0.45	3.91	8.88	0.96
4	5.40	0.32	7.91	8.12	0.97
5	4.87	0.16	3.03		0.99
6	5.46	0.17	21.68		0.98

Table 6.1. Sequence VI A tests: correlation equations

In table 6.1, A_0 is the constant term, R^2 is the correlation coefficient and all the remaining terms are the coefficients that multiply the parameter which is the header of the respective column.

By normalising the coefficients, the relative importance of different lubricant properties could be estimated as for the Sequence VI case. Figure 6.5 shows such an attempt.

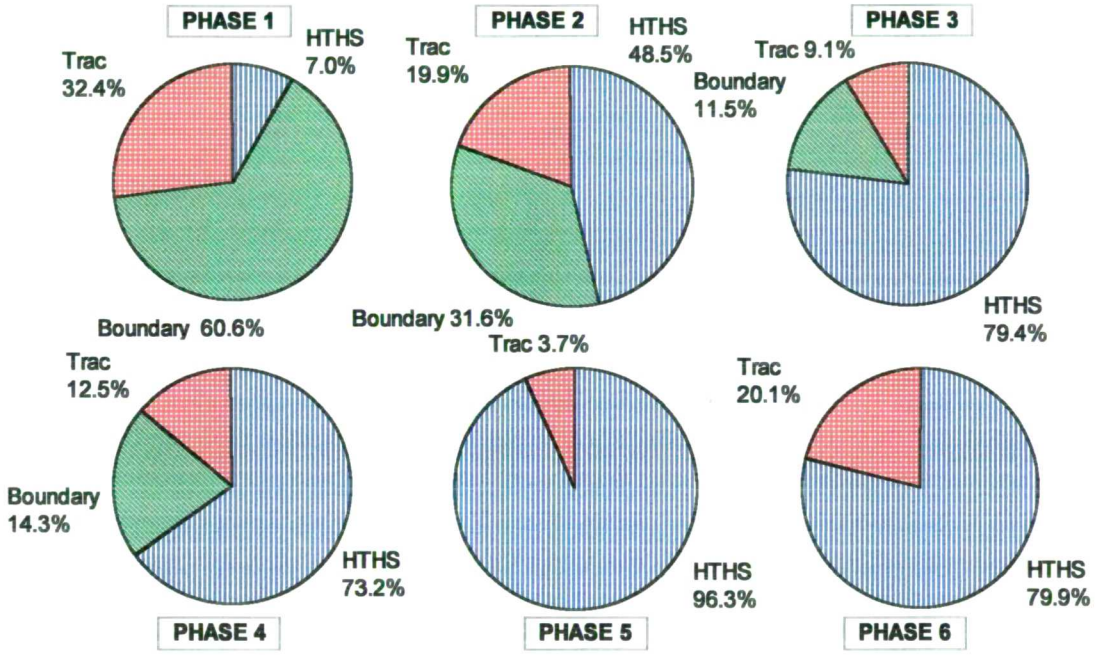


Fig.6.5. Contribution of lubrication regimes to all Sequence VI A stages

Phase 1 of the test is run at the highest temperature (105°C) which means that the viscosity of the oil and the film thickness will be at their lowest. In this stage the dominant factor in determining fuel economy is the coefficient of boundary lubrication. There is a large contribution from the traction coefficient and only a small contribution from HTHS viscosity. Boundary lubrication, as will be seen, is much less important in the other, lower temperature phases of the test.

Phase 2 differs from phase 1 only in that the temperature of the oil is lower (70°C) and hence the viscosity and oil thickness are higher. This should lead to a shift of emphasis towards the mixed and hydrodynamic regimes. The analysis confirms this; boundary

friction has decreased in importance (but is still significant), HTHS viscosity has increased in importance and EHD traction coefficient has decreased. All of this is consistent with the shift from boundary to mixed/hydrodynamic lubrication.

Phase 3 is run at the same temperature as phase 2 but at a higher speed. This would imply in theory that the oil thickness in phase 3 to be higher than in phase 2. The analysis shows that phase 3 is dominated more by the HTHS viscosity than is phase 2 and that both traction and boundary friction have become much less significant. Again these observations are entirely consistent with established theory.

Phase 4 of the test differs from phase 3 in that the applied load is increased. This should result in a reduction in hydrodynamic oil film thickness and a consequential shift towards the mixed and boundary regimes. The significance of boundary and traction coefficients is increased whilst the importance of HTHS viscosity is diminished.

Phase 5 is run at a lower temperature (45°C) than phase 4. As a consequence of this the viscosity and film thickness are increased. The increase in the contribution of HTHS viscosity and the decrease in the importance of boundary and traction terms is consistent with this.

The last phase is run at the same temperature as phase 5, but the engine speed is further reduced. This results in a decrease in film thickness which is consistent with the observed increase in the contribution from the EHD traction term on the correlation equation.

6.1.3. Comparison of Sequence VI and VI A tests

The overall performance of the reference oils in the two tests are shown in figure 6.6. These are obtained by combining the correlation coefficients for each lubricant property in each test phase according to the Sequence VI (equation E3.1) and Sequence VIA (equation E3.5) rules for determining the overall engine test efficiency from measured test phase results.

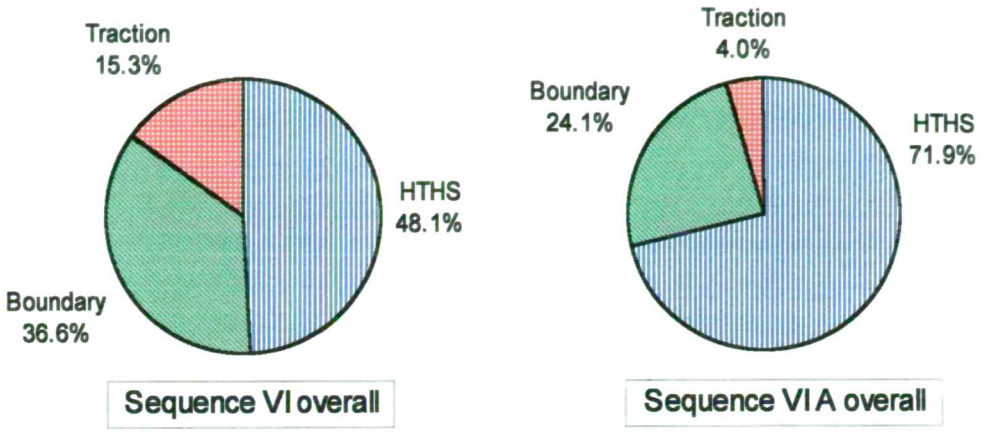


Fig.6.6. Contribution of lubrication regimes to overall Sequence VI and VI A performance

This analysis confirms that the new Sequence VIA test differs significantly from its predecessor in the balance between the various lubrication regimes. It is more responsive to viscometric changes and less responsive to mixed and boundary friction changes than Sequence VI test.

This difference in balance is probably due to a combination of differences in engine design and the lower temperatures encountered in the Sequence VIA test. The small contribution of EHD traction to efficiency in the Sequence VIA may well reflect the use of roller followers rather than sliders as used in the Sequence VI engine.

Both tests, however, respond to changes in viscometric, EHD traction/film thickness and boundary friction properties of lubricants.

6.2. Discriminant function analysis

Another approach to statistical analysis of the data available was to use discriminant functions. Like linear regression, discriminant function analysis is a multivariate technique and as with most such methods, they are interchangeable [**6.1**] and can be used as complementary techniques. Thus discriminant function (DF) can be considered as a multiple regression analysis with the dependent variable taken as the criterion for division into subgroups. The most influential parameters identified from DF analysis to

produce good discrimination can then be used in a regression analysis to give the best fit for the dependent variable.

Discriminant function technique is suited to multi-variable dependent problems and results in a series of weighting parameters which quantify the relevance of each variable to the overall outcome. The most common situation is that of a population which needs to be separated into two groups of individuals based on measurements for these individuals of several variables. The probability that a given individual comes from either of the two groups depends upon both the separation of the group means and the variance within the groups. Thus if the group means are widely separated and the variation within each group is relatively small, the probability of a good classification is quite high. In general, if several properties of the individuals are given or measured, it may be found that some linear function of these variables is more efficacious in distinguishing the groups than is any one of them. When the purpose of the analysis is to determine a linear function of the variables that distinguishes most clearly between the two groups, the linear function is known as a "discriminant function" (DF). This linear expression contains many variables from each observation of the groups involved, but with each variable weighted by a constant that represents the discriminatory ability of that particular variable. The values of the constants (or weights) are found by maximising the overall ratio of group mean separation to within-group variation. When the number of data is big enough for both groups, the separation criterion usually used is the midpoint of the interval between the average of discriminant functions of the two groups.

In order to quantify the level of discrimination achieved, a more general concept of distance needs to be used. The most widely accepted method is the calculation of the Mahalanobis distance (D^2) which represents the squared difference between the group means. It is defined as:

$$D^2 = \left(\bar{x}_1 - \bar{x}_2\right)' S^{-1}\left(\bar{x}_1 - \bar{x}_2\right)$$

where $\bar{x}_1$, $\bar{x}_2$ represent the means for group 1 and 2 respectively and S^{-1} is the inverse of the covariance matrix ($p \times p$, p is the number of parameters).

More detailed theoretical explanations can be found in many textbooks dealing with discriminant function and multivariate analysis such as references **[6.2]**, **[6.3]**.

6.2.1. Data sample employed

Initially the data available for the nine Sequence VIA oils were used for the discriminant function analysis. Two groups were formed, the separation being based on the overall EFEI efficiency data. Thus oils that showed low EFEI were ascribed to group 1 whereas those with EFEI greater than 1 were classified in group 2. A Fortran 77 program listed in appendix H was developed which could calculate the best linear combination of 6, 5,...down to 2 parameters. The use of 6 and 5 parameters was not appropriate because the more parameters, the higher the risk of correlation to each other thus increasing the instability of the covariance matrix. Unfortunately only two oils had fuel efficiency greater than 1 which made the grouping quite unbalanced. The DF analysis basically requires a normal distribution of data and a set of only two data can not fit any probability density function. Thus to improve the data quality and enable the calculation of statistical parameters, more data were needed. Finally, data for another 5 oils supplied by Exxon Chemical Ltd. with known efficiency were added to the initial 9 which increased the group separation balance to 9:5. The following table shows the oils used together with the data on fuel efficiency.

Nr	Oils	SAE grade	%EFEI
	group 1		
1	BO-2	5W30	0.01
2	R530	20W50	-1.699
3	R531	10W30	0.377
4	R532	5W30	0.683
5	R533	5W30	0.673
6	R534	5W30	0.599
7	R1002	10W30	0.400
8	i11	5W30	0.908
9	i14	5W30	0.741
	group 2		
10	R535	5W20	1.411
11	R536	5W30	1.066
12	F14	na	1.453
13	i13	5W20	1.765
14	i15	5W20	1.264

Table 6.2. Two group separation based on efficiency data

The parameters used for discriminant function analysis are those from chapter 5, tables 5.9 to 5.12 for the nine reference oils. The viscosity data, EHD film thickness, EHD friction and boundary friction data for the additioned 5 oils are shown below:

Nr	Oils	Kvisc40 cSt	Kvisc100 cSt	HTHS100 cP	HTHS150 cP
1	F14	65	10.53	6.64	3.08
2	i11	52.64	10.22	6.36	2.92
3	i13	41.59	8.25	5.41	2.52
4	i14	52.65	10.37	6.38	3.05
5	i15	44.14	8.33	5.72	2.61

Table 6.3. Viscometric data for additional 5 oils

Nr	Oils	EHD 40°C	EHD 60°C	EHD 80°C	EHD 100°C
1	F14	0.184	0.114	0.077	0.053
2	i11	0.197	0.115	0.07	0.03
3	i13	0.153	0.096	0.051	0.033
4	i14	0.176	0.104	0.057	0.042
5	i15	0.173	0.106	0.064	0.04

Table 6.4. Film thickness data for the 5 added oils at 1m/s (μm)

Nr	Oils	Trac40°C	Trac60°C	Trac80°C	Trac100°C	Trac50%SR
1	F14	0.059	0.053	0.048	0.042	0.05
2	i11	0.051	0.042	0.033	0.025	0.045
3	i13	0.052	0.043	0.037	0.032	0.052
4	i14	0.063	0.056	0.051	0.047	0.08
5	i15	0.05	0.043	0.036	0.03	0.038

Table 6.5. Limiting traction coefficient and traction at 50% sliding for the 5 additional oils

Nr	Oils	μ 40°C	μ 60°C	μ 80°C	μ 100°C	μ 120°C	μ 140°C
1	F14	0.108	0.12	0.124	0.128	0.129	0.136
2	i11	0.089	0.073	0.068	0.08	0.102	0.117
3	i13	0.103	0.078	0.069	0.063	0.094	0.114
4	i14	0.122	0.123	0.121	0.124	0.126	0.126
5	i15	0.096	0.077	0.067	0.068	0.089	0.102

Table 6.6. Boundary friction coefficient for the 5 additional oils

The data on measured properties were used to calculate discriminant functions for all the possible combinations of any specified number of variables available. Selection of the best combination was based on maximising the Mahalanobis distance (D^2) which is related to the differences between the group means of the discriminant functions. Having calculated the coefficients (weights) for each parameter, the discriminant functions are defined and can be used as a classificatory device for oils with unknown fuel efficiency data. Because the variables have values which vary in magnitude, the direct comparison of coefficients as a measure of variable significance becomes difficult. To overcome this, variables from each data column were normalised by subtracting the mean and dividing by the standard deviation.

6.2.2. Results

When all 14 oils were used in the discriminant function analysis, the best combination with three parameters was found to be with HTHS viscosity @150°C, friction coefficient @ 120°C and limiting traction coefficient @ 100°C. The results are shown in the following figure where each dot represents the value of discriminant function calculated for each oil. The blue points are the DF for oils with low fuel efficiency (group 1) and the pink ones for oils with high fuel efficiency (group 2).

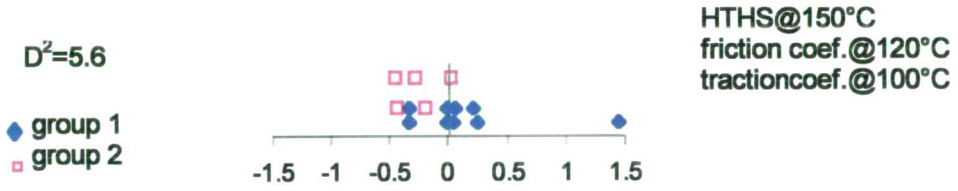


Fig.6.7. Discriminant functions distribution for the best three parameters for 14 oils

Two main findings need to be mentioned.

(i) the viscosity is the main parameter for best separation. The fact that a good discrimination was obtained (D^2=5.6) is due to the presence of oil no.2 with high viscosity and shows that the technique is able to detect parameters which improve the separation. However, the certainty of results would be increased if more data on oils with high viscosity were available.

(ii) the method is able to find the singularities in the data set. Although the separation came out quite significant (Mahalanobis distance D^2 was 5.6), it was misleading since there was not a good discrimination between the two groups. The discriminant functions distributions for the two groups almost overlapped each other, with only one value being away from the group: the DF for oil no.2. (figure 6.7.). Thus the anomalous property, the high viscosity in this case, is highlighted by the discriminant function analysis.

In the next stage, oil no.2 was removed from the data sheet and the result of discrimination for the same three parameters was as follows:

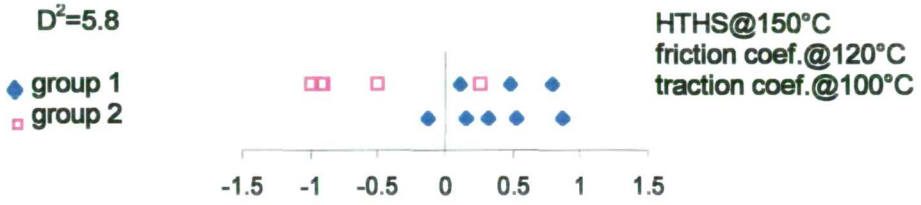


Fig.6.8. Discriminant functions distribution for the best three parameters for 13 oils

It is clear that by removing the exceptional data the discrimination has improved. The Mahalanobis distance is similar to that in the previous case but this time the magnitude is true since the values of DFs are grouped reasonably close and no values are far away from the group.

6.2.3. The influence of the number of parameters

It is mentioned in the literature [**6.4**] that the number of parameters used for DFs analysis should not be too large; the more parameters the higher the amount of calculation needed. The use of a larger number of variables also increases the risk of correlation between some of them and as a result, the instability of the covariance matrix. On the other hand, if the choice of variables is satisfactory, any additional variable will make an insignificant contribution. The number of parameters is also dependent on the amount of data available. For the current study with a relatively small number of data, the analysis was performed with 4, 3 and 2 parameters and the best combinations are shown in the following plots.

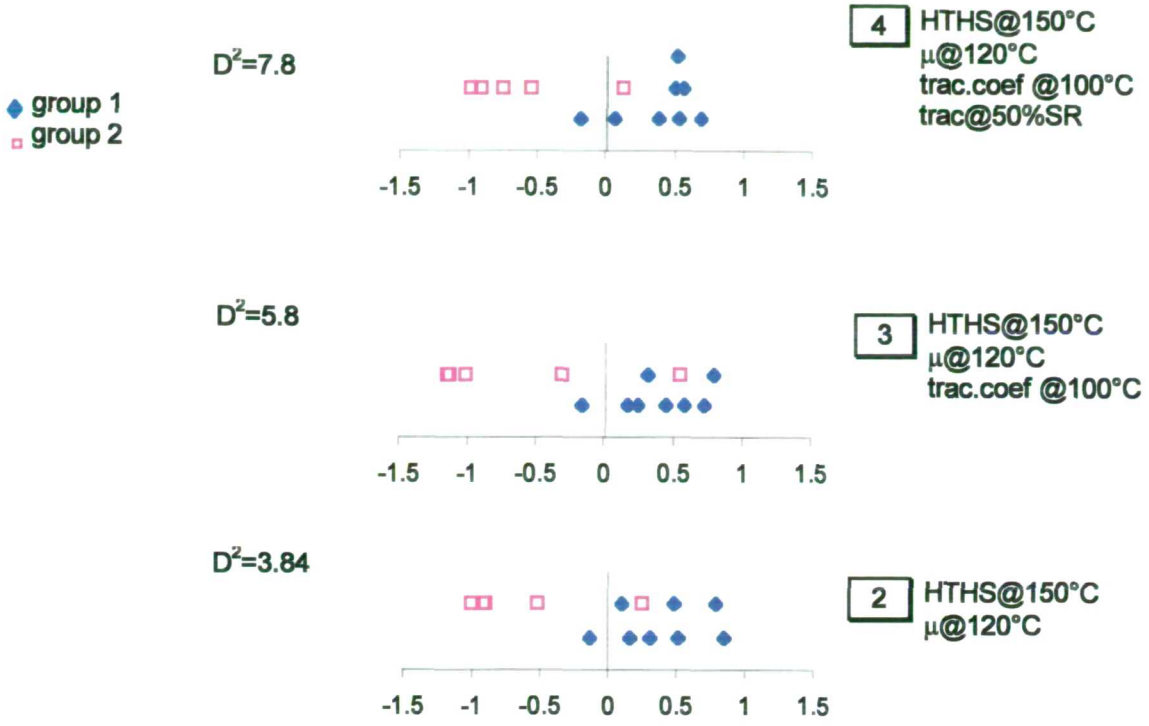


Fig.6.9. Discrimination plots for the best combination of 4, 3 and 2 parameters

It is clear from the above diagrams that the four parameter case i.e. HTHS viscosity, friction coefficient, limiting traction coefficient and traction coefficient at 50% sliding shows the best discrimination. However, for the reasons outlined above and also for reducing the measurement effort, decreasing the number of parameters is desirable. Thus when using three parameters the separation is still quite good and the data which cross the center line are not too far from it. With only 2 parameters though, the discrimination starts to deteriorate and the singular good data (pink empty square) is shifted more towards the centre of the bad data group (blue squares). But even so the discrimination given by HTHS viscosity and friction is still satisfactory which shows that traction is not such an important parameter since by removing it the separation was not significantly changed. This correlates well with the findings from the linear regression analysis that viscometrics are more important than friction from EHD and boundary regime.

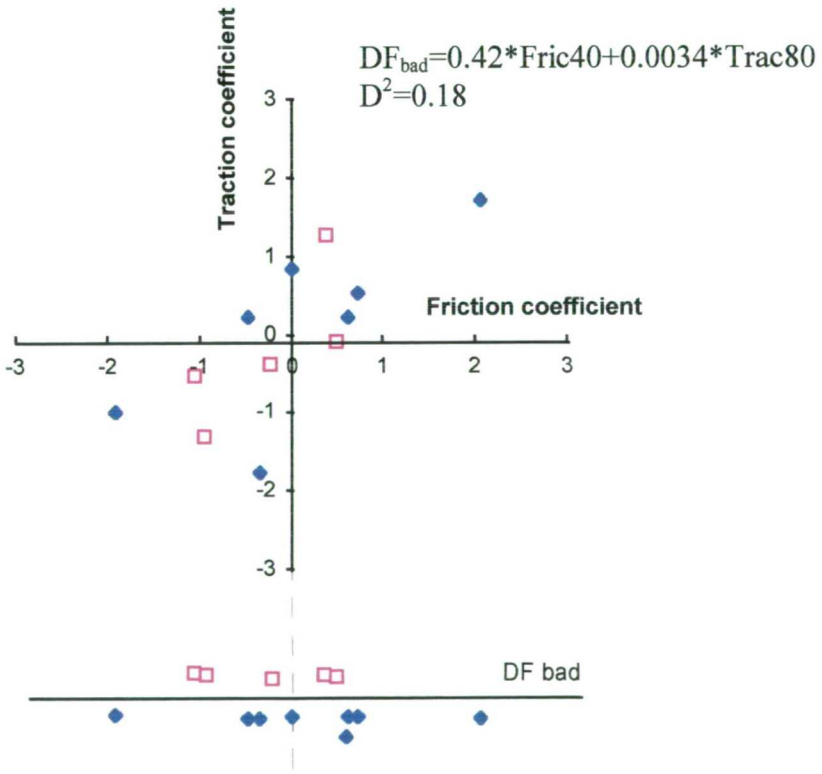
Figures 6.10a and b below compare bad and good choice of parameters. For better visualisation of the discriminant function, these two variable cases are represented in a plane of co-ordinates with the variables being on x and y axes. The data shown are

normalised as mentioned before. Having calculated the coefficients for the discriminant function in both cases, the discriminant direction can also be plotted and it is shown in a position shifted from the data area. The orthogonal projections of the normalised data on the discriminant direction give the distribution according to that particular direction (represented by the discriminant function).

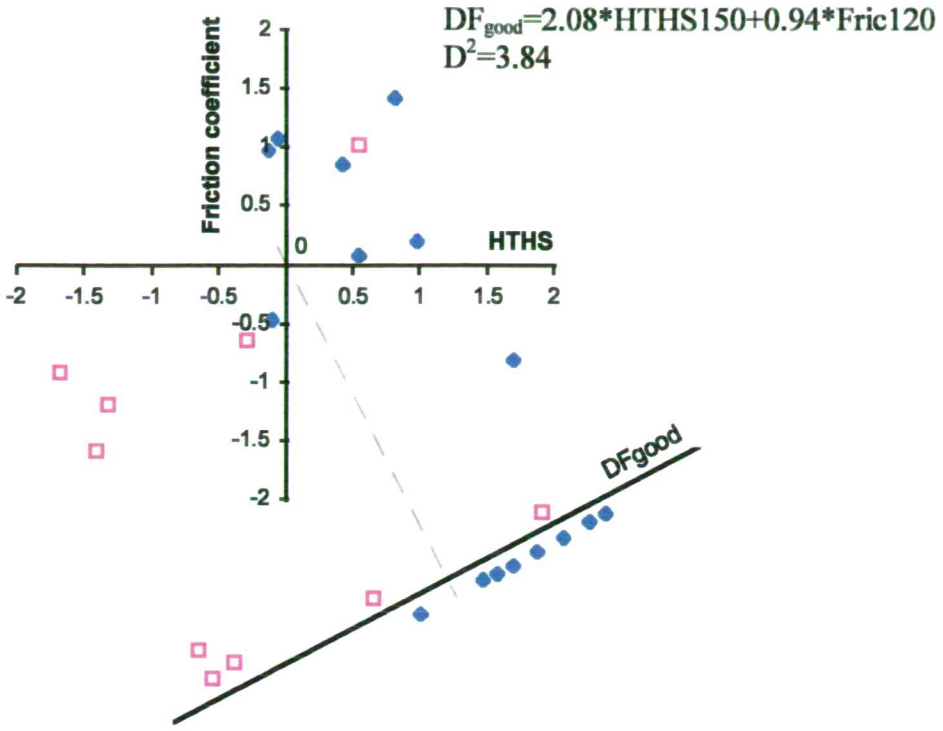
The discriminant function expressions for both situations are given below. The analysis of coefficients can give an indication on the significance of each individual variable. Although the sample size is not too large, the oils used are representative for the range used in industrial practice, their properties covering most of it. This enables us to directly compare the coefficients in order to establish the importance of parameters. It can be seen that HTHS has a higher coefficient than friction which shows that is the most important among the two.

$$DF_{good}=2.08*HTHS+0.94*Fric$$

$$DF_{bad}=0.42*Fric+0.0034*Trac$$



a) discrimination given by a bad choice of parameters



b) good choice discrimination

Fig.6.10. Parameter choice-comparison for two variable case

For the bad case, the coefficient for traction is extremely low. Thus traction can be neglected which leaves the friction plane to be the discriminant one (in figure 6.10a the discriminant direction is parallel to the friction axis). It is obvious that the separation is extremely poor, the projections of the data points for the pair of observations are overlapping and the Mahalanobis distance is insignificant (0.18). Since the chosen variables that give such a bad separation are friction coefficient @ 40°C and traction @80°C it can be concluded that friction at low temperatures is not so important for the test conditions from Sequence VI A.

6.2.4. Discussion

The use of discriminant functions was shown to be a useful tool for finding the singularities in the data set and for assigning an observation of unknown origin to one of the two groups. The calculated discriminant functions can be used as a mean for predicting the fuel efficiency for new oils which could be a real advantage both financially and time-wise.

It should be mentioned that the results obtained are representative for the sample of data used in the study and a larger sample would have been desirable from the statistical point of view. For the number of data available, the discriminant function analysis has shown that 3 parameters are enough for a good discrimination. The importance of HTHS viscosity as the main discriminatory parameter has been outlined. Boundary friction at high temperature is also a significant parameter whilst friction in EHD (traction) is the least important. From the regression work on Sequence VIA fuel efficiency prediction, it can be seen that traction is the least important parameter (4%) whereas dynamic viscosity (HTHS) has the highest impact on fuel efficiency (71.9%). Thus discriminant function analysis used as a means of grouping data, emphasised the same conclusion of regression fitting that, for Sequence VIA test conditions, the viscometrics are more important than mixed and boundary friction.

6.3. Conclusions

This work has shown the contribution of different types of friction to engine fuel efficiency. The changes in importance of these regimes when shifting from one test phase to another are entirely consistent with established theory. The study clearly shows that boundary friction is a major factor in high temperature engine test stages: 66% in R275 stage of Sequence VI and 60.6% in stage one of Sequence VI A tests. Low temperature stages however are dominated by hydrodynamic and mixed/EHD friction which are represented by HTHS viscosity and EHD traction, respectively.

The fuel economy study has shown that both engine tests, Sequence VI and VIA, respond to changes in viscometric, EHD traction/film thickness and boundary friction properties of lubricants. Although the new Sequence VIA test differs significantly from its predecessor being more responsive to viscometric changes, boundary friction coefficient still played an important role in predicting fuel economy. These results are confirmed by a subsequent prediction study carried out at Ford Motor Co. [**6.5**].

Similar trends were found when discriminant function analysis was used for an increased number of oils of known Sequence VI A efficiency data. For the sample analysed it highlighted the importance of HTHS viscosity and that of high temperature friction coefficient. Although a larger number of data would have been desirable, the attempt has shown that discriminant function analysis can be successfully used as a means of predicting the fuel economy for new oils due to its capacity for assigning an observation of unknown origin to the appropriate group.

The study also outlined the importance of bench tests in predicting lubricant-related friction losses in a typical internal combustion engine. They can be a useful and reasonable cheap tool for assessing new formulated oils from the fuel efficiency point of view.

This concludes the first part of this study on engine fuel efficiency. By developing correlations between bench tests and engine fuel efficiency it has been shown that boundary friction coefficient plays an important and quantifiable role in determining fuel economy in engine tests. The second part of this thesis will be concerned with a study of friction modifying additives in order to determine the extent to which this role can be maximised.

REFERENCES

[6.1] Van de Geer J.P., "Introduction to Multivariate Analysis for Social Sciences", p. 92, Freeman and Co., San Francisco, 1971,

[6.2] Anderson T. W., "An Introduction to Multivariate Statistical Analysis", Wiley & Sons, second edition, 1984,

[6.3] Lachenbruch P. A., "Discriminant Analysis", Hafner Press, New York, 1975,

[6.4] Williams E.J., "Regression Analysis", p. 194, Wiley&Sons, New York, 1966,

[6.5] Gangopadhyay A.K., Sorab J. et al., "Prediction of ASTM Sequence VI and VIA Fuel Economy Based on Laboratory Bench Tests", SAE paper 961140, pp. 13-21, 1996

CHAPTER 7

OILINESS ADDITIVES: A REVIEW

The chapter contains a review of previous work carried out on oiliness-type boundary additives as an attempt to examine the mechanisms by which they work. Numerous studies have been carried out to compare the friction reducing and adsorption properties of long chain surfactant solutions but the basic problem of whether they form thick or thin boundary films is still unclear.

7.1. General introduction

The use of additives to enhance specific chemical or physical properties of the base oil goes back to the middle of the nineteenth century [7.1] but only at the beginning of the twentieth century, when the internal combustion engine became a mass-produced article and mineral oils the most common form of lubricants, did lubricant additive technology began to develop on an industrial scale. A well documented history of lubricant additives has been outlined by Barwell [7.2].

Modern oil formulations for gasoline and diesel engines incorporate a wide range of additives used to control deposits, wear, corrosion, oxidation and rust. Some, such as antioxidants, corrosion inhibitors and detergents, protect the lubricant or the lubricated

system against chemical changes during use, whereas others, such as antiwear and oiliness additives make a direct contribution to lubricating effectiveness when the hydrodynamic action of the lubricant is weak or absent. This is the case in boundary lubrication regime (see chapter 2) when a coherent oil film can no longer be maintained between the surfaces and considerable friction and wear occurs unless a *boundary lubricant* is present. Good boundary lubrication is thus a result of a certain property of lubricants, other than viscosity, which has been called "oiliness" or "lubricity". The effectiveness of boundary lubricants is governed by their ability to interact physically or chemically with the sliding surfaces and to form adsorbed films, firmly bound to metal surfaces but also able to slide easily over each other. Such low shear strength films can be formed by polar additives dissolved in the bulk lubricant in quite a low percentage (1-2% wt.). Because of their polarity they are believed to orient themselves with the polar end towards the metal surface whereas the non-polar part remains suspended in the lubricant. Many molecules pack in as closely as possible and strengthen the film with lateral cohesive forces between the non-polar groups of adjacent molecules. The attachment to the substrate is due to adsorption which can be physical or chemical (see chapter 2). It is practical impossible to disentangle the mechanisms by which different additives react with metal surfaces, although. It is believed that all boundary additives act initially by physical adsorption [7.3]. If the temperature subsequently rises sufficiently, electron transfer can take place and films due to chemisorption and chemical reaction are formed.

7.2. Types of boundary additives

Depending on the effect they are intended to achieve, boundary additives are generally of three types:

(i) lubricity or oiliness (friction modifiers FM)

(ii) anti-wear(AW)

(iii) extreme-pressure(EP)

Since this work is concerned mainly with friction modifiers, the other two groups will be briefly described, the emphasis being on the first group.

7.2.1. Anti-wear additives

Additives that reduce mild wear are traditionally called *anti-wear additives*, whilst additives that reduce or prevent severe wear are called *extreme-pressure additives*. In practice there is not always a clear distinction and some substances can act as both anti-wear and EP additives. AW additives encompass several classes of chemicals most of them containing sulphur, oxygen and/or phosphorus. Perhaps the most important and most effective is zinc dialkyldithiophosphate (ZDDP) which has combined anti-wear, antioxidant and corrosion-preventing properties. Other important AW additives are organic phosphorus compounds such as tricresyl phosphate (TCP) and dilauryl phosphate and compounds containing sulphurized fats and fats derivatives [7.4]. Another group of AW additives is that of oil-soluble molybdenum-sulphur compounds such as molybdenum dithiocarbamates and dithiophosphates which combine both friction and wear reduction properties. Anti-wear additives are believed to chemisorb onto the metal surfaces forming a much stronger bond than simple physical adsorption. Chemisorption is a mechanism that takes place when electron transfer occurs between an adsorbed molecule and the substrate. This produces either a covalent or an electrovalent bond so that chemisorbed molecules are only removed when the element of surface to which they are attached is removed by wear [7.3]. With phosphorus-containing additives it is now believed that they give a thick protective film, probably of a phosphate-glass which forms over time on hot rubbing surfaces [7.5].

7.2.2. Extreme-pressure additives

If the sliding conditions are too severe, anti-wear additives will be inadequate to prevent severe wear or seizure. More highly-reactive additives are then needed to form stronger films on the surfaces. This protective film can sometimes form the substrate for further polar adsorption, which can be much stronger than on the metal itself [7.6]. Most of the chemicals used as *extreme-pressure* additives contain sulphur or chlorine which by reaction with the metal surfaces form a film of metal sulphide or chloride. Since they are working by chemical reaction, their use involves possible corrosion problems through the repeated cycle of reaction and wear. Thus the selection of an EP additive is a compromise between desirable EP protection and undesirable corrosion.

7.2.3. Oiliness additives

Typical *oiliness additives* are long chain fatty acids (palmitic, stearic, oleic), salts or esters of carboxylic acids, alcohols and amines. They are designed to work mainly at low temperatures up to 100 and 150°C. As long ago as the middle of the 19th century Little [7.7] proposed the mixing of fatty acid soap with mineral oils to produce lubricating greases. The first deliberate use of additives to improve the boundary properties of liquid lubricants was reported by Wells and Southcombe in 1920 [**7.8**]. They showed that the addition of small proportions of long chain carboxylic acids to mineral oils reduced friction and ameliorated seizure tendencies to such an extent that a refined mineral oil attained comparable boundary lubricating properties to a natural animal or vegetable oil. Since then quite a wide range of chemically formulated additives has been developed to improve the properties of oils, but only relatively recent the attention has been focused on the development of friction modifying additives. Following the Gulf crisis in 1978, fuel economy for all vehicles became an international issue. This lead to the introduction of FM into automotive crankcase lubricants, the objective being to improve fuel efficiency via lubricant formulation. Chemically, friction modifiers can be any molecule that is adsorbed onto a surface and forms a film that is tenacious to vertical pressure but easily sheared laterally. Oiliness-type FM are amphiphilic molecules containing an oleophilic hydrocarbon chain (minimum 10 carbon atoms) covalently bonded to a polar terminal group such as: phosphates, phosphites, thiophosphates, thiocarbamates, amine, amide, carboxylic acids, esters, sulfurized esters, etc. [**7.8**].

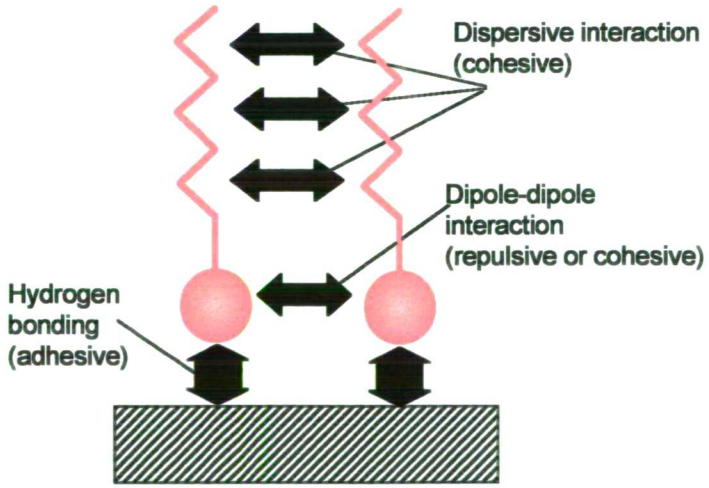


Fig.7.1. Key interactions between adsorbate molecules (from ref 7.9)

They are thought to operate by forming a cohesive monomolecular layer on metal and metal oxides. A "carpet" of surfactant molecules is physically adsorbed by Van der Waals forces on to the surfaces. This layer keeps all but the highest asperities from adhering and provides a low shear strength layer between opposing surfaces thus reducing the friction coefficient. It tends to be effective at low temperatures and moderate loads. The adsorbed molecules lower the free energy of the surface and the greater the reduction in free energy, the greater will be the stability of the adsorbed film [7.10].

7.3. Oiliness additives - monolayer or multilayer ?

As described above, oiliness additives form surface films which are beneficial for reducing friction and wear. To study these films of nanometric dimensions, concealed within contacts - in realistic conditions of speed, pressure, temperature, etc. - was practically impossible until recently when in-situ analytical techniques were developed such as: force balance [7.11], ultrathin interferometry [7.12] and scanning tunneling and atomic force microscopy [7.13].

Previous studies of oiliness additives mechanisms were based mainly on two alternative approaches: one was to measure friction properties in real contacts and deduce the nature and properties of the films from the observed behaviour and to relate them to surfactant, chain length, concentration, surface type or temperature. The second approach was based on adsorption studies i.e. to examine the state and chemical composition of surface films using techniques such as X-ray diffraction, scanning electron microscopy or infrared analysis. The main drawback of these techniques is that the films are not analysed in situ and thus the conditions are different and usually far gentler than those prevailing in real contacts.

7.3.1. Monolayer issue

Despite the extensive research undergone for almost a century, the true nature and the origins of "oiliness" in real lubricated contacts still remains unclear. A remarkable amount of work on this phenomenon started at the beginning of the 1920 with the pioneering work carried out by Hardy [**7.14**]. Initially, different possible explanations for oiliness were proposed but soon the attention was focused on the role of adsorbed layers of surfactants which, in Hardy's view, were reducing the field of force between sliding surfaces thus decreasing friction. The technique developed by Blodgett [**7.15**] for transferring monolayers of fatty acids or their salts spread on a water surface on a solid surface, enabled films of controlled thickness to be obtained and analysed in friction tests. Numerous studies were carried out to compare the friction reducing and adsorption properties of long chain surfactant solutions.

It was shown by Desvaux [**7.16**], Langmuir [**7.17**] and later by Bowden [**7.18**] that single monolayers of surfactant deposited on surfaces were able to reduce friction coefficient down to values characteristic of those found using surfactant solutions in hydrocarbons. This approach was extended by Gregory [**7.20**] who calculated the minimum fatty acid coverage required to provide effective lubrication. The thickness was found to be of the order of 1 to 2 molecular layers. Another demonstration to support the idea of monolayer sufficiency has been provided by Bailey and Courtenay-Pratt [**7.21**]. Monolayers of calcium stearate were spread on two sheets of mica and rubbed together. Using multiple beam interferometry they showed that throughout the experiment, the film remained at a thickness of about 5 nm which was consistent with previous assumptions that monolayers presumably slid with their methyl heads in contact. The work had some limitations however in that, owing to the delicate nature of mica substrate, the contact pressures used were of the order of 10^6 Pa, about 1000 times lower than the pressures encountered in normal engineering practice.

Friction studies have shown that a monolayer of fatty acid greatly reduced friction coefficient, but the film is easily worn away. By using multiple deposited layers of fatty acids it was shown that although layers in excess of the first one did not significantly reduce friction, they did greatly enhance the film's durability [**7.18, 7.22**]. There was however evidence that surface films produced by reaction, for example copper stearate,

were inherently more durable than layers deposited on solid with a Langmuir trough [7.23]. This led to the conclusion that reaction between lubricant and the metal substrate is an important feature for good lubrication properties of boundary films. Studies of stearic acid and metal stearates deposited on different metals, carried out by Greenhill [7.24], showed that, with some unreactive metals such as platinum, at least 7 molecular layers must be present for effective lubrication.

The shear strength and other tribological properties of surfactant monolayers have been the subject of many relatively recent studies. Briscoe et al. [7.25] used curved mica surfaces to study the influence of contact pressure on the sliding behaviour of stearic acid and calcium stearate monolayers among other organic materials. Briscoe and Evans [7.26] investigated the shear properties of deposited monolayers of fatty acids (C14 to C22) and of fluorinated fatty acids on mica surfaces. They reported that the shear strength of a wide range of organic materials varied linearly with pressure, temperature and the logarithm of sliding velocity. They also suggested that all these materials shear by a similar process involving the sliding of linearly orientated methylene groups over one another. More recently Timsit and Pelow [7.27] examined the shear strength and durability properties of stearic acid monolayers deposited on glass and Al surfaces. They found that shear properties, as evaluated with bare-glass or Al-coated glass sliders, were nearly independent of the shearing interface. In agreement with the results of earlier work, they also have shown that shear strength increased nearly linearly with contact stress. The work has been extended to include gold surfaces [7.28]. Measurements of shear strength in lubricated Au/Au interfaces revealed that stearic acid does not sustain shear in this interface and is expelled from the contact. Lubricant function was restored only when one side of the interface was replaced by a surface to which the acid adheres (i.e. glass or Al).

It was demonstrated by Hardy [7.14] that the extent of friction reduction increased with surfactant chain length up to a critical number of carbon atoms, above which it remained constant. The increase in hydrocarbon chain length increases the number of cohesion forces between the chains which results in better friction reducing properties [7.26]. For homologous series of additives and monolayer coverage, only the cohesive dispersion interactions between the hydrocarbon chains are obviously chain length dependent. It has been found that solutions where the hydrocarbon chain has the same length as the n-

alkane carrier gives higher transition temperatures than those of a similar concentration of either higher or lower acids in the same solvent [7.29, 7.30]. Also in order to be effective, the chain needs to be straight rather than branched [7.31] since complete surface coverage is more difficult to achieve with a branched molecular shape chain, thus increasing the probability of metallic contact. More recent studies have shown that the position of polar group is also of great influence. The best position for the polar moiety is at the very end of the hydrocarbon chain and any change from this location can result in a disruption of the packing of surfactant on the surface [7.32]. The adsorption properties of oiliness additives can be accounted for by hydrogen bonding to surfaces and the lateral interactions between adsorbate molecules. It has been shown [7.9] that polarity itself is not a sufficient condition for adsorption; the polar group must also have hydrogen bonding capability. Polarity, however, is important for the various lateral surface interactions through strong electrostatic dipole-dipole interactions.

It has been suggested that the effectiveness of adsorbed additives ceases when the temperature reaches a specific desorption value, a "critical temperature" Tc, normally between 80 and 150°C in the case of friction modifiers. A marked increase in friction has been shown to occur when the oiliness film desorbs or melts. Electron difraction studies [7.33] have shown that the initially highly-oriented film gives a more difuse difraction pattern when the temperature aproaches Tc, indicating a more random orientation. For pure hydrocarbons it was shown that this temperature is similar to the melting point [7.34] whereas for fatty acids it is higher than the bulk melting point and increases with molecular weight. Bowden and Tabor explained this effect by the formation of a metallic soap at the surface due to chemical reaction of the fatty acid with the metal or metal oxide [7.35]. This was supported by early evidence of chemical interactions that arose from the realisation that Langmuir-Blodgett layers formed by spreading fatty acid on a surface of water containing metal ions, consist not of acid itself but of the soap formed by the reaction of the acid with the ions [7.36]. Analysis of the retracted monolayers using electron diffraction [7.33] indicated that the hydrocarbon chains are more closely packed on more reactive metals like copper and iron than the chains in monolayers on silver and platinum. This led to the conclusion that the soap monolayers (formed in situ) are more closely packed than the fatty acid monolayers on unreactive metals. Considerable reaction between fatty acids solutions and iron and copper has also been detected by Sakurai and Baba [7.37]. They suggested that the

resulting soap might adsorb on the surface to form a lubricating film. Some authors ascribed the loss of effectiveness of boundary layers not to desorption but to their solubility in the bulk lubricant medium [7.38]. Studies of copper surfaces lubricated by fatty acids in cetane (n-hexadecane) have shown that the solubility of the generated soap does not increase continuously with temperature, the soap remains insoluble in the bulk lubricant up to a certain temperature when sudden solubilisation occurs [7.38].

Most of the data available on adsorption films has been obtained under controlled conditions including cleaning of the specimen surfaces, deposition of the lubricant films and stabilisation for many hours to allow chemical and thermal equilibrium to be reached. The friction tests themselves are performed at quite low sliding speeds with several minutes between successive slidings. Bearing in mind that in reality, working conditions are far from those described above, some researchers have made attempts to study the differences between a dynamic form of adsorption and the classic equilibrium model. Okabe et al. [7.39] measured the coefficient of friction of several fatty acids (C11 to C21) in pure hexadecane as a function of surfactant concentration in a ball and cylinder apparatus. They found a "transition concentration" around 0.5 mol/m^3 for all the surfactants tested where the friction coefficient declined sharply. This was considered to be the minimum concentration where the fatty acids will replenish the damaged adsorbate film under conditions of repetitive sliding. These findings came to confirm the idea stemming from the 1940s that effective oiliness requires a self-healing ability [7.15, 7.40]. The influence of additive concentration upon friction coefficient was investigated more recently by Jahanmir et al. [7.41]. It was shown that under boundary lubrication conditions, friction coefficient is reduced by increasing the additive concentration and approaches a minimum value at higher concentrations.

More thorough reviews of long chain surfactant monolayers deposited on solids can be found in references [7.42] and [7.43]. Recently Lockwood et al. [7.44] have presented a review of lubricant-solid adsorption theories and analysed how the liquid-surface interactions affect boundary lubrication.

7.3.2. Multimolecular films

Work showing practical evidence on films more than one molecule thickness is much less abundant than that on monomolecular research. This is probably due to the fact that monolayer adsorption model seemed by the 1930s to have been almost unanimously accepted. However, there were still some researchers who were in favor of the presence of a quite thick oiliness friction modifier layer between the lubricated surfaces. Even Hardy in his later work had comments on the possibility of boundary films thicker than monolayers [7.45]. In the 1930s, Trillat used X-ray diffraction to show that a lubricant could form an organised layer many molecules thick up to 5 microns distant from the surface [7.46]. Evidence of a thick film, sometimes hundreds of nanometers thick, has been demonstrated by Deryaguin and his co-workers. Studies of the film profile of a lubricant droplet on a solid surface when blown-off with a stream of air indicated that the liquid layers within a few nanometers of solid surfaces might exhibit anomalous viscosity [7.47]. They reported that layers exhibited an ordered structure 10 to 100 nm deep and advanced the hypothesis that these layers were in a state similar to that of liquid crystals. Later in the 1980s using the force balance technique, Israelachvili [7.48] came to a similar conclusion that on very smooth mica surfaces, molecules have an effectively layered structure, several molecular diameters out from the surface. He has shown that for simple molecular organic liquids, the normal force is an oscillatory function of distance from the surface resulting from this layering of molecules. In order to overcome the limitations imposed by the low pressures used by Israelachvili, Georges and his colleagues [7.49] have applied the force balance technique to study the contact of a ball on a flat both made of steel or cobalt-coated glass. They showed that simple molecular liquids form immobile layers with anomalous viscometric properties typically 1 nm out of surface. With low molecular weight polymers the phenomenon was detected up to 10 nm [7.50].

Work carried out in the 1940s and 1950s brought supporting evidence to the idea that more than a monolayer films could be present in lubricated systems. Further evidence of long-range action near solid surfaces was produced by studies of flow through narrow passages, or from between approaching surfaces. Bastow and Bowden [7.51] studied the flow of water, various organic liquids and ionic solutions, radially through a narrow gap between circular glass and stainless steel plates. Flow anomalies were detected only

in the case of ammonium oleate, which was known to contain colloidal particles and which behaved as a liquid crystal, and ethyl palmitate, in which case the observed clogging was attributed to the presence of suspended particles. Researchers such as Needs [7.52] and Fuks [7.53] studying the normal approach of lubricated, loaded flats found that low molecular weight hydrocarbons such as benzene, hexane, cyclohexane, iso-octane and decane were expelled from the interface and did not form a residual film. On the contrary, when fatty acids were added to a low molecular weight hydrocarbon, a residual separating film, resistant to high loads was produced, typically hundreds of nanometers in thickness. Fuks concluded that, close to the solid surfaces, the fatty acid in mineral oil solution behaved like a plastic solid. He also reported that the surface films increase in thickness with increasing fatty acid concentration, with surface energy of the boundary surfaces (from aluminium oxide to steel) and with increasing molecular weight of both solvent and solute. When normal stress was applied, the thick films exhibited elastic properties, shrinking when compressed and expanding when released, recovering a significant portion of the residual thickness. Despite the considerable evidence yielded by these results, there were many sceptics who attributed such behaviour to other reasons than the existence of a thick boundary film. Their explanation of results was either due to the presence of dirt in the fluids and the asperities on the flats or due to particles of solid fatty acid or the formation of micelles caused by the presence of water. The controversial subject of multy-layer boundary films is reviewed by Allen and Drauglis [7.54] who supported the idea of a long range order on the films.

Later in the 1970s, Smith [7.55] investigated the formation of thick films of stearic acid from hexadecane on to steel. He used a method of displacing lubricant from a steel ball using mercury and measured the capacitance of the remaining film. He found that when moisture was present, viscous layers of micron thickness were formed on the steel surfaces and were far more slowly displaced than the bulk fluid. Other authors including Sherwood [7.56], Smith and co-workers [7.57] also showed that the presence of moisture was necessary for the formation of a thick film of fatty acid. Also Hirst [7.58] obtained thicker adsorbed films of stearic acid on zinc and copper when moisture was deliberately introduced. A possible explanation might be the one given by Tingle [7.59] that the presence of water may lead to the formation of a loose hydroxide or hydrated oxide layer of a character suitable for penetration and reaction by the fatty acid.

Alternatively water may promote oxidation of the metal and thus the formation of a metal soap [**7.59**].

There have also been indications that lubricants may degrade chemically during rubbing to form polymerised, protective layers [**7.60, 7.61**]. Such polymerisation, especially of unsaturated and aromatic components, might be promoted by the high pressures and temperatures at the asperity contacts and possibly by the added catalytic action of freshly exposed surfaces. It is worth noting that most friction studies used to test boundary layers properties have used very mild conditions of slow speed and smooth surfaces where such polymerisation effects are least likely to be seen.

Despite its long history and extensive research undertaken, the question of the existence of such rheological anomalies at solid-fluid interfaces still remains unsolved. Although there has been many experimental evidence of long range surface forces in boundary lubricant films formed close to metal surfaces, the experimental techniques have in general been ambiguous and the conditions of cleanliness have not always been appropriate thus leading to alternative interpretations. Nor is there any substantial evidence to indicate if thick films do form, whether they are present in rubbing contacts. An important aim of the work described in this thesis was to investigate this question.

REFERENCES

[7.1] Dowson D., "History of Tribology", Longman Group Ltd., p. 348, 1979,

[7.2] Barwell F. T., "Lubricant Additives-The History of their Introduction and Assessment", Proc. 5th Int. Colloq. Esslingen, "Additives for Lubricants and Operational Fluids", vol. 1, 14-16 Jan, 1986,

[7.3] Lansdown A.R., "Extreme-pressure and anti-wear additives" from "Chemistry and Technology of Lubricants", Mortier R.M. and Orszulik S.T editors, p. 274, Blackie and Son, 1992,

[7.4] Kajdas C., "Engine Oil Additives: A General Overview", Proc. 7th Int. Colloq. Esslingen, "Automotive Lubrication" 16-18 Jan, 1990,

[7.5] Bell J.C., Delagry K.M. and Seeney A.M., "The Removal of Substrate Material through Thick Zinc Dithiophosphate Anti-Wear Films", Proc. 18th Leeds-Lyon Symposium on Tribology, Wear Particles, ed. D. Dowson et al., publ. Elsevier, Amsterdam, 1992,

[7.6] Spikes H.A., "Physical and Chemical Adsorption in Boundary Lubrication", PhD Thesis, Imperial College, p. 16, London, 1971,

[7.7] Little, Brit. Patent 12,571, 1849, (from ref. 7.6)

[7.8] Papay A.G., "Friction Reducers for Engine and Gear Oils-A Review of the State of the Art", Proc. 5th Int. Colloq. Esslingen, "Additives for Lubricants and Operational Fluids", 14-16 Jan, 1986,

[7.9] Beltzer M. and Jahanmir S., "Effect of Additive Molecular Structure on Friction", Lub. Sci. 1-1, pp. 3-26, 1988,

[7.10] Groszek A.J., "Role of Adsorption in Liquid Lubrication", Proc. NASA Sposored Symp. on Interdisciplinary Approach to Liquid Lubricant Technology, Cleveland, Ohio, Jan. 11-13, pp. 477-525, 1972,

[7.11] Israelachvili J.N. and Tabor D., "The Measurement of Van der Waals Dispersion Forces in the Range 1.5 to 130 nm", Proc. Roy. Soc. Lond. A331, pp. 19-38, 1972,

[7.12] Foord C.A., Hamman W.C. and Cameron A., "Evaluation of Lubricants Using Optical Elastohydrodynamics", ASLE Trans, 11, pp. 31-43, 1968,

[7.13] Andoh Y., Oguchi S., Kaneko R. and Miyamoto J., "Evaluation of Very Thin Lubricant Films", J. Phys. D 25, pp. A71-A75, 1992,

[7.14] Hardy H. B. and Doubleday I., "Boundary Lubrication - The Paraffin Series", Proc. Roy. Soc. Lond. A100, pp. 550-757, 1922,

[7.15] Blodgett K.B., "Molecular Films of Fatty Acids on Glass" Communication to the editor, J. Am. Chem. Soc. 56, nr. 2, p. 495, 1934,

[7.16] Desvaux H., "Le Frottement des Solides: Epaisseur Minimum d'un Enduit Lubrefiant", J. de Phys. et la Radium, 5, p. 845, 1924,

[7.17] Langmuir I, "The Mechanism of the Surface Phenomena of Flotation", Trans. Farad. Soc. 15, pp. 62-74, 1920,

[7.18] Bowden F.P. and Leben L., "The Friction of Lubricated Metals", Phil. Trans. Roy. Soc. Lond. A239, pp. 1-27, 1940,

[7.19] Bowden F.P. and Tabor D., "The Friction and Lubrication of Solids", Clarendon Press, Oxford, 1954,

[7.20] Gregory J.N., C.S.I.R. (Australia) Tribophysics Div. Report, A74, 1943, Taken from reference 7.14

[7.21] Bailey A. and Courtenay-Pratt J.S., "The Area of Real Contact and the Shear Strength of Monomolecular Layers of a Boundary Lubricant", Proc. Roy. Soc. Lond. A227, p. 500, 1955,

[7.22] Cottington R.L., Shafrin E.G.and Zisman W.A., "Physical Properties of Monolayers at the Solid/Air Interface. III. Friction and Durability of Films on Stainless Steel", J. Phys. Chem. 62, no. 5, pp. 513-518, 1958,

[7.23] Rowe G.W., "The Chemistry of Tribology", RIC Reviews, 1, p.135, 1968,

[7.24] Greenhill E.B., "The Lubrication of Metal Surfaces by Mono- and Multi-Molecular Layers", Trans. Farad. Soc. 45, pp. 631-635, 1949,

[7.25] Briscoe B.J., Scruton B. and Willis F.R., "The Shear Strength of Thin Lubricant Films", Proc. Roy. Soc. Lond. A333, pp. 99-114, 1973,

[7.26] Briscoe B.J. and Evans D.C.B. "The Shear Properties of Langmuir-Blodgett Layers", Proc. Roy. Soc. Lond. A380, pp. 389-407, 1982,

[7.27] Timsit R.S. and Pelow C.V., "Shear Strength and Tribological Properties of Stearic Acid Films - Part I: On Glass and Aluminium-Coated Glass", ASME Trans, Journal of Tribology. 114, pp. 150-158, 1992,

[7.28] Timsit R.S. and Pelow C.V., "Shear Strength and Tribological Properties of Stearic Acid Films - Part II: On Gold-Coated Glass", ASME Trans, Journal of Tribology. 114, pp. 159-166, 1992,

[7.29] Askwith R., Crouch R.F. and Cameron A., "Chain Length of Additives in Relation to Lubricants in Thin Film and Boundary Lubrication", Proc. Roy. Soc. Lond. A291, pp. 500-519, 1966,

[7.30] Hirano F. and Sakai T., "The Chain Matching Effect", J. Japan Soc., Lub. Eng. 21, pp. 606-613, 1976,

[7.31] Levine O. and Zisman W.A., "Physical Properties of Monolayers Adsorbed at the Solid Interface. Wettability of Aliphatic Polar Compounds and the Effect of Halogenation", J. Chem. Phys. 61, pp. 1068-1077, 1957,

[7.32] Papay A.G.and Devlin M.T., "Friction and Friction Modifiers in Lubricants", in "Tribology-solving Friction and Wear Problems", 10th International Colloquium, Esslingen, Jan. 1996,

[7.33] Chapman J.A. and Tabor D., "An Electron Diffraction Study of Retracted Monolayers", Proc. Roy. Soc. Lond. A242, pp. 96-107, 1957,

[7.34] Tabor D., "Effect of Temperature on Lubricant Films", Nature 145, p. 308, 1940,

[7.35] Bowden F.P. and Tabor D., "Lubrication of Metal Surfaces by Fatty Acids", Nature,156, p. 97, 1945,

[7.36] Clark J.L., Sterrett R.R. and Leppla P.W., "X-Ray Diffraction Studies of Built-up Films of Long Chain Compounds", J. Am. Chem. Soc. 57, p. 330, 1935,

[7.37] Sakurai T. and Baba T., "Surface Chemical Behaviour of Polar Compounds in Non-Aqueous Liquids. Dispersing Effect of Soap Solutions", Wear 3, p. 286, 1960,

[7.38] Kreuz K.L., Fein R.S. and Rand S.J., "Solubilization Effects in Boundary Lubrication", Symposium on Deposit, Wear and Emission Control by Lubricant and Fuel Additives, Am. Chem. Soc., pp. 126-138, New York, Sept. 1969,

[7.39] Okabe H., Masuko M. and Sakurai K, "Dynamic Behaviour of Surface-Adsorbed Molecules under Boundary Lubrication", ASLE Trans. 24, pp. 467-473, 1981,

[7.40] Adams N.K., "Molecular Forces in Friction and Boundary Lubrication", I. Mech. E. Proc. of the General Discussion on Lubrication and Lubricants 2, pp. 197-201, 1937,

[7.41] Jahanmir S. and Beltzer M., "Effect of Additive Molecular Structure on Friction Coefficient and Adsorption", Journal of Tribology 108, pp. 109-116, 1986,

[7.42] Harding R.D., "Studies in the Surface Chemistry of Boundary Lubrication", PhD Thesis, University of London, 1968,

[7.43] Kipling J.J., "Adsorption from Solutions of Non-Electrolytes", Academic Press, New York, 1965,

[7.44] Lockwood F. E. and Bridger K., "Liquid Wetting on Metal Surfaces and the Heat of Immersion/Adsorption in Lubrication", ASLE Trans. 30, pp. 339-354, 1987,

[7.45] Hardy W., "Problems of the Boundary State", Phil. Trans. Roy. Soc. Lond. A203, pp. 1-37, 1931,

[7.46] Trillat J.J., "The Adsorption of Oils in Relation to Lubrication", I. Mech. E. Proc. of the General Discussion on Lubrication and Lubricants 2, pp. 55-59, 1937,

[7.47] Deryaguin B.V., Karassev V.V., Zakhavaeva N.N. and Lazarev V.P., "The Mechanism of Boundary Lubrication and the Properties of the Lubricating Film - Short and Long-Range Action in the Theory of Boundary Lubrication", Wear 1, pp. 277-289, 1957/58,

[7.48] Israelachvili J.N., Fisher L.R., Horn R.G. and Christenson H.K., "Measurement of Adhesion and Short-Range Forces between Molecularly Smooth Surfaces in Undersaturated Vapours and in Organic Liquids", Microscopic Aspects of Adhesion and Lubrication, Tribol. Series, 7, J.M.Georges, Ed. Elsevier Scientific Pub. Co., Amsterdam, pp. 55-69, 1982,

[7.49] Tonck A., Georges J.M. and Loubet J.L., "Measurements of Intermolecular Forces and the Rheology of Dodecane between Alumina Surfaces", J. Coll. and Interface Sci. 126, nr. 1, pp. 150-163, 1988,

[7.50] Georges J.M., Millot S., Loubet J.L. and Tonck A., "Drainage of Thin Liquid Films Between Relatively Smooth Surfaces", J. Chem Phys. 98, nr.9, pp. 7345-60, 1993,

[7.51] Bastow S.H. and Bowden F.P., "Physical Properties of Surfaces II-Viscous Flow of Liquid Films. The Range of Action of Surface Forces", Proc. Roy. Soc. Lond. A151, p. 220, 1935,

[7.52] Needs S.J., "Boundary Film Investigations", Trans. ASME 62, pp. 331-339, 1940,

[7.53] Fuks G.I., "The Properties of Solutions of Organic Acids in Liquid Hydrocarbons at Solid Surfaces", Research in Surface Forces, vol. 1, 1960, ed. B.V. Deryaguin, Transl. by Consultants Bureau, NY, 1963,

[7.54] Allen C.M. and Drauglis E., "Boundary Layer Lubrication: Monolayer or Multilayer", Wear 14, pp. 363-384, 1969,

[7.55] Smith A.J. and Cameron A., "Rigid Surface Films", Proc. Roy. Soc. Lond. A328, pp. 541-560, 1972,

[7.56] Sherwood A.F. and Rybicka S.M., "Surface Properties of Titanium Dioxide Pigments", J. Oil Col. Chem. Assoc. 40, p. 648, 1966,

[7.57] Smith H.A. and McGill R.M., "The Adsorption of n-Nonadecanoic Acid on Mechanically Activated Metal Surfaces", J. Phys. Chem. 61, p. 1025, 1957,

[7.58] Hirst W. and Lancaster J.K., "Effect of Water on the Interaction between Stearic Acid and Fine Powders", Trans. Farad. Soc. 47, p. 315, 1951,

[7.59] Tingle E.P., "The Influence of Water on the Lubrication of Metals", Nature 160, p. 710, 1947,

[7.60] Furey M.J., "The Formation of Polymeric Films Directly on Rubbing Surfaces to Reduce Wear", Wear 26, pp. 369-392, 1973,

[7.61] Fein R.S. and Kreuz K.L., "Chemistry of Boundary Lubrication of Steel by Hydrocarbons", ASLE Trans. 8, pp. 29-38, 1965

CHAPTER 8

FATTY ACID STUDY

Long-chain fatty acids, known for their lubricating properties, were investigated in this study. The film forming capabilities of hexadecanoic (palmitic), octadecanoic (stearic) and oleic acids were assessed in pure rolling conditions using the ultra-thin interferometry technique described in chapter 4. The influence of several factors such as chain length, concentration, rolling time and cleaning methods was investigated. Unfortunately the results were not entirely repeatable, showing two alternate modes of behaviour: thick and thin surface film formation. The observed behaviour appeared to be extremely sensitive to surface cleanliness.

8.1. Materials employed

In order to make the interpretation of the experimental results more straightforward and to give greater control over the possible chemical reactions of the lubricants, solutions with simple chemical constitution were used, consisting of a pure surfactant dissolved in a base fluid. Long-chain carboxylic acids used in this study are listed in the table below, together with the chemical formula, number of carbon atoms in the molecule, melting point and supplier name.

ADDITIVE	CHEMICAL FORMULA	CARBON ATOMS	MELTING POINT °C	MOLECULAR WEIGHT	SUPPLIER
Decanoic acid	$CH_3(CH_2)_8COOH$	10	31	172	BDH
Lauric acid	$CH_3(CH_2)_{10}COOH$	12	44-46	200	BDH
Palmitic acid	$CH_3(CH_2)_{14}COOH$	16	62.5-64	256	BDH
Stearic acid	$CH_3(CH_2)_{16}COOH$	18	67-69	284	Aldrich
Oleic acid	$CH_3(CH_2)_7CH = CH(CH_2)_7COOH$	18	13-14	282	Aldrich

Table 8.1. Carboxylic acid additives

Decanoic and lauric acids with shorter chain length were only employed in an initial attempt to study the influence of chain length on surfactants behaviour.

The stearic acid and oleic acid were 99+ puriss. grade and were used as received from the supplier company. The palmitic acid was recrystallised from ethanol.

For these tests at 25°C, the lubricant base fluid used was hexadecane because the solvent had to fulfil two main requirements: to be temperature stable and non-volatile. A simple solvent was also necessary in order to clearly distinguish the effect of boundary additives in film thickness measurements. Hexadecane is a straight chain hydrocarbon with 16 carbon atoms and since it has been employed quite extensively in the literature this made it useful for comparison purposes. Hexadecane solvent of viscosity 3.48 cSt at 25°C, with a specific gravity of 0.773 g/cm^3, was supplied by Aldrich Chemical Co. and was 99% pure. Very pure solvent was essential for boundary lubrication work since any contaminant would have interfered directly with the surface phenomena, producing erroneous results. Although the fluid arrived in brown sealed bottles, for the sake of experiments, it was necessary to purify it before use to remove polar impurities and water. The purification method employed activated silica gel and alumina as in ref. **[8.1]**. The mixture was oven heated at 100°C for about 2 hours and then left to cool down at room temperature. When added to hexadecane, the ratio of solid to liquid was approximately 1:2 by volume. The whole mixture was stored away from light for about 10-12 days. Prior to use, the purified solvent was filtered by passing it through a filter paper grade 1 purchased from Whatman International Ltd.

The carboxylic acids were blended in hexadecane, mainly in concentrations of 0.1% by weight. A wider range of concentrations from 0.05% up to 2% wt. was employed when its effect on additive film formation was tested.

8.2. Cleaning and testing procedures

The cleanliness of surfaces in boundary lubrication studies is extremely important since any impurities will strongly affect surface phenomena. Although many researchers have stressed the idea that in industrial practice metal surfaces are not perfectly clean but are covered with an oxide layer and many contaminants, for more fundamental studies it is necessary to ensure that the working surfaces have a good and repeatable standard of cleanliness. As will be indicated in the results, the thickness of the films formed appeared to be very dependent upon the cleaning technique used.

8.2.1. Cleaning techniques

Film thickness measurements were performed using the ultra-thin interferometry technique described in chapter 4. Since one of the employed surfaces is glass coated with chromium and silica layers, it was not possible to use more powerful techniques such as ionic bombardment which can cause excessive damage to the surface. The alternative was to use chemical cleaning methods based on solvents such as analar toluene and analar acetone. The ball support and the glass disc were heated in boiling analar toluene for about 30 minutes. They were then cooled to about 80°C, removed from the toluene and rinsed with analar acetone.

Two different techniques were used for cleaning the steel ball. In one the ball was boiled in toluene and then rinsed in acetone in a similar fashion to the glass disc. In the second, the ball was soxhletted in analar chloroform for one hour and then rinsed in analar propan-2-ol (isopropanol) before being dried in an oven at 60°C for ten minutes.

For friction and EHD traction studies the HFRR specimens and the metal disc, ball and ball support were cleaned in analar toluene and acetone using an ultrasonic bath. The cleaning time in each solvent was around 10 minutes.

8.2.2. Measurement techniques

The ultra-thin interferometry technique was used for testing the film forming capacities of fatty acids in hexadecane. The technique and the test rig employed was fully described in chapter 4. For this study the only difference from normal testing procedure was that the ball was not half-immersed in the lubricant, so tests were not fully-flooded. Instead, a small quantity of solution, typically 3 cm^3 per test, was applied directly on the ball at the beginning of the test after measuring the spacer layer thickness for the dry contact. The whole contact was contained in a temperature-controlled chamber where the temperature was maintained at 25°C ± 0.5°C.

The second EHD property, traction, was measured using a similar rig to the one employed for film thickness measurements whilst the boundary friction coefficient was determined on a high frequency reciprocated rig (HFRR). Both rigs were described in chapter 4.

8.3. Film thickness results

Film thickness tests were generally performed immediately after lubricant application, although with some tests, ball and disc were held stationary at the set temperature for a fixed "presoak" period of about 30 minutes to one hour before the motion was started. This was to investigate the existence of any time-dependent future adsorption effects. Test procedure was to determine the variation of film thickness with increasing rolling speed for a range of speeds from 0.002 m/s up to 1 m/s (with some tests the upper speed limit was 0.5 m/s since for speeds beyond this value the lubrication was fully hydrodynamic and the film thickness line was already coincident with that of the solvent).

8.3.1. Film thickness of purified hexadecane

Firstly the film thickness formed by the solvent was tested in order to have a base line for comparison purposes. Figure 8.1 shows a plot of log(film thickness) versus

log(rolling speed) for purified hexadecane at 25°C ± 0.5°C. Four sets of results are included to indicate the level of repeatability.

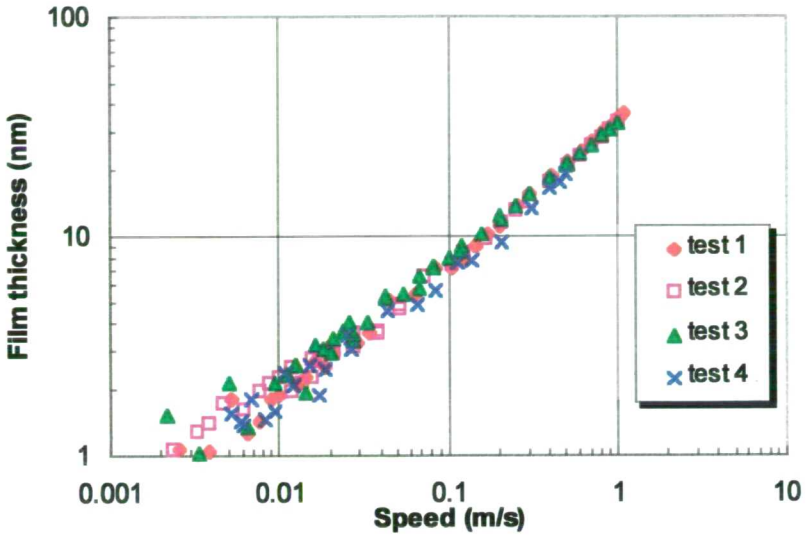


Fig.8.1. Film thickness vs. speed for hexadecane @ 25°C

According to the elastohydrodynamic theory, central film thickness h_c, is given by [**8.2**]:

$$h_c \approx k(U\eta)^{0.67}\,\alpha^{0.53} \qquad (E8.1)$$

where U is the mean rolling speed (U1+U2)/2, η is the dynamic viscosity of the lubricant in the inlet at atmospheric pressure and α is the pressure-viscosity coefficient of the lubricant (dlnη/dp). Thus a log/log plot should be a straight line of gradient about 0.67. Figure 8.1 shows that hexadecane obeys EHD theory and forms a straight line plot close to this gradient down to 1 nm film. There is maybe a small deviation from the straight line at slow speeds, but this is less than 1 nm which is below the measurement accuracy of the rig. It is worth noting that EHD film thickness is determined not by the viscosity of the lubricant within the contact itself but by the viscosity of the fluid in the immediate contact inlet, where the film gap reduces from about $2h_c$ to h_c at the inlet edge [**8.3**]. Thus the fact that the equation 8.1 is obeyed down to 1 nm thickness for hexadecane indicates that its viscosity remains at the bulk value within 2 nm of the surfaces. These findings are consistent with previous work carried out with other saturated hydrocarbon fluids [**8.3**].

Since the proposed use of hexadecane as a solvent for the polar additives was based on the assumption that, should anomalous behaviour be detected in the boundary regime, it

would be due to the action of the additive alone, the results described above indicate that the chosen solvent suits the purpose .

8.3.2. Film thickness of surfactant solutions

Toluene/acetone cleaning

Using hexadecane purified as above, solutions of fatty acids at a concentration 0.1% by weight were prepared and their film forming capacities were tested at 25°C ± 0.5°C in the EHD rig using ultrathin film interferometry technique. A fresh solution was employed every time a test was performed, prepared from hexadecane filtered prior to use. Figure 8.2 shows the results of two tests using 0.1% palmitic acid in hexadecane with the toluene/acetone cleaning method described above. The solid line represents the behaviour of hexadecane. Two sets of data points are included for each test. One shows how film thickness varies as speed is steadily increased (fwd) in the first half of a test whilst the second shows the response of film thickness to the speed being subsequently decreased (back).

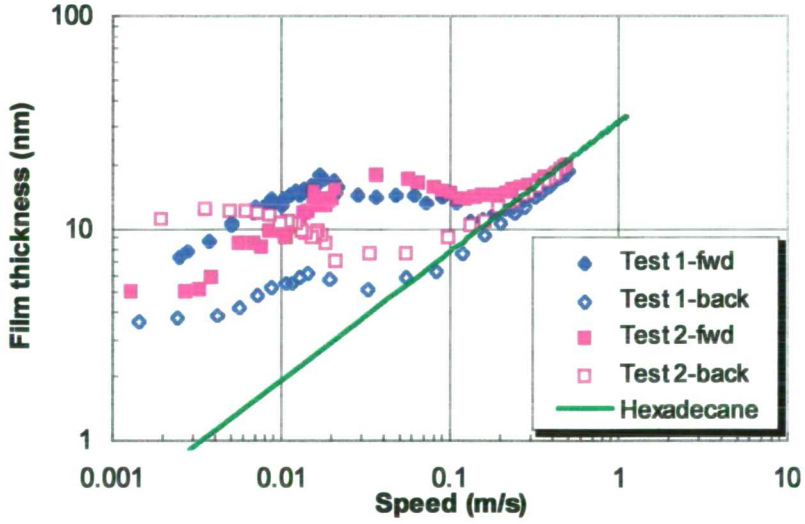


Fig. 8.2. Film thickness vs. speed for 0.1% wt. palmitic acid @ 25°C

It can be seen that both tests give quite similar, thick boundary films of about 10-15 nm thickness at slow speed. In the second stage of each test, this boundary film thickness seems to form again at low speeds but is somewhat reduced, to between 4 and 8 nm

thickness. The behaviour at high speeds follows the classical Dowson and Hamrock relationship with a log(film thickness)/log(speed) gradient of about 0.7.

Similar results were also obtained with stearic acid in hexadecane. Figure 8.3 shows two tests at two concentrations.

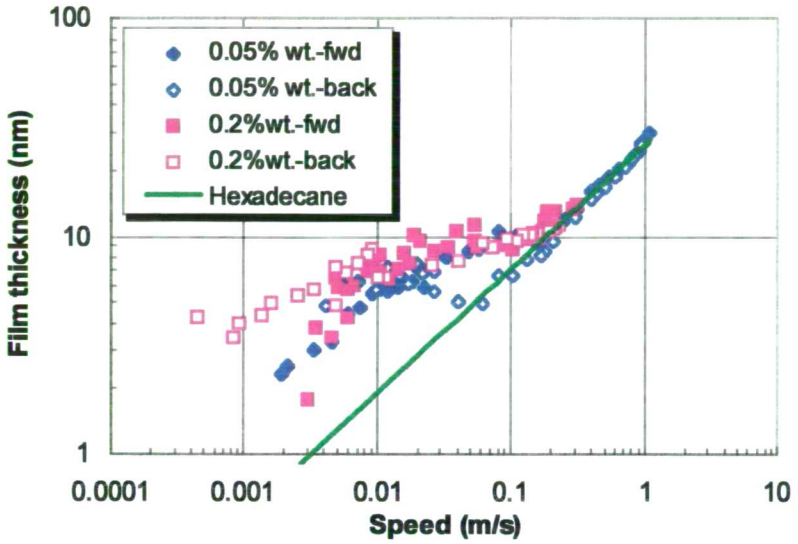


Fig. 8.3. Film thickness vs. speed for stearic acid solutions @ 25°C

It can be seen that the behaviour is broadly similar to that for 0.1% wt. palmitic acid although the boundary film is considerably thinner, maximum values do not exceed 7, mostly 10 nm. There appears to be no concentration effect and none was also noted for oleic and palmitic acid.

A large number of tests were carried out using the same cleaning procedure and test conditions. Whilst many showed the thick boundary film behaviour exemplified in figure 8.2 and 8.3, in others a much thinner boundary film only about 2 nm thick formed initially, although sometimes a thicker film was evident in the second stage of the test. Thin film behaviour is exemplified in figure 8.4 for palmitic and oleic acid showing only the first stage of the test i.e. when speed is gradually increased.

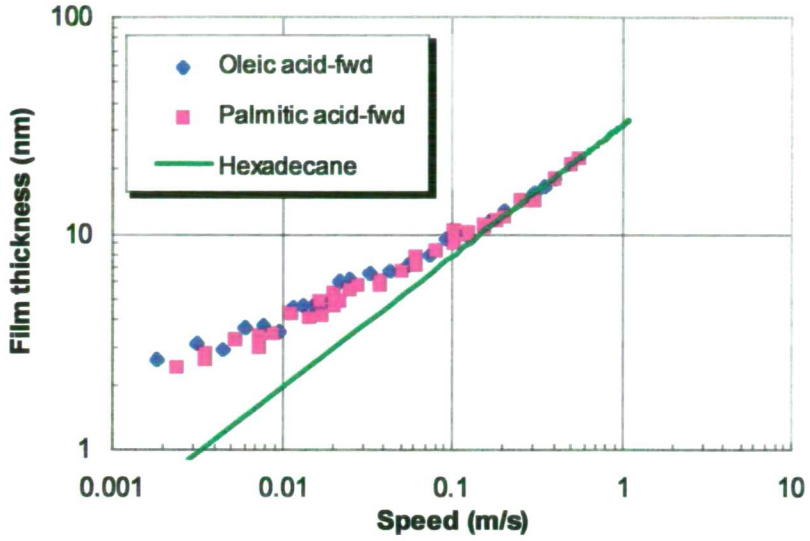


Fig. 8.4. Thin films of palmitic and oleic acids - forward plots @ 25°C

Figure 8.5 shows film thickness/speed results from a test with 0.1% wt. palmitic acid where no boundary film was detected in the initial, increasing speed stage whilst in the second stage of the test (back) the film grew with decreasing the speed quite contrary to the classical EHD behaviour.

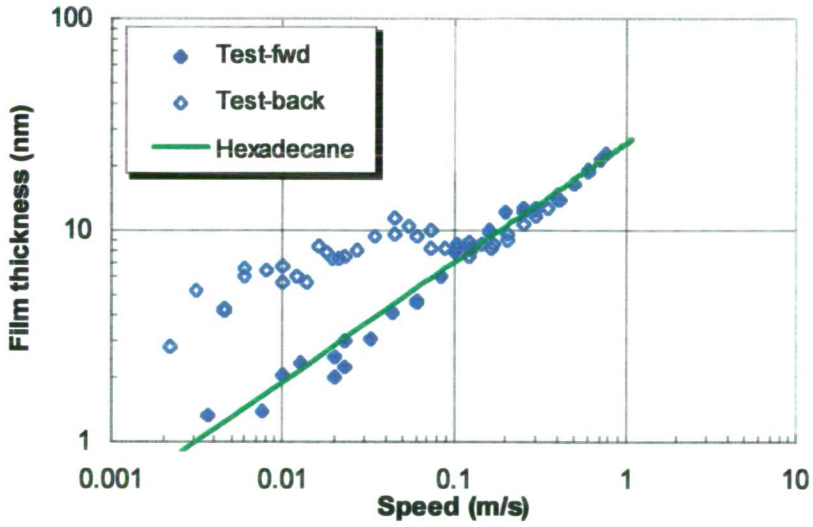


Fig. 8.5. Boundary film reformation in the second stage of the test for 0.1% palmitic acid @ 25°C

The variation in test results was disappointing and a number of factors were investigated in order to try to discover the origin of the variability and to eliminate it.

Presoaking

One possibility was that thick film formation was time-dependent and varied depending upon the time interval between adding the test lubricant and starting the measurement. To investigate this, one change in the test procedure was to presoak the ball in the additive solution for 30 min up to 1 hour to allow for any physical or chemical adsorption. However, this soaking did not seem to influence film formation.

Chloroform/IPA cleaning

In an attempt to reduce scatter, a second, more rigorous cleaning procedure involving chloroform and isopropanol as outlined in the previous section was adopted. This did not completely remove the variation but increased the proportion of tests in which the thick film was formed.

Test time effect

The fact that many tests showed a reformation of the boundary film in the second stage of the test, suggested that there it might be a running time effect. Thus the normal film measurement procedure was deliberately extended. The normal test procedure was first carried out, measuring film thickness as the speed was raised and then lowered. Then the whole measurement procedure was repeated.

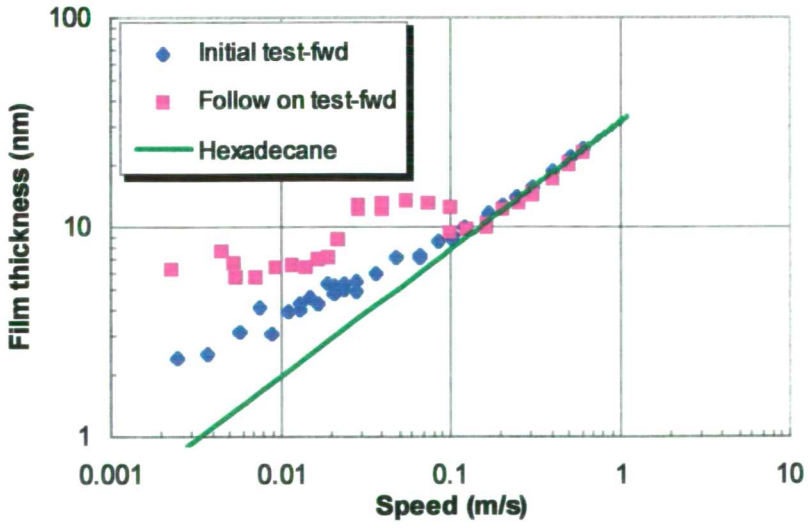


Fig. 8.6. Two stage film thickness vs. speed results for palmitic acid solution @ 25°C (chloroform/IPA cleaning)

Figure 8.6 shows the result of such a test and it can be seen that there is a time effect; the boundary film initially being about 2 nm thick but increasing during running to about 8 to 10 nm. The time effect was explored further. Results from an extended test are shown in figure 8.7. Solution of 0.1% wt. oleic acid was used and the toluene/acetone cleaning procedure was employed.

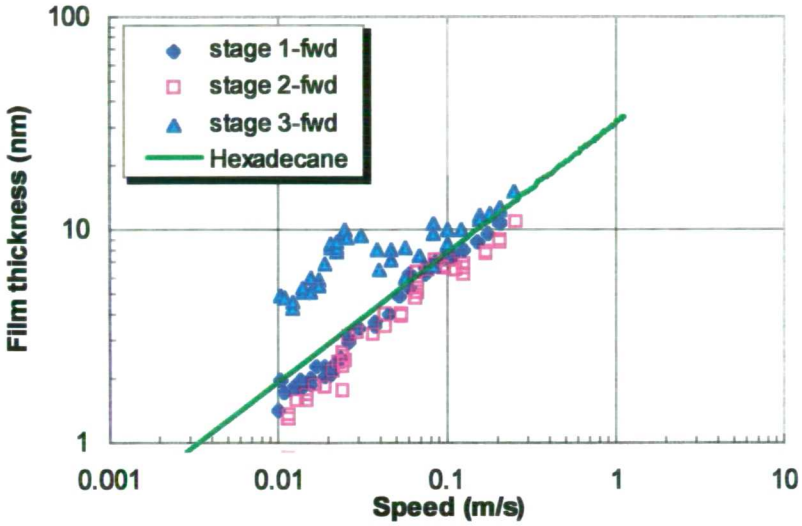


Fig. 8.7. Three stage film thickness vs speed results for oleic acid solution @ 25°C (toluene/acetone cleaning)

Three successive sets of film thickness measurements were made, each separated by one hour period during which the ball was rolled against the disc at 0.1 m/s. The first two stages show no measurable film formation and, indeed, a thinner film than for hexadecane (probably due to some removal of spacer layer). By the third stage, however, a boundary film about 6-8 nm in thickness has clearly formed

Acid cleaning

Bearing in mind that the surface phenomena are extremely sensitive to surface cleanliness, the search for a more efficient cleaning method was further pursued. Thus a third chemical method, developed by Dr. M. Ratoi was employed. Ball cleaning was carried out as follows: a new ball was wiped with toluene, immersed firstly in isopropanol (IPA) and secondly in a solution of 3% wt. hydrochloric acid in IPA for 10-20 sec. Finally the ball was rinsed with distilled water and dried immediately with a hot air gun. The glass disc was cleaned with toluene followed by IPA and wiped dried. Then was immersed in (H_2O_2 + KOH) boiling solution for 10-20 sec, rinsed with

distilled water and dried clean with the hot air gun. In order to check the efficiency of this new cleaning method, measurements of the contact angle of metal and glass surfaces cleaned as above were performed. The results were very encouraging since the contact angles were much lower than for the classical toluene/acetone method showing that the surfaces were freer of organic. Thus for the ball cleaning technique the contact angle value, θ dropped from 65-66° to 13-14° and for the disc from 40-47° to 4-5°. Despite these assuring results, however, film thickness tests still showed a lot of scatter.

Effect of adsorbed moisture

One possibility for the variation in film formation was the varying presence of water, either in the lubricant or in the rubbing surfaces. In this context it is noteworthy that some of the studies reviewed in chapter 7 concluded that moisture was necessary for thick boundary films formation [**8.5** to **8.8**]. A series of tests were therefore performed in which the influence of water vapour was investigated. Two modifications were made to the normal experimental method to accomplish this. In one set of tests, the metal ball and the glass disc previously cleaned with the toluene/acetone method were suspended in a closed glass vessel which contained a pool of water in the bottom. The specimens were left in this atmosphere of 82% relative humidity for 4 hours before the normal film thickness test was performed. The second procedure was to leave the palmitic acid solution in the same conditions of humidity but for longer time, 24 hours.

These experiments were not found to favour thick film formation and, indeed, films no thicker than those formed by hexadecane were detected and there was no measurable difference even after one hour of extensive running. It is possible that the ball and disc surfaces became covered with a monolayer of solvent from cleaning with toluene/acetone and that water molecules were not able to displace these solvent molecules in order to adsorb on to the solid surface. On the other hand it is possible that it is not the amount of adsorbed water that is important but the changes in the surface chemistry produced by it, which could depend on factors such as the nature of lubricant, rubbing conditions and probably the amount of oxygen molecules capable to form the metal oxide layer beneficial in promoting boundary films formation.

8.3.3. Concentration influence

According to previous studies [**8.4**], the film thickness of fatty acids solutions increases with concentration, all other conditions being held constant. However, in this study, film thickness tests of stearic, palmitic and oleic acids solutions at different concentrations did not show any significant difference. Figures 8.8 and 8.9 show such results for oleic and palmitic acid solutions in hexadecane at three concentrations: 0.1, 0.5 and 1%.

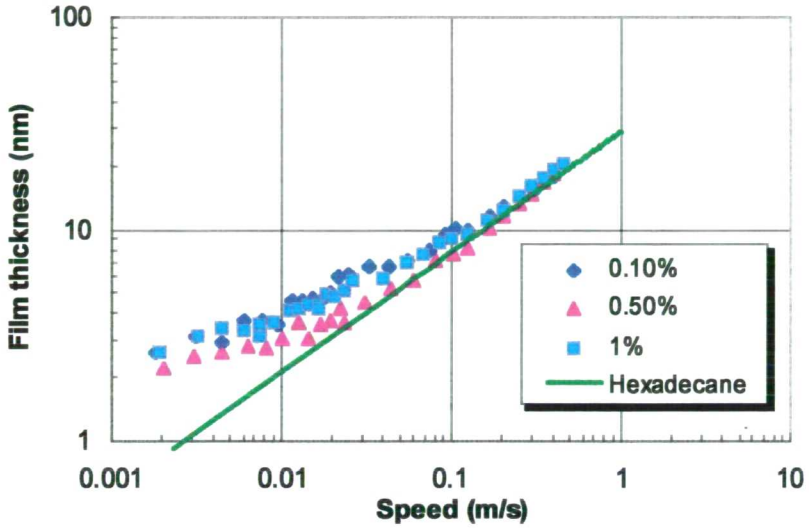


Fig. 8.8. Film thickness vs. speed for oleic acid solution in hexadecane-concentration influence @ 25°C

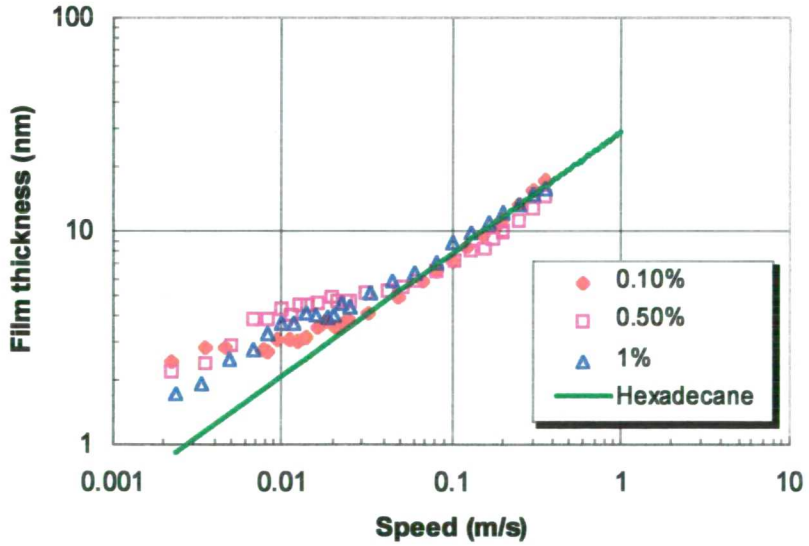


Fig. 8.9. Film thickness vs. speed for palmitic acid solution in hexadecane-concentration influence @ 25°C

The data points represent the film thickness variation as speed is steadily increased. Stearic acid response to concentration variation is exemplified in figure 8.3.

8.4. Discussion

It is clear that in some conditions, long chain carboxylic acids form quite thick films, up to and even in excess of 10 nm thickness in high pressure, slow speed rolling conditions. Since the surfactants employed in this study have chain lengths of between 2 and 2.5 nm when fully aligned [**8.9**], such thick films imply many equivalent monolayers. These boundary films appear to become thinner at very slow speeds and are also partially lost on halting the rolling motion. This type of behaviour has previously been seen with polar polymer solutions and is believed to indicate the presence of a surface film of enhanced viscosity [**8.10**]. It is not yet known whether these films represent ordered multilayers or a more disordered, paste-like material. As the speed is raised, these films often exhibit some instability, reflected in a very variable and often decreasing film thickness in the intermediate speed range of about 0.1 m/s. This might be regarded as a starvation of a thick, lumpy film which, as the speed is raised and the separation becomes higher, is less entrained in the contact thus resulting in a collapse of the film. At high speeds the influence of boundary films on overall film thickness appears minimal. The boundary films formed by palmitic acid were consistently higher than those formed with stearic acid. This may possibly be related to a "chain matching" effect since palmitic acid and hexadecane have the same number of carbon atoms [**8.11**].

From the results carried out in this study it appears that the extent of thick film formation is determined by a coupling of cleaning method and running time. The formation of multilayers may be critical contingent on the initial formation of a coherent monolayer to provide the template for further layer formation. Thus thick boundary film formation will be especially sensitive to surface cleanliness and it is possible that the extended rolling helps to form the crucial single monolayer by conditioning the surfaces. Alternatively, it is possible that, whilst monolayers can be formed by direct adsorption of surfactant, multilayers can only be formed by carboxylic acid salts or soaps. In this case, cleanliness might determine the accessibility of metallic oxides for reaction with surfactant and extended running might promote the formation of insoluble soaps on the surfaces.

This concept will be further discussed after results on commercial friction modifier additives are presented in the next chapter.

REFERENCES

[8.1] Spikes H.A. and Cameron A., "A Comparison of Adsorption and Boundary Lubricant Failure", Proc. Roy. Soc. Lond. A336, pp. 407-419, 1974,

[8.2] Hamrock B.J. and Dowson D., "Ball Bearing Lubrication: the Elastohydrodynamics of Elliptical Contacts", publ. J.Wiley, New York, 1981,

[8.3] Guangteng G. and Spikes H.A., "Boundary Film Formation by Lubricant Base Fluids", Trib. Trans. 39, pp. 448-454, 1996,

[8.4] Fuks G.I., "The Properties of Solutions of Organic Acids in Liquid Hydrocarbons at Solid Surfaces", Research in Surface Forces, vol. 1, 1960, ed. B.V. Deryaguin, Transl. by Consultants Bureau, NY, 1963,

[8.5] Smith A.J. and Cameron A., "Rigid Surface Films", Proc. Roy. Soc. Lond. A328, pp. 541-560, 1972,

[8.6] Sherwood A.F. and Rybicka S.M., "Surface Properties of Titanium Dioxide Pigments", J. Oil Col. Chem. Assoc. 40, p. 648, 1966,

[8.7] Smith H.A. and McGill R.M., "The Adsorption of n-Nonadecanoic Acid on Mechanically Activated Metal Surfaces", J. Phys. Chem. 61, p. 1025, 1957,

[8.8] Hirst W. and Lancaster J.K., "Effect of Water on the Interaction between Stearic Acid and Fine Powders", Trans. Farad. Soc. 47, p. 315, 1951,

[8.9] Cameron A., "Basic Lubrication Theory", 3rd edition, Ellis Horwood, Chichester, chapt. 15, 1981,

[8.10] Smeeth M., Gunsel S. and Spikes H.A., "The Formation of Viscous Surface Films by Polymer Solutions: Boundary or Elastohydrodynamic Lubrication", Trib. Trans. 39, pp. 720-725, 1996,

[8.11] Hirano F., Sakai T., Kuwano N. and Ohno N., "Chain Matching Between Hydrocarbon and Fatty Acid as Interfacial Phenomena", Tribology Int. 20, pp. 186-204, 1987

CHAPTER 9

COPPER OLEATE AND C_{36} DIMER STUDY

Film thickness and friction results obtained with solutions of copper oleate and a commercial additive, C_{36} dimer acid ester, are presented in this chapter. A similar approach to fatty acids was used for film thickness measurements with emphasis on time dependence and temperature effects. The influence of shear on film formation was studied by varying the slide/roll ratio in the EHD film test. Traction coefficient variation with mean entrainment speed was also determined which enabled a correlation with film thickness to be obtained.

9.1. Materials employed

It has been extensively reported in the literature [**9.1, 9.2, 9.3, 9.4**] that long-chain carboxylic acids when in contact with reasonably reactive metals such as copper and iron react with the metal or metal oxide to form metallic salts or soaps which are more durable than the physically adsorbed acid and help reducing friction between rubbing surfaces up to the melting-point of the metal soap. In view of these reports, a study was carried out in which the additive used was a salt of oleic acid, copper oleate. This compound, with the chemical formula $[CH_3(CH_2)_7CH{=}CH(CH_2)_7COO^-]_2Cu^{2+}$ and the molecular weight 626.42, was supplied by ICN Pharmaceuticals Ltd. Copper oleate is

also commercially used as a friction modifying additive which made a study of its behaviour particularly interesting.

In a first series of tests at room temperature, the solvent employed was hexadecane which was chosen for the reasons outlined in the previous chapter. Tests were then carried out at higher temperatures and with sliding using a mineral oil, 100SN, supplied by Exxon Chemical Ltd. as a solvent. This is a paraffinic base oil that has relatively high paraffinic content and is characterised by good viscosity/temperature characteristics (high VI), good stability and adequate low temperature properties. In oil industry terminology they are frequently referred to as solvent neutrals (SN) where solvent means that the base oil has been solvent refined and neutral means that the oil is of neutral pH [**9.5**]. An alternative designation is high viscosity index (HVI) base oil. Typical physical properties for 100SN are shown in the table below. Low shear rate kinematic viscosity was measured using a conventional capillary viscometer and the refractive index, required for converting measured optical film thicknesses to absolute spatial values, was measured using an Abbe refractometer.

GRADE	FLASH POINT(°C)	DENSITY (g/cm^3)	VISCOSITY (cSt)			REFRACTIVE INDEX		
		20°C	25°C	40°C	100°C	25°C	60°C	100°C
100SN	195	0.872	40.3	19.8	4.5	1.4725	1.4618	1.4496

Table 9.1. Physical properties for 100SN base oil

In addition to copper oleate, studies were performed with a commercial additive C_{36} dimer acid ester. This is formed from a mixture of the long chain C_{36} dimer of linoleic acid and ethylene glycol and is reported to be very effective in reducing valve train wear in automotive engines [**9.6, 9.7**]. Figure 9.1 shows the chemical formula for this compound.

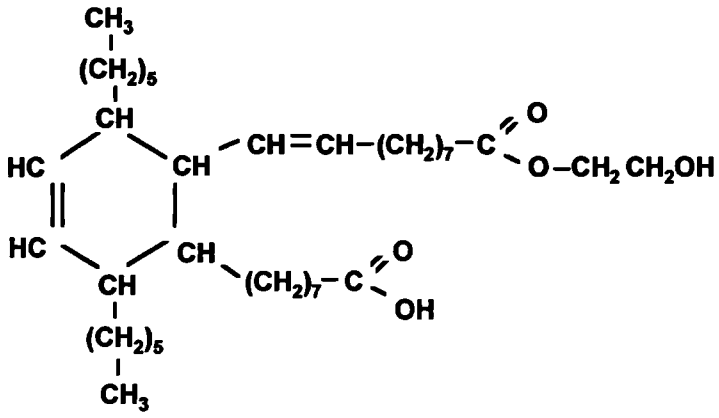


Fig. 9.1. Chemical formula for C_{36} dimer acid / ethylene glycol (from ref. **9.7**)

Since both the dimer acid and glycol are quite soluble in hydrocarbons [**9.6**], it was relatively easy to form solutions of 0.1% wt. in hexadecane and in paraffinic oil as solvents.

9.2. Film thickness results

Solutions of 0.1% wt. copper oleate and C_{36} dimer acid ester in hexadecane were employed for film thickness tests using the ultra-thin interferometry technique described in chapter 4. Their film forming capabilities were assessed under pure rolling conditions at 25°C using a similar test procedure to the one described in chapter 8. A chemical cleaning method based on toluene and acetone was used (see chapter 8). Since in practical conditions these additives are normally dissolved in mineral oils, room temperature tests were also performed using 100SN mineral oil as a solvent. The influence of temperature was investigated by carying out tests at 60 and 100°C and the resistance to shear of the films formed was tested under mixed sliding/rolling conditions. All tests were fully flooded except for those using hexadecane solvent at room temperature. These results are shown in the subsequent sections.

9.2.1. Film thickness of hexadecane and 100SN mineral oil

The film thickness variation with speed for the additive-free lubricants was tested initially. Hexadecane results have already been presented in the previous chapter in figure 8.1. The results for the mineral oil at three temperatures are shown in the plot

below. Several sets of results are included to show the level of repeatability which was ±1 nm below 10 nm.

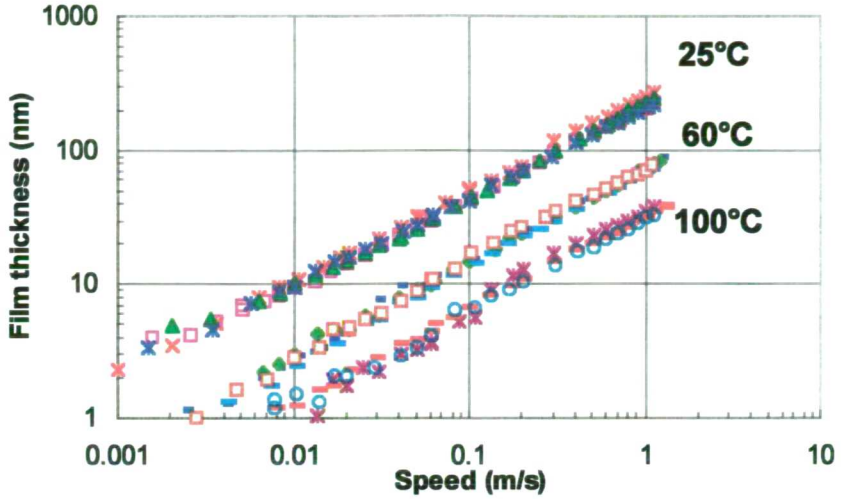


Fig.9.2. Film thickness vs. speed for 100SN mineral oil at three temperatures

It can be seen that the film thickness is proportional to $(speed)^{0.67}$ and forms a straight line in a log/log plot with a gradient close to 0.67, i.e. 0.66 and 0.7 for 25°C and 60°C and 0.68 for 100°C. This shows that the EHD theory is obeyed down to 1 nm thickness which demonstrates that any roughness or boundary lubricant effects occur only at thicknesses of less than 1 nm. As expected, film thickness is lower at higher temperature, primarly because of the effect of temperature on viscosity.

9.2.2. Film thickness results for additive-containing solutions at 25°C

With hexadecane as solvent

Figure 9.3. depicts three tests with copper oleate 0.1% wt. solution in hexadecane at room temperature. For clarity, the film formed by the hydrocarbon is shown by a continuous line rather than individual data points. It can be clearly seen that all three tests show a similar behaviour both in the first half of the test when speed is steadily increased (fwd) as well as in the second part when speed is decreased (back). Films of 10 to 20 nm are formed in the low speed region in a very similar manner to that observed with fatty acid "thick film" behaviour (chapter 8).

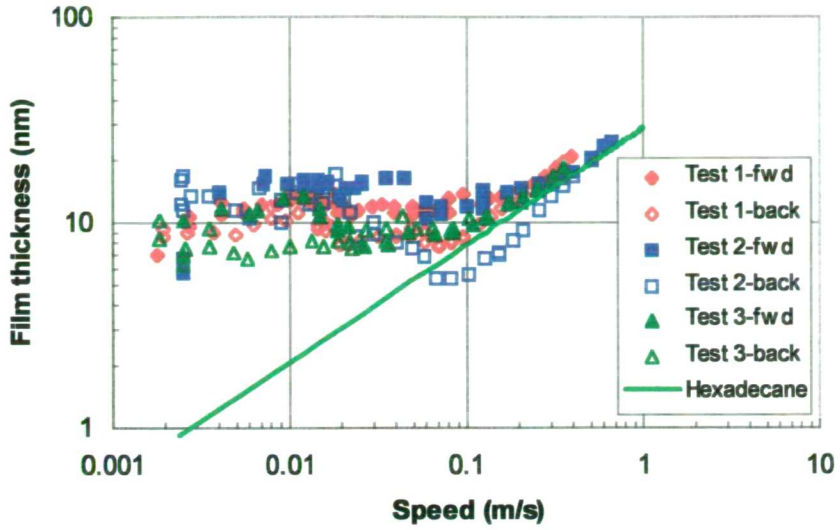


Fig.9.3. Film thickness vs. speed for 0.1% Cu Oleate in hexadecane @ 25°C

These films appear to collapse at a speed around 0.1 to 0.2 m/s and join the film thickness curve of hexadecane, at higher speeds behaving in a pure hydrodynamic fashion. It is interesting to note that even in the second part of the test, whilst speed is decreased, the film gradually increases to values just slightly less than those obtained at the beginning of the test. Another type of behaviour on the "back" plot is shown in figure 9.4. where the boundary film reformed at slow speeds exceeds the initial values from the first half of the test.

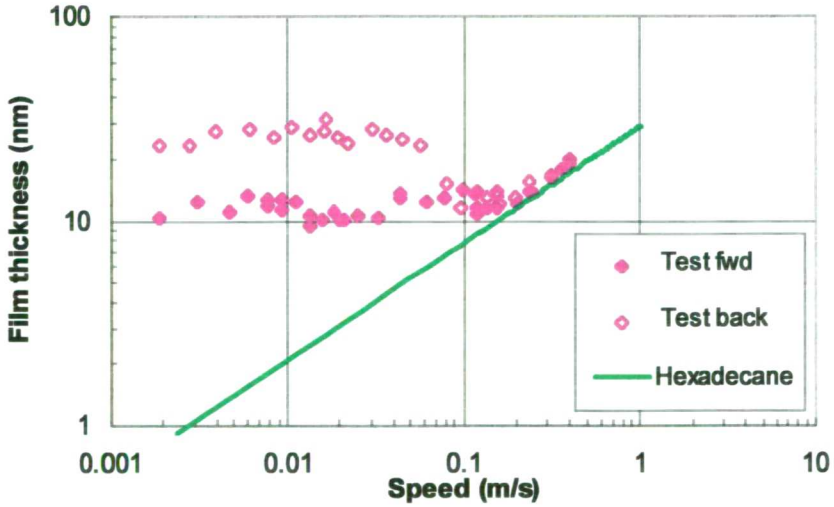


Fig.9.4. Reformation of thicker film at slow speeds for 0.1% Cu Oleate in hexadecane @ 25°C

Since there were some questions as to the solubility of copper oleate in hexadecane at the concentration of 0.1% wt., tests were carried out at 0.01% wt.

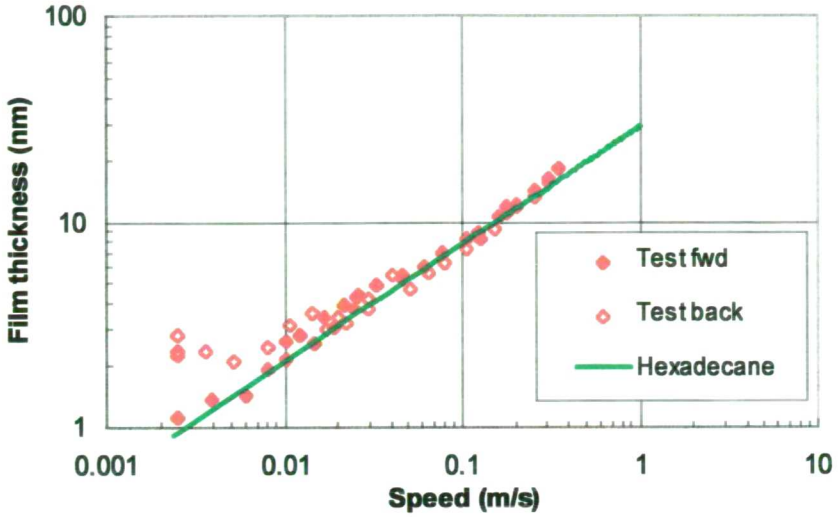


Fig.9.5. Film thickness vs. speed for 0.01% Cu Oleate in hexadecane @ 25°C

As it can be seen from figure 9.5, the effect of additive in this case was insignificant. Another way to increase the solubility was to add a more polar compound to the initial solution which would help the polar molecules of copper oleate to dissolve. Tripropylene glycol monomethylether (TPGME) with chemical formula H-(OCH (CH_3) $CH_2)_3$ - OCH_3 and molecular weight 206, has been used for this purpose in synthetic oils [**9.9**]. The solubility parameters for all three components were calculated using the formula developed by Fedors and Small [**9.10**] and the values obtained are as follows: 8.01 for hexadecane, 9.18 for copper oleate and 9.98 for TPGME. Since close values with differences of less than unity are an indication of good solubility, it was believed that the combination would be successful. Several tests were carried out but much thinner films were obtained possibly due to the competition for the adsorption sites between the polar solvent and the copper oleate molecules.

The problem of initial solubility of copper oleate was eventually overcome by slightly raising the temperature during stirring the solution.

Film thickness tests at room temperature were also carried out using the commercial additive C_{36} dimer acid ester in hexadecane and results are shown in figure 9.6.

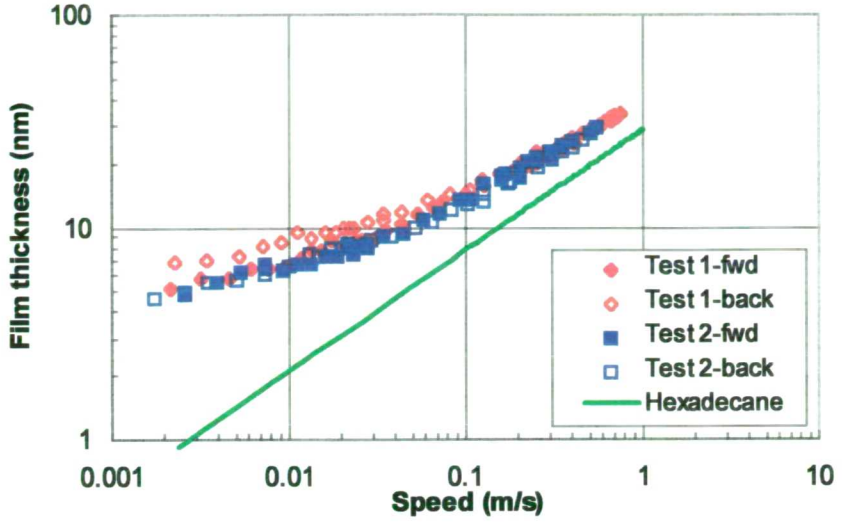


Fig.9.6. Film thickness vs. speed for 0.1% C_{36} dimer acid ester in hexadecane @ 25°C

Boundary films no more than 10 nm thick were detected, less than with the copper oleate. These were still present when speed was gradually decreased. The film also shows quite an even, steady behaviour which was confirmed by the low values of standard deviation during measurement. It is interesting to note that at higher speeds in the hydrodynamic regime, the film thickness tendency to join the solvent line is much slower than with copper oleate, the difference of about 5 nm still being present up to 1 m/s, suggesting that the film formed at interfaces might make a detectable contribution even in thick film lubrication regime.

With 100SN as solvent

Film thickness results for solutions of copper oleate and C_{36} dimer acid ester in mineral oil at 25°C are shown in figures 9.7 and 9.8 respectively. These show that both additives form films of insignificant thickness compared to the base oil. This may be because mineral oils, unlike hexadecane, contain a slight amount of natural polar compounds which might compete with the additive molecules for adsorption at the interfaces.

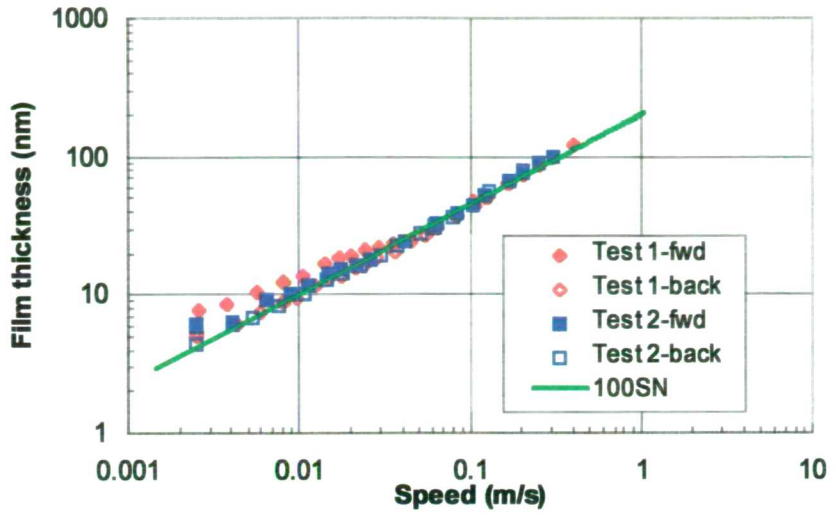


Fig.9.7. Film thickness vs. speed for 0.1% Cu Oleate in 100SN @ 25°C

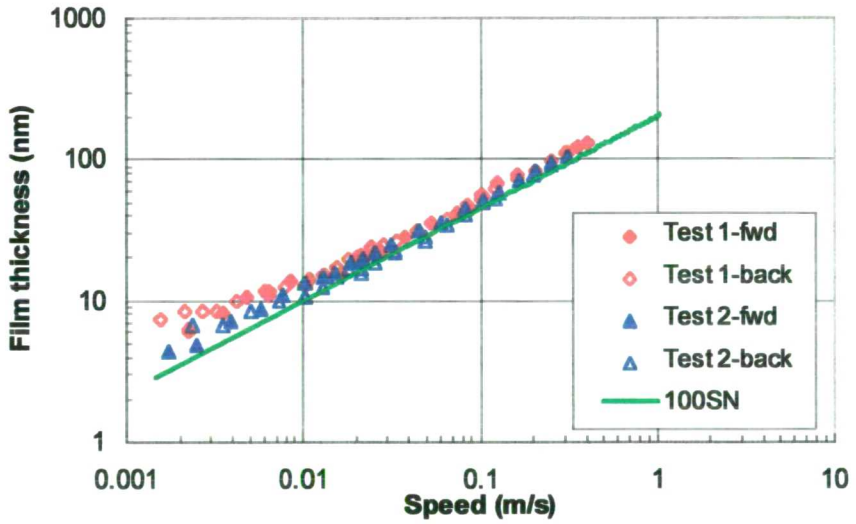


Fig.9.8. Film thickness vs. speed for 0.1%C_{36} dimer acid ester in 100SN @ 25°C

9.2.3. Film thickness results for additive-containing solutions at 60°C

Higher temperature tests were only performed with solutions in mineral oil as solvent and not with hexadecane. This was mainly to avoid the risk of oxidation of hexadecane. Typical results are shown in figures 9.9 and 9.10 with Cu oleate and C_{36} dimer acid ester solutions in 100SN at 60°C. Both additives behave in a similar manner in that they formed thick boundary films of 10 to 15 nm after extensive running i.e. in the second half of the test when speed was subsequently decreased after maximum test speed was

reached. There was also a small contribution in the first part of the test, in the "forward" plot, where the film thickness showed an enhancement of 2.5 to 3 nm compared to the base oil. This observed behaviour may be ascribed to the increase in test temperature since the results at room temperature showed no boundary film formation, all other test conditions being the same.

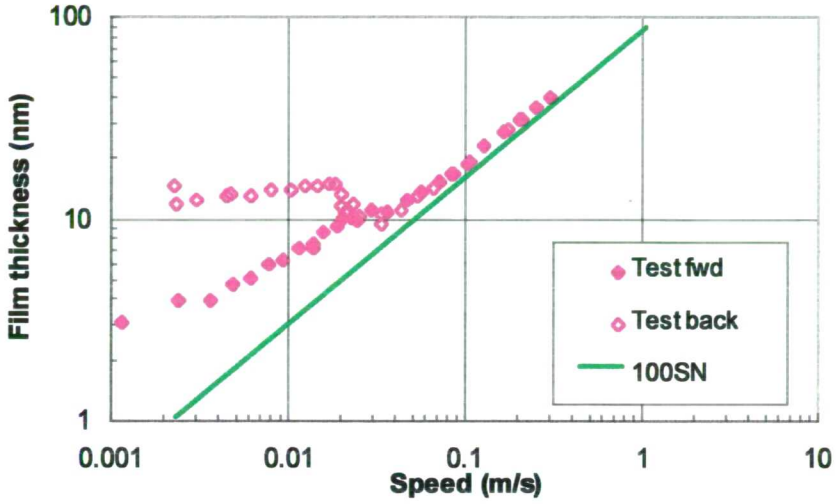


Fig.9.9. Film thickness vs. speed for 0.1% Cu oleate in 100SN @ 60°C

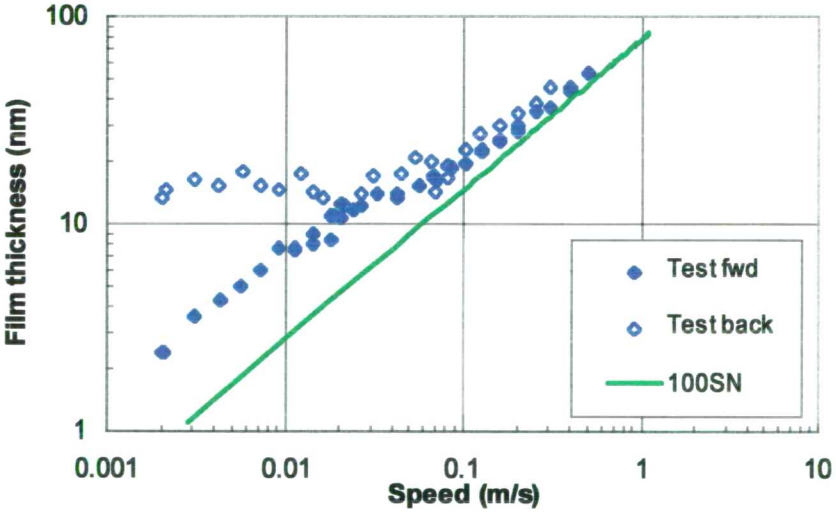


Fig.9.10. Film thickness vs. speed for 0.1% C_{36} dimer acid ester in 100SN @ 60°C

Time effect

Since it was noticed that the increase in film thickness tendency was more pronounced towards the end of the test, the effect of running time was explored further. Thus to

investigate the kinetics of boundary film reformation at slow speeds, the test procedure was changed to eliminate the second stage in which the speed was gradually decreased. After measuring the film thickness at the maximum test speed in the forward part, the speed was very rapidly reduced to 0.011 m/s and subsequent measurements were taken at fixed time intervals (2 minutes) whilst the rig was left running at the same speed. The results of such tests are shown in figure 9.11.

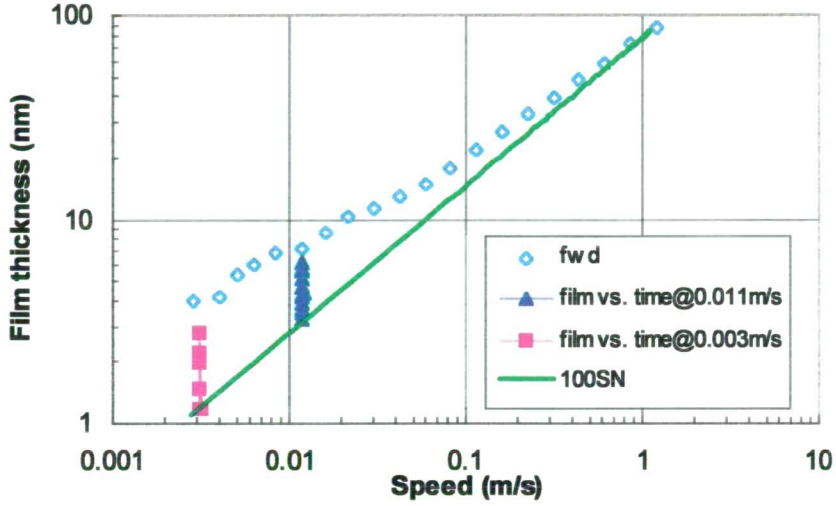


Fig.9.11. Film thickness vs. speed for 0.1%Cu oleate in 100SN @ 60°C, pure rolling, time effect

It can be seen that the first measurement taken at 0.011 m/s (bottom blue triangle) gave a low value for the film thickness which was comparable to the base oil value at the same speed and not to the previous film thickness measured on the forward plot. This was an indication that boundary films do not survive in high speed conditions. The film thickness then increased with time and eventually reached the boundary film values. The same time dependence analysis was also applied for a lower speed, 0.003 m/s when the film build up was recorded at 4 minutes intervals. The speed was again increased up to the maximum value and then immediately reduced to 0.003 m/s. It is interesting to note from figure 9.12 that the film thickness increase rate is not as high as expected from the results from previous tests (figure 9.10) and there are several fluctuations which might suggest a temporary loss of film or an uneven deposition on the surfaces.

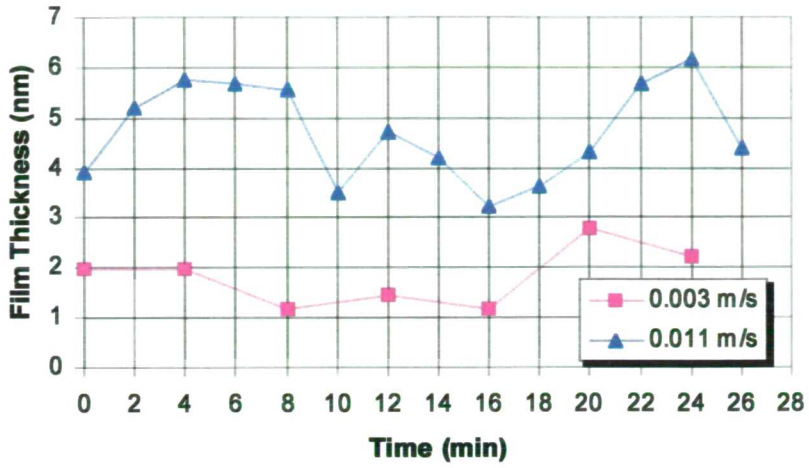


Fig.9.12. Film thickness growth with time for 0.1% Cu oleate in 100SN solution @ 60°C, pure rolling

9.2.4. Film thickness results for additive-containing solutions in mixed sliding/rolling conditions

The above tests were carried out in nominally pure rolling. In practice, friction modifier films must withstand sliding and therefore tests were also carried out to measure film thickness in mixed sliding-rolling conditions. To enable this, the set-up from traction measurements was used i.e. the ball and disc were driven by separate DC motors in order to control the slide/roll ratio. Film thicknesses were determined at 50% slide/roll ratio for a range of speeds from 3 mm/s up to 1m/s. When plotted against speed in a log/log scale, the entrainment speed was calculated as the average between the ball and the disc speed. Figure 9.13 shows the behaviour of 0.1% wt. Cu oleate in 100SN at 25°C under 50% sliding. As with the pure rolling case (figure 9.7), the room temperature test shows no enhancement in film thickness and, indeed, at low speeds, the measured film is less than the base oil value, probably due to some loss of silica layer. This was confirmed by negative film values obtained when the thickness in the trigger point was checked at the end of test.

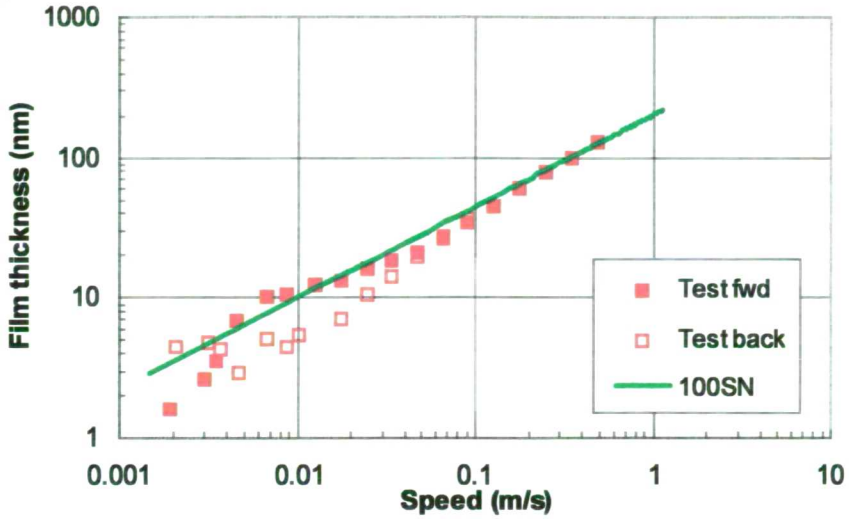


Fig.9.13. Film thickness vs. speed for 0.1% Cu oleate in 100SN @ 25°C, 50% SRR

A totally different behaviour was observed at higher temperatures and figures 9.14 and 9.15 show some typical film thickness results obtained when 50% sliding was introduced from the beginning of the test. It can be seen that the enhanced film thickness due to surfactant at slow speeds is present in the mixed sliding/rolling contact just as in pure rolling. Films of 30-40 nm were measured for copper oleate which collapsed at speeds of about 0.2 m/s. The films formed by the dimer are not as spectacular but still quite significant, at 10-15 nm, and seem to gradually join the base oil line without the sharp decrease found with copper oleate.

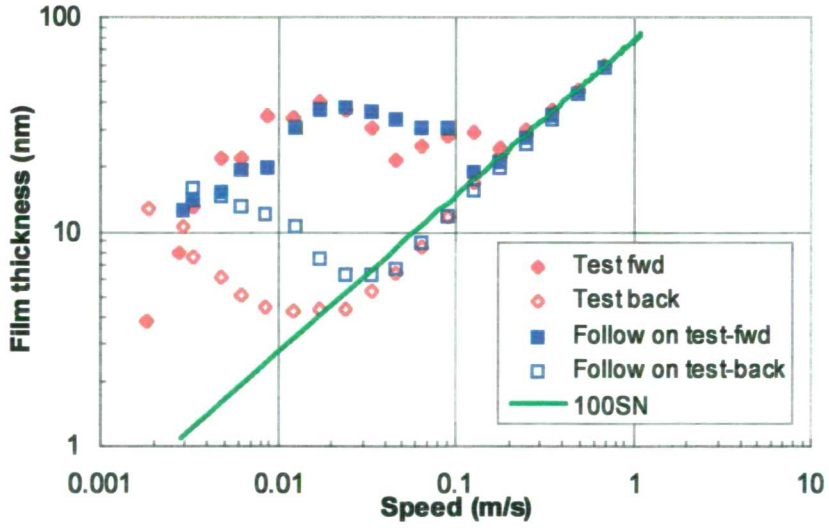


Fig.9.14. Film thickness vs. speed for 0.1% Cu oleate in 100SN @ 60°C, 50% SRR

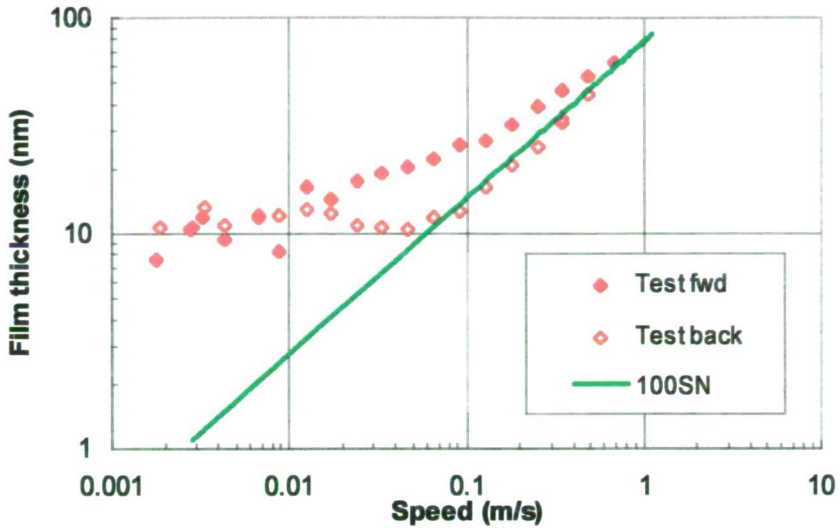


Fig.9.15. Film thickness vs. speed for 0.1% C_{36} dimer acid ester in 100SN @ 60°C, 50% SRR

This behaviour is similar to that of some viscosity index improvers which form much thicker films than predicted from EHD theory [**9.11**].

Tests were also carried out at 100°C with 50% sliding. These revealed the formation of very thick films up to 60-80 nm for Cu oleate and up to 30 nm for C_{36} dimer acid. The results are presented in figures 9.16 and 9.17 and it can be seen that the overall pattern of behaviour is the same as in the 60°C tests.

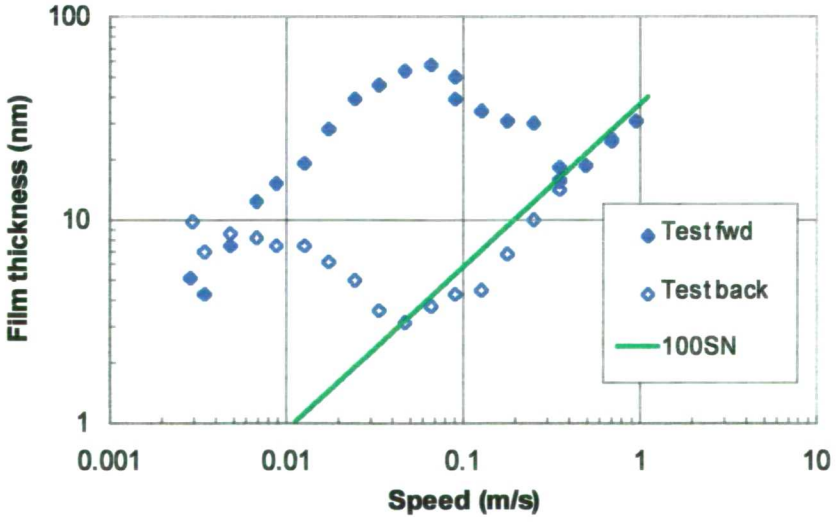


Fig.9.16. Film thickness vs. speed for 0.1% Cu oleate in 100SN @ 100°C, 50% SRR

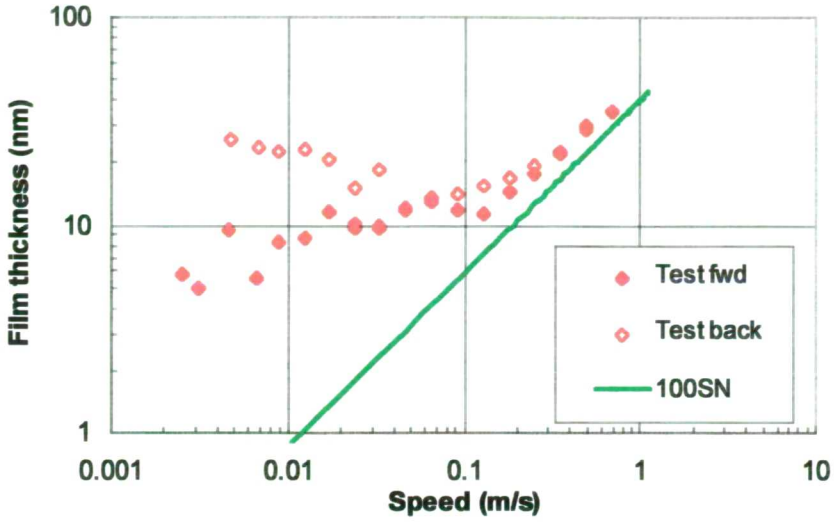


Fig.9.17. Film thickness vs. speed for 0.1% C_{36} dimer acid ester in 100SN @ 100°C, 50% SRR

It is interesting to note the reformation of the thick film in the second stage of the test which is a general characteristic for high temperature tests.

Influence of test time

The kinetics of boundary film reformation at slow speeds was explored in mixed rolling/sliding conditions in a similar way to the pure rolling tests described in section 9.2.3. Results for copper oleate and C_{36} dimer acid ester in 100SN are presented in figures 9.18 to 9.21 at 60°C in rolling with 50% sliding conditions

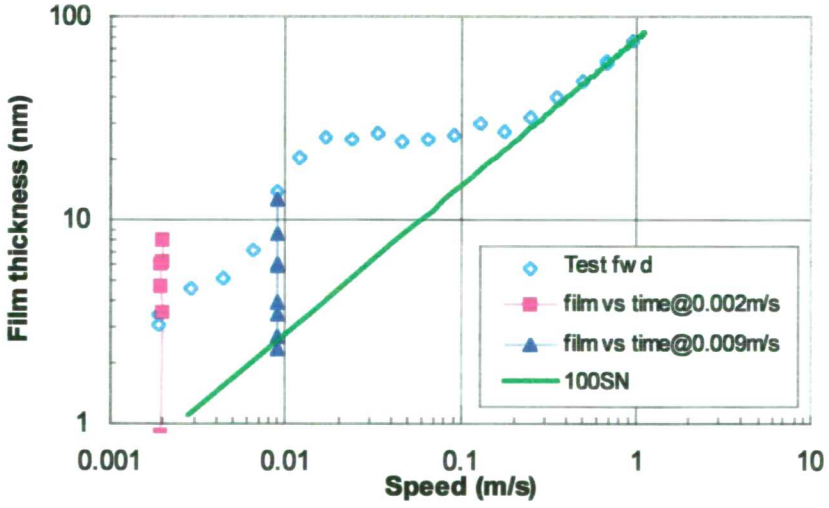


Fig.9.18. Film thickness vs. speed for 0.1%Cu oleate in 100SN @ 60°C, 50% SRR, time effect

It can be seen that the rate of film formation is higher than in the pure rolling conditions (figure 9.12) for both speeds tested. This suggests again that sliding is beneficial for the film growth in the low speed region, up to 0.1 m/s. It is interesting to note that with copper oleate, the films start to form after rapid reduction in entrainment speed from values characteristic to the base oil whilst with the C_{36} dimer there is a shift of about 4-5 nm from the base oil line. This confirms that for solutions of C_{36} dimer acid ester, the boundary film formed at interfaces in the first stage of the test is not completely removed due to shear at high speeds.

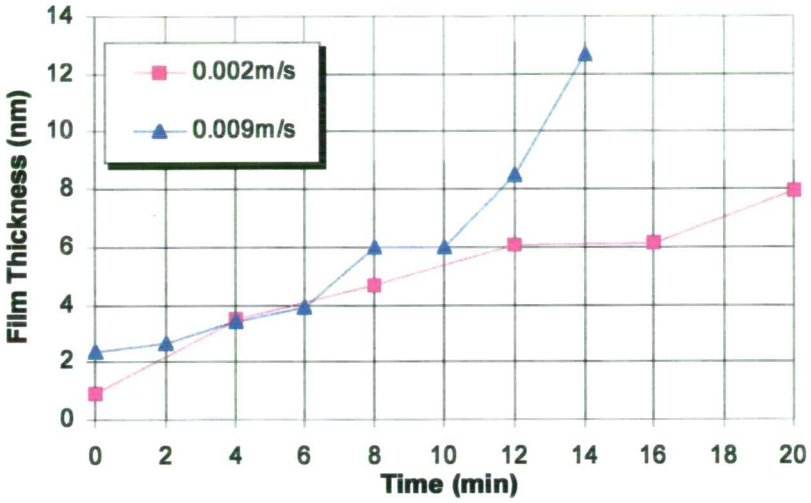


Fig.9.19. Film thickness growth with time for 0.1% Cu oleate in 100SN solution @ 60°C, 50% SRR

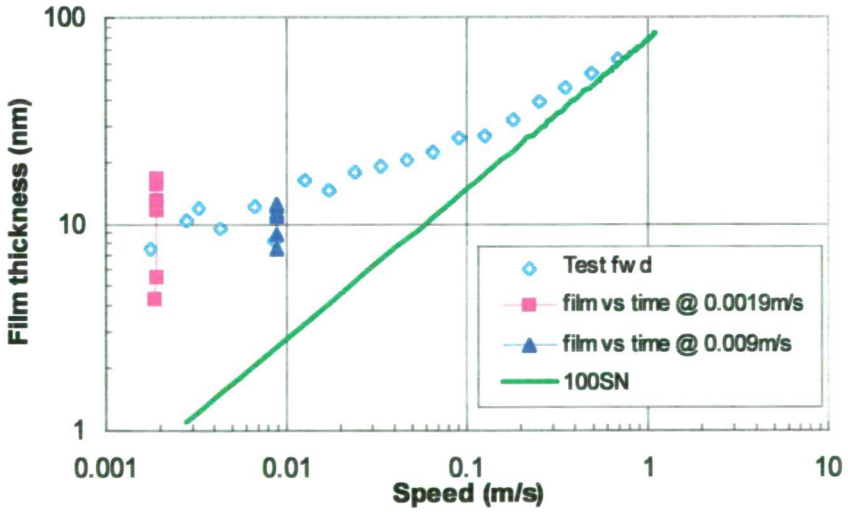


Fig.9.20. Film thickness vs. speed for 0.1%C_{36} dimer acid ester in 100SN @ 60°C, 50% SRR, time effect

It is interesting to note that with copper oleate, the films start to form after rapid reduction in entrainment speed from values characteristic to the base oil whilst with the C_{36} dimer there is a shift of about 4-5 nm from the base oil line. This confirms that for solutions of C_{36} dimer acid ester, the boundary film formed at interfaces in the first stage of the test is not completely removed due to shear at high speeds.

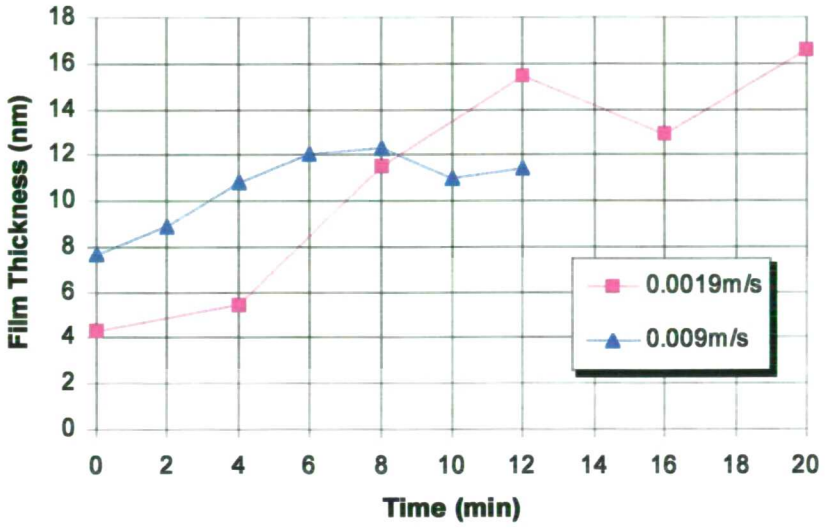


Fig.9.21. Film thickness growth with time for 0.1% C_{36} dimer acid ester in 100SN solution @ 60°C, 50% SRR

The time effect was also studied for temperatures of 100°C and typical results are shown in figure 9.22.

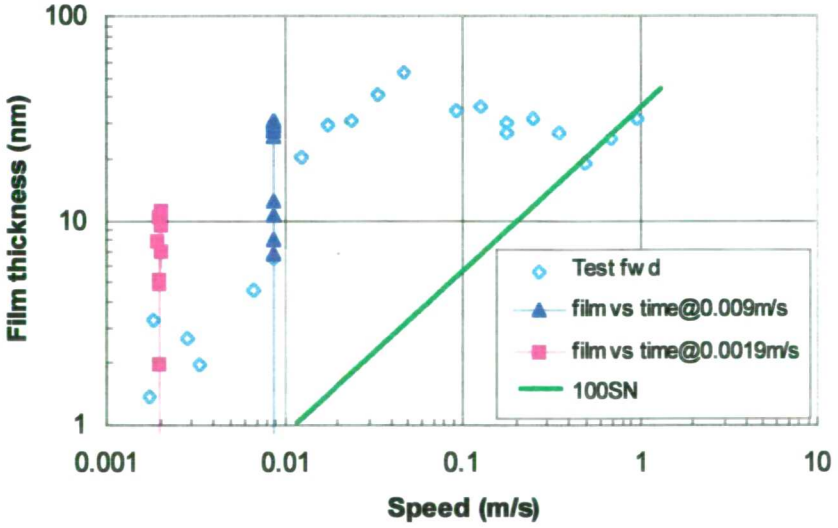


Fig.9.22. Film thickness vs. speed for 0.1% Cu oleate in 100SN @ 100°C, 50% SRR, time effect

In most cases, film thickness after rapid speed reduction and before growth at constant speed was lower than the base oil line, probably due to silica layer damage which was accelerated by the fact that the lubricant had lower viscosity at higher temperature.

The diagram presented in figure 9.23 shows the film thickness variation with time for two tests at 100°C. Both are showing a similar trend in that the growth rate is higher for the high speed tests as well as the maximum film values attained.

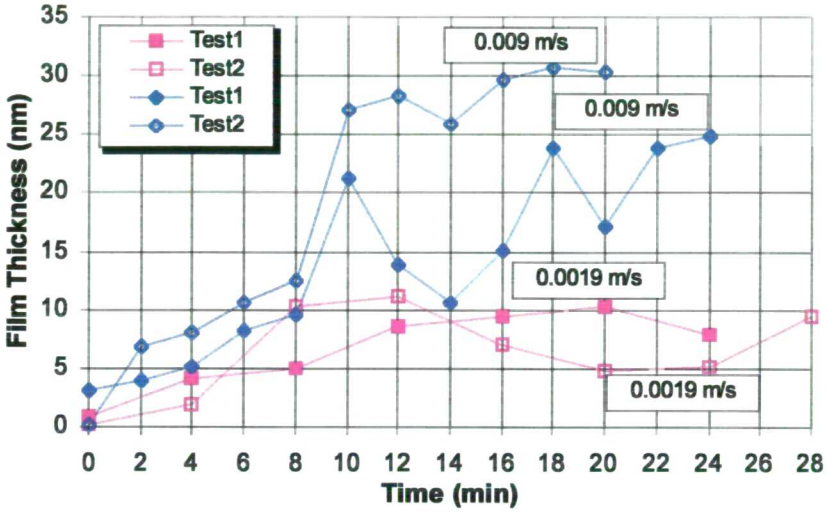


Fig.9.23. Film thickness growth with time for two solutions of 0.1% Cu oleate in 100SN @ 100°C, 50% SRR

An attempt was made to measure film thickness under sliding conditions at a still higher temperature of 135°C but the results were not reliable since it was noticed at the end of the test that the colour of the solution has changed from blue to yellow probably due to oxidation products and also that there was a lot of damage to the spacer layer on the surface.

Visual evidence

It was noticed that whilst the tests were performed, there was a visible change in the aspect of the interference fringes on the monitor screen. These were captured on photographs taken at different test times and speeds and are presented in figure 9.24.

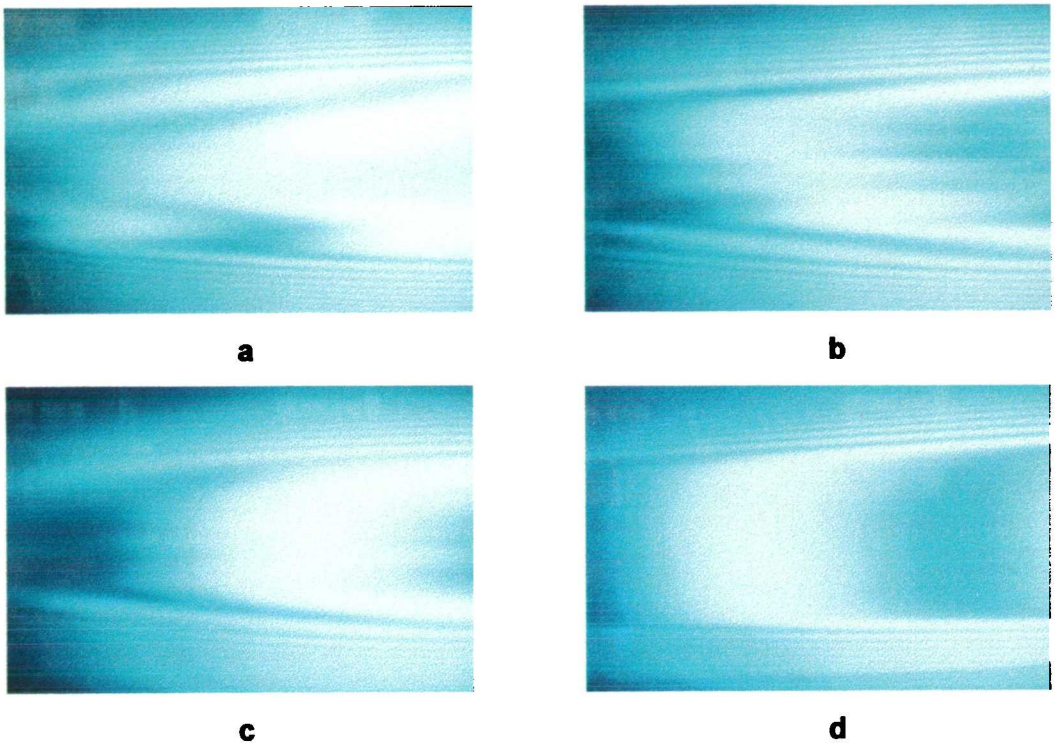


Fig.9.24. Photographs of the monitor screen showing the dispersed contact images

When thick films were forming, the image of the broad band which covers most of the screen and represents the centre of the contact area, was becoming more and more unclear and additional fringes were forming. In these circumstances, the standard deviation of the measurements was also increasing, suggesting that the boundary film thickness might also be very uneven over the contact area. This situation is represented in figure 9.24a which shows the interference pattern when measuring the film thickness at 0.002 m/s after a film versus time test of 20 min. The central fringe image was changing with speed as it can be seen from figures 9.24b and 9.24c taken at 0.005 and 0.008 m/s respectively and was still maintaining a fuzzy, blurred appearance as long as the boundary film was present. This was suggesting that the transparency of the medium in the contact was partially reduced due to the presence of some amorphous deposition. Only after running at high speeds up to 1 m/s, the image became clear, with distinct contours as it normally appears for a film test (figure 9.24d at 0.002 m/s speed).

Negative sliding

All mixed sliding/rolling results shown so far have had the disc moving faster than the ball (positive sliding). It was of interest to see how the film forming behaviour would vary if the ball was made to go faster than the disc. Previous work **[9.12]** has shown that the central film thickness decreases at high slide/roll ratios in an asymmetrical way

with respect to whether the ball or disc surface moves faster. However the reasons for this are not yet clear.

The velocity gradient in the lubricant film would change depending on which surface moves faster so that if the ball speed were higher than the disc speed, the fluid in the proximity of the ball surface would flow faster than that closer to the disc surface and the other way around when the slide/roll ratio were positive. Thus if the boundary film were deposited on one of the surfaces unevenly in random patches, a positive or negative slide/roll ratio might have different effects on the film environment. This was recently shown by Kaneta **[9.13, 9.14]** when studying how dents and grooves behave in contacts. Such a defect has a "leading edge" relative to the lubricant film which can be closer or further from the contact inlet and the local effects which take place at the defect leading or trailing edge will take place on different sides of the defect depending on whether the disc is travelling faster or slower than the ball.

Several tests were therefore performed at 60°C and 50% negative sliding and typical results are shown in figure 9.25.

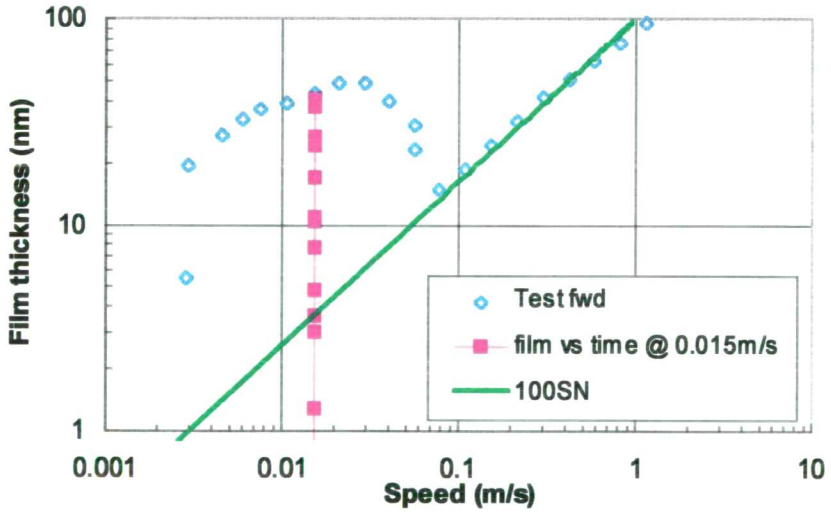


Fig.9.25. Film thickness vs. speed for 0.1%Cu oleate in 100SN @ 60°C, 50% negative SRR, time effect

As a general observation, thicker films of 30-50 nm are formed which tend to collapse slightly earlier than in the positive SRR tests, below 0.1 m/s speed. This is probably a consequence of the fact that the decrease in film thickness is faster at negative rather than positive slide/roll ratios for the same conditions of sliding and speed **[9.12]**. The

influence of time was also tested and it was noticed that the growth rate was delayed but became much faster towards the end of test. The results for two tests are shown in figure 9.26.

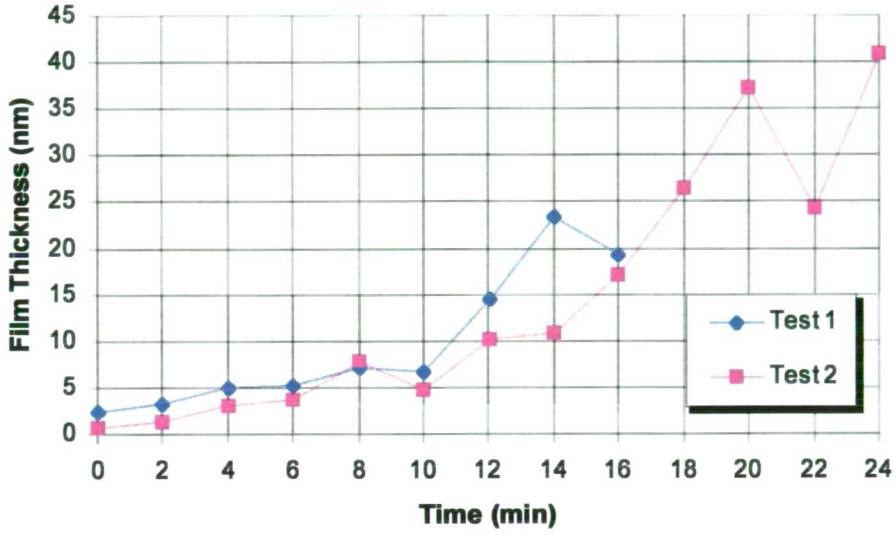


Fig.9.26. Film thickness growth with time for two solutions of 0.1% Cu oleate in 100SN @ 60°C, 50% negative SRR

9.2.5. Traction results

Friction or traction in EHD was measured for 0.1% wt. solutions in hexadecane and in 100SN mineral oil. The technique and the rig employed have been previously described in section 4.1.2. Two types of friction measurements were made. In one, the entrainment speed was held constant at 1 m/s and the friction coefficient measured as a function of slide/roll ratio. Because the film thickness at 1 m/s is normally quite high, this type of test measures the EHD film friction (traction) coefficient. In the second type of friction experiment the slide/roll ratio was held constant and the mean rolling speed progresively reduced. The speed decrease produces a corresponding reduction in film thickness and the results can be used for exploring the variation of friction with film thickness going from EHD through mixed to boundary lubrication like in a "Stribeck"-type curve. Such curves are important for measuring and understanding the behaviour of friction modifier additives, otherwise there is always the danger that friction modifier response is being assesed in the full EHD regime.

Traction results for surfactant solutions in hexadecane

Figures 9.27 and 9.28 show the influence of speed on EHD friction coefficient at two temperatures for pure hexadecane. The slide/roll ratio is held constant at 50% whilst the rolling speed and thus the EHD film thickness is gradually reduced.

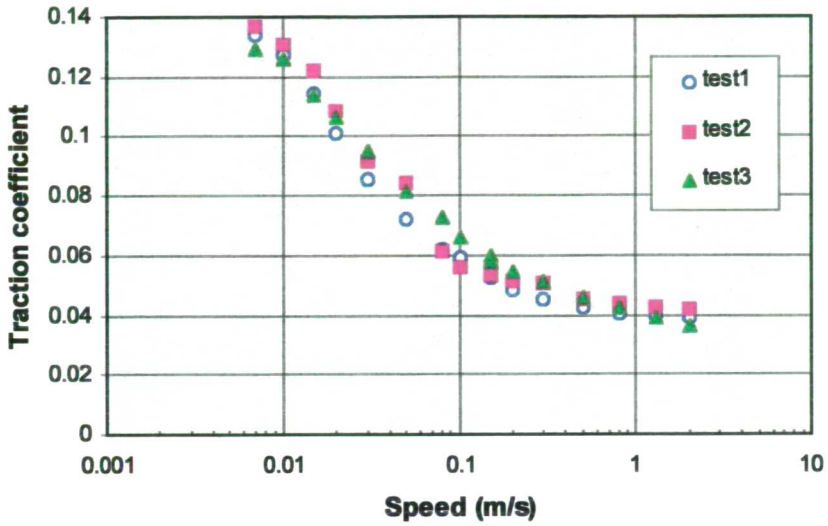


Fig.9.27. Traction coefficient vs. speed for pure hexadecane @ 50% SRR, 25°C

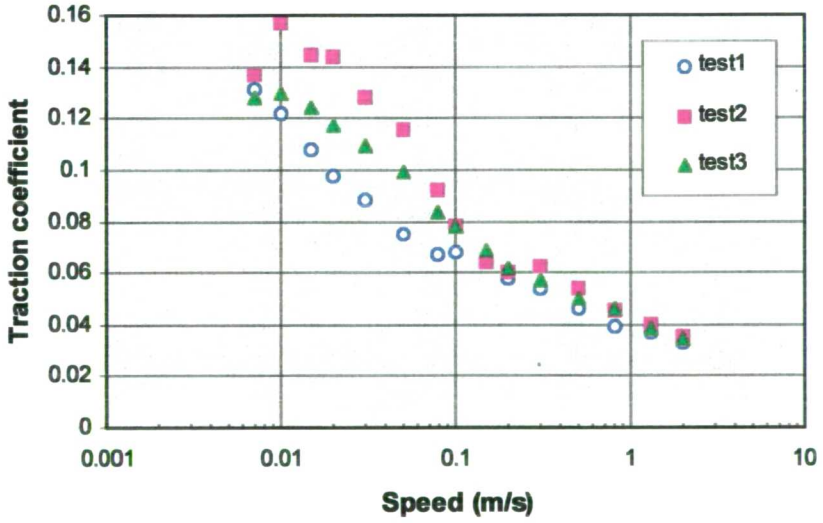


Fig.9.28. Traction coefficient vs. speed for pure hexadecane @ 50% SRR, 60°C

Hexadecane has low viscosity and is a very poor lubricant. The film thickness at 1 m/s is comparable to the composite surface roughness thus friction will be influenced by the surface asperities which is reflected in the increased amount of scatter mainly for results at high temperature.

With friction modifier solutions, the variation of friction coefficient with speed shows quite a different behaviour. Results are shown in figures 9.29 and 9.30 for Cu oleate and in 9.31 and 9.32 for C_{36} dimer solutions in hexadecane.

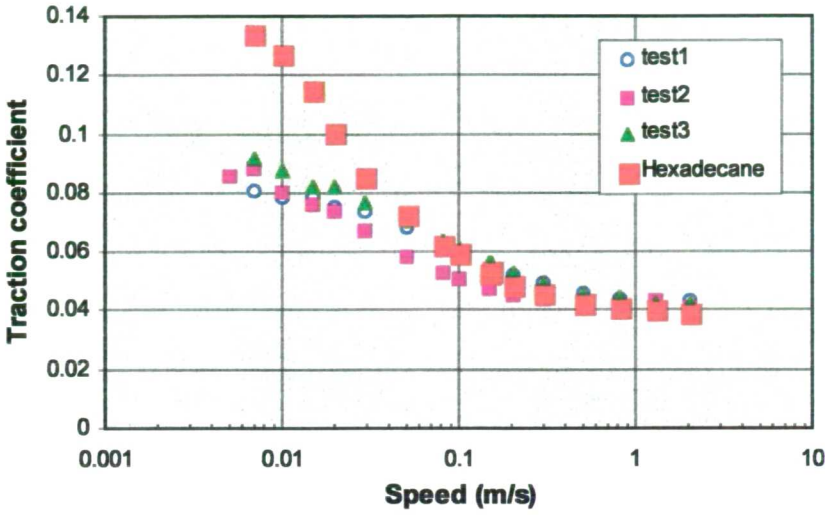


Fig.9.29. Traction coefficient vs. speed for 0.1% wt. Cu oleate in hexadecane @ 50% SRR, 25°C

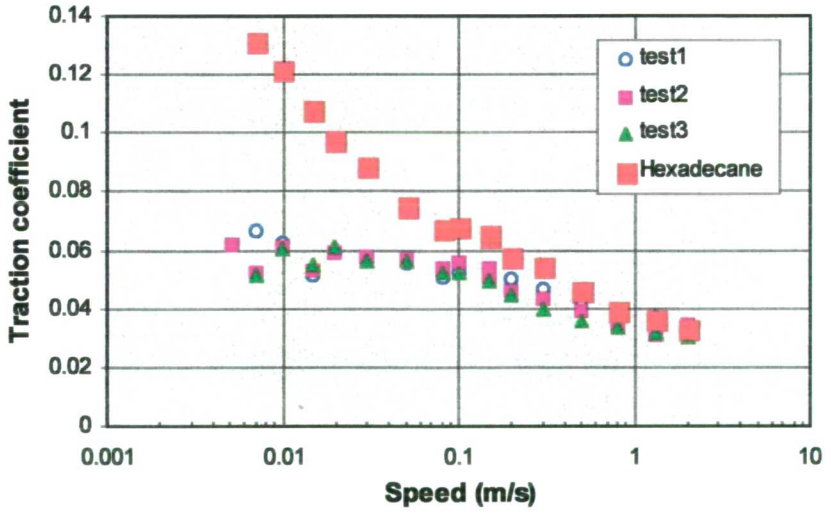


Fig.9.30. Traction coefficient vs. speed for 0.1% wt. Cu oleate in hexadecane @ 50% SRR, 60°C

At high speeds the EHD friction has values comparable to the base fluid corresponding to a limiting traction value but as the speed is reduced, a much smaller rise in friction is noticed. For copper oleate the additive begins to be effective below about 0.1 m/s whilst the contribution of the dimer acid can only be seen below 0.02 m/s. The effect of copper oleate additive at 60°C is very striking since it reduces friction down to 0.06 at slow speeds.

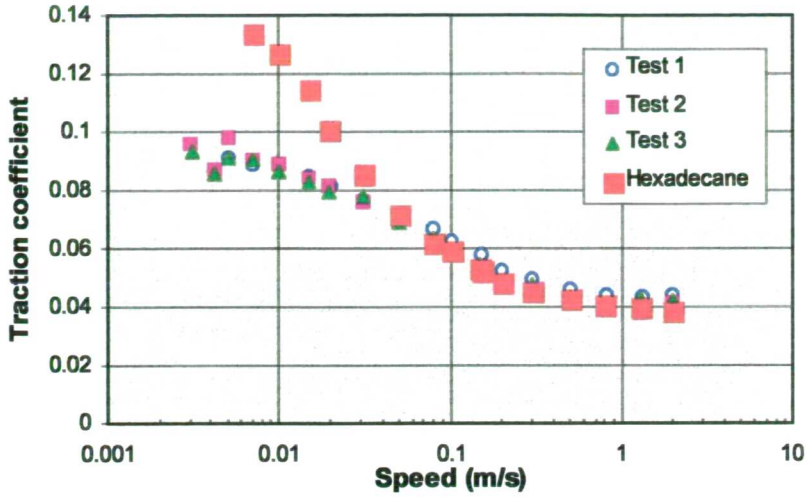


Fig.9.31. Traction coefficient vs. speed for 0.1% wt. C_{36} dimer acid ester in hexadecane @ 50% SRR, 25°C

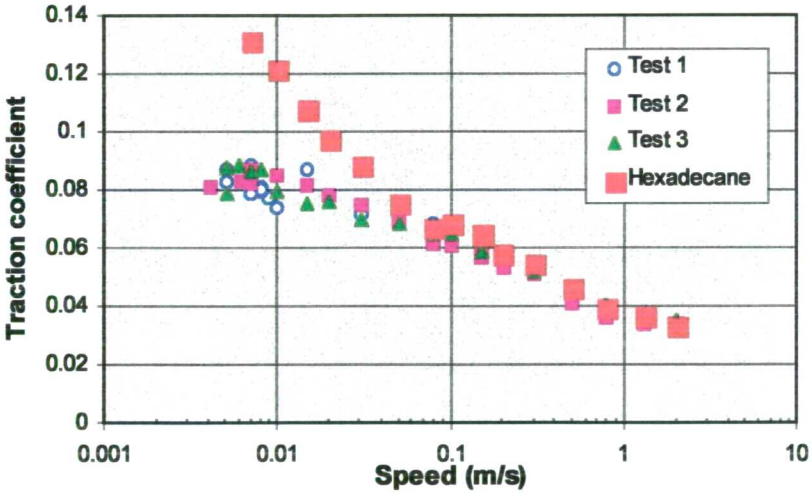


Fig.9.32. Traction coefficient vs. speed for 0.1% wt. C_{36} dimer acid ester in hexadecane @ 50% SRR, 60°C

Both types of surfactants showed similar behaviour in that they produced a much lower friction in the slow speed region.

Traction results for surfactant solutions in mineral oil

Traction results for the additive-free mineral oil are presented in figures 9.33 and 9.34. In figure 9.33 is shown the variation of traction coefficient with slide/roll ratio for three temperatures, 25, 60 and 100°C and figure 9.34 illustrates how traction coefficient varies with entrainment speed when the slide/roll ratio is kept constant at 50%, also for three temperatures. At least two tests are included to show the level of repeatability.

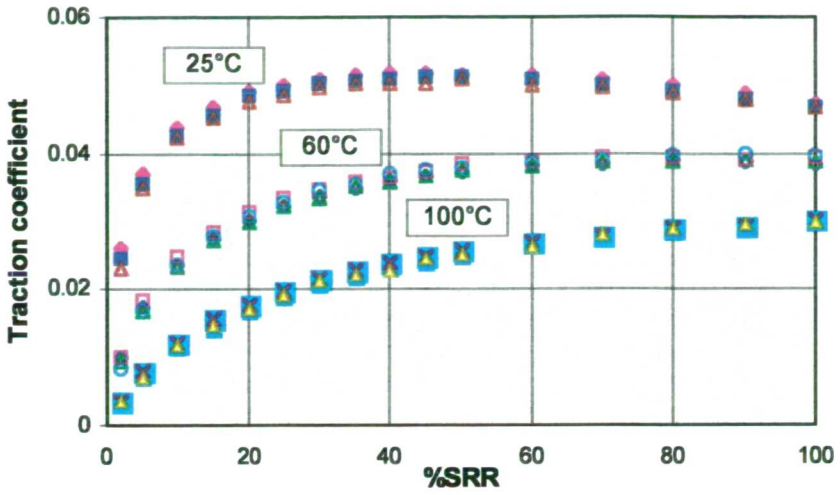


Fig.9.33. Traction coefficient vs. slide/roll ratio for 100SN at three temperatures

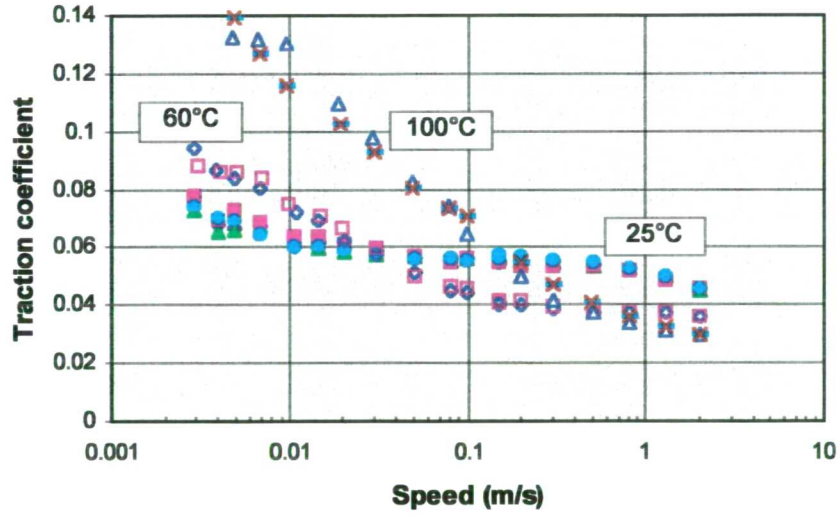


Fig.9.34. Traction coefficient vs. speed for 100SN @ 50% SRR and three temperatures

It was unfortunate that for the tests at 100°C a different batch of mineral oil had to be used since the previous one has been consumed in other tests. It can be seen that the Stribeck-type friction is quite high at slow speeds showing an earlier entry to boundary lubrication which may be a consequence of a higher degree of lubricant refining.

When surfactant solutions were tested, the variation with slide/roll ratio at 1 m/s constant speed showed no significant difference from the base oil results. The results show classical EHD friction behaviour, with friction coefficient increasing with slide/roll ratio to reach a limiting, maximum value before falling slightly due to inlet shear heating. The results are more scattered at 60 and 100°C but it can still be concluded that

the presence of surfactant has little effect on EHD friction. This has been observed by other researchers with VII polymers [**9.15**]. Figure 9.35 shows the results obtained with copper oleate solutions.

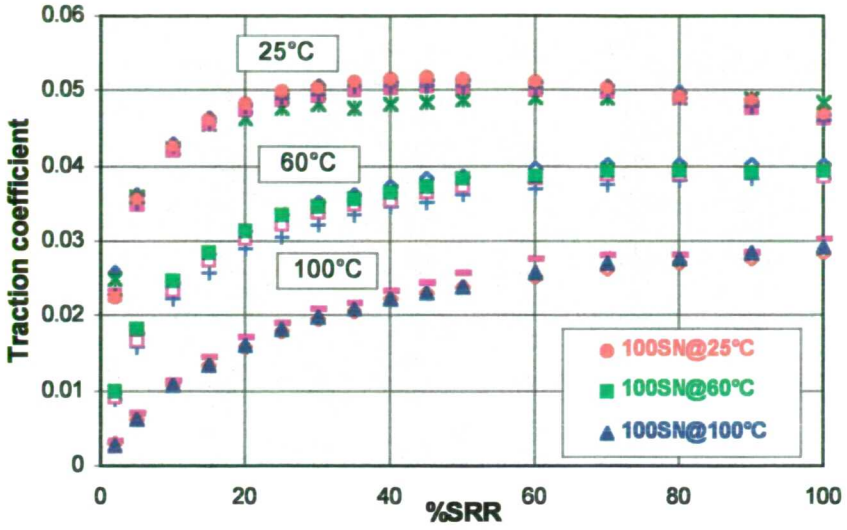


Fig.9.35. Traction coefficient vs. slide/roll ratio for 0.1% wt. Cu oleate in 100SN at three temperatures

In the second type of tests traction variation with entrainment speed was tested. Figures 9.36 and 9.37 show such behaviour for copper oleate solutions.

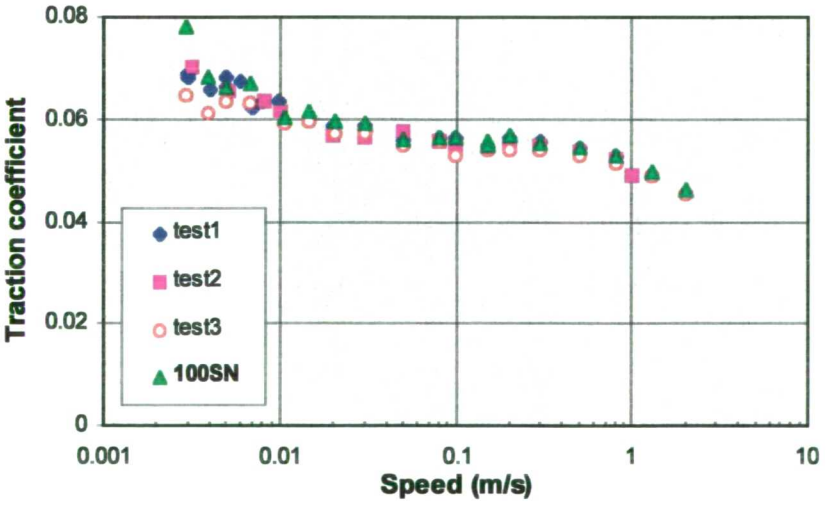


Fig.9.36. Traction coefficient vs. speed for 0.1% wt. Cu oleate in 100SN @ 25°C

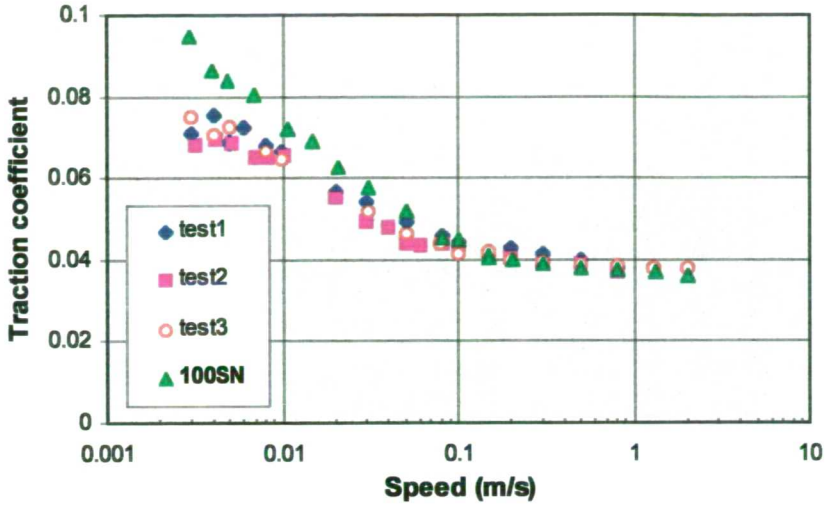


Fig.9.37. Traction coefficient vs. speed for 0.1% wt. Cu oleate in 100SN @ 60°C

It can be seen that the results at 25°C overlap the mineral oil values and that those at 60°C show only a slight reduction in friction coefficient but it should be mentioned that the base oil friction is still in the range of mixed lubrication and thus any additive effect would be slight.

However, the results at 100°C in mineral oil show quite a significant friction reduction (down to 0.06) in the intermediate speed range below 0.1 m/s. This is followed by a slight increase in friction as the boundary regime is reached.

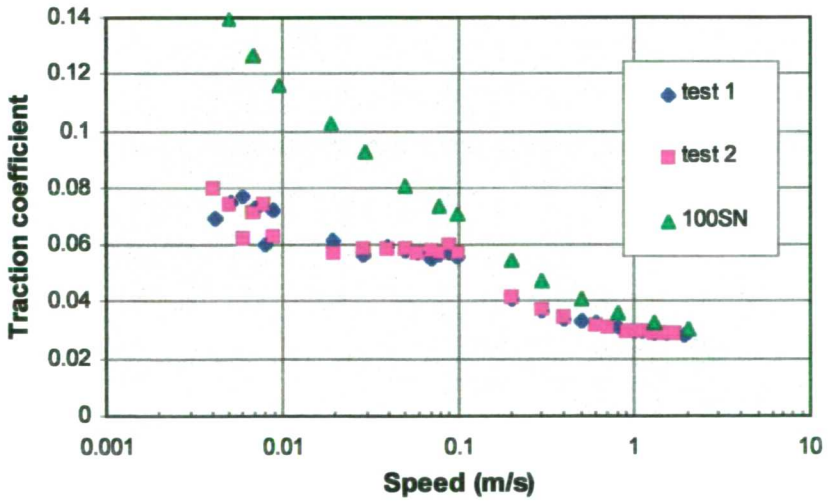


Fig.9.38. Traction coefficient vs. speed for 0.1% wt. Cu oleate in 100SN @ 100°C

The solutions of C_{36} dimer acid ester behaved in a very similar manner to copper oleate and the traction coefficient variation with speed is plotted in figures 9.39 and 9.40.

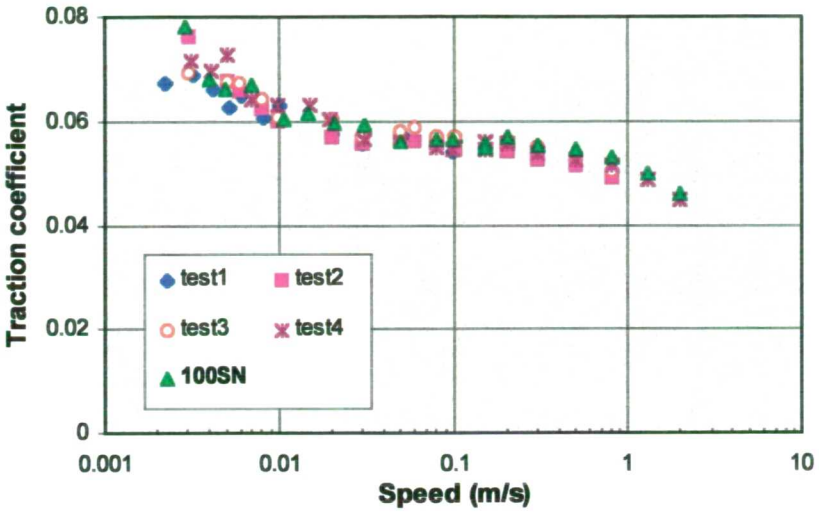


Fig.9.39. Traction coefficient vs. speed for 0.1% wt. C_{36} dimer acid ester in 100SN @ 25°C

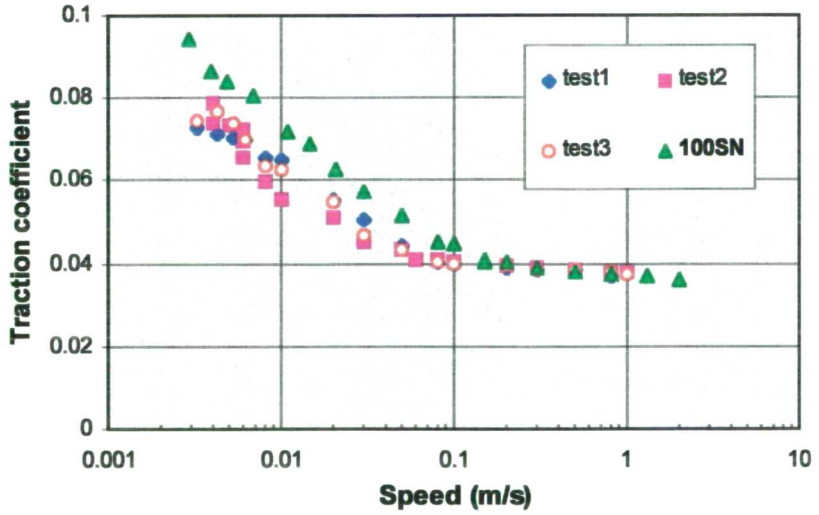


Fig.9.40. Traction coefficient vs. speed for 0.1% wt. C_{36} dimer acid ester in 100SN @ 60°C

9.2.6. Discussion

The results presented show that copper oleate and, to a lesser extent, dimer acid friction modifiers can form thick, boundary films in both rolling and rolling-sliding high pressure contacts. These films are much thicker than predicted from EHD theory in the very thin film regime. The film formation at slow speeds is a kinetic process which depends upon time rather than rolling speed. The thickness of the films depends upon both

temperature and base fluid. In hexadecane, copper oleate forms films 10 to 20 nm thick at 25°C. In mineral oil, there is negligible film formation at 25°C but rapid formation at 60°C and 100°C. At 100°C, films up to 70 nm thick were observed with copper oleate and 30 nm thick with dimer. These values are comparable with those suggested by Allen and Drauglis [**9.16**] in their disscussion of thin versus thick film boundary lubrication.

An important characteristic of these films is that they start to decrease as the speed is raised above about 0.02 m/s. With copper oleate the thick boundary film appeared to be completely destroyed above about 0.1 m/s, with the film thickness reverting to the EHD value of the base fluid. For the dimer acid, a residual film remained which continued to augment the film thickness by about 5 nm up to high speed, thick EHD film conditions. This observation is in contradiction to a previous work which suggested that friction modifiers might promote thick film formation in high speed but not in slow speed conditions [**9.17**].

The fact that the boundary film is destroyed at high speeds makes it possible to study the kinetics of film built-up by suddenly reducing the speed from a high value down to film forming conditions. This tests indicated that film formation is time dependent, with films taking around 20 minutes to fully develop within a slow speed rubbing contact. Film formation rate is faster at higher temperature and is also increased when sliding is present in the contact.

The boundary film appears to increase with increasing speed in the very slow speed region. Such behaviour suggests that the film is not a "solid-like" coating but a rather highly viscous surface layer, whose high viscosity promotes entrainment. This can be associated with the behaviour of some viscosity index improving polymer solutions in thin film conditions [**9.11**] where the contact effectively operates within the viscous material forming much thicker films than predicted from the bulk viscosity of the lubricant. It is possible to estimate the viscosity of the boundary film in the slow speed region by using the film thickness versus speed measurements. By making some assumptions about how the inlet viscosity influences film thickness and applying simple EHD analysis to the film forming behaviour it is possible to evaluate what viscosity should give the observed film thickness. The approach is described in reference [**9.18**].

From EHD theory, central film thickness depends upon the speed and lubricant properties according to equation [9.19]:

$$h = k_1 U^{0.67} \eta^{0.67} \alpha^{0.53}$$

where U is the mean entrainment speed, η is the dynamic viscosity of the lubricant in the inlet and α is the pressure-viscosity coefficient of the lubricant. The coefficient k_1 depends upon the geometry and elastic properties of the two surfaces and upon the applied load. Assuming the pressure-viscosity coefficient of any boundary film to be, to a first approximation, the same as that of the bulk fluid, for the same speed condition the ratio of the bulk film thickness and the boundary layer thickness can be written as:

$$\frac{h_{bulk}}{h_{bound}} = \left(\frac{\eta_{bulk}}{\eta_{bound}} \right)^{0.67}$$

which gives the ratio of the viscosities of the films. Since the bulk fluid viscosity is a known parameter, follows that the boundary layer viscosity can be easily estimated. Taking for example the film thickness versus speed mesurements from figure 9.16, for the same speed of 0.01 m/s the calculations showed that the viscosity of the boundary layer is around 150 cP which is about 40 times higher than the bulk fluid viscosity in the same test conditions. The impressive increase of viscosity in the inlet explains the formation of the thick films detected in the centre of the contact.

There is a striking similarity of copper oleate behaviour to that observed with fatty acids in the thick-film forming tests. The fact that pure fatty acids gave the thick films only intermittently whilst copper oleate always showed this kind of behaviour, supports the idea that thick films are formed by metal soaps and that fatty acids must form such soaps in order to exhibit thick film behaviour. However insufficient work has been carried out to determine the composition of such films so it is not yet known whether the films are based on the copper soap itself or on iron oleate as a result of a chemical reaction.

The friction behaviour of additive solutions has been assessed in EHD friction tests in order to establish whether the thick boundary films have any significant effect on friction. To demonstrate this, it is necessary to show higher friction reduction than single, adsorbed monolayers which are expected to reduce friction down to about 0.08 at slow speeds with a proportionate contribution throughout the mixed regime. A

at slow speeds with a proportionate contribution throughout the mixed regime. A viscous layer, on the other hand, would be expected to help maintaining full or partial EHD lubrication down to lower speeds, effectively shifting the Stribeck curve to the left as shown by the diagram in figure 9.41.

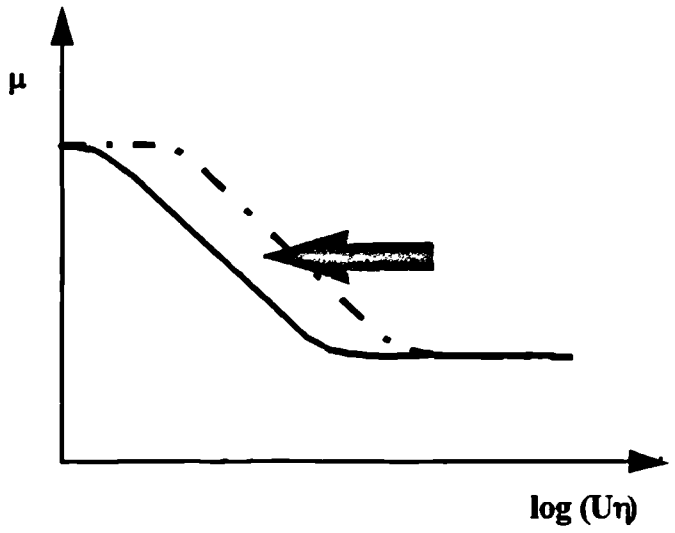


Fig.9.41. Shifted Stribeck curve for viscous films

The behaviour would however be more complicated if viscous layer formation were time dependent. The reduction in friction showed by copper oleate and dimer acid solutions in mineral oil at low temperature is ambiguous and could derive from either thick or thin films. A more straight-forward conclusion can be derived from high temperature results which are strongly supportive of a thick film contribution below 0.1 m/s. The additive appears to reduce friction at slow speeds down to levels reminiscent of full film EHD rather than boundary lubrication making a significant contribution to friction reduction in the intermediate speed range. This is shown schematically in figure 9.42. by using the high temperature friction results for copper oleate. It is interesting to note that Beeck in 1940 found a similar behaviour with fatty acid additives i.e. they promoted the onset of mixed lubrication so that the transition from boundary to mixed took place at lower speeds [9.20].

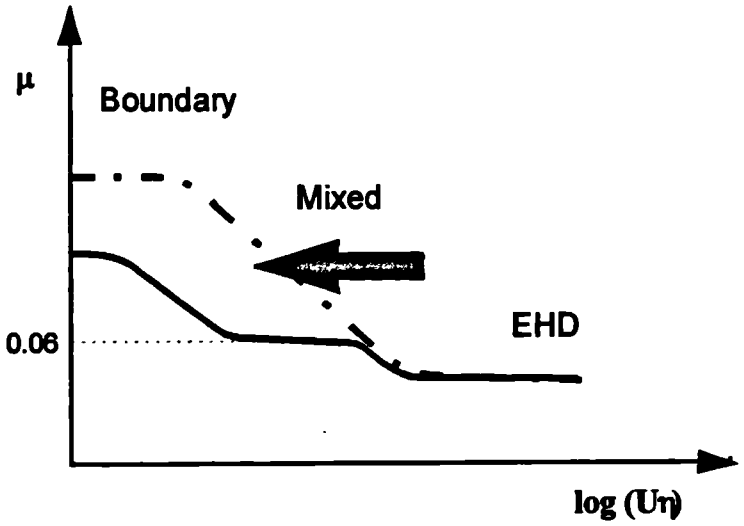


Fig.9.42. Friction reduction mechanism of thick boundary films

The dotted line shows the Stribeck-type curve in the form of friction coefficient against log(speed × viscosity) for a non-boundary film forming lubricant. At slow speeds the system operates in the high friction boundary regime but as speed is raised, the friction falls as an EHD film develops. The solid line shows the possible influence of thick, viscous films which would make the transition to EHD lubrication at slower speeds but the contact would then operate for a time within that viscous layer before emerging into the bulk, low viscosity fluid. It is noteworthy the low friction coefficient 0.06 attained in mixed regime which is indeed characteristic for EHD lubrication levels. Once EHD regime is reached, any boundary film effect disappears, friction values corresponding to those of the bulk lubricant.

However, the fact that thick films are destroyed at high speed and take time to reform may affect their practicality in realistic applications such as pistons where there would not be enough time for them to develop during stroke reversal. Further work needs to be done in non-steady state contacts to see whether thick boundary films exist in such conditions and also to investigate their structure and composition. A discussion about possible structures of thick boundary films will be included in the last chapter of the thesis.

REFERENCES

[9.1] Bowden F.P. and Tabor D., "Lubrication of Metal Surfaces by Fatty Acids", Nature 156, p. 97, 1945,

[9.2] Clark J.L., Sterrett R.R. and Leppla P.W., "X-Ray Diffraction Studies of Built-up Films of Long Chain Compounds", J. Am. Chem. Soc. 57, p. 330, 1935,

[9.3] Sakurai T. and Baba T., "Surface Chemical Behaviour of Polar Compounds in Non-Aqueous Liquids. Dispersing Effect of Soap Solutions", Wear 3, p. 286, 1960,

[9.4] Bowden F.P. and Tabor D., "The Friction and Lubrication of Solids", Part I, 2nd edition, chap. 10, Clarendon Press, 1954,

[9.5] Mortier R.M. and Orszulik S.T., "Chemistry and Technology of Lubricants", Blackie Academie & Professional, second edition, 1997,

[9.6] Furey M.J., "The Formation of Polymeric Films Directly on Rubbing Surfaces to Reduce Wear", Wear 26, pp. 369-392, 1973,

[9.7] Furey M.J., Ghasemi H., Kajdas C. et al., "Tribochemistry of the Antiwear Action of Dimer Acid/Glycol Monoester on Alumina", Trib. Trans. 37, 1, pp. 67-74, 1994,

[9.8] Dorinson A. and Ludema K.C., "Mechanics and Chemistry in Lubrication", p. 236, Tribology Series, 9, Elsevier, Amsterdam, 1985,

[9.9] Hideaki Mitsui, "The Behaviour of Low Molecular Weight Polymer Solutions in Concentrated Contacts", PhD Thesis submitted in 1995, Imperial College, London,

[9.10] Fedors R.F., "A Method for Estimating Both the Solubility Parameters and Molar Volumes of Liquids", Polymer Engineering and Science 14, p. 147, 1974,

[9.11] Smeeth M., Günsel S. and Spikes H.A., "Boundary Film Formation by Viscosity Index Improvers", Trib. Trans, 39, 3, pp. 726-734, 1996,

[9.12] Smeeth M. and Spikes H.A., "The Influence of Slide/Roll Ratio on the Film Thickness of an EHD Contact Operating within the Mixed Lubrication Regime", Proc. 22nd Leeds-Lyon Symposium on Tribology, "The Third Body Concept. Interpretation of Tribological Phenomena", p. 61, ed. D. Dowson, Elsevier, Amsterdam, 1996,

[9.13] Kaneta M., Sakai T. and Nishikawa H., "Optical Interfrometric Observations of the Effects of a Bump on Point Contact EHL", ASME Trans., Journal of Tribology 114, pp. 770-784, 1992,

[9.14] Kaneta M. and Nishikawa H., "Local Reduction in Thickness of Point Contact EHL Films Caused by a Transversely Oriented Mooving Groove and Its Recovery", ASME Trans., Journal of Tribology 116, pp. 635-639, 1994,

[9.15] Sharma S.K., Forster N.H. and Geschewender L.J., "Effect of Viscosity Index Improvers on the Elastohydrodynamic Lubricating Characteristic of a Chlorotrifluoroethylene and Polyalphaolefin Fluid", Trib. Trans, 36, pp. 555-564, 1993,

[9.16] Allen C.M. and Drauglis E., "Boundary Layer Lubrication: Monolayer or Multilayer", Wear 14, pp. 363-384, 1969,

[9.17] Jahanmir S., "Chain Length Effects in Boundary Lubrication", Wear 102, pp. 331-349, 1985

[9.18] Guangteng G., Smeeth M., Cann P.M. and Spikes H.A., "Measurement and Modelling of the Boundary Film Properties of Polymeric Lubricant Additives", Proc.I.Mech.E., 210, Part J, pp. 1-8, 1996,

[9.19] Hamrock B.T. and Dowson D., "Ball Bearing Lubrication: the Elastohydrodynamics of Elliptical Contacts", Publ. J. Wiley, New York, 1981,

[9.20] Beeck O., Givens J.W. and Smith A.E., "On the Mechanism of Boundary Lubrication. I. The Action of Long Chain Polar Compounds", Proc. Roy. Soc. Lond. A117, pp. 90-102, 1940

CHAPTER 10

ADDITIONAL TECHNIQUES APPLIED TO BOUNDARY FILM STUDY

In this chapter, results from a number of other in situ methods used to study boundary films in contacts are described. Video recording techniques were used to take images from the EHD contact and two mapping techniques were also: an ultra-scan method and a spacer layer imaging method (SLIM). Both give information not only on central film thickness but are also able to provide 2-D and 3-D film thickness maps from an EHD contact operating in the thin film regime. In order to obtain information about the chemistry of lubricant films, in contact reflection-absorption Fourier transform infra-red (FTIR) microspectroscopy was employed.

10.1. Video image analysis

In order to investigate some of the distribution characteristics of the thick boundary films observed, a colour video camera was used to obtain and record interference images of the contact. The presence of the spacer layer meant that small changes in film thickness across the contact were visible as interference colour variations. The video camera model JVC (TK-107E) was mounted on top of the microscope on the EHD rig and the light was shone into the contact through the beam splitter. Visual images of the contact interferogram were initially obtained by taking images in static conditions after

performing a film thickness test. Figure 10.1 shows such images of the Hertzian contact from a film thickness test with copper oleate solution in mineral oil at 60°C, in pure rolling conditions.

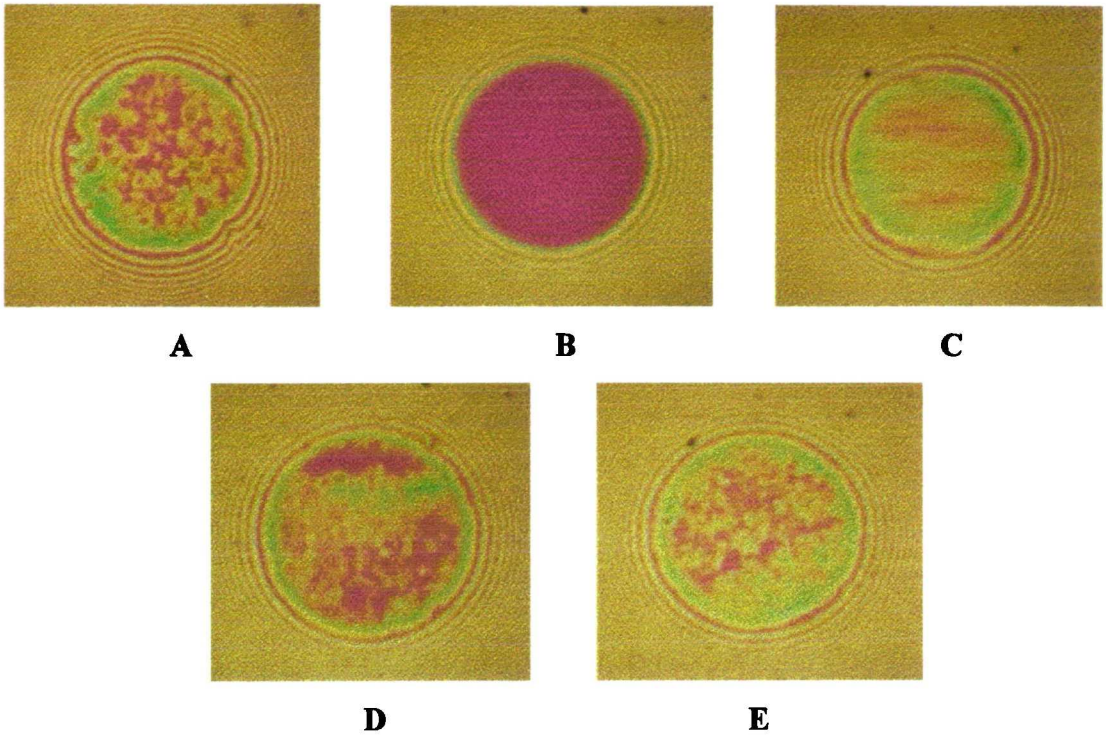


Fig.10.1. Photographs of the Hertzian contact

The test was run in the usual way, measuring the film thickness variation with increasing speed and after about 15 min of test time, when a thick, lumpy film was detected, the video camera set-up was used and images of the stationary contact were taken (figure A). After speed was gradually increased up to 1 m/s, the motion was then stopped and the images were recorded. In this case, the contact image looked like figure B, clear purple colour corresponding to the silica layer thickness of about 600 nm augmented with the thin oil layer existing in the contact. No trace of boundary film is seen. The motion was then restarted with speeds varying from 0.0025 m/s up to 0.02 m/s and figure C shows the contact image when surfaces were rolling at very slow speed i.e. 0.0025m/s. After about 20 min of rolling, stationary images indicated the reformation of the lumpy film as seen in figure D. Then the disc track radius was changed and the new image of the contact (E) was obtained, very similar to the one taken when the original radius was used. This might lead to the conclusion that the film is mainly deposited on the ball surface since it was still visible when an out-of-track disc area was used.

However, the possibility of an area larger than the track width where the thick substance was trapped has to be considered. Very similar contact images were obtained when a solution of C_{36} dimer acid ester in 100SN was used.

Video images of the contact were also recorded during film thickness versus time tests, to obtain insight into the kinetics of boundary film formation. Figure 10.2 shows four images of the contact taken at different conditions in a test with copper oleate solution in 100SN, 60°C and 50% sliding.

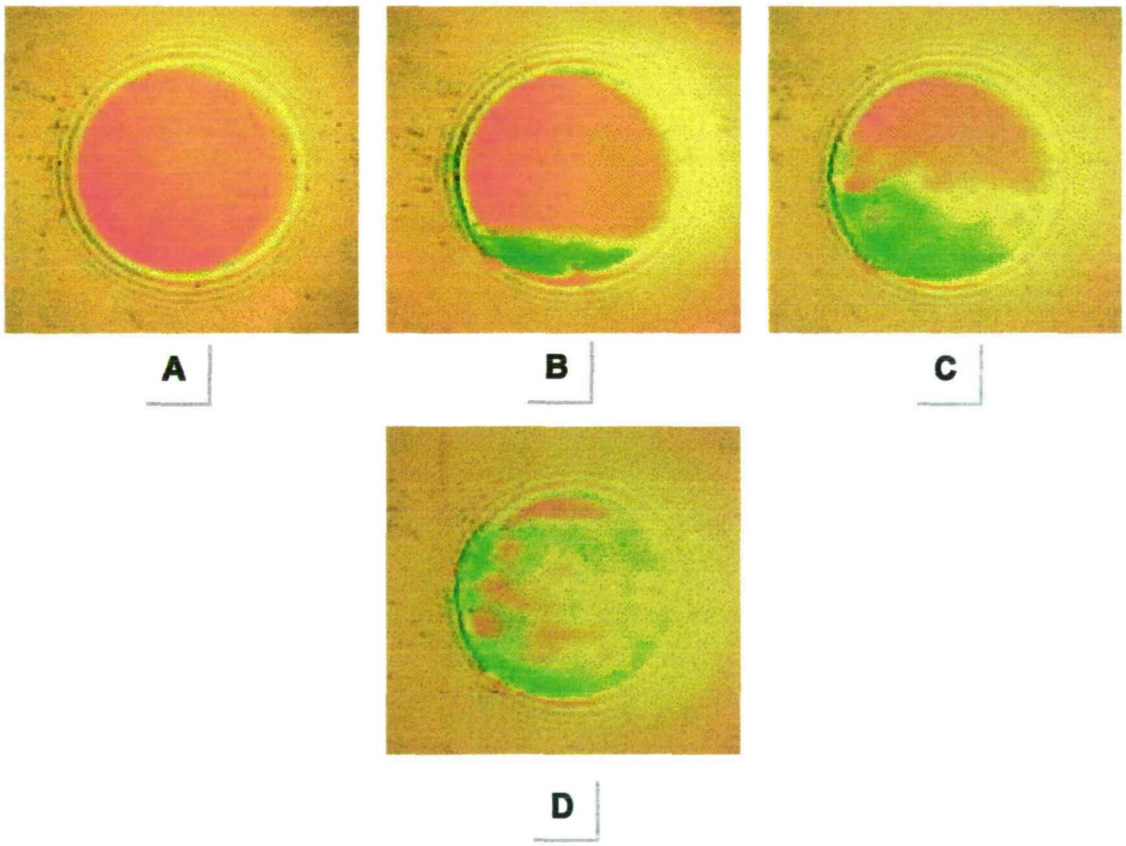


Fig.10.2. Video images of the contact during a time dependence test

Figure A shows the image of the contact before motion was started, then figures B, C and D represent the images after running at 0.009 m/s for 5, 20 and 30 min, respectively. The images were taken during running and represent visual evidence that the film was increasing with time. It can be clearly seen that, over time, the colours in the contact are changing from purple to green, the area becoming covered almost

entirely by a thick, patchy film. After running at high speeds, this thick film disappeared leaving a clear contact image.

From this visual evidence, it was quite straight-forward to obtain information on the spatial distribution of the surface films. In order to accomplish this, two additional methods were employed since ultra-thin film interferometry technique gives information only upon film thickness values in the centre of the Hertzian contact (see chapter 4). One is a modified ultra-thin film technique which is able to measure the film thickness distribution across a thin segment of the contact resulting in a two dimensional plot of the film profile. The second one called SLIM (Spacer Layer Imaging Method) which can produce either a 2-D or a 3-D map of the contact by analysing the colours from video images recorded during film thickness tests.

10.1.1. 2-D profiling

The original development of the technique belongs to Gohar **[10.1, 10.2]** whose aim was to measure the two dimensional film thickness across the contact and to validate the results by comparison with theoretical predictions. Due to the limitations of the conventional film thickness technique imposed by the colour resolution of the human eye, Gohar was able to produce contact profiles with a maximum resolution of about 30 nm. Ultra-thin film technique overcome these limitations, as shown in chapter 4, and with the new developments of the system it is possible to measure how film thickness varies across the contact with a resolution of the order of ±1 nm.

The technique used in this study for obtaining the film profile across the contact is shown schematically in figure 10.3. Work on contact profiling has been previously reported by Aderin **[10.3]** and Smeeth **[10.4]** who used it to measure the central and minimum film thickness in high pressure contacts.

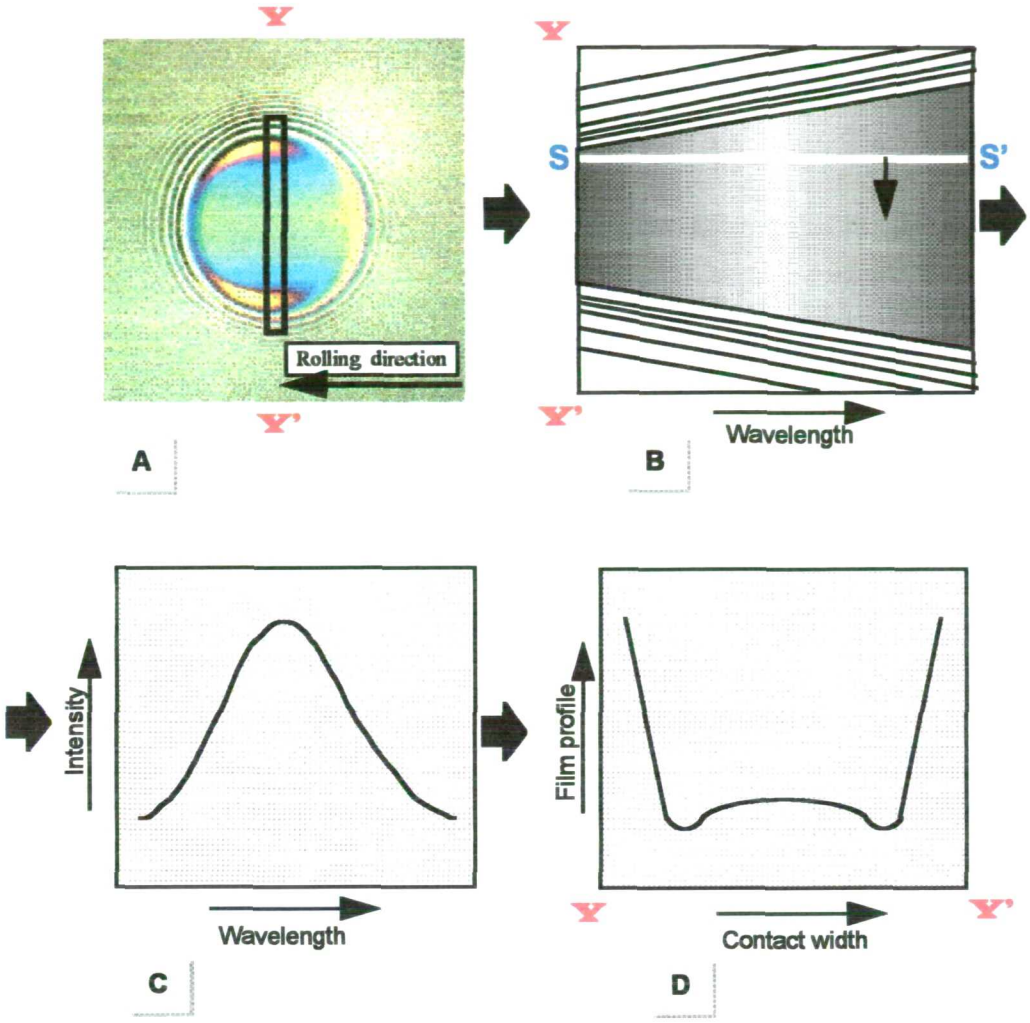


Fig.10.3. Schematic of the procedure for film thickness profiling

The same rig as for the ultra-thin film tests is used but with a modified image analysis software. The whole contact area is viewed by the microscope but only a section of it, passing through a narrow slit area YY' is projected into the spectrometer (figure 10.3, A). In the spectrometer the selected section is dispersed into its component wavelengths which are displayed on the screen through the video camera. Figure 10.3, B shows the dispersed image in detail. The light from the contact has been dispersed horizontally by wavelength, so the x-axis corresponds to wavelength of light whilst the y-axis represents the distance across the contact. The flat, central contact region can be seen as the broad band filling most of the image. For central film thickness measurements, the intensity across most of the central band of the contact is averaged for each wavelength in order to determine the wavelength of maximum constructive interference and thus the average central film thickness. For the technique used in this study, just a thin strip of 1-2 pixels (marked SS' in figure 10.3, B) is scanned. For every position of this strip, along

the Y-Y' direction, an intensity profile is generated (figure 10.3, C) and the film thickness associated with that part of the contact area is produced. The results are stored in terms of film thickness versus screen position and after all the contact is scanned the resulted film thicknesses are put together to give the complete profile (figure 10.3, D). The system has also a facility to measure the central film thickness at the same time as film profiling.

Figure 10.4 represents the film profiles at different speeds measured with the above technique for 0.1% wt. solution of Cu oleate in hexadecane at 25°C and in pure rolling conditions.

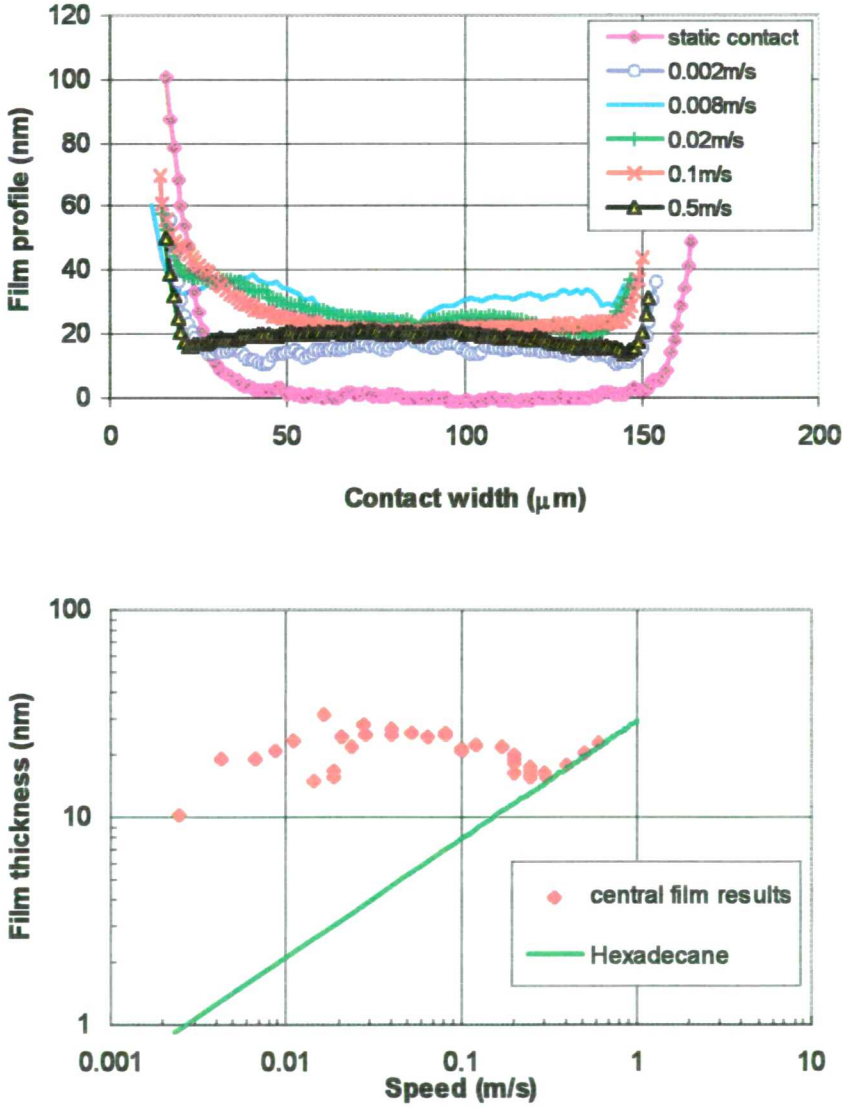


Fig.10.4. Film profile and central film thickness for 0.1% wt. Cu oleate in hexadecane @ 25°C, pure rolling

The graph of central film thickness measured simultaneously is shown for comparison purposes.

Figure 10.5 shows typical 2-D profiles corresponding to several test speeds for 0.1% wt. Cu oleate in 100SN mineral oil at 60°C, with 50% sliding. Also shown is the plot of the central film thickness measured conventionally with the average film values calculated from the film profiles.

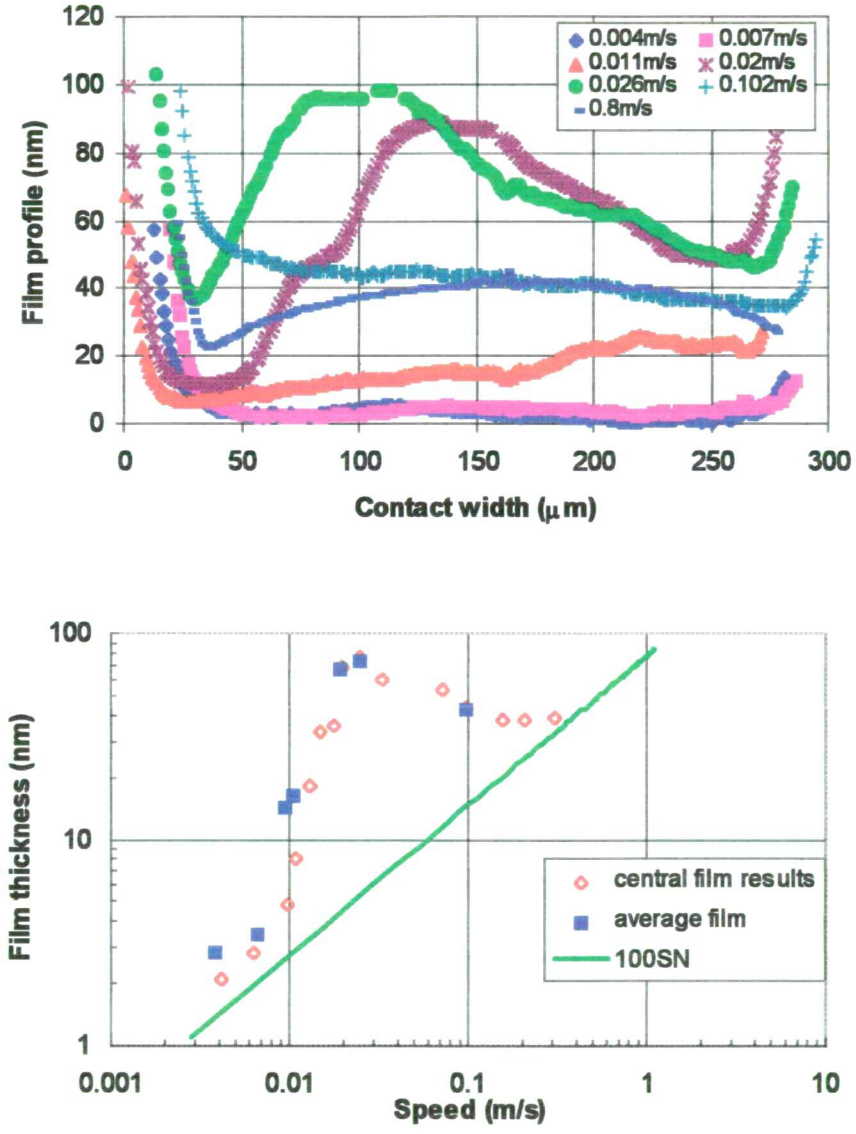


Fig.10.5. Film profile and central film thickness for 0.1% wt. Cu oleate in 100SN, 50% SRR, 60°C

It can be seen that the profiles for the thick films are quite unevenly distributed across the contact width. As the speed increases and the film collapses to the base oil values, the profile becomes smoother and closer to the classical EHD shape with a flat, almost constant film thickness covering most of the central Hertzian area and with the side grooves corresponding to the two lobes of reduced film thickness.

10.1.2. 3-D profiling

The SLIM technique employed for 3-D film profiling was recently developed and is fully described in reference [**10.5**]. Unlike other colour image analysis work [**10.6**] which was concerned with the classical EHD regime, this technique uses a spacer layer so that it can explore the film shape in the thin film regime i.e. to study boundary films between 10 to 80 nm. A schematic of the system is shown in figure 10.6.

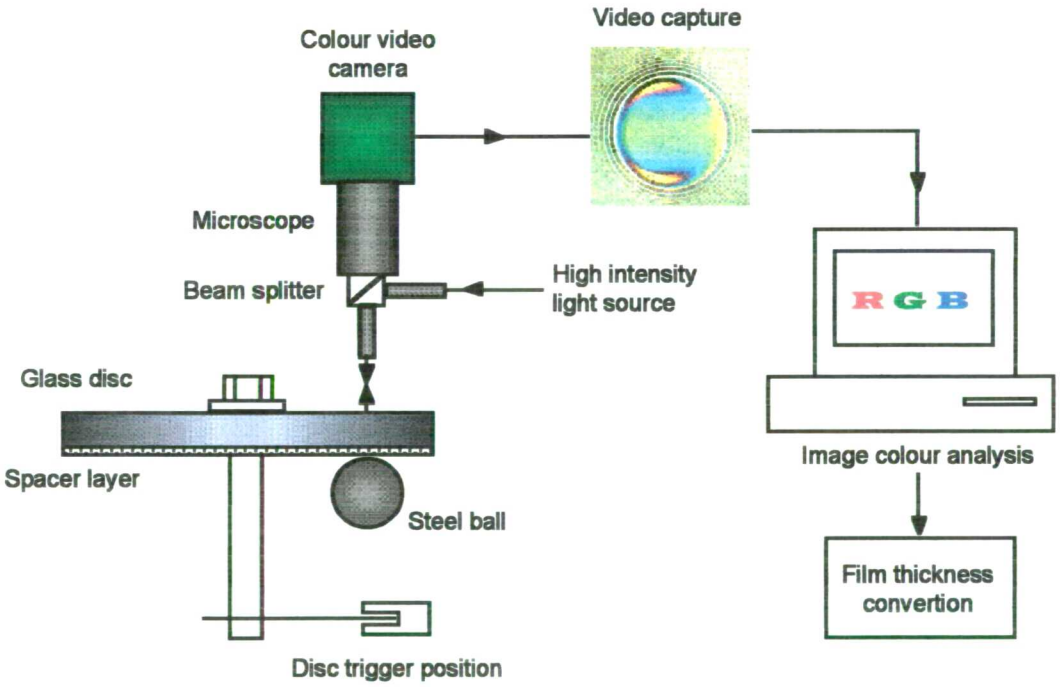


Fig.10.6. Schematic of the spacer layer imaging system

The test rig is essentially that used for ultra-thin film interferometry. However, a colour video camera is mounted on the microscope instead of the eye piece, a tungsten halogen light source of a higher intensity is used with a fibre optic light guide, a Zeiss ×5 objective to illuminate the contact and a software for image colour analysis are also used. The colour video camera used is JVC (TK-107E) with a variable shutter speed

down to 10^{-4} seconds which enables it to take clear images of local features in a fast-moving contact. The objective combines efficient light gathering with a long working distance and is corrected for chromatic aberration.

The S-VHS output from the camera contains two signals: chrominance and luminance **[10.5]**. Through the frame grabber, these are converted into separate RGB (red, green and blue) signals which are digitised and stored for further conversion into hue, saturation and intensity. At present, it is the hue value that is used to define the image colour and is calibrated against film thickness. Out of the 360 hue values, "pure red" was arbitrarily assigned to zero, "pure blue" to 240 and "pure green" to 120 **[10.5]**.

In order to use this method, a calibration of hue values against wavelength and subsequently film thickness, is needed. This was achieved with the help of the existing ultra-thin film technique which, by analysing the wavelength of the constructive interference, gives the measurement of the local silica layer thickness. Replacing the thin film optics by the imaging camera, the corresponding hue value for the same encoder position is measured. Since the thin film technique measures an average thickness across the contact, to obtain a representative hue value it was necessary to sample from several areas within the contact and calculate the average. To obtain hue versus silica film thickness variation for different orders, a phase change correction is applied and the film is divided by the silica refractive index. The hue/silica thickness results are curve fitted and a suitable calibration developed which is used to determine the "zero" silica film thickness at the start of the test, and the additional lubricant film developed during the test. This is obtained by subtracting the zero silica layer thickness from the combined measurement (silica layer + oil film thickness). With this calibration, the estimated film thickness resolution is 5 nm **[10.5]**. The contact geometry can be plotted as a 3-D map or as 2-D film thickness profiles taken either transverse or parallel to the rolling direction. Figure 10.7 is an example of a captured image and the resulting film thickness profile. In this case, the speed was 0.006 m/s and the solution tested was 0.1% wt. Cu oleate in mineral oil at 60°C. The images were recorded after running the test for 20 min at 0.01 m/s during which time the central film thickness measured with optical interferometry has reached values of about 30 nm. The 3-D plot represents only a

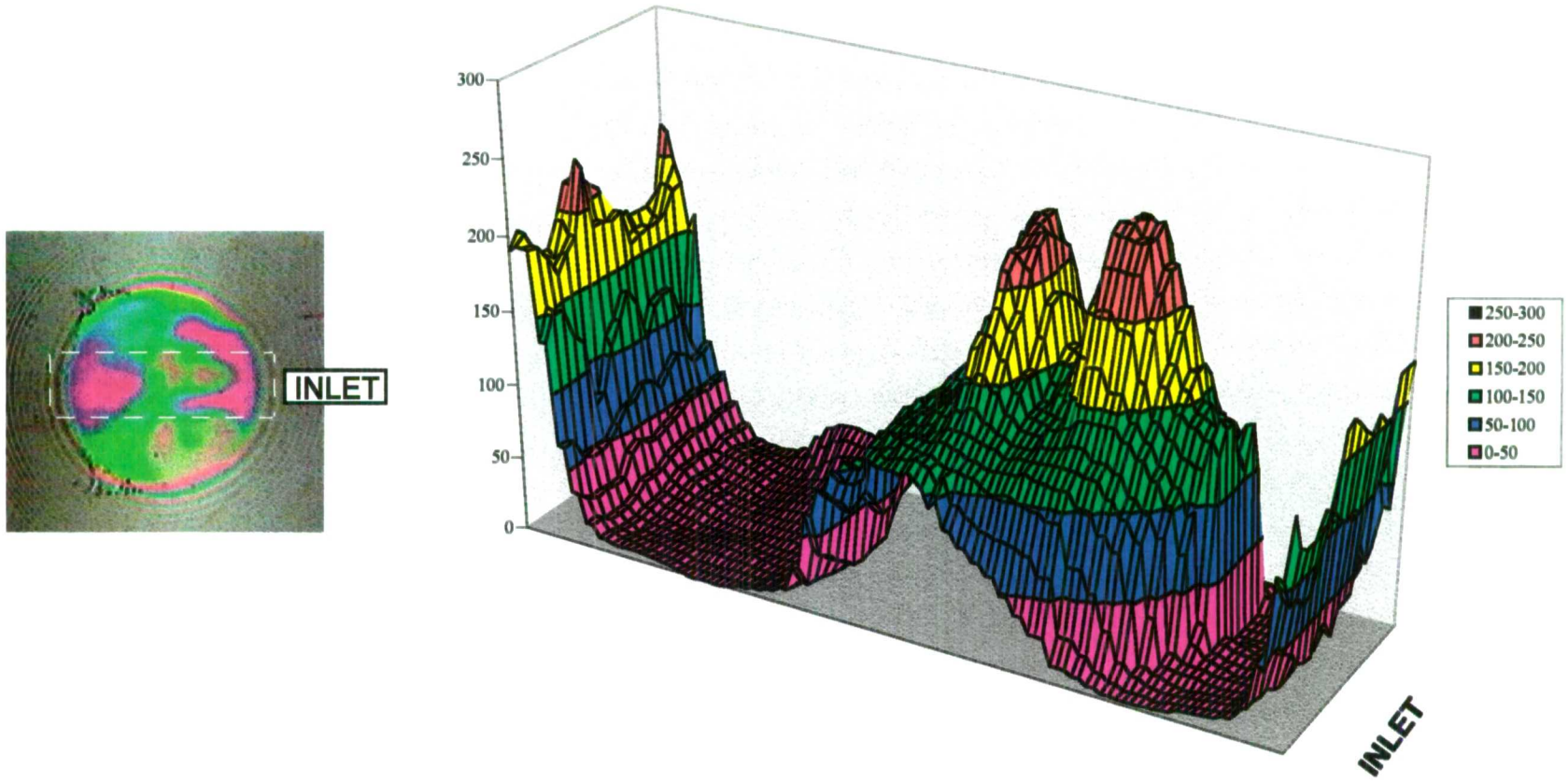


Fig.10.7. 3-D film thickness map for a strip area across the contact (nm)

selected area of the contact where the spatial variation of film thickness is mostly prominent. It can be seen that there are local deflections of film thickness with peaks of hundreds of nanometers.

10.2. Infrared spectroscopy

10.2.1. General

Infrared (IR) analysis has been used for many years to study unknown structures and specific chemical groups, chemical bonding and electronic structure, molecular geometry etc. It has been used both on bulk materials and on thin films on surfaces. It is a non-destructive method which needs little sample preparation and the incorporation of an optical microscope permits selection of an analysis area which can be as small as 10 μm in FTIR.

The underlying basis of infrared absorption spectroscopy is the fact that practically all organic substances selectively absorb certain frequencies in the infrared portion of the electromagnetic spectrum. The atoms of any molecule not at absolute zero are constantly oscillating about their position of equilibrium. The amplitudes of these oscillations are extremely minute (10^{-9} to 10^{-10} cm) and their frequencies are high (10^{13} to 10^{14} cycles per second) **[10.7]**. Since these frequencies are of the same order of magnitude as those of infrared radiation, some direct relationship might be expected to exist between the motions of the atoms within molecules and their effects on infrared radiation incident upon them. It is therefore possible to identify substances from the spectral plot because each substance possesses a different spectrum. In IR spectroscopy, the vibrational excitation is achieved by radiating the sample with a broad-band source of radiation in the infrared region, which is generally 2.5-50 μm. The wavenumber, $\bar{\nu}$ in cm^{-1} , is the number of waves per centimetre. It is equal to the reciprocal of the wave length λ in cm and is equal to the frequency ν divided by c, the velocity of light (cm sec^{-1}). The molecule is excited to a higher vibrational state by directly absorbing the infrared radiation. The transmittance at a given wavenumber can be calculated according to the following relation **[10.8]**:

$$T = I / I_0$$

where T is transmittance, I_0 is the intensity of the entering radiation (before sample absorption) and I is the intensity of the transmitted light (after sample absorption). The transmission spectrum is then obtained by plotting the transmittance versus the IR wavenumber. Similarly, the absorbance at a given wavenumber can be obtained by using the Beer-Lambert equation **[10.8]**:

$$A = \log(I_0 / I) = abc$$

where A is absorbance, a is absorptivity, b is cell thickness and c is concentration. A plot of absorbance versus wavenumber yields an absorption spectrum which is characteristic of the sample studied.

10.2.2. Infrared spectra of carboxylic acid salts

A carboxylic acid salt like the one used in the current study, possess a number of characteristic, well-documented IR absorption bands due to the fact that the C=O and C-O bonds are replaced by two equivalent carbon-oxygen bonds which are intermediate in force constant between the C=O and C-O.

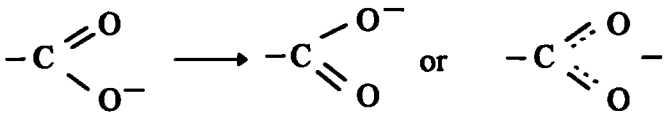


Fig.10.8. Diagram of carbon-oxygen bonds in a fatty acid salt (from ref.10.3)

These two "bond and a half" oscillators are strongly coupled, resulting in a strong asymmetric CO_2 stretching vibration at 1650-1540 cm^{-1} and a somewhat weaker symmetric CO_2 stretching vibration at 1450-1360 cm^{-1} **[10.9]**. Of these bands, the former is very much more characteristic, as it is generally more constant in frequency whilst many other skeletal vibrations occur in the wide range 1450-1360 cm^{-1}.

10.2.3. Description of the system employed

The technique has been recently developed **[10.10]** and employs an FTIR microscope in conjunction with a sliding point contact device. A lubricated contact is formed between a rotating steel ball and a stationary, infrared transparent flat. For the pure sliding conditions employed in this study, a small diamond flat of 3 mm diameter is used. Diamond is suitable since it can transmit infrared wavelengths through the entire mid-IR

range of 2 to 40 μm, although some loss of resolution is experienced in the 4 to 5.5 μm range [**10.10**]. Infrared radiation is focused into the contact using the FTIR microscope system and this is reflected at the lubricant/steel interface and collected by the microscope optics for analysis by the IR detector. Discrete areas of the contact can be scanned, typically 72-200 μm in diameter, the size being defined by the aperture used. For spectra taken in this study, an aperture of 100 μm was employed which compares to a Hertzian contact diameter of 165 μm.

A schematic of the sliding rig used is shown in figure 10.9. The ball is immersed in lubricant and the whole test chamber, containing the ball and lubricant, is heated and maintained at fixed temperature.

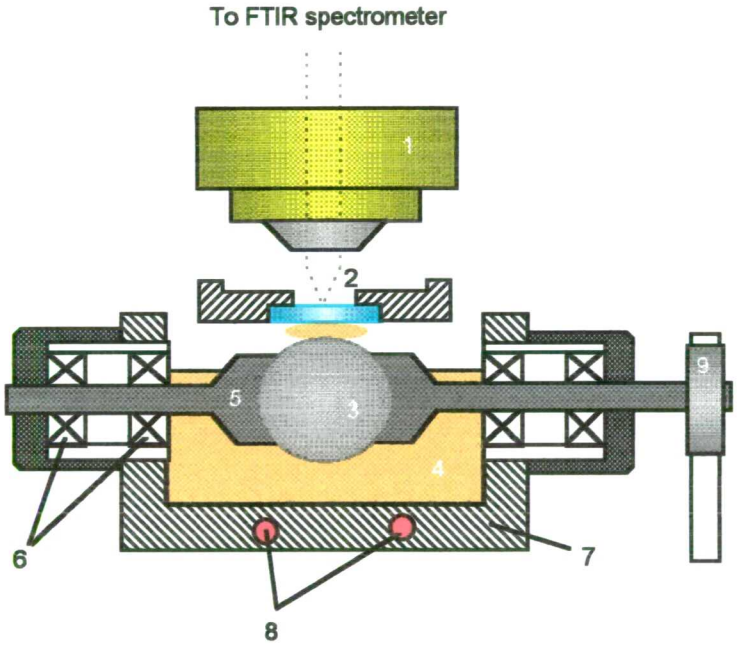


Fig.10.9. Sliding optical EHD device

The numbers in the diagram represent: 1-IR microscope, 2-diamond window, 3-steel ball, 4-lubricant, 5- specimen holder and shaft, 6-bearings, 7-oil bath, 8-heating rods, 9-belt and pulley drive. The sliding device is mounted on a X-Y-Z micropositioning table underneath the FTIR microscope. Thus the entire contact area, inlet and exit regions can be examined through the movement of the table. The Hertzian contact of about 165 μm width is defined by the formation of interference fringes due to the high refractive index of the IR window so that the relative position of the target spot is accurately

known. A complete description of the system is given in reference [10.10]. The test conditions employed in this study are shown in the following table.

Temperature range	25 and 60 °C
Speed range	0.001 to 1 m/s
Load	13 N
Hertzian pressure	0.83 GPa
Hertzian width	165 μm
Ball properties	M 52100 steel, 25.4 mm diameter
(sliding)	Young's modulus 210 GPa
Disc properties	diamond, 3 mm diameter, R I 2.4
(static)	Young's modulus 1143 GPa

Table 10.1. Test conditions for the sliding rig

The spectrometer used was a Perkin Elmer 1740 FTIR instrument with a Spectra Tech IR Plan microscope, computer controlled. Background spectra were usually taken from the diamond/steel interface at the middle of the static, loaded contact. The sample spectra were ratioed against the background spectra in order to remove spurious absorption bands due to IR optics and atmosphere. At least 500 scans were taken for each individual spectra with a resolution of 8 cm^{-1}.

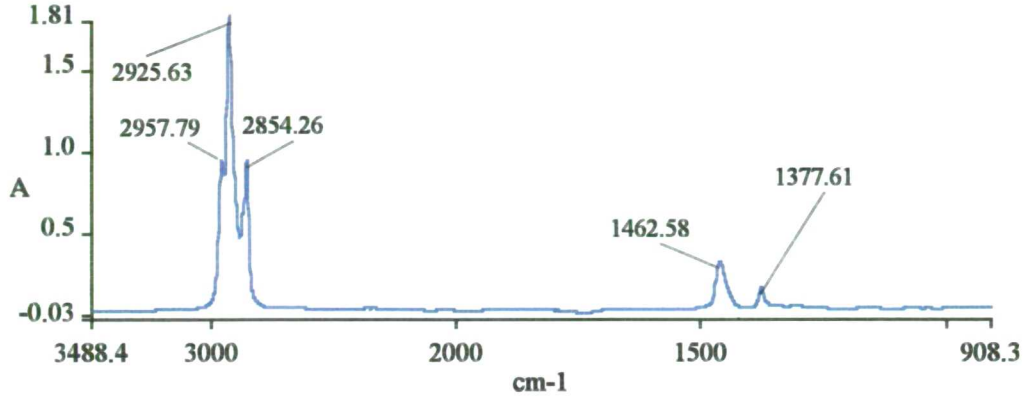
In this study, IR analysis was used as a means for analysing the thick films detected with ultra-thin interferometry technique, to better identify the species of such films in a sliding contact. In this respect, solutions of 0.1% wt. copper oleate in hexadecane were tested at 25 and 60°C both in transmission and reflection mode. The results obtained in transmission tests were subsequently used as a basis for analysing the spectra from the tests performed in the sliding device. This correlation was possible since in both modes the film thickness is thin, of comparable dimensions. Results are presented in the next section.

10.2.4. Spectra results for copper oleate

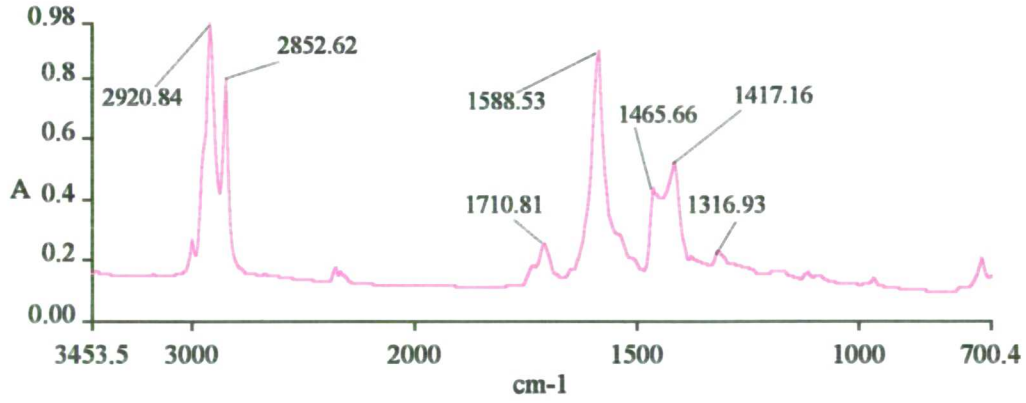
Transmission tests

For the transmission tests, the sample to be analysed was held in a potassium bromide (KBr) cell which is transparent to infrared radiation. A drop of the liquid to be analysed forms a capillary film of ~ 0.01 nm thick between the two transparent salt plates. Since

the pure copper oleate is not in liquid state but a thick paste, a minute quantity was smeared in a very thin layer on one of the plates. The IR radiation passes through the cell and is than analysed by the IR detector. Both basic components of the solution, hexadecane and copper oleate, were analysed in this way and the spectra results are presented in figure 10.10 a and b.



(a) Pure hexadecane



(b) Pure copper oleate

Fig.10.10. Transmission spectra for pure hexadecane and copper oleate

According to the spectral database for an alkane, the CH_3 asymmetrical and symmetrical stretching vibrations occur near 2962 and 2872 cm^{-1} respectively **[10.8]**. The intensities of these vibrations are strong and their frequencies are characteristic. The asymmetric and symmetric CH_2 stretching vibrations appear strongly at about 2926 and 2853 cm^{-1} and the spectral positions vary no more than ± 10 cm^{-1} for acyclic -CH_2- groups **[10.8]**. Also the asymmetric and symmetric CH_3 bending vibrations occur at 1470-1430 cm^{-1} and 1395-1365 cm^{-1} respectively. All these absorbance peaks can be easily identified in

the spectrum for pure hexadecane. For pure carboxylic acid salts, the strong absorptions corresponding to CH_2 stretching vibrations and CH_3 bending vibrations are still present, in addition specific vibrations appear due to the CO_2 moiety [**10.9**]. Thus the absorbancies at 1588 and 1417 cm^{-1} represent the "fingerprints" for the presence of the carboxylate.

Figure 10.11 shows a small portion of the infrared spectrum (1500 cm^{-1} region expanded) for pure hexadecane, pure copper oleate and their solution all on the same plot.

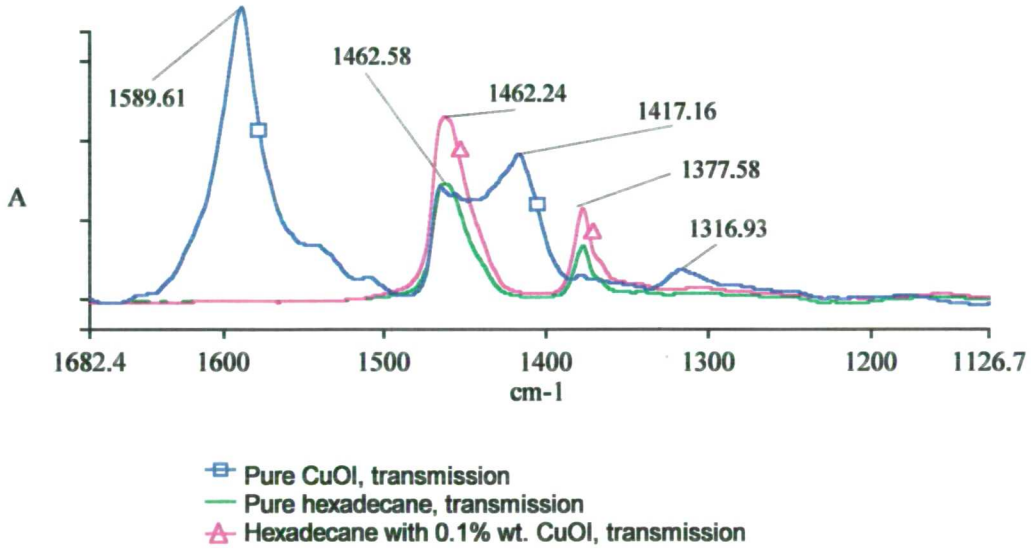


Fig.10.11. Spectra comparison for pure Cu oleate, hexadecane and their 0.1% wt. solution

The purpose of this is to compare the absorbance peaks position, so there is no scale shown on the Y axis. It can be seen that there is no discernible difference between the absorption spectra of hexadecane and the solution of copper oleate, the additive concentration being too small.

Reflection tests

Room temperature results

A series of spectra were taken from the inlet and the exit of the contact in static conditions and at different speeds. It was not possible to obtain spectra results from the central area of the contact due to the very small film thickness, so spectra from the inlet region were used to obtain an insight on the film behaviour. This approach was based

on the EHD theory statement that the film thickness in the contact is controlled by the rheology of the lubricant in the inlet [**10.11**].

Although test condition was that of pure sliding instead of pure rolling or mixed sliding/rolling, an attempt was made to follow the same test procedure as in the ultra-thin film tests using those results for guidance in the IR analysis. Thus the time effect was investigated by recording spectra at constant time intervals whilst keeping the sliding speed constant and spectra from the inlet region were taken when speed was increased as well as decreased corresponding to "forward" and "back" plots from the film thickness measurements.

Figure 10.12 shows a portion of the infrared spectra at 25°C taken from the inlet region at three speeds when speed was gradually increased.

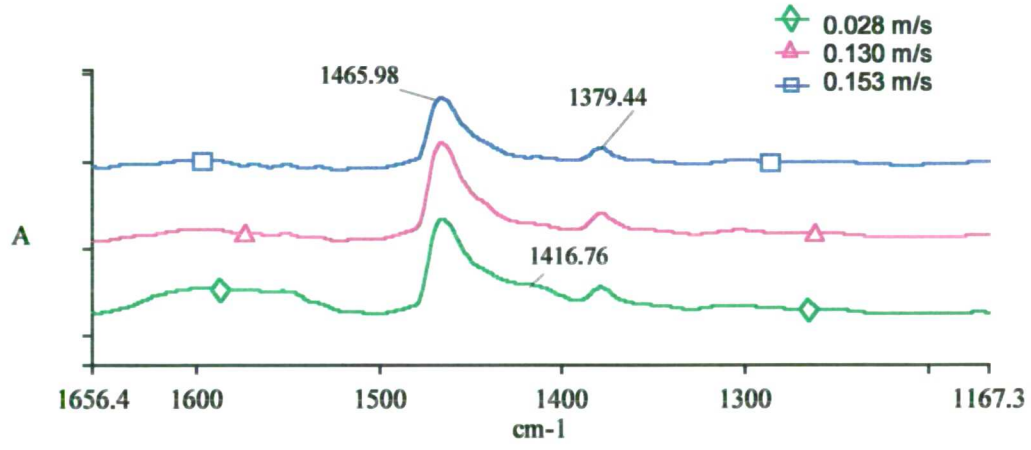


Fig.10.12. IR spectra around 1500 cm^{-1}, inlet region for 0.1% wt. Cu oleate in hexadecane at 3 speeds and 25°C

It is noticeable from this plot that the oleate absorption peak at 1416 cm^{-1} visible at 0.028 m/s disappears as the speed increases, which suggests that the composition in the inlet is changing with speed, less of the carboxylate is entrained in the contact at higher speeds. The fact that the oleate peak is not visible in transmission but is present at slow sliding speeds suggests that there is an increase in oleate concentration in the inlet due to the actual motion and the running time.

There is also a significant difference between the spectra taken at the same speed but at different stages of the test. Figure 10.13 shows such comparison results at 0.0034 m/s and 25°C.

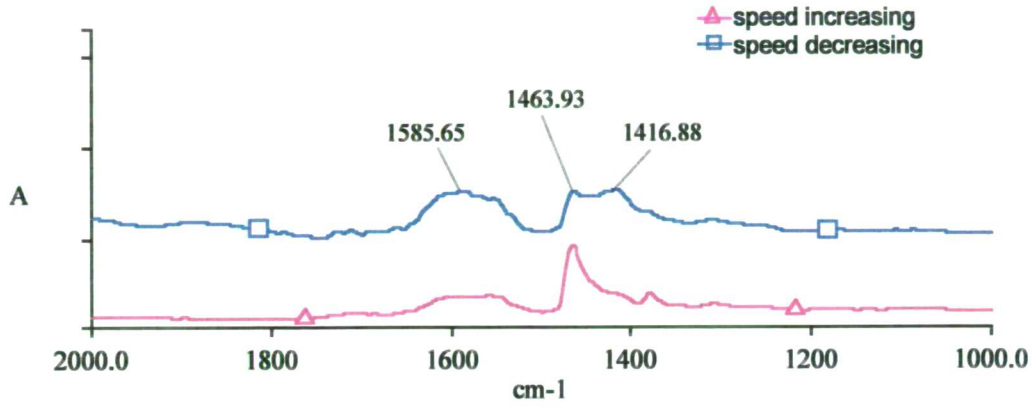


Fig.10.13. IR spectra from 0.1% Cu oleate in hexadecane at 25°C, 0.0034 m/s, for two test stages

The spectra from the second stage, when speed is decreasing, shows a much stronger absorption peak at 1416 cm^{-1}. The absorption band at 1585 cm^{-1} is also more apparent, however it is also more broader which suggests that a number of similar species are present, not only the oleate.

A test to monitor the film build-up was also performed at 25°C, slow speed 0.0034 m/s with copper oleate solution in hexadecane. Spectra were taken from the contact inlet at regular intervals in an attempt to simulate the conditions from the optical tests where film growth with time was recorded as described in chapter 9. Several scans made at the start of the test together with those taken after 10, 20 and 30 minutes of running are shown in figure 10.14.

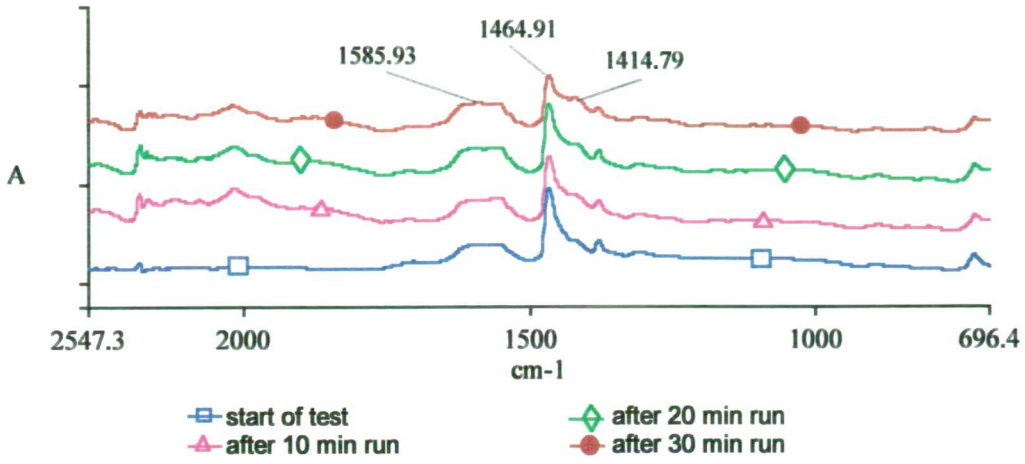


Fig.10.14. IR spectra from the inlet region for 0.1% wt. Cu oleate in hexadecane at 0.0034 m/s, 25°C - time dependence

It can be seen that the shoulder at 1414 cm^{-1} is becoming more visible as the test time is increasing. This corresponds to the absorption peak characteristic of a symmetric COO- stretch structure. There was also visual evidence of some kind of aggregation in the inlet which probably caused the formation of the thick films detected with ultra-thin interferometry.

Immediately after the ball was halted, a spectra was taken from the inlet region and is compared in figure 10.15 with the similar observation taken before the test has started.

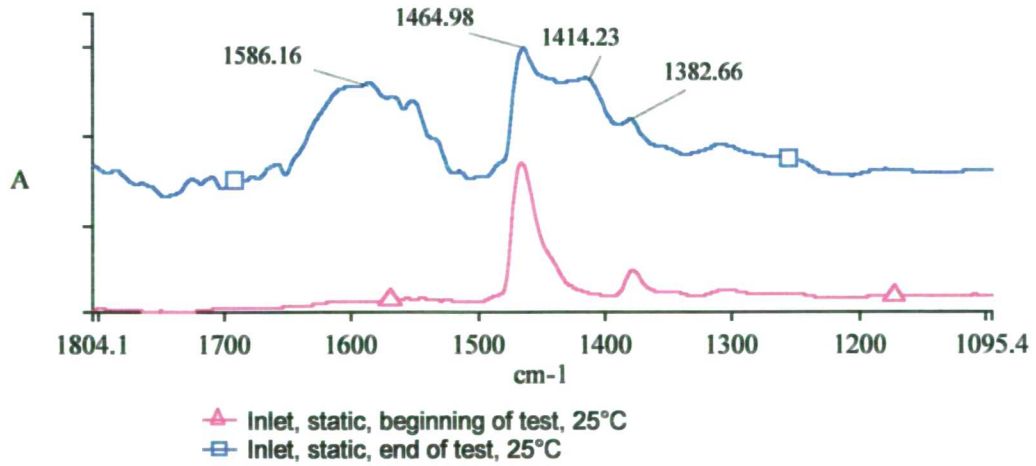


Fig.10.15. Comparison between IR spectra taken in the beginning and at the end of test for 0.1% wt. Cu oleate solution in hexadecane at 25°C

It can be clearly seen that the presence of the oleate salt in the inlet is still strong even after sliding has stopped which suggests that the material is probably deposited or somehow trapped between the surfaces.

Results at 60°C

Higher temperature tests were a confirmation of the results obtained at 25°C. The fact that the oleate salt is present in the inlet mainly at slow speeds was also revealed in spectra taken at 60°C and the results are shown in figure 10.16.

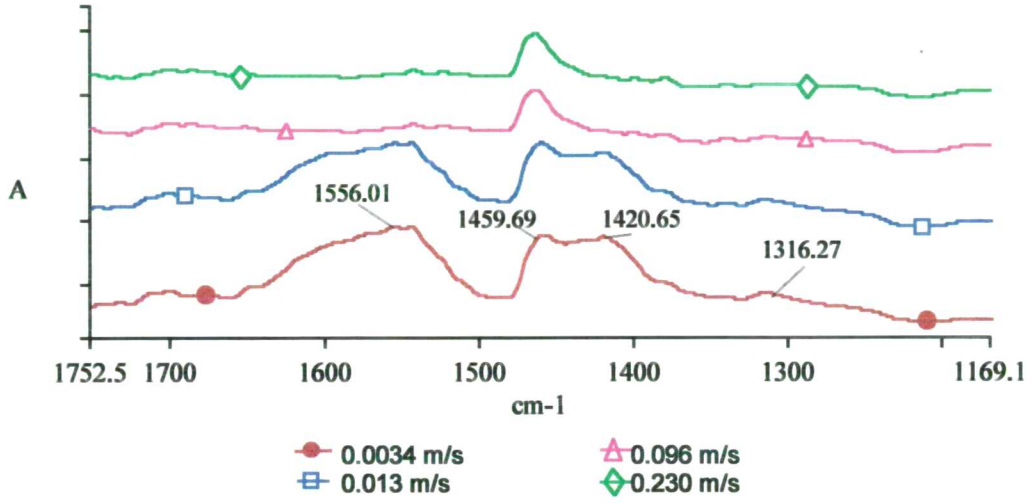


Fig.10.16. IR spectra from the inlet region for Cu oleate solution in hexadecane at 4 speeds, 60°C

Other tests also support the idea that there is an increased concentration of carboxylate salt in the inlet region. Spectra were taken from the inlet region of the contact and also from further out of inlet region at 0.0034 m/s and the results showing the presence of oleate in the inlet region only are shown in figure 10.17. Observations taken from inlet and outlet regions are presented in figure 10.18.

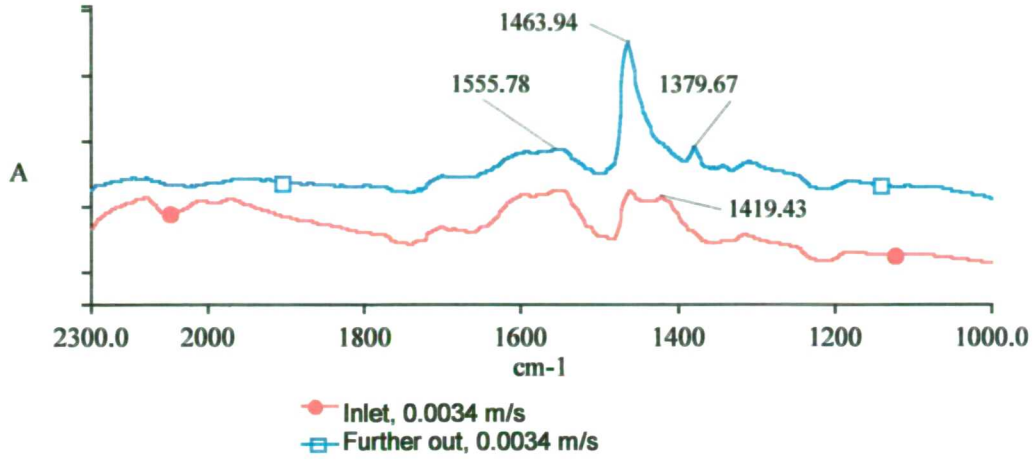


Fig.10.17. IR spectra for Cu oleate solution in hexadecane taken in the inlet and further out regions at 0.0034 m/s and 60°C

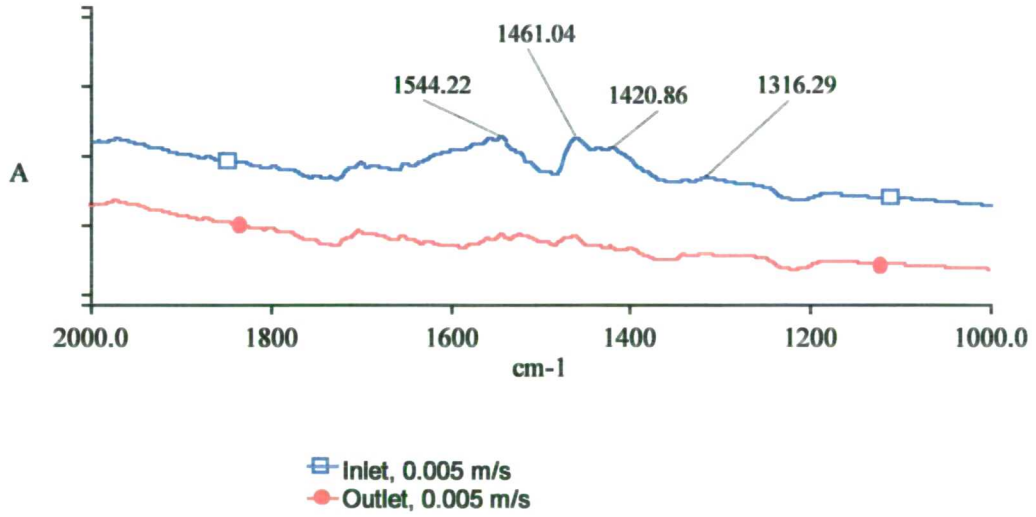


Fig.10.18. IR spectra for Cu oleate solution in hexadecane taken in the inlet and outlet regions at 0.005 m/s and 60°C

There is clear evidence that the oleate compound is present in the inlet of the contact in a higher concentration than in the bulk of solution. This is only noticeable after extending sliding which agrees with the observation from optical tests that thick films formation is a time dependent phenomenon.

10.3. Discussion

This section considers the results of work carried out on friction modifier additives and discusses the interpretation of the properties and possible origins of the boundary films identified in this study.

10.3.1. Physico-chemical characteristics

Video image analysis and mapping techniques have confirmed the presence of a thick boundary film at slow speeds which is destroyed by high shear conditions. 2-D and 3-D maps have shown that the film is patchy, unevenly distributed over the contact area and has high local peaks. Both video recording and IR analysis have shown in tests run at slow speeds that the film formation is strongly time dependent.

As to the composition of the boundary films, IR analysis provides a body of evidence which supports the idea that thick films formed by copper oleate might consist mainly of carboxylate but no information whether the metal ion is copper or iron is available yet. One possibility could be that of cation exchange between copper and iron compounds to form an insoluble iron oleate as has been observed with iron and zinc species in ZDDP containing formulations [10.12]. Here it was found that iron from the steel substrate displaced Zn from the ZDDP and replaced it forming FeDDP. It has also been suggested in the literature [10.13] that redox-type reactions between copper and iron species might also occur at surfaces, a mechanism which is believed to inhibit oil oxidation in steel systems [10.14]. What is definitely clear is that in the contact inlet there is a much higher concentration of the carboxylic acid salt than in the bulk solution and this was not detected in the contact outlet or in remote areas. Further work is needed to clarify the composition of these films.

It is noteworthy that film formation became faster and a thicker film was formed at high temperature. This supports the possibility of a chemical reaction process. It is unfortunate in retrospect that the carboxylic acid tests were carried out in hexadecane only at 25°C. If thick film formation requires soap formation, then results made at higher temperature may well have more repeatability given thick films.

As discussed earlier, there was visual evidence of some kind of substantial aggregation in the contact inlet region which was clearly visible on video image recordings and also during IR analysis in sliding tests. This "material" seemed to have quite a thick consistency and to be clearly identified with the formation of the thick boundary films. From interferometric measurements it appears to have high viscosity, almost 40 times higher than the bulk solution. It is also evident that the material was somehow better entrained in the inlet when sliding was present than in pure rolling, as evidenced by the higher film thicknesses obtained in sliding conditions.

10.3.2. Low and high shear rate behaviour

From the fact that boundary film thickness increases with rolling speed at slow speeds, it appears that the boundary film is behaving in an essentially "hydrodynamic" way, in a fashion similar to that reported for adsorbed polymers from solutions [**10.15**]. At slow speed/thin film conditions, the contact inlet is effectively filled with deposited, highly viscous material which, because of its viscosity, is strongly entrained even though the speed is low. Figure 10.19 shows a schematic representation of this situation.

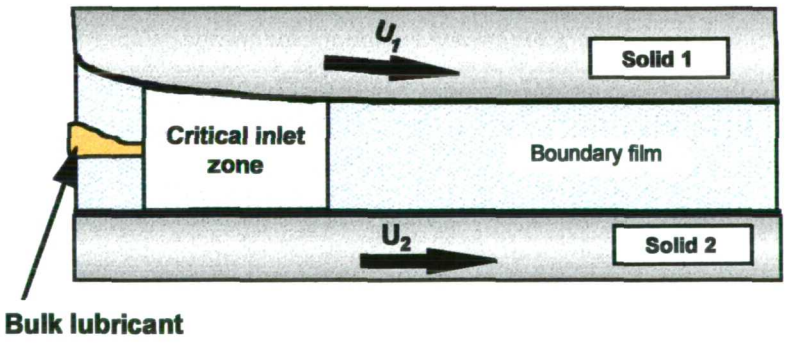


Fig.10.19. Contact inlet zone for slow speeds/small clearances

Thus up to a certain film thickness, the contact is effectively lubricated by a viscous surface layer, yielding a much thicker EHD film than would be formed by the bulk solution. As the speed is raised, the film thickness grows higher than the surface layer so that the inlet is now filled with bulk solution resulting in a reversion to the level of EHD film thickness expected of the solution. The behaviour of copper oleate boundary film was, however, significantly different from that of polymer solutions in that the film

thickness at high speeds did not revert to that of EHD film thickness of solution plus boundary film but seems to collapse down to the EHD film thickness alone. This implies that at high speeds the boundary film was either destroyed or failed to form, so the resulting film thickness was that of the bulk solution alone. This thick film collapse at high speeds above about 0.07 to 0.1 m/s was also confirmed by video recorded images. This behaviour may hold clues as to the nature of the boundary film material itself.

There are several possible explanations for the high speed behaviour of thick boundary films.

(i) *repulsion of inlet material.* The viscous material which is entrained at slow speeds may be only weakly (or not at all) bonded to the solid surfaces. Thus, as the speed increases, fluid forces in the inlet region may reject this material which may be swept around the contact sides due to reverse shear before it enters the critical inlet zone. This type of behaviour has been found with PTFE and solid particles suspended in solutions when as the speed is raised, less particles are entrained in the contact **[10.16, 10.17]**.

(ii) *removal of deposited film material.* It is possible that, due to the high shear rates in the contact, the thick film suffers a mechanical degradation and the film continuity is destroyed. It might be even that the thick material structure is broken before reaching the concentrated inlet region, effectively being washed off the solid surface out of contact by fluid shear forces close to the surfaces, so that the substance available in the inlet to build the film in the contact is no longer present as in low speed conditions.

(iii) *shear thinning of inlet material.* The response of the thick material to the high strain rates in the inlet region, which are often suggested to be about 1.5 times higher than in the contact itself **[10.18]**, might be severe shear thinning or temporary viscosity loss. The effective shear rate at 0.1 m/s and a 20 nm film would be 0.75×10^{7} s^{-1}. As with greases **[10.19]** when the external stresses exceed the threshold level of shear, the semi-solid material may turn into a flowing liquid. This will have a much lower viscosity, that of the base oil and in consequence the film at high speeds may only be due to the base lubricant alone.

It is worth mentioning that mechanisms one and two are supported by the IR results which have shown that the oleate presence in the inlet was not detected when the speed was exceeding 0.1 m/s. However, this evidence does not support the shear thinning hypothesis. It is important to note that in the copper oleate case, with either of the mechanisms suggested, the result is that at high shear stresses, the thick, viscous material fails to fill the contact inlet and as a consequence, the film thickness is only equal to that provided by the pure base oil.

The dimer acid behaviour at high shear rates seems to conform more to the adsorbing polymer additive model in that the boundary film continued to partially augment the base oil film thickness in full-film hydrodynamic conditions. Although the films formed by the dimer acid are less than that of copper oleate, they appear to be somehow stronger attached to the surfaces. It has been shown in the literature **[10.20]** that dicarboxylic acids are better adsorbed than monocarboxylic acids from polar solvents. Their adsorption film is more stable showing superior oiliness effect which was attributed to their immediate replenishment when removed by friction.

10.3.3. Possible structure of thick boundary films

In their discussion on thick versus thin boundary lubricating films, Allen and Drauglis **[10.21]** proposed several possible models for thick film structure. One was the formation of a multimolecular micellar film resulted from the formation of viscous laminar or cubic inverted micelles next to polar surfaces. It is known that in non-aqueous solutions, a micelles' structure is such that the polar heads of the molecules being repelled from the solvent, are grouped together to form the central core of the micelle **[10.22]**. The consequent micellar material might, because of its high viscosity, be entrained in rolling and sliding contacts even at very slow speeds.

It is suggested that initially a monolayer is adsorbed on to the metal surfaces which may already contain an oxidised iron layer in the manner suggested by Godfrey **[10.23]** for stearic acid and that micelles form on top of this. It has been shown that fatty acid salts can form micelles in hydrocarbons **[10.22]**. Small amounts of water or other polar

impurities can affect the size and shape of the micelles formed in hydrocarbon solvents. The polar compounds formed may possibly create a molecular "network" structure similar to the soap structure found in greases [**10.24**]. In support of this idea it should be mentioned that the video images of the contact interferograms for thick films of fatty acid salts are strikingly similar to those of greases recorded recently by other researchers [**10.25**]. The formation of these micelles could explain the aggregation observed in the inlet and the thick films detected at slow speeds. The film behaviour at high shear rates could be due to rejection from or breakdown in the contact inlet of the micellar species by a mechanism discussed in the previous section.

A second possible structure of the boundary film could be a local, ordered, liquid film, also postulated by Allen and Drauglis [**10.21**]. It is possible that specific adsorption of surfactant molecules due to dipole interactions between fluid molecules and solid will itself produce a layer of reduced mobility and thus enhanced viscosity. Such adsorption may lead to local layering through the mutual short-range molecular interactions which can produce long-range order and explain the existence of films over one molecular layer thickness. It was mentioned in previous work [**10.26**] that thick films exhibit an ordered structure similar to liquid crystals. In the ordered liquid film model [**10.21**] it is postulated that a close packed monomolecular layer is firstly adsorbed on the surfaces. A second close packed layer is then deposited, stability being induced by the combined effect of van der Waals forces between the terminal methyl groups of the acids, and a residual field due to the Fe-O bond at the surfaces. A third layer is then held in place by hydrogen bonding [**10.27**] between the adjacent carboxyl groups thus forming dimers in the form of linear chains with the two carboxyl groups in the middle. These dimers can aggregate by London forces acting between the methylene groups thus forming an ordered structure of lamellar or rod-shaped molecules. When a triple layer is thus formed, further dimer layers may be deposited in a similar manner and built up the thick films. Since the model is based mainly on the short range physical interactions it is likely that high amounts of shear would destroy its structure. On the other hand, in low shear conditions, the slip plane will be located between the nonpolar methyl-methyl ends where the bonding energy is lowest. The lamellar structure would thus provide a low shear strength layer which would reduce friction as long as it is present in the contact. Classical examples of such long-range order in a fluid are liquid crystal structures formed by long chain organic molecules. Such liquid crystalline compositions have been

recognised as potential lubricants, by a great number of researchers in the last 20 years [10.28]. Recently, non-aqueous lamellar liquid crystalline compositions claimed to be useful as lubricants or as friction-modifying additives have been patented [10.29].

One possible explanation for the thick films formed by the dimer acid might be given by the concept of friction polymer. This was used by Furey [10.30, 10.31] to account for the wear reduction of more than 40% on alumina surfaces, produced by solutions of the same dimer acid compound. Such polymerisation might be promoted by the high pressures and temperatures at asperity contact or by exoelectrons emitted during metallic plastic deformation. The first step may involve concentration of the dimer acid on the solid surface by an adsorption process. In a dynamic system, the polymer films continually form and wear away. However, the system tends to have a built-in control: the very formation of the polymer film will tend to reduce contact and friction and therefore the rate at which the film continues to form. As the polymer is physically worn away, friction and surface temperatures will tend to increase thereby causing the rate of film-formation to increase.

It must be emphasised that these models are largely conjectural, based on measurements of mainly physical phenomena made in this study. Clearly more chemical work needs to be done in future to clarify these assumptions and some suggestions as to how this might be carried out will be proposed in the next chapter.

REFERENCES

[10.1] Cameron A. and Gohar R., "Theoretical and Experimental Studies of the Oil Film in Lubricated Point Contacts", Proc. Roy. Soc. Lond., A291, pp. 520-536, 1966,

[10.2] Gohar R. and Cameron A., "The Mapping of Elastohydrodynamic Contacts", ASLE Trans. 10, pp. 215-225, 1967,

[10.3] Aderin M.E., "Interferometric Studies of Very Thin Lubricant Films in Concentrated Contacts", PhD Thesis, Imperial College, University of London, 1994,

[10.4] Smeeth M. and Spikes H.A., "Central and Minimum Elastohydrodynamic Film Thickness at High Contact Pressure", Trans. ASME J. of Trib. 119, pp. 291-296, 1997,

[10.5] Cann P.M., Spikes H.A. and Hutchinson J, "The Development of a Spacer Layer Imaging Method (SLIM) for Mapping Elastrodynamic Contacts", Trib. Trans., 39, pp. 915-921, 1996,

[10.6] Gustafsson L., Höglund E. and Marklund O., "Measuring Lubricant Film Thickness with Image Analysis", Proc. IMechE, 209, pp. 109-205, 1994,

[10.7] Barnes R.B. et al., "Infrared Spectroscopy. Industrial Applications and Bibliography", Reinhold Publishing Co., New York, 1944,

[10.8] Lin-Vien D., Colthup N.B. et al., "The Handbook of Infrared and Raman Characteristic Frequencies of Organic Molecules", p. 2, Academic Press, 1991,

[10.9] Colthup N.B., Daly L.H. and Wimberley S.E. " Introduction to IR and Raman Spectroscopy", 3rd edition, Academic Press Inc., 1990,

[10.10] Cann P.M. and Spikes H.A., "In Lubro Studies of Lubricants in EHD Contacts using FTIR Absorption Spectroscopy", Trib. Trans. 34, pp. 248-256, 1991,

[10.11] Guangteng G. and Spikes H.A., "Boundary Film Formation by Lubricant Base Fluids", Trib. Trans. 39, pp. 448-454, 1996,

[10.12] George J.M., Martin J.M., Matima T., Kapsa P.H., Meill G. and Montes H., "Mechanism of Boundary Lubrication with Zinc Dithiophosphate", Wear 53, p. 9, 1979,

[10.13] Colclough T., "Role of Additives and Transition Metals in Lubricating Oil Oxidation", Ind. Eng. Chem. Res., 26, pp. 1888-1895, 1987,

[10.14] Günsel S. and Lockwood F.E., "The Influence of Copper-Containing Additives on Oil Oxidation and Corrosion", Trib. Trans. 38, pp. 485-496, 1995,

[10.15] Smeeth M., Günsel S. and Spikes H.A., "Boundary Film Formation by Viscosity Index Improvers", Trib. Trans, 39, 3, pp. 726-734, 1996,

[10.16] Palios S., Cann P. M. and Spikes H.A., "Behaviour of PTFE Suspensions in Rolling/Sliding Contacts", Proc. 22nd Leeds-Lyon Symposium on Tribology, "The Third Body Concept: Interpretation of Tribological Phenomena", Lyon, Sept. 1995, pp. 141-151, ed. D. Dowson et al., publ. Elsevier, Amsterdam, 1996,

[10.17] Wan G.T.Y. and Spikes H.A., "The Behaviour of Suspended Particles in Rolling and Sliding Elastroydrodynamic Contacts", STLE Trans. 31, pp. 12-21, 1988,

[10.18] Dyson A. and Wilson A.R., "Film Thickness in Elastohydrodynamic Lubrication by Silicone Fluids", Proc. I.Mech.E, 180, Pt. 3k, pp. 97-112, 1965-66,

[10.19] Gow G., "Lubricating Grease", in "Chemistry and Technology of Lubricants", 2nd edition, ed. Mortier R.M. and Orszulik S.T., 1997,

[10.20] Minami I., Kikuta S, Masuko M. and Okabe H., "Lubricating Functions of Dicarboxylic Acids in Polar Base Oils", J. Journal of Trib. , 35, p. 505, 1990,

[10.21] Allen C.M. and Drauglis E., "Boundary Layer Lubrication: Monolayer or Multilayer", Wear 14, pp. 363-384, 1969,

[10.22] Shinoda K., "Colloidal Surfactants", p.81, Academic Press, New York, 1963,

[10.23] Godfrey D., "Symposium on Properties of Surfaces", ASTM Spec. Publ. No. 340, p. 109, 1962,

[10.24] Smith A.J., "The Thinning of Liquid Films on Metal Surfaces", PhD Thesis, Imperial College, University of London, 1971,

[10.25] Cann P.M. "Grease Lubricant Film Distribution in Rolling Contacts", Presented at NLGI Conference 1996, to be published in NLGI Spokesman,

[10.26] Deryaguin B.V., Karassev V.V., Zakhavaeva N.N. and Lazarev V.P., "The Mechanism of Boundary Lubrication and the Properties of the Lubricating Film - Short and Long-Range Action in the Theory of Boundary Lubrication", Wear 1, pp. 277-289, 1957/58,

[10.27] Trillat J.J., "The Adsorption of Oils in Relation to Lubrication", I. Mech. E. Proc. of the General Discussion on Lubrication and Lubricants 2, pp. 55-59, 1937,

[10.28] Lockwood F.E., Benchaita M.T. and Friberg S.E., "Study of Lyotropic Liquid Crystals in Viscometric Flow and Elastohydrodynamic Contact", ASLE Trans., 30, pp. 539-548, 1987,

[10.29] Lockwood F.E. et al., "Non-Aqueous Lamellar Liquid Crystalline Lubricants", United States Patent No. 4,999,122, Mar. 1991,

[10.30] Furey M.J., "The Formation of Polymeric Films Directly on Rubbing Surfaces to Reduce Wear", Wear 26, pp. 369-392, 1973,

[10.31] Furey M.J., Ghasemi H. et al., "Tribochemistry of the Antiwear Action of a Dimer Acid/Glycol Monoester on Alumina", Trib. Trans., 37, pp. 67-74, 1994

CHAPTER 11

CONCLUSIONS AND FUTURE WORK RECOMMENDATIONS

11.1. Conclusions

This study has been in two parts and the conclusions from the fuel efficiency work have already been presented in chapter 6. This last chapter outlines the conclusions from the second part of the study which was concerned with studying boundary film formation in-situ. A number of experimental methods were employed to investigate such films, all were in-contact techniques able to examine additive film properties under realistic conditions of pressure, temperature and shear. The main conclusions drawn from this research are as follows.

(a) Thin-film interferometry has demonstrated that carboxylic acid salts and, occasionally, fatty acids themselves form thick boundary films of the order of tens of nanometers thickness in concentrated contacts under low speed conditions. These films are thicker than predicted from the classical EHD theory based upon the bulk viscosity of the lubricant. The films survive in slow speed mixed rolling/sliding conditions and their formation appears to be promoted by sliding. The films also exhibit a viscous nature since they are

speed dependent and appear to result from a contact inlet viscosity up to 40 times higher than the bulk viscosity of the fluid. The film formation is also a time dependent process and is influenced by temperature and the nature of the base fluid.

(b) It appears that these thick films can make a significant contribution to friction reduction in the mixed/boundary regime, decreasing friction down to levels reminiscent to full film EHD lubrication. This means that contacts which would otherwise operate mainly in the boundary regime are able, for much more of their contact cycle, to operate in the lower friction, mixed or EHD regime.

(c) Evidence of increased oleate presence in the contact inlet detected using the IR analysis suggests that when copper oleate was used as additive the composition of these films is mainly metal salt. Whether the metal is copper or iron remains to be investigated in future work. If thick films are formed by soaps then fatty acids must form such soaps in order to exhibit thick film forming behaviour. The fact that fatty acids only showed this behaviour intermittently suggests that there must be some critical conditions such as degree of cleanliness, temperature and rolling time which might promote the formation of soaps at the surface.

(d) The films formed by the dimer acid additive were not as thick as the copper oleate films. However research done by other authors have found them able to reduce wear by impressive amounts. Their formation is explained by the concept of in-situ polymerisation i.e. formation of friction polymeric films directly on the rubbing surfaces under conditions of high temperature and pressures. They reduce friction and wear thus protecting the surfaces and they continually form and wear away showing a built-in control. The film formed by this additive appeared to persist, to some extent, in high speed conditions and augment the base fluid EHD film.

(e) Three hypothesis have been advanced to explain the collapse of the thick films of copper oleate at high shear rates. One is the lack of entrainment of the thick,

more viscous material in the contact inlet zone as the speed is increased. A second suggests removal of deposited film material from the out of contact solid surfaces due to high speed motion through the bulk fluid. The third is a possible mechanical degradation or shear thinning of surface film material in the inlet due to high shear rates.

(f) The current study has shown that thick boundary films exist between solid and liquid phases in slow speed, high load conditions but was not able to clarify their actual structure. However, some possibilities have been suggested based on the suggestions of Allen and Drauglis. These include a micellar network structure and an ordered liquid structure.

(g) It has been demonstrated that the additives studied can reduce friction in mixed/boundary regime. However, since the film formed is entirely or partially destroyed by shear and takes time to reform, they might not be suitable for non-steady state practical applications such as engine pistons. Further study in non-steady state contacts will help clarify whether these films exist in such conditions.

11.2. Future work recommendations

(a) More work needs to be done to delineate more clearly the conditions under which fatty acids form thick boundary films. This will require work to establish a standard, reliable cleaning procedure in order to reduce the scatter of the results. Boundary lubrication is very sensitive to surface contamination and vigorous cleaning is a very important condition to achieve repeatable results.

(b) It will be useful to explore further the role of temperature, time and speed conditions on film formation and friction and also the influence of humidity, concentration and the nature of the substrate. This is especially the case for fatty acid additives.

(c) The study would be usefully supported by work in which Langmuir-Blodgett multilayers of fatty acids were deposited and the ultra-thin film technique used to investigate their behaviour under rolling and mixed sliding/rolling conditions.

(d) Further work should be carried out to study the influence of solvent upon the thickness of boundary layers. Using different types of solvents might help clarify whether the film formation sensitivity is influenced by the solubility of the material of the film in the solvent.

(e) The current work should be expanded to other carboxylic acid salts and other metals besides copper.

(f) The test rig needs to be modified to allow for even lower speed traction measurement and to enable simultaneous traction and film thickness determination in order to make measurements at exactly the same test conditions,

(h) Further work to investigate the behaviour of thick films in non-steady state conditions simulating the reciprocating motion of pistons in an engine.

(i) Further work is needed to determine the composition and structure of boundary films. The XANES (X-ray absorption near edge structure) approach shows considerable promise in being able to analyse oiliness films using electron transmission from the carbon atom directly into rubbing contacts thus producing reliable molecular information on very thin films **[11.1]**.

(j) Some work has already been started in the Tribology Section, Imperial College, to study the behaviour of oiliness additives under applied potential conditions. Such research might help explaining the conditions which promote the thick film formation especially for fatty acids.

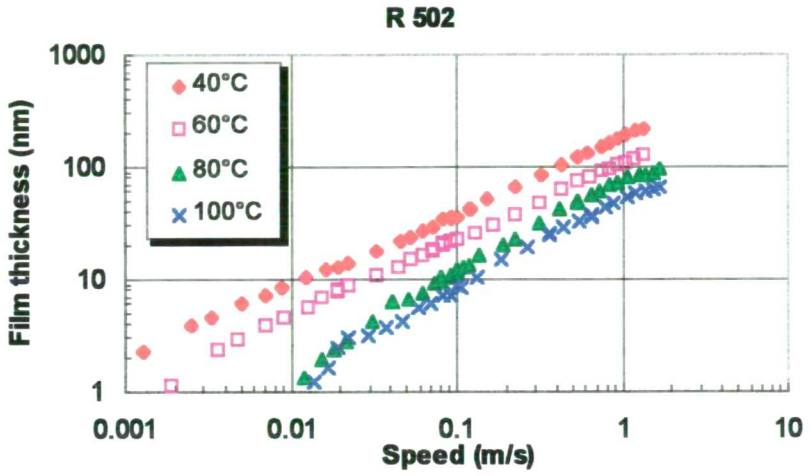
This research has provided, for the first time, direct evidence on the existence of thick boundary films. The proposed work together with more advanced techniques will perhaps help a proper understanding of boundary lubrication in the near future.

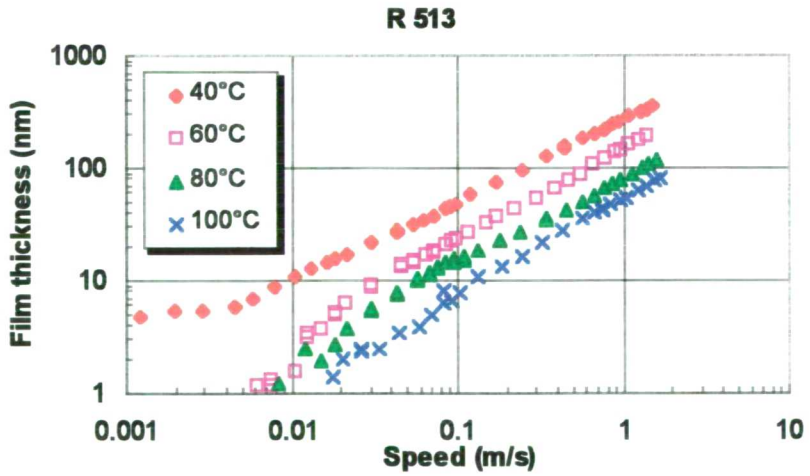
REFERENCES

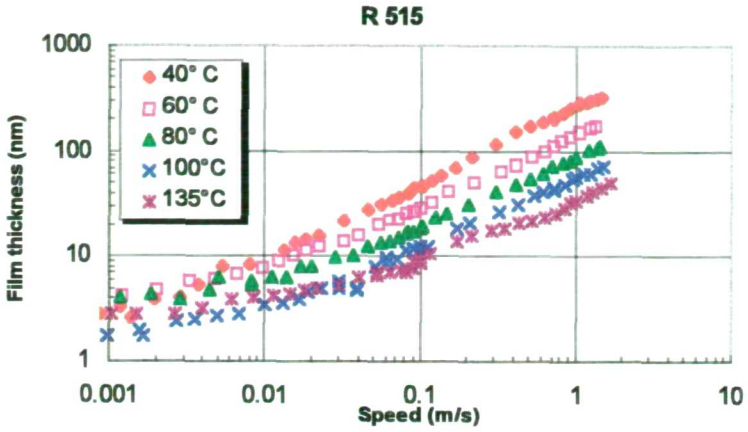
[11.1] Hastie G.P. and Roberts K.J., "Structural Characterisation of Long-Chain Hydrocarbon Thin Films Using Ultra-Soft Polarised Near Edge X-ray Absorption Spectroscopy", Langmuir, 11, pp. 4170-4172, 1995

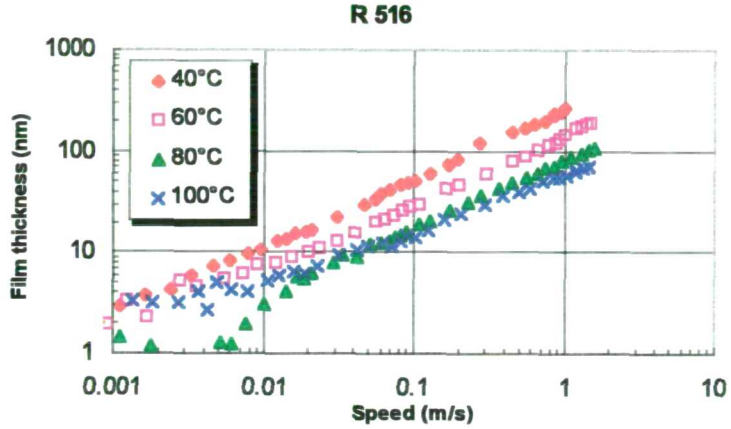
APPENDIX A

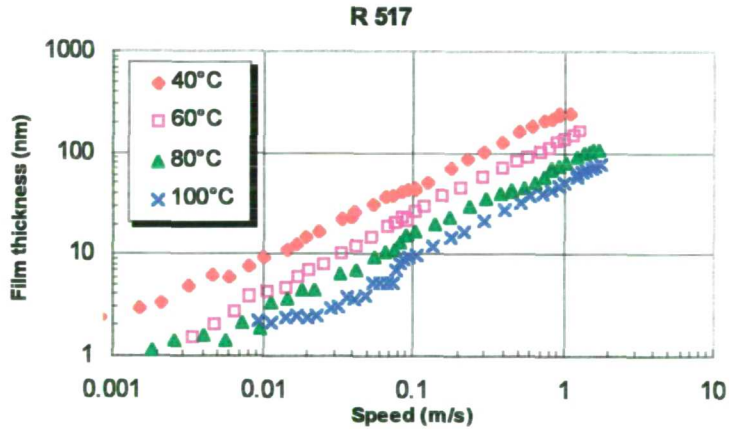
EHD film thickness vs speed results for Sequence VI oils

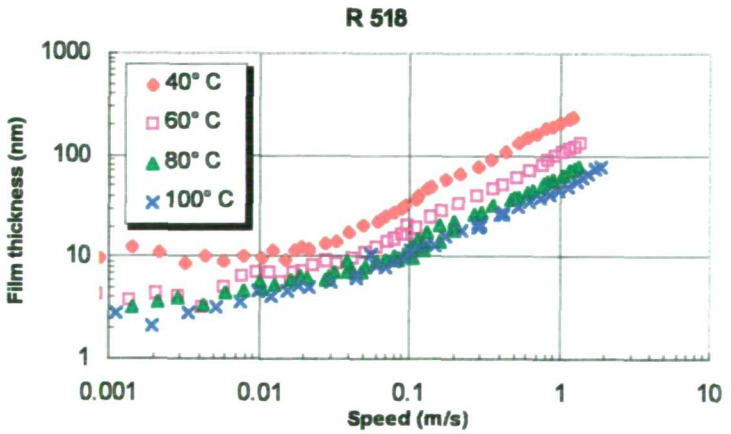


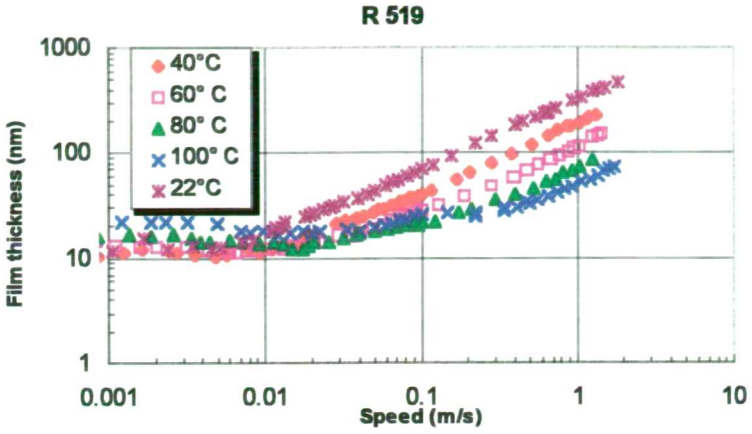


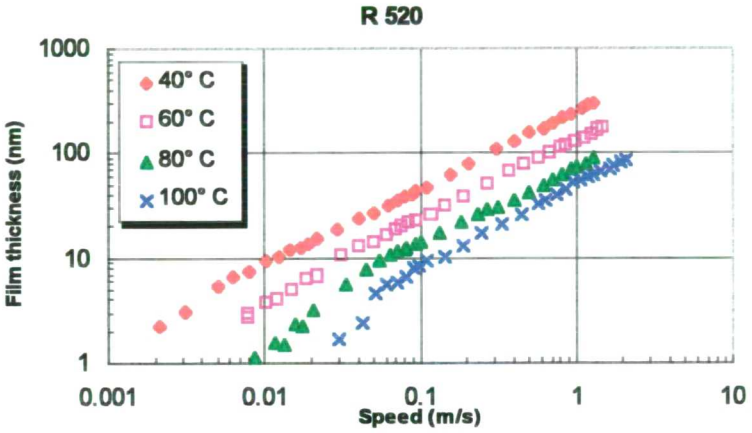

R 515
1000
100
10
1
Film thickness (nm)
40° C
60° C
80° C
100°C
135°C
0.001
0.01
0.1
1
10
Speed (m/s)

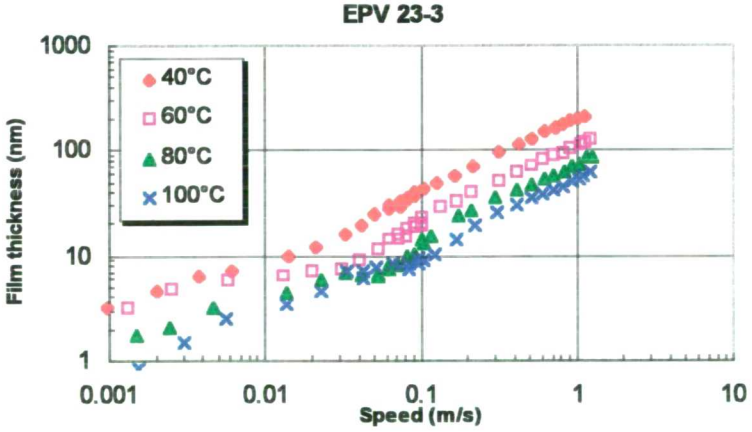

R 516
1000
100
10
1
Film thickness (nm)
40°C
60°C
80°C
100°C
0.001
0.01
0.1
1
10
Speed (m/s)

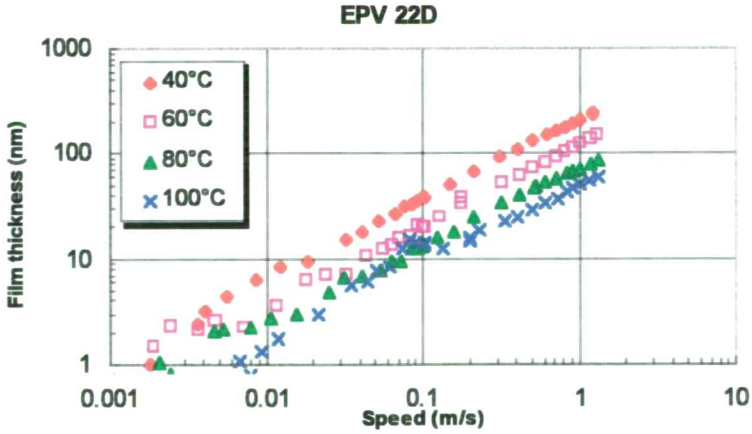

R 517
1000
100
10
1
Film thickness (nm)
40°C
60°C
80°C
100°C
0.001
0.01
0.1
1
10
Speed (m/s)


R 518
1000
100
10
1
Film thickness (nm)
40° C
60° C
80° C
100° C
0.001
0.01
0.1
1
10
Speed (m/s)


R 519
1000
100
10
1
Film thickness (nm)
40°C
60° C
80° C
100° C
22°C
0.001
0.01
0.1
1
10
Speed (m/s)

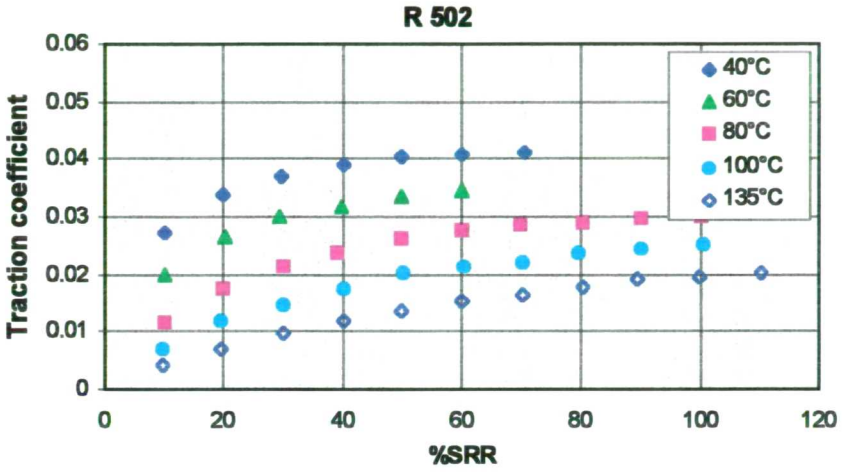

R 520
1000
100
10
1
Film thickness (nm)
40° C
60° C
80° C
100° C
0.001
0.01
0.1
1
10
Speed (m/s)

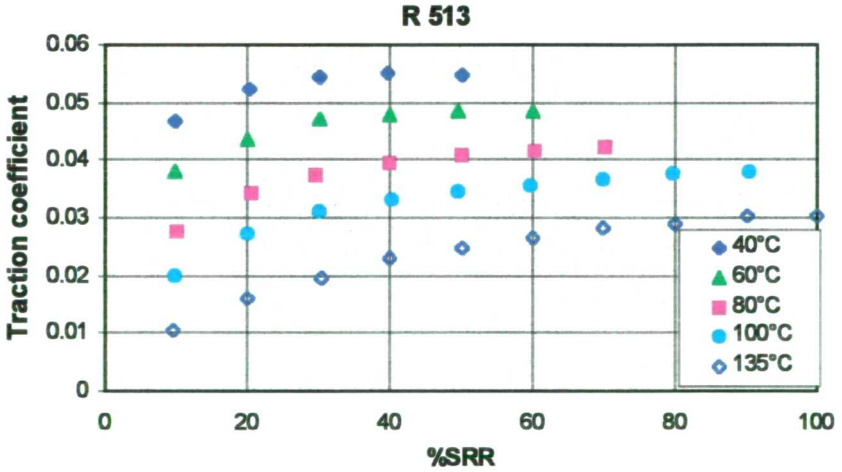

EPV 23-3
1000
100
10
1
Film thickness (nm)
40°C
60°C
80°C
100°C
0.001
0.01
0.1
1
10
Speed (m/s)

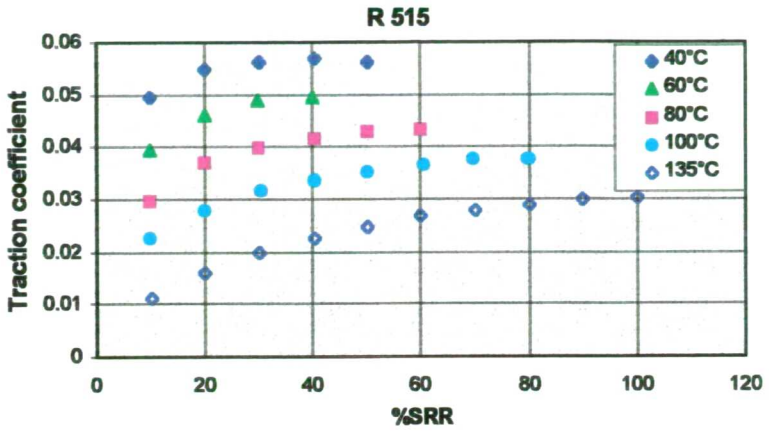

EPV 22D
1000
100
10
1
Film thickness (nm)
40°C
60°C
80°C
100°C
0.001
0.01
0.1
1
10
Speed (m/s)

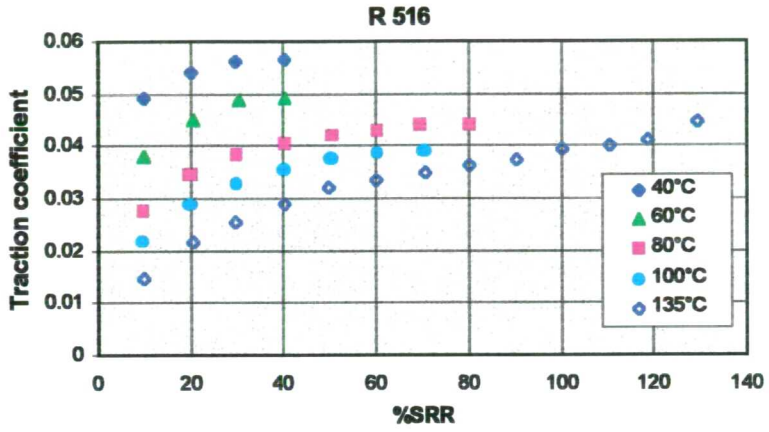
APPENDIX B

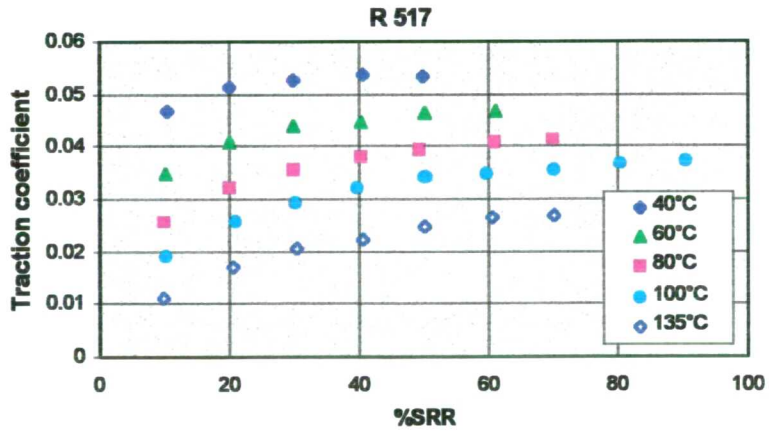
EHD traction coefficients vs slide/roll ratio results

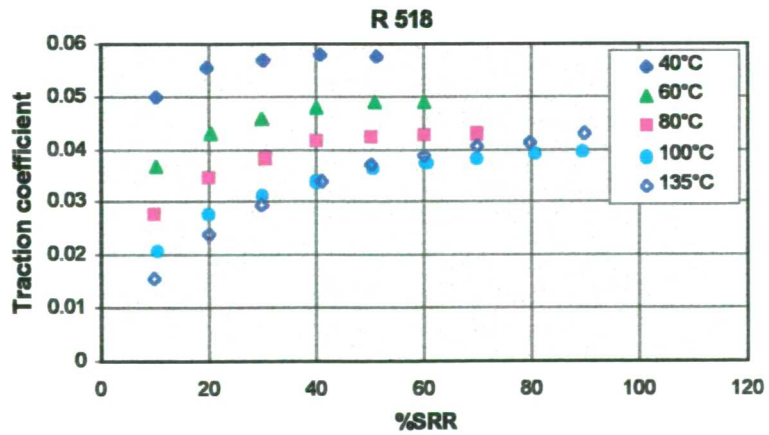


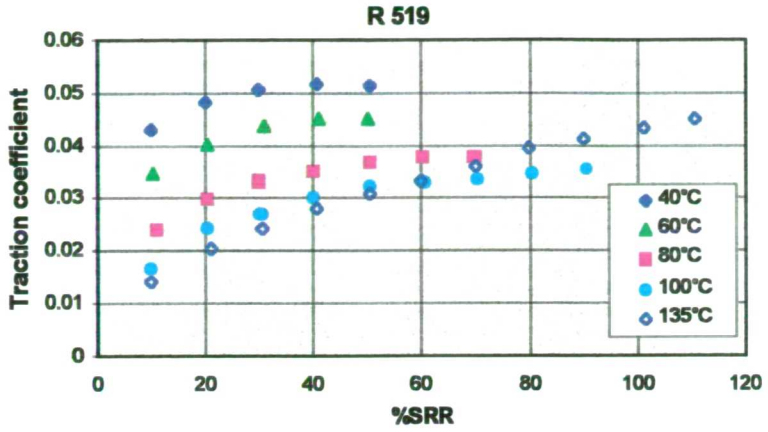


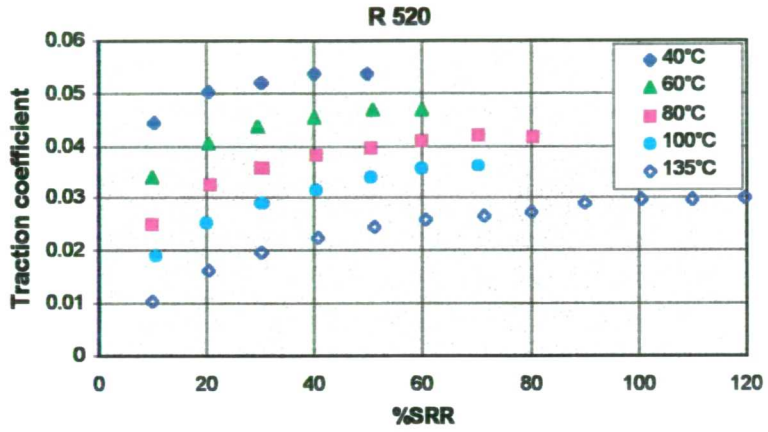

R 515
Traction coefficient
0.06
0.05
0.04
0.03
0.02
0.01
0
0
20
40
60
80
100
120
%SRR
40°C
60°C
80°C
100°C
135°C

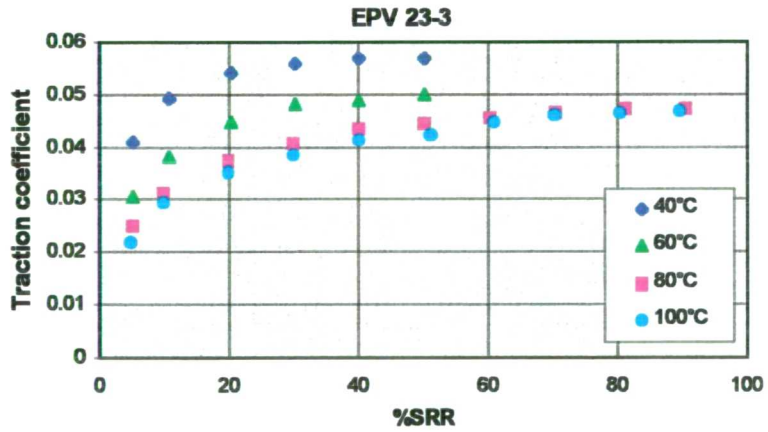

R 516
Traction coefficient
0.06
0.05
0.04
0.03
0.02
0.01
0
0
20
40
60
80
100
120
140
%SRR
40°C
60°C
80°C
100°C
135°C

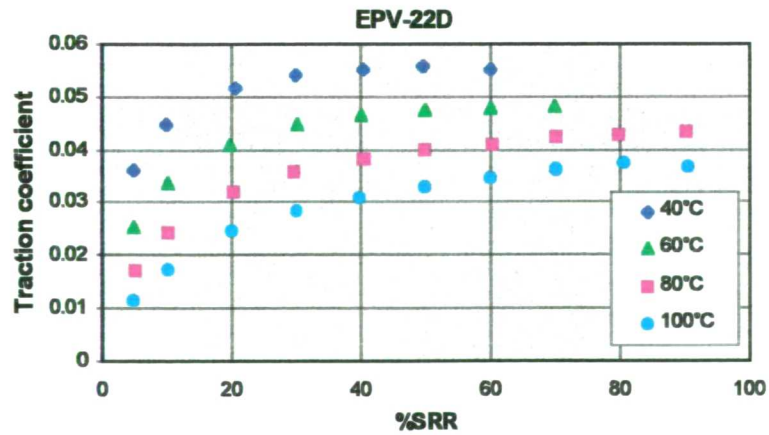

R 517
Traction coefficient
0.06
0.05
0.04
0.03
0.02
0.01
0
0
20
40
60
80
100
%SRR
40°C
60°C
80°C
100°C
135°C


R 518
Traction coefficient
0.06
0.05
0.04
0.03
0.02
0.01
0
0
20
40
60
80
100
120
%SRR
40°C
60°C
80°C
100°C
135°C


R 519
Traction coefficient
0.06
0.05
0.04
0.03
0.02
0.01
0
0
20
40
60
80
100
120
%SRR
40°C
60°C
80°C
100°C
135°C

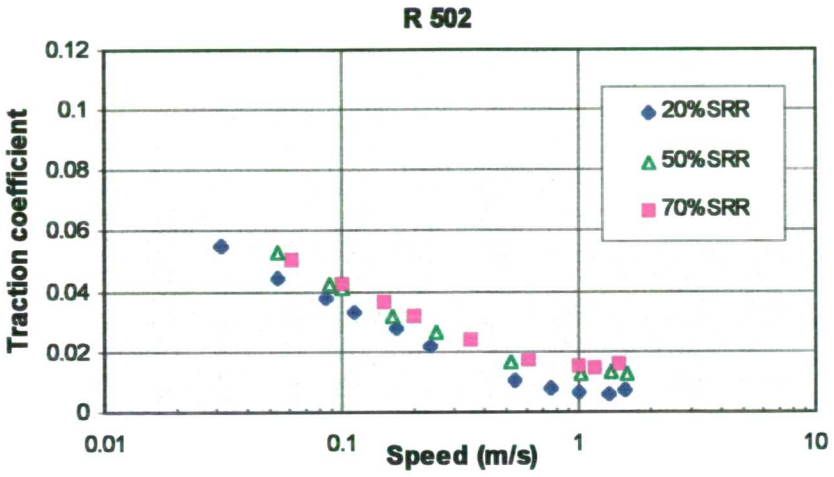

R 520
Traction coefficient
0.06
0.05
0.04
0.03
0.02
0.01
0
0
20
40
60
80
100
120
%SRR
40°C
60°C
80°C
100°C
135°C

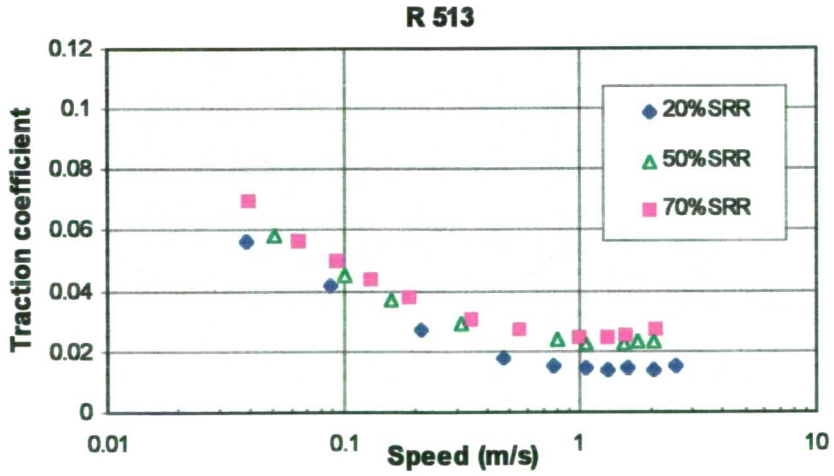

EPV 23-3
Traction coefficient
0.06
0.05
0.04
0.03
0.02
0.01
0
0
20
40
60
80
100
%SRR
40°C
60°C
80°C
100°C

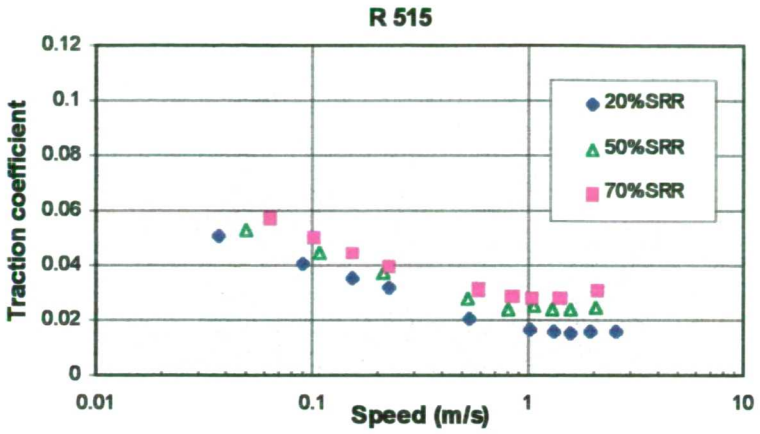

EPV-22D
Traction coefficient
0.06
0.05
0.04
0.03
0.02
0.01
0
0
20
40
60
80
100
%SRR
40°C
60°C
80°C
100°C

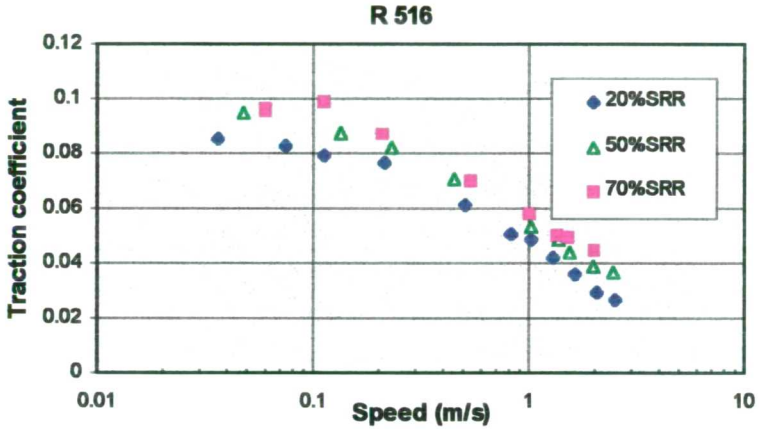
APPENDIX C

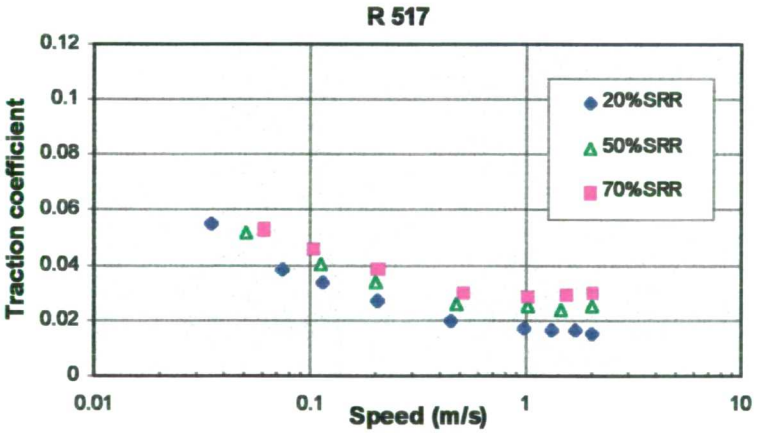
EHD traction coefficient vs entrainment speed results

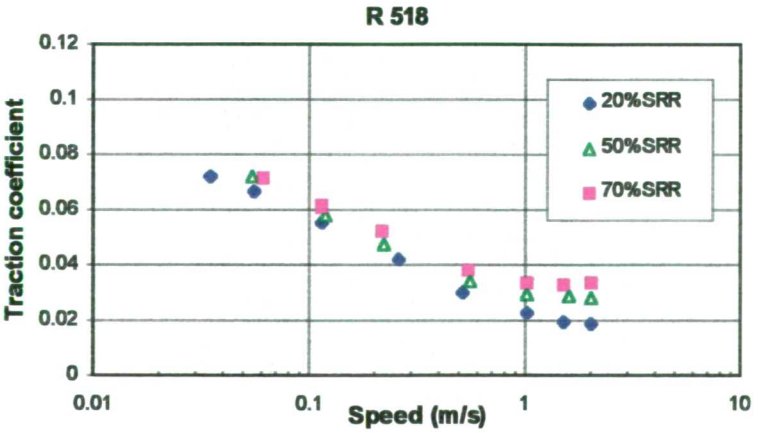


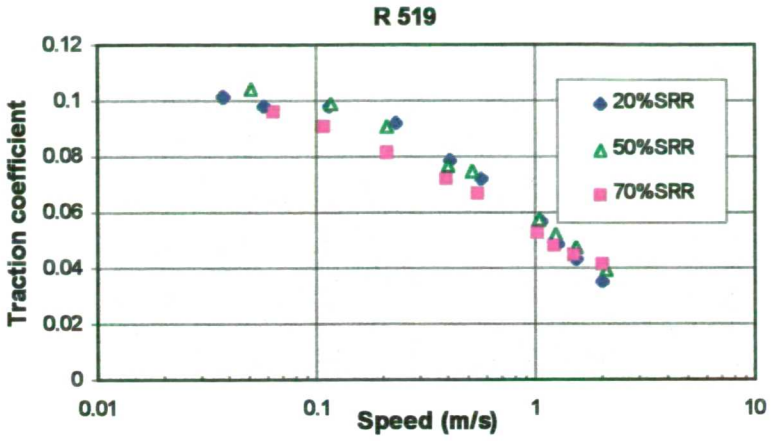


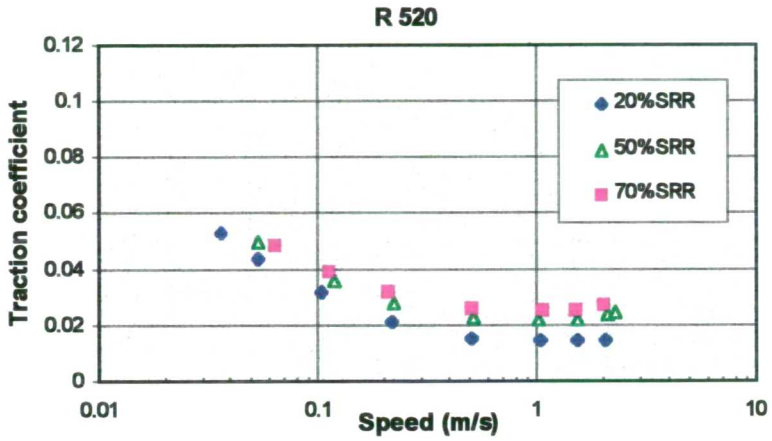

R 515
Traction coefficient
0.12
0.1
0.08
0.06
0.04
0.02
0
0.01
0.1
1
10
Speed (m/s)
20%SRR
50%SRR
70%SRR

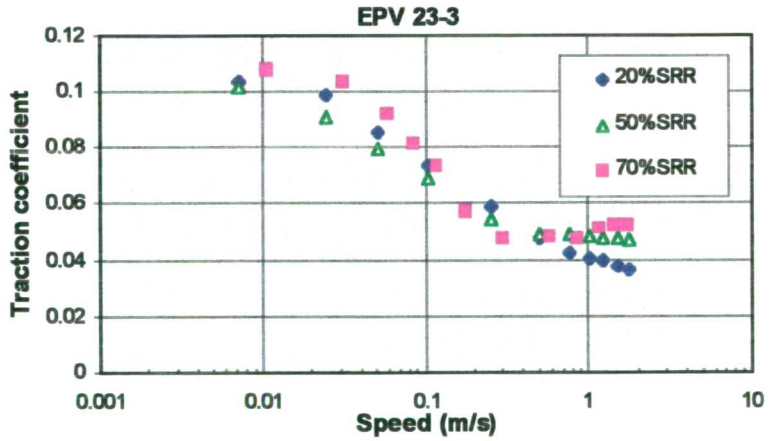

R 516
Traction coefficient
0.12
0.1
0.08
0.06
0.04
0.02
0
0.01
0.1
1
10
Speed (m/s)
20%SRR
50%SRR
70%SRR

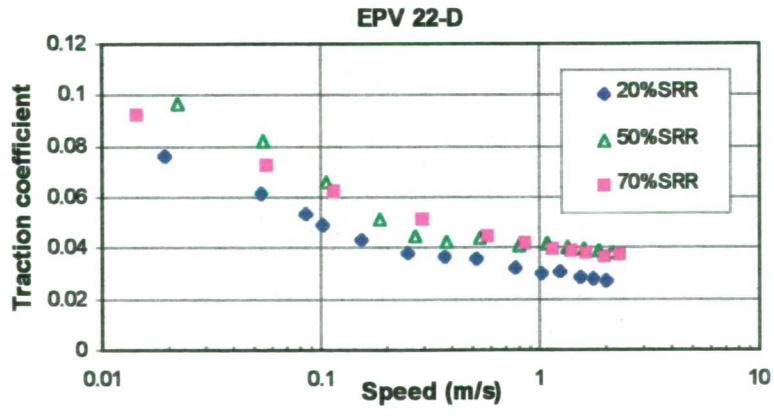

R 517
Traction coefficient
0.12
0.1
0.08
0.06
0.04
0.02
0
0.01
0.1
1
10
Speed (m/s)
20%SRR
50%SRR
70%SRR


R 518
Traction coefficient
0.12
0.1
0.08
0.06
0.04
0.02
0
0.01
0.1
1
10
Speed (m/s)
20%SRR
50%SRR
70%SRR


R 519
Traction coefficient
0.12
0.1
0.08
0.06
0.04
0.02
0
0.01
0.1
1
10
Speed (m/s)
20%SRR
50%SRR
70%SRR


R 520
Traction coefficient
0.12
0.1
0.08
0.06
0.04
0.02
0
0.01
0.1
1
10
Speed (m/s)
20%SRR
50%SRR
70%SRR


EPV 23-3
Traction coefficient
0.12
0.1
0.08
0.06
0.04
0.02
0
0.001
0.01
0.1
1
10
Speed (m/s)
20%SRR
50%SRR
70%SRR


EPV 22-D
Traction coefficient
0.12
0.1
0.08
0.06
0.04
0.02
0
0.01
0.1
1
10
Speed (m/s)
20%SRR
50%SRR
70%SRR

APPENDIX D

FORTRAN77 Program for regression fitting

```
C       REGRESS    15/7/95
C
C     Fits:
C           y = a0 + a1*x1^p1 + a2*x2^p2 + a3*x3^p3 + ...
C
C     where y is a fuel economy measure
C         x1,x2,x3 are lubricant parameters
C         a0,a1,a2,a3 are constants
C         p1,p2,p3 are constant indices
C
C     NSIZE         = number of lubricant parameters to be fitted
C     IX(1 to NSIZE)  = column of the data file they are
C     IY            = column the fuel efficiency data is in
C     RLIM          = regression coeff. above which data is printed out
C     P1, P2, P3    = indices of fitted equations
C     STPOW         = increment by which P1, P2, P3 are raised
C     NPROPLO       = start column number of property data in input file
C     NPROPHI       = end column number of property data in input file
C     NFELO         = start column number of fuelec data in input file
C     NFEHI         = end column number of fuelec data in input file
C
      PROGRAM REGRESS
      PARAMETER (NCOLMX=100,NROWMX=15,NSIZMX=10)
      DOUBLE PRECISION X,A,C
      COMMON /GEN/ NFELO,NFEHI,NPROPLO,NPROPHI,RLIM,P1,P2,P3,STPOW
      COMMON /DATIN/ DATCON(NCOLMX,NROWMX),IX(NSIZMX),IY
      COMMON /DSIZE/ NDATA,NCOLS,NSIZE
      COMMON /CALC/ X(10),A(10,10),C(10)
      COMMON /TIT/ TITLE,DATE,TITCOL(NCOLMX)
      COMMON /DATUSE/ DAT(NSIZMX,NROWMX),FUELEC(NROWMX)
      CHARACTER SIG(10)*1
      CHARACTER TITLE*12,DATE*12,TITCOL*12
      CHARACTER FILEOUT*12
      CHARACTER TIXNOW*12
      DIMENSION DATAV(NROWMX)
C
C Input performance data from data file
C
      CALL DATAIN
C
C Set index data.  Currently just unity (linear regression)
C
      P1=1.
      P2=1.
      P3=1.
      STPOW=1.
C
C Set number of parameters to be fitted at once (1 to 3)
```

```
C
 1  PRINT*,' '
    PRINT*,'ENTER NUMBER OF PARAMETERS TO FIT, 1 to 3'
    READ(*,*)NSIZE
    IF(NSIZE.LT.1.OR.NSIZE.GT.3) GO TO 1
C
C
C Set threshold regression coeff. above which fits are printed out
C
 2  PRINT*,' '
    PRINT*,'ENTER REGRESSION COEFF THRESHOLD PRINT VALUE (0 to 1)'
    READ(*,*)RLIM
C
C create output file
C
    FILEOUT='VALULT311'
    OPEN(2,FILE=FILEOUT,STATUS='NEW')
    WRITE(2,*)TITLE,DATE
    WRITE(2,100)'NSIZE  ',NSIZE
100 FORMAT(A6,I1)
C
C carry out regression fitting, writing results to output file
C
    IF (NSIZE.EQ.1) CALL REG1
    IF (NSIZE.EQ.2) CALL REG2
    IF (NSIZE.EQ.3) CALL REG3
C
C close output file
C
    CLOSE(2)
    STOP
    END
C
C-------------------------------------------------------
C  This routine reads in all the lubricant performance data from
C  an input file whose name is entered by the user into an array DATCON(,)
C
    SUBROUTINE DATAIN
    PARAMETER (NCOLMX=100,NROWMX=15,NSIZMX=10)
    COMMON /DATIN/ DATCON(NCOLMX,NROWMX),IX(NSIZMX),IY
    COMMON /TITIN/ TITROW(2,NROWMX)
    COMMON /DSIZE/ NDATA,NCOLS,NSIZE
    COMMON /TIT/ TITLE,DATE,TITCOL(NCOLMX)
    CHARACTER TITLE*12,DATE*12,TITCOL*12,TITROW*12
    CHARACTER FILEIN*12
C
C Choose and open input file
C
    PRINT*,'ENTER DATAFILE IN'
    READ(*,*)FILEIN
    OPEN(1,FILE=FILEIN,STATUS='OLD')
C
C TITLE = title of input file
C DATE  = date file was created
C NCOLS = Number of columns of property data in file
C NDATA = number of rows of oil data in fileC
C Also read start and end column numbers of property values
C in input file
```

```
C
      READ(1,*)NONE
      WRITE(*,*)NONE
      READ(1,*)TITLE,DATE,NCOLS,NDATA,NPROPLO,NPROPHI
      WRITE(*,*)TITLE,DATE,NCOLS,NDATA,NPROPLO,NPROPHI
      NFELO=NPROPHI+1
      NFEHI=NCOLS
C
C  Now read titles of property column data into TITCOL()
C
      READ(1,*)(TITCOL(JCOL),JCOL=1,NCOLS)
      WRITE(*,*)(TITCOL(JCOL),JCOL=1,NCOLS)
C
C  Now read all data into DATCON(,)
C
       DO 1 IROW=1,NDATA
       READ(1,*)TITROW(1,IROW),TITROW(2,IROW),
     1         (DATCON(JCOL,IROW),JCOL=3,NCOLS)
       WRITE(*,*)TITROW(1,IROW),TITROW(2,IROW),
     1         (DATCON(JCOL,IROW),JCOL=3,NCOLS)
  1    CONTINUE
C
      CLOSE(1)
      RETURN
      END
C
C-------------------------------------------------------
C   This routine fits 1-variable regression equations to all possible
C   combinations of oil properties and fuel economy data
C   Only results with REGR COEFF > RLIM are printed out
C
      SUBROUTINE REG1
      PARAMETER (NCOLMX=100,NROWMX=15,NSIZMX=10)
      DOUBLE PRECISION X,A,C
      COMMON /GEN/ NFELO,NFEHI,NPROPLO,NPROPHI,RLIM,P1,P2,P3,STPOW
      COMMON /DATIN/ DATCON(NCOLMX,NROWMX),IX(NSIZMX),IY
      COMMON /CALC/ X(10),A(10,10),C(10)
      COMMON /TIT/ TITLE,DATE,TITCOL(NCOLMX)
      CHARACTER SIG(10)*1
      DIMENSION DATAV(NROWMX)
C
      DO 40 LL=NFELO,NFEHI
      DO 30 II=NPROPLO,NPROPHI
      IX(1)=II
      IX(2)=JJ
      IY=LL
      A3=1.
      A2=1.
        DO 1 A1=P1,P2,STPOW
          CALL POWER(A1,A2,A3,DATAV)
          CALL COEFFAC
          CALL CHOL
          CALL CALCR(REG)
          CALL SIGN(SIG)
          IF (REG.GT.RLIM) THEN
          WRITE(2,100)(SIG(L+1),TITCOL(IX(L)),L=1,NSIZE),
     #     TITCOL(IY),REG,X(1),(DATAV(L)*X(L+1),L=1,NSIZE)
 100       FORMAT(2(A1,1X,A10,5X),A10,3(5X,F8.4))
```

```
        ENDIF
  1    CONTINUE
 30  CONTINUE
 40  CONTINUE
     RETURN
     END
C
C-------------------------------------------------------
C    This routine fits 2-variable regression equations to all possible
C    combinations of oil properties and fuel economy data
C    Only results with REGR COEFF > RLIM are printed out
C
     SUBROUTINE REG2
     PARAMETER (NCOLMX=100,NROWMX=15,NSIZMX=10)
     DOUBLE PRECISION X,A,C
     COMMON /GEN/ NFELO,NFEHI,NPROPLO,NPROPHI,RLIM,P1,P2,P3,STPOW
     COMMON /DATIN/ DATCON(NCOLMX,NROWMX),IX(NSIZMX),IY
     COMMON /CALC/ X(10),A(10,10),C(10)
     COMMON /TIT/ TITLE,DATE,TITCOL(NCOLMX)
     CHARACTER SIG(10)*1
     DIMENSION DATAV(NROWMX)
C
     DO 40 LL=NFELO,NFEHI
     DO 30 II=NPROPLO,NPROPHI
     DO 20 JJ=II+1,NPROPHI-1
     IX(1)=II
     IX(2)=JJ
     IY=LL
     A3=1.
      DO 2 A2=P1,P2,STPOW
       DO 1 A1=P1,P2,STPOW
        CALL POWER(A1,A2,A3,DATAV)
        CALL COEFFAC
        CALL CHOL
        CALL CALCR(REG)
        CALL SIGN(SIG)
        IF (REG.GT.RLIM) THEN
        WRITE(2,100)(SIG(L+1),TITCOL(IX(L)),L=1,NSIZE),
    #    TITCOL(IY),REG,X(1),(DATAV(L)*X(L+1),L=1,NSIZE)
 100     FORMAT(2(A1,1X,A10,5X),A10,4(5X,F8.4))
        ENDIF
  1    CONTINUE
  2   CONTINUE
 20  CONTINUE
 30  CONTINUE
 40  CONTINUE
     RETURN
     END
C-------------------------------------------------------
C    This routine fits 3-variable regression equations to all possible
C    combinations of oil properties and fuel economy data
C    Only results with REGR COEFF > RLIM are printed out
C
     SUBROUTINE REG3
     PARAMETER (NCOLMX=100,NROWMX=15,NSIZMX=10)
     DOUBLE PRECISION X,A,C
     COMMON /GEN/ NFELO,NFEHI,NPROPLO,NPROPHI,RLIM,P1,P2,P3,STPOW
     COMMON /DATIN/ DATCON(NCOLMX,NROWMX),IX(NSIZMX),IY
```

```
      COMMON /CALC/ X(10),A(10,10),C(10)
      COMMON /TIT/ TITLE,DATE,TITCOL(NCOLMX)
      CHARACTER SIG(10)*1
      DIMENSION DATAV(NROWMX)
C
      DO 40 LL=NFELO,NFEHI
      DO 30 II=NPROPLO,NPROPHI
      DO 20 JJ=II+1,NPROPHI-1
      DO 10 KK=JJ+1,NPROPHI-2
      IX(1)=II
      IX(2)=JJ
      IX(3)=KK
      IY=LL
      DO 3 A3=P1,P2,STPOW
       DO 2 A2=P1,P2,STPOW
        DO 1 A1=P1,P2,STPOW
         CALL POWER(A1,A2,A3,DATAV)
         CALL COEFFAC
         CALL CHOL
         CALL CALCR(REG)
         CALL SIGN(SIG)
         IF (REG.GT.RLIM) THEN
         WRITE(2,100)(SIG(L+1),TITCOL(IX(L)),L=1,NSIZE),
     #    TITCOL(IY),REG,X(1),(DATAV(L)*X(L+1),L=1,NSIZE)
  100     FORMAT(3(A1,1X,A10,5X),A10,5(5X,F8.4))
         ENDIF
    1   CONTINUE
    2  CONTINUE
    3 CONTINUE
   10 CONTINUE
   20 CONTINUE
   30 CONTINUE
   40 CONTINUE
      RETURN
      END
C-------------------------------------------------------
C  This routine selects the required columns of data from DATCON(,)
C  raises them to the required powers
C  then stores them in DAT(,)
C  and puts the required fuel economy column in FUELEC()
C
      SUBROUTINE POWER(A1,A2,A3,DATAV)
      PARAMETER (NCOLMX=100,NROWMX=15,NSIZMX=10)
      COMMON /DATIN/ DATCON(NCOLMX,NROWMX),IX(NSIZMX),IY
      COMMON /DSIZE/ NDATA,NCOLS,NSIZE
      COMMON /DATUSE/ DAT(NSIZMX,NROWMX),FUELEC(NROWMX)
      DIMENSION P(10),DATAV(NROWMX)
      P(1)=A1
      P(2)=A2
      P(3)=A3
       DO 2 IROW=1,NDATA
        DO 1 L=1,NSIZE
         DAT(L,IROW)=DATCON(IX(L),IROW)**P(L)
    1   CONTINUE
      FUELEC(IROW)=DATCON(IY,IROW)
    2 CONTINUE
      DO 4 L=1,NSIZE
       SUM=0.0
```

```
      DO 3 IROW=1,NDATA
       SUM=SUM+DAT(L,IROW)
 3     CONTINUE
       DATAV(L)=SUM/NDATA
 4    CONTINUE
     RETURN
     END
C
C-------------------------------------------------
C  This routine calculates matrix values needed for solving the
C  regression fit equations
C
     SUBROUTINE COEFFAC
     PARAMETER (NCOLMX=100,NROWMX=15,NSIZMX=10)
     DOUBLE PRECISION X,A,C
     COMMON /DSIZE/ NDATA,NCOLS,NSIZE
     COMMON /DATUSE/ DAT(NSIZMX,NROWMX),FUELEC(NROWMX)
     COMMON /CALC/ X(10),A(10,10),C(10)
      DO 2 J=1,NSIZE+1
       DO 1 I=1,NSIZE+1
       A(I,J)=0.
 1     CONTINUE
      C(J)=0.
 2    CONTINUE
C
      DO 5 M=1,NDATA
       DO 4 J=1,NSIZE+1
       IF (J.EQ.1) THEN
         COL=1.
              ELSE
         COL=DAT(J-1,M)
       ENDIF
        DO 3 I=1,NSIZE+1
        IF (I.EQ.1) THEN
          ROW=1.
               ELSE
          ROW=DAT(I-1,M)
        ENDIF
        A(I,J)=A(I,J)+ROW*COL
 3      CONTINUE
        C(J)=C(J)+FUELEC(M)*COL
 4     CONTINUE
 5    CONTINUE
     RETURN
     END
C
C -------------------------------------------------
C  This routine solves the regression fit matrix by Cholesky's method
C
     SUBROUTINE CHOL
     DOUBLE PRECISION X,A,C
     COMMON /DSIZE/ NDATA,NCOLS,NSIZE
     COMMON /CALC/ X(10),A(10,10),C(10)
C
     PRINT*,'THE COMPUTER IS CALCULATING PERCENT FUEL ECONOMY'
      NT=NSIZE+1
       DO 40  I=1,NT
       A(I,NT+1)=C(I)
```

```
 40   CONTINUE
      DO 70  K=1,NT
      PIVOT=A(K,K)
      IL=K
       DO 50 L=K+1,NT
       IF(ABS(A(L,K)).LT.ABS(PIVOT)) GOTO 50
       PIVOT=A(L,K)
       IL=L
 50     CONTINUE
      IF (IL.EQ.K)  GOTO 70
       DO 60 LL=1,NT+1
       TER=A(K,LL)
       A(K,LL)=A(IL,LL)
       A(IL,LL)=TER
 60     CONTINUE
 70   CONTINUE
      DO 80 J=2,NT+1
      A(1,J)=A(1,J)/A(1,1)
 80   CONTINUE

      DO 90  L=2,NT
       DO 100  I=L,NT
       S1=0.
        DO 110 K=1,L-1
        S1=S1+A(I,K)*A(K,L)
 110      CONTINUE
       A(I,L)=A(I,L)-S1
 100    CONTINUE
       DO 120 J=L+1,NT+1
       S1=0.
        DO 130 K=1,L-1
        S1=S1+A(L,K)*A(K,J)
 130      CONTINUE
       A(L,J)=(A(L,J)-S1)/A(L,L)
 120    CONTINUE
 90   CONTINUE
     X(NT)=A(NT,NT+1)
      DO 210 M=1,NT-1
      I=NT-M
      S1=0.
       DO 200 J=I+1,NT
       S1=S1+A(I,J)*X(J)
 200    CONTINUE
      X(I)=A(I,NT+1)-S1
 210  CONTINUE

     RETURN
     END
C
C-------------------------------------------------------
C  This routine calculates the regression coefficient from the
C  fitted equation and the Actual data
C
     SUBROUTINE CALCR(REG)
     PARAMETER (NCOLMX=100,NROWMX=15,NSIZMX=10)
     DOUBLE PRECISION X,A,C
     COMMON /DSIZE/ NDATA,NCOLS,NSIZE
     COMMON /DATUSE/ DAT(NSIZMX,NROWMX),FUELEC(NROWMX)
```

```
      COMMON /CALC/ X(10),A(10,10),C(10)
      SR=0.
      SFUEL=0.
       DO 1 I=1,NDATA
       FUELPR=X(1)
        DO 2 J=2,NSIZE+1
        FUELPR=FUELPR+X(J)*DAT(J-1,I)
 2      CONTINUE
       DIFF=FUELEC(I)-FUELPR
       SR=SR+DIFF*DIFF
       SFUEL=SFUEL+FUELEC(I)
 1     CONTINUE
      ST=0.
      AMEAN=SFUEL/NDATA
       DO 3 J=1,NDATA
       DELTA=FUELEC(J)-AMEAN
       ST=ST+DELTA*DELTA
 3     CONTINUE
      REG=(ST-SR)/ST
      RETURN
      END
C
C-------------------------------------------------------
C  This routine determines the coefficient signs as + or - for output
C
      SUBROUTINE SIGN(SIG)
      PARAMETER (NCOLMX=100,NROWMX=15,NSIZMX=10)
      DOUBLE PRECISION X,A,C
      COMMON /DSIZE/ NDATA,NCOLS,NSIZE
      COMMON /CALC/ X(10),A(10,10),C(10)
      CHARACTER SIG(10)*1
C
      DO 1 I=2,NSIZE+1
      IF (X(I).GE.0.0) THEN
        SIG(I)='+'
              ELSE
        SIG(I)='-'
      ENDIF
 1    CONTINUE
      RETURN
      END
```

APPENDIX E

Single parameter correlations with R150 and R275 test stages

a) R150 stage

Sequence VI stage		Parameter, X	R^2	a_0	a_1
R150	-	EHD40	0.515	7.174	-4.223
R150	-	EHD60	0.373	6.937	-3.986
R150	-	EHD80	0.291	7.840	-4.889
R150	-	EHD100	0.139	10.471	-7.520
R150	-	HSVisc60	0.174	5.548	-2.597
R150	-	HSVisc80	0.094	5.101	-2.150
R150	-	HTHS100	0.366	7.167	-4.216
R150	-	HTHS150	0.291	7.077	-4.126
R150	-	KVisc40	0.503	5.671	-2.720
R150	-	KVisc60	0.490	5.938	-2.987
R150	-	KVisc80	0.475	6.174	-3.223
R150	-	KVisc100	0.459	6.384	-3.433
R150	-	KVisc120	0.443	6.563	-3.612
R150	-	KVisc150	0.435	6.951	-4.000
R150	-	TracC40	0.004	3.629	-0.678
R150	-	TracC60	0.013	4.021	-1.070
R150	+	TracC80	0.003	2.515	0.436
R150	+	TracC100	0.024	1.917	1.035
R150	-	µ40	0.496	10.517	-7.566
R150	-	µ60	0.670	9.604	-6.653
R150	-	µ80	0.641	8.327	-5.376
R150	-	µ100	0.635	7.322	-4.371
R150	-	µ120	0.672	7.934	-4.983
R150	-	µ140	0.544	8.499	-5.548
R150	+	HTHSK60	0.412	-1.218	4.169
R150	+	HTHSK80	0.486	-1.691	4.642
R150	+	HTHSK100	0.180	-0.791	3.742
R150	+	HTHSK150	0.270	-4.079	7.030
R150	+	Trac20SR	0.032	2.677	0.274
R150	+	Trac50SR	0.017	2.711	0.240
R150	+	Trac70SR	0.024	2.629	0.323
R150	+	07FilmKv40	0.191	0.497	2.454
R150	-	07FilmKv60	0.027	4.414	-1.463
R150	-	07FilmKv80	0.069	4.294	-1.343
R150	-	07FilmKv100	0.029	3.671	-0.720
R150	-	20Tr01Tr1	0.001	2.993	-0.042
R150	-	50Tr01Tr1	0.001	2.990	-0.039
R150	+	70Tr01Tr1	0.001	2.904	0.047
R150	-	K40K100	0.355	9.889	-6.938

b) R275 stage

Sequence VI stage		Parameter, X	R^2	a_0	a_1
R275	-	EHD40	0.093	12.893	-5.413
R275	-	EHD60	0.033	11.043	-3.563
R275	-	EHD80	0.103	16.613	-9.133
R275	-	EHD100	0.163	32.543	-25.063
R275	-	HSVisc60	0.003	8.373	-0.893
R275	+	HSVisc80	0.003	6.893	0.593
R275	-	HTHS100	0.053	12.233	-4.753
R275	-	HTHS150	0.033	11.923	-4.443
R275	-	KVisc40	0.153	12.203	-4.723
R275	-	KVisc60	0.153	12.573	-5.093
R275	-	KVisc80	0.143	12.893	-5.413
R275	-	KVisc100	0.133	13.183	-5.703
R275	-	KVisc120	0.123	13.433	-5.943
R275	-	KVisc150	0.123	14.083	-6.603
R275	+	TracC40	0.013	3.633	3.853
R275	+	TracC60	0.013	4.753	2.733
R275	+	TracC80	0.043	2.163	5.323
R275	+	TracC100	0.063	2.403	5.083
R275	-	μ40	0.503	31.223	-23.743
R275	-	μ60	0.653	28.063	-20.573
R275	-	μ80	0.693	24.923	-17.443
R275	-	μ100	0.763	22.473	-14.993
R275	-	μ120	0.703	23.383	-15.893
R275	-	μ140	0.633	26.203	-18.713
R275	+	HTHSK60	0.273	-3.143	10.623
R275	+	HTHSK80	0.303	-3.913	11.393
R275	+	HTHSK100	0.103	-1.453	8.933
R275	+	HTHSK150	0.203	-11.593	19.083
R275	-	Trac20SR	0.113	9.093	-1.613
R275	-	Trac50SR	0.143	9.693	-2.213
R275	-	Trac70SR	0.113	9.693	-2.213
R275	+	07FilmKv40	0.233	-0.953	8.433
R275	-	07FilmKv60	0.013	9.743	-2.263
R275	-	07FilmKv80	0.033	10.453	-2.973
R275	-	07FilmKv100	0.033	9.723	-2.243
R275	+	20Tr01Tr1	0.003	7.453	0.033
R275	-	50Tr01Tr1	0.003	7.733	-0.253
R275	-	70Tr01Tr1	0.023	8.343	-0.863
R275	-	K40K100	0.123	20.293	-12.813

APPENDIX F

Three parameter correlations with R150

		Param 1		Param 2		Param 3	R^2	a_0	a_1	a_2	a_3
R150	-	EHD40	-	EHD60	-	μ120	0.906	10.292	-1.599	-1.537	-4.205
R150	-	EHD40	-	EHD80	-	μ60	0.908	12.687	-1.557	-2.565	-5.613
R150	-	EHD40	-	EHD80	-	μ80	0.891	11.432	-1.947	-2.1	-4.434
R150	-	EHD40	-	EHD80	-	μ120	0.907	10.476	-2.523	-0.993	-4.009
R150	-	EHD40	+	EHD100	-	μ100	0.883	6.05	-3.769	4.111	-3.44
R150	-	EHD40	+	EHD100	-	μ120	0.92	6.918	-3.707	3.722	-3.983
R150	-	EHD40	+	EHD100	-	μ140	0.894	7.837	-4.224	3.948	-4.61
R150	-	EHD40	+	HSVisc60	-	HTHS100	0.906	8.888	-4.269	12.123	-13.791
R150	-	EHD40	-	HSVisc60	-	μ120	0.903	10.122	-2.689	-0.422	-4.06
R150	-	EHD40	+	HSVisc80	-	HTHS100	0.881	6.76	-2.072	11.124	-12.862
R150	-	EHD40	-	HSVisc80	-	μ120	0.903	10.18	-2.784	-0.391	-4.055
R150	-	EHD40	-	HTHS100	-	μ60	0.891	11.54	-2.097	-1.358	-5.134
R150	-	EHD40	-	HTHS100	-	μ80	0.888	10.724	-2.205	-1.398	-4.17
R150	-	EHD40	-	HTHS100	-	μ100	0.886	10.005	-2.155	-1.5	-3.399
R150	-	EHD40	-	HTHS100	-	μ120	0.909	10.234	-2.545	-0.832	-3.905
R150	-	EHD40	-	HTHS150	-	μ100	0.881	10.102	-2.418	-1.347	-3.387
R150	-	EHD40	-	HTHS150	-	μ120	0.911	10.409	-2.605	-0.94	-3.913
R150	-	EHD40	-	KVisc40	-	μ60	0.883	10.7	-2.299	-0.641	-4.808
R150	-	EHD40	-	KVisc40	-	μ80	0.888	9.903	-2.266	-0.807	-3.88
R150	-	EHD40	-	KVisc40	-	μ100	0.89	9.184	-2.18	-0.905	-3.149
R150	-	EHD40	-	KVisc40	-	μ120	0.921	9.729	-2.33	-0.748	-3.701
R150	-	EHD40	-	KVisc40	-	μ140	0.884	10.743	-2.953	-0.563	-4.277
R150	-	EHD40	-	KVisc60	-	μ60	0.88	10.791	-2.405	-0.624	-4.811
R150	-	EHD40	-	KVisc60	-	μ80	0.885	10.012	-2.369	-0.827	-3.865
R150	-	EHD40	-	KVisc60	-	μ100	0.89	9.316	-2.253	-0.978	-3.134
R150	-	EHD40	-	KVisc60	-	μ120	0.923	9.841	-2.366	-0.837	-3.687
R150	-	EHD40	-	KVisc60	-	μ140	0.886	10.817	-2.955	-0.661	-4.25
R150	-	EHD40	-	KVisc80	-	μ80	0.883	10.103	-2.453	-0.836	-3.863
R150	-	EHD40	-	KVisc80	-	μ100	0.889	9.434	-2.319	-1.037	-3.127
R150	-	EHD40	-	KVisc80	-	μ120	0.923	9.948	-2.405	-0.912	-3.681
R150	-	EHD40	-	KVisc80	-	μ140	0.887	10.9	-2.967	-0.746	-4.237
R150	-	EHD40	-	KVisc100	-	μ80	0.881	10.178	-2.52	-0.839	-3.867
R150	-	EHD40	-	KVisc100	-	μ100	0.889	9.538	-2.376	-1.086	-3.125
R150	-	EHD40	-	KVisc100	-	μ120	0.924	10.047	-2.439	-0.978	-3.679
R150	-	EHD40	-	KVisc100	-	μ140	0.889	10.985	-2.982	-0.822	-4.23
R150	-	EHD40	-	KVisc120	-	μ100	0.888	9.628	-2.427	-1.124	-3.126
R150	-	EHD40	-	KVisc120	-	μ120	0.924	10.137	-2.473	-1.033	-3.681
R150	-	EHD40	-	KVisc120	-	μ140	0.889	11.066	-3.001	-0.886	-4.228
R150	-	EHD40	-	KVisc150	-	μ100	0.889	9.788	-2.469	-1.265	-3.103
R150	-	EHD40	-	KVisc150	-	μ120	0.925	10.282	-2.511	-1.163	-3.657
R150	-	EHD40	-	KVisc150	-	μ140	0.891	11.189	-3.022	-1.02	-4.197
R150	-	EHD40	+	TracC40	-	μ60	0.906	9.195	-3.285	2.19	-5.149
R150	-	EHD40	-	TracC40	-	μ120	0.907	10.929	-2.683	-1.036	-4.259
R150	-	EHD40	-	TracC40	-	μ140	0.885	12.574	-3.077	-1.442	-5.105

		Param 1		Param 2		Param 3	R^2	a_0	a_1	a_2	a_3
R150	-	EHD40	+	TracC40	+	HTHSK60	0.933	-3.688	-4.136	6.066	4.709
R150	-	EHD40	+	TracC40	+	HTHSK80	0.951	-4.943	-3.654	6.346	5.202
R150	-	EHD40	+	TracC40	+	HTHSK100	0.898	-8.688	-4.871	9.036	7.474
R150	-	EHD40	+	TracC60	-	µ60	0.903	9.46	-3.392	1.968	-5.085
R150	-	EHD40	-	TracC60	-	µ120	0.906	10.757	-2.65	-0.907	-4.25
R150	-	EHD40	-	TracC60	-	µ140	0.884	12.432	-2.997	-1.356	-5.128
R150	-	EHD40	+	TracC60	+	HTHSK60	0.915	-2.353	-4.425	5.301	4.427
R150	-	EHD40	+	TracC60	+	HTHSK80	0.936	-3.608	-3.988	5.617	4.931
R150	-	EHD40	+	TracC80	-	µ60	0.899	9.402	-3.337	1.681	-4.795
R150	-	EHD40	-	TracC80	-	µ120	0.903	10.438	-2.795	-0.5	-4.192
R150	-	EHD40	+	TracC80	+	HTHSK60	0.902	-0.784	-4.175	4.178	3.733
R150	-	EHD40	+	TracC80	+	HTHSK80	0.915	-1.652	-3.791	4.306	4.088
R150	-	EHD40	+	TracC100	-	µ60	0.888	9.921	-3.074	0.975	-4.871
R150	-	EHD40	-	TracC100	-	µ120	0.905	10.52	-2.813	-0.501	-4.255
R150	-	EHD40	-	TracC100	-	µ140	0.882	12.215	-3.215	-0.847	-5.202
R150	-	EHD40	+	µ40	-	µ60	0.913	8.849	-2.705	7.436	-10.629
R150	-	EHD40	-	µ40	-	µ120	0.908	10.638	-2.904	-1.317	-3.466
R150	-	EHD40	-	µ40	-	µ140	0.898	12.096	-3.2	-2.312	-3.633
R150	-	EHD40	-	µ60	-	µ120	0.914	10.513	-2.835	-2.012	-2.715
R150	-	EHD40	-	µ60	-	µ140	0.918	11.505	-3.001	-2.897	-2.657
R150	-	EHD40	-	µ60	-	HTHSK100	0.884	13.193	-2.829	-6.016	-1.396
R150	-	EHD40	-	µ60	-	HTHSK150	0.88	14.33	-2.713	-6.343	-2.323
R150	-	EHD40	-	µ60	+	Trac20SR	0.89	10.746	-2.42	-5.619	0.245
R150	-	EHD40	-	µ60	+	Trac50SR	0.889	10.768	-2.52	-5.58	0.284
R150	-	EHD40	-	µ60	+	Trac70SR	0.891	10.693	-2.507	-5.568	0.333
R150	-	EHD40	-	µ60	+	07FilmKv60	0.906	9.792	-2.925	-5.792	1.877
R150	-	EHD40	-	µ60	+	07FilmKv80	0.888	10.754	-2.999	-5.573	0.77
R150	-	EHD40	-	µ60	+	07FilmKv100	0.882	10.781	-2.929	-5.416	0.514
R150	-	EHD40	-	µ60	-	20Tr01Tr1	0.9	11.468	-2.962	-5.301	-0.254
R150	-	EHD40	-	µ60	-	50Tr01Tr1	0.882	11.237	-2.909	-5.207	-0.171
R150	-	EHD40	-	µ80	-	µ120	0.904	10.052	-2.935	-0.993	-3.174
R150	-	EHD40	-	µ80	-	µ140	0.9	10.898	-3.133	-2.156	-2.657
R150	-	EHD40	-	µ80	+	07FilmKv60	0.908	8.76	-3.072	-4.782	2.046
R150	-	EHD40	-	µ80	+	07FilmKv80	0.897	9.808	-3.179	-4.716	1.038
R150	-	EHD40	-	µ80	+	07FilmKv100	0.891	9.86	-3.088	-4.555	0.734
R150	-	EHD40	+	µ100	-	µ120	0.902	9.971	-2.997	0.574	-4.597
R150	-	EHD40	-	µ100	-	µ140	0.889	10.488	-3.183	-1.574	-2.78
R150	-	EHD40	-	µ100	+	07FilmKv40	0.88	8.121	-3.068	-3.003	0.901
R150	-	EHD40	-	µ100	+	07FilmKv60	0.901	7.912	-3.084	-3.864	1.986
R150	-	EHD40	-	µ100	+	07FilmKv80	0.915	8.863	-3.227	-4.087	1.401
R150	-	EHD40	-	µ100	+	07FilmKv100	0.916	8.943	-3.108	-4.008	1.124
R150	-	EHD40	-	µ120	+	µ140	0.901	9.82	-2.946	-4.279	0.356
R150	-	EHD40	-	µ120	+	HTHSK60	0.923	8.039	-2.824	-3.433	1.169
R150	-	EHD40	-	µ120	+	HTHSK80	0.923	7.801	-2.7	-3.422	1.272
R150	-	EHD40	-	µ120	+	HTHSK100	0.917	8.4	-2.843	-3.807	1.201
R150	-	EHD40	-	µ120	+	HTHSK150	0.92	7.371	-2.933	-3.575	2.088
R150	-	EHD40	-	µ120	+	Trac20SR	0.901	9.863	-2.938	-4.003	0.029
R150	-	EHD40	-	µ120	+	Trac50SR	0.901	9.857	-2.943	-4.004	0.041
R150	-	EHD40	-	µ120	+	Trac70SR	0.901	9.885	-2.962	-3.994	0.022
R150	-	EHD40	-	µ120	+	07FilmKv40	0.916	8.798	-3.054	-3.581	0.789
R150	-	EHD40	-	µ120	+	07FilmKv60	0.924	8.851	-3.094	-4.25	1.445
R150	-	EHD40	-	µ120	+	07FilmKv80	0.954	9.498	-3.251	-4.651	1.355
R150	-	EHD40	-	µ120	+	07FilmKv100	0.96	9.565	-3.136	-4.625	1.147
R150	-	EHD40	-	µ120	-	20Tr01Tr1	0.901	9.938	-2.994	-3.974	-0.019

		Param 1		Param 2		Param 3	R^2	a_0	a_1	a_2	a_3
R150	-	EHD40	-	µ120	-	50Tr01Tr1	0.901	9.921	-2.979	-3.989	-0.003
R150	-	EHD40	-	µ140	+	HTHSK60	0.908	8.548	-3.176	-3.856	1.436
R150	-	EHD40	-	µ140	+	HTHSK80	0.918	8.067	-2.973	-3.845	1.702
R150	-	EHD40	-	µ140	+	HTHSK100	0.898	9.139	-3.258	-4.389	1.459
R150	-	EHD40	-	µ140	+	HTHSK150	0.907	7.569	-3.317	-4.05	2.749
R150	-	EHD40	-	µ140	+	07FilmKv40	0.886	9.797	-3.489	-4.105	0.747
R150	-	EHD40	-	µ140	+	07FilmKv80	0.905	10.777	-3.732	-5.125	1.031
R150	-	EHD40	-	µ140	+	07FilmKv100	0.921	10.838	-3.664	-5.246	1.023
R150	-	EHD40	+	HTHSK60	-	HTHSK100	0.935	6.593	-2.862	12.253	-13.033
R150	-	EHD40	+	HTHSK60	-	20Tr01Tr1	0.883	2.363	-3.363	4.632	-0.681
R150	-	EHD40	+	HTHSK80	-	HTHSK100	0.887	4.304	-1.957	10.939	-10.335
R150	-	EHD60	-	EHD80	-	µ60	0.891	13.045	-1.244	-2.833	-6.018
R150	-	EHD60	-	EHD80	-	µ120	0.9	10.714	-2.994	-0.305	-4.464
R150	-	EHD60	+	EHD100	-	µ120	0.911	8.432	-3.713	2.799	-4.567
R150	-	EHD60	-	HSVisc60	-	µ120	0.9	10.605	-3.125	-0.048	-4.481
R150	-	EHD60	-	HSVisc80	-	µ120	0.9	10.624	-3.126	-0.063	-4.484
R150	-	EHD60	+	HSVisc80	-	µ140	0.883	11.544	-4.342	1.087	-5.339
R150	-	EHD60	-	HTHS100	-	µ120	0.901	10.672	-2.901	-0.415	-4.406
R150	-	EHD60	-	HTHS150	-	µ120	0.904	10.825	-2.862	-0.62	-4.393
R150	-	EHD60	-	KVisc40	-	µ100	0.885	9.632	-2.305	-0.863	-3.513
R150	-	EHD60	-	KVisc40	-	µ120	0.916	10.25	-2.489	-0.693	-4.117
R150	-	EHD60	-	KVisc60	-	µ100	0.886	9.776	-2.383	-0.933	-3.509
R150	-	EHD60	-	KVisc60	-	µ120	0.918	10.362	-2.522	-0.784	-4.105
R150	-	EHD60	-	KVisc80	-	µ100	0.885	9.905	-2.454	-0.987	-3.513
R150	-	EHD60	-	KVisc80	-	µ120	0.919	10.472	-2.559	-0.859	-4.102
R150	-	EHD60	-	KVisc100	-	µ100	0.885	10.017	-2.514	-1.033	-3.519
R150	-	EHD60	-	KVisc100	-	µ120	0.92	10.575	-2.594	-0.927	-4.103
R150	-	EHD60	-	KVisc120	-	µ100	0.884	10.116	-2.568	-1.07	-3.527
R150	-	EHD60	-	KVisc120	-	µ120	0.92	10.671	-2.628	-0.985	-4.108
R150	-	EHD60	-	KVisc120	-	µ140	0.881	11.876	-3.247	-0.803	-4.875
R150	-	EHD60	-	KVisc150	-	µ100	0.885	10.276	-2.611	-1.202	-3.512
R150	-	EHD60	-	KVisc150	-	µ120	0.921	10.816	-2.667	-1.107	-4.092
R150	-	EHD60	-	KVisc150	-	µ140	0.882	11.993	-3.265	-0.927	-4.85
R150	-	EHD60	+	TracC40	-	µ60	0.882	10.181	-3.252	1.865	-5.844
R150	-	EHD60	-	TracC40	-	µ120	0.917	12.112	-2.784	-1.579	-4.798
R150	-	EHD60	-	TracC40	-	µ140	0.899	14.304	-3.243	-2.18	-5.929
R150	-	EHD60	+	TracC40	+	HTHSK60	0.885	-4.318	-4.205	6.134	5.339
R150	-	EHD60	+	TracC40	+	HTHSK80	0.913	-5.698	-3.644	6.457	5.836
R150	-	EHD60	+	TracC60	-	µ60	0.881	10.414	-3.376	1.716	-5.803
R150	-	EHD60	-	TracC60	-	µ120	0.913	11.772	-2.727	-1.327	-4.767
R150	-	EHD60	-	TracC60	-	µ140	0.895	13.918	-3.128	-1.934	-5.905
R150	-	EHD60	+	TracC60	+	HTHSK80	0.903	-4.434	-4.075	5.828	5.632
R150	-	EHD60	-	TracC80	-	µ120	0.912	11.796	-2.821	-1.166	-4.859
R150	-	EHD60	-	TracC80	-	µ140	0.886	13.686	-3.344	-1.462	-5.929
R150	-	EHD60	-	TracC100	-	µ120	0.913	11.673	-2.94	-0.895	-4.887
R150	-	EHD60	-	TracC100	-	µ140	0.897	14.007	-3.437	-1.415	-6.204
R150	-	EHD60	+	µ40	-	µ60	0.901	9.403	-2.773	7.719	-11.399
R150	-	EHD60	-	µ40	-	µ120	0.908	11.402	-3.09	-1.495	-3.866
R150	-	EHD60	-	µ40	-	µ140	0.9	13.145	-3.454	-2.593	-4.147
R150	-	EHD60	-	µ60	-	µ120	0.914	11.18	-3.014	-2.084	-3.132
R150	-	EHD60	-	µ60	-	µ140	0.921	12.399	-3.24	-3.088	-3.12
R150	-	EHD60	-	µ60	+	Trac20SR	0.889	11.29	-2.463	-6.18	0.304
R150	-	EHD60	-	µ60	+	Trac50SR	0.887	11.343	-2.585	-6.16	0.353
R150	-	EHD60	-	µ60	+	Trac70SR	0.889	11.254	-2.577	-6.136	0.41

		Param 1		Param 2		Param 3	R^2	a_0	a_1	a_2	a_3
R150	-	EHD60	-	μ60	-	20Tr01Tr1	0.884	12.135	-3.016	-5.922	-0.247
R150	-	EHD60	-	μ80	-	μ120	0.902	10.692	-3.119	-0.839	-3.783
R150	-	EHD60	-	μ80	-	μ140	0.897	11.765	-3.369	-2.22	-3.225
R150	-	EHD60	+	μ100	-	μ120	0.9	10.595	-3.164	0.037	-4.518
R150	-	EHD60	-	μ100	-	μ140	0.893	11.29	-3.419	-1.922	-2.998
R150	-	EHD60	-	μ100	+	Trac20SR	0.892	9.539	-2.755	-4.131	0.298
R150	-	EHD60	-	μ100	+	Trac50SR	0.892	9.593	-2.867	-4.127	0.352
R150	-	EHD60	-	μ100	+	Trac70SR	0.887	9.545	-2.897	-4.059	0.362
R150	-	EHD60	-	μ120	+	μ140	0.9	10.578	-3.159	-4.515	0.046
R150	-	EHD60	-	μ120	+	HTHSK60	0.928	8.453	-3.031	-3.805	1.333
R150	-	EHD60	-	μ120	+	HTHSK80	0.929	8.18	-2.886	-3.777	1.434
R150	-	EHD60	-	μ120	+	HTHSK100	0.926	8.726	-3.063	-4.21	1.498
R150	-	EHD60	-	μ120	+	HTHSK150	0.933	7.276	-3.217	-3.894	2.787
R150	-	EHD60	-	μ120	+	Trac20SR	0.902	10.443	-3.076	-4.49	0.075
R150	-	EHD60	-	μ120	+	Trac50SR	0.902	10.451	-3.101	-4.492	0.092
R150	-	EHD60	-	μ120	+	Trac70SR	0.901	10.472	-3.119	-4.477	0.075
R150	-	EHD60	-	μ120	+	07FilmKv40	0.906	9.872	-3.163	-4.242	0.485
R150	-	EHD60	-	μ120	+	07FilmKv60	0.906	10.002	-3.147	-4.631	0.728
R150	-	EHD60	-	μ120	+	07FilmKv80	0.917	10.246	-3.156	-4.902	0.763
R150	-	EHD60	-	μ120	+	07FilmKv100	0.919	10.241	-3.06	-4.89	0.66
R150	-	EHD60	-	μ120	+	20Tr01Tr1	0.9	10.577	-3.151	-4.49	0.015
R150	-	EHD60	-	μ120	+	50Tr01Tr1	0.9	10.564	-3.146	-4.497	0.029
R150	-	EHD60	-	μ140	+	HTHSK60	0.914	9.134	-3.449	-4.373	1.639
R150	-	EHD60	-	μ140	+	HTHSK80	0.927	8.597	-3.226	-4.33	1.909
R150	-	EHD60	-	μ140	+	HTHSK100	0.908	9.647	-3.552	-4.971	1.827
R150	-	EHD60	-	μ140	+	HTHSK150	0.927	7.6	-3.689	-4.53	3.57
R150	-	EHD60	+	HTHSK60	-	HTHSK100	0.905	6.277	-2.827	13.046	-13.545
R150	-	EHD80	+	HSVisc60	-	KVisc40	0.893	6.93	-5.646	7.331	-5.664
R150	-	EHD80	-	HSVisc60	-	μ60	0.904	13.643	-3.209	-1.2	-6.284
R150	-	EHD80	+	HSVisc80	-	KVisc40	0.918	5.149	-4.124	7.288	-5.362
R150	-	EHD80	+	HSVisc80	-	KVisc60	0.895	6.381	-4.609	6.768	-5.589
R150	-	EHD80	-	HSVisc80	-	μ60	0.9	13.98	-3.512	-1.158	-6.359
R150	-	EHD80	-	HTHS100	-	μ60	0.909	13.471	-3.157	-1.499	-5.863
R150	-	EHD80	-	HTHS100	-	μ80	0.885	12.312	-2.917	-1.76	-4.684
R150	-	EHD80	-	HTHS150	-	μ60	0.898	13.714	-3.632	-1.219	-5.912
R150	-	EHD80	-	KVisc40	-	μ60	0.917	12.677	-3.436	-0.933	-5.357
R150	-	EHD80	-	KVisc40	-	μ80	0.908	11.513	-3.185	-1.17	-4.206
R150	-	EHD80	-	KVisc40	-	μ100	0.901	10.53	-2.933	-1.296	-3.351
R150	-	EHD80	-	KVisc40	-	μ120	0.902	10.624	-2.625	-1.294	-3.755
R150	-	EHD80	-	KVisc60	-	μ60	0.913	12.852	-3.565	-0.98	-5.357
R150	-	EHD80	-	KVisc60	-	μ80	0.905	11.726	-3.328	-1.259	-4.189
R150	-	EHD80	-	KVisc60	-	μ100	0.901	10.782	-3.067	-1.428	-3.337
R150	-	EHD80	-	KVisc60	-	μ120	0.904	10.88	-2.752	-1.435	-3.741
R150	-	EHD80	-	KVisc80	-	μ60	0.909	13.005	-3.667	-1.015	-5.372
R150	-	EHD80	-	KVisc80	-	μ80	0.901	11.915	-3.445	-1.333	-4.185
R150	-	EHD80	-	KVisc80	-	μ100	0.901	11.009	-3.181	-1.544	-3.333
R150	-	EHD80	-	KVisc80	-	μ120	0.905	11.114	-2.861	-1.562	-3.739
R150	-	EHD80	-	KVisc100	-	μ60	0.906	13.135	-3.75	-1.039	-5.394
R150	-	EHD80	-	KVisc100	-	μ80	0.898	12.078	-3.542	-1.397	-4.189
R150	-	EHD80	-	KVisc100	-	μ100	0.9	11.211	-3.278	-1.648	-3.333
R150	-	EHD80	-	KVisc100	-	μ120	0.905	11.325	-2.954	-1.679	-3.742
R150	-	EHD80	-	KVisc120	-	μ60	0.903	13.247	-3.819	-1.058	-5.419
R150	-	EHD80	-	KVisc120	-	μ80	0.895	12.225	-3.626	-1.451	-4.197
R150	-	EHD80	-	KVisc120	-	μ100	0.899	11.395	-3.366	-1.741	-3.337

		Param 1		Param 2		Param 3	R^2	a_0	a_1	a_2	a_3
R150	-	EHD80	-	KVisc120	-	µ120	0.905	11.52	-3.038	-1.783	-3.748
R150	-	EHD80	-	KVisc150	-	µ60	0.901	13.386	-3.874	-1.129	-5.432
R150	-	EHD80	-	KVisc150	-	µ80	0.891	12.41	-3.694	-1.573	-4.191
R150	-	EHD80	-	KVisc150	-	µ100	0.898	11.644	-3.437	-1.929	-3.327
R150	-	EHD80	-	KVisc150	-	µ120	0.903	11.769	-3.114	-1.969	-3.735
R150	-	EHD80	-	TracC40	-	µ120	0.93	15.466	-3.724	-3.702	-5.089
R150	-	EHD80	-	TracC40	-	µ140	0.908	18.307	-4.291	-4.71	-6.355
R150	-	EHD80	+	TracC40	+	HTHSK60	0.882	-0.854	-5.54	3.55	5.796
R150	-	EHD80	+	TracC40	+	HTHSK80	0.904	-2.798	-4.689	4.227	6.212
R150	-	EHD80	-	TracC60	-	µ120	0.922	14.609	-3.424	-3.185	-5.049
R150	-	EHD80	-	TracC60	-	µ140	0.9	17.297	-3.901	-4.129	-6.316
R150	-	EHD80	+	TracC60	+	HTHSK80	0.894	-1.646	-5.043	3.566	6.074
R150	-	EHD80	-	TracC80	-	µ60	0.881	13.908	-4.183	-0.474	-6.3
R150	-	EHD80	-	TracC80	-	µ120	0.906	14.558	-3.505	-2.806	-5.296
R150	-	EHD80	-	TracC100	-	µ120	0.88	13.651	-3.566	-1.857	-5.277
R150	-	EHD80	+	TracC100	+	HTHSK80	0.886	0.365	-4.78	2.084	5.282
R150	-	EHD80	+	µ40	-	µ60	0.882	12.415	-3.884	2.528	-8.109
R150	-	EHD80	-	µ40	-	µ120	0.885	14.031	-4.188	-4.243	-2.65
R150	-	EHD80	-	µ40	+	Trac20SR	0.899	15.696	-4.525	-8.713	0.493
R150	-	EHD80	-	µ40	+	Trac50SR	0.898	15.844	-4.699	-8.791	0.597
R150	-	EHD80	-	µ40	+	Trac70SR	0.903	15.664	-4.558	-8.852	0.697
R150	-	EHD80	-	µ60	+	µ80	0.882	13.814	-4.197	-8.816	2.151
R150	-	EHD80	-	µ60	-	µ120	0.89	12.908	-3.923	-4.61	-1.424
R150	-	EHD80	-	µ60	-	µ140	0.894	13.519	-4.053	-5.022	-1.493
R150	-	EHD80	-	µ60	+	HTHSK60	0.895	10.637	-4.612	-4.628	1.554
R150	-	EHD80	-	µ60	+	HTHSK80	0.889	10.806	-4.366	-4.84	1.351
R150	-	EHD80	-	µ60	+	HTHSK100	0.882	12.414	-4.378	-5.815	0.73
R150	-	EHD80	-	µ60	+	HTHSK150	0.88	11.898	-4.391	-5.705	1.149
R150	-	EHD80	-	µ60	+	Trac20SR	0.927	12.919	-3.723	-6.596	0.352
R150	-	EHD80	-	µ60	+	Trac50SR	0.922	13.005	-3.86	-6.598	0.404
R150	-	EHD80	-	µ60	+	Trac70SR	0.918	12.87	-3.8	-6.551	0.431
R150	-	EHD80	-	µ60	+	07FilmKv40	0.892	12.207	-4.377	-5.66	0.782
R150	-	EHD80	-	µ60	+	07FilmKv60	0.884	12.74	-4.03	-6.536	0.776
R150	-	EHD80	-	µ60	+	50Tr01Tr1	0.884	13.412	-4.362	-6.212	0.113
R150	-	EHD80	-	µ80	+	HTHSK60	0.896	8.603	-4.777	-3.197	2.322
R150	-	EHD80	-	µ80	+	HTHSK80	0.892	8.342	-4.449	-3.24	2.299
R150	-	EHD80	-	µ100	+	HTHSK60	0.908	7.49	-4.749	-2.475	2.685
R150	-	EHD80	-	µ100	+	HTHSK80	0.9	7.152	-4.375	-2.484	2.659
R150	-	EHD80	-	µ100	+	HTHSK100	0.882	8.338	-4.705	-3.282	2.599
R150	-	EHD80	-	µ100	+	HTHSK150	0.881	6.147	-4.871	-2.868	4.543
R150	-	EHD80	-	µ120	+	HTHSK60	0.94	7.507	-4.513	-2.892	2.849
R150	-	EHD80	-	µ120	+	HTHSK80	0.942	7.1	-4.111	-2.927	2.889
R150	-	EHD80	-	µ120	+	HTHSK100	0.932	7.988	-4.531	-3.756	3.249
R150	-	EHD80	-	µ120	+	HTHSK150	0.922	5.662	-4.695	-3.267	5.251
R150	-	EHD80	-	µ140	+	HTHSK60	0.923	7.718	-4.937	-3.104	3.273
R150	-	EHD80	-	µ140	+	HTHSK80	0.94	7.304	-4.461	-3.269	3.377
R150	-	EHD80	-	µ140	+	HTHSK100	0.903	8.508	-5.073	-4.269	3.786
R150	-	EHD80	-	µ140	+	HTHSK150	0.905	5.53	-5.224	-3.606	6.251
R150	-	EHD80	+	HTHSK60	-	HTHSK100	0.936	6.064	-4.439	11.928	-10.602
R150	-	EHD80	+	HTHSK60	-	20Tr01Tr1	0.906	2.807	-5.216	5.899	-0.539
R150	-	EHD80	+	HTHSK80	-	HTHSK100	0.898	4.093	-3.212	10.717	-8.647
R150	-	EHD80	+	HTHSK80	-	20Tr01Tr1	0.895	1.974	-4.427	5.924	-0.52
R150	-	EHD80	+	07FilmKv40	-	07FilmKv60	0.885	10.818	-6.579	4.891	-6.179
R150	-	EHD100	-	µ60	+	Trac20SR	0.883	16.198	-6.892	-6.884	0.53

		Param 1		Param 2		Param 3	R^2	a_0	a_1	a_2	a_3
R150	-	EHD100	+	HTHSK60	-	20Tr01Tr1	0.937	9.2	-12.338	6.967	-0.877
R150	-	EHD100	+	HTHSK80	-	20Tr01Tr1	0.905	6.946	-9.934	6.727	-0.787
R150	-	HSVisc60	+	µ40	-	µ60	0.932	8.869	-2.856	12.301	-15.363
R150	-	HSVisc60	-	µ40	-	20Tr01Tr1	0.889	17.041	-3.808	-9.392	-0.891
R150	-	HSVisc60	-	µ60	+	Trac20SR	0.896	11.65	-2.241	-6.897	0.439
R150	-	HSVisc60	-	µ60	+	Trac50SR	0.893	11.73	-2.38	-6.923	0.524
R150	-	HSVisc60	-	µ60	+	Trac70SR	0.903	11.654	-2.436	-6.89	0.624
R150	-	HSVisc60	-	µ60	-	20Tr01Tr1	0.926	13.717	-3.435	-6.804	-0.527
R150	-	HSVisc60	-	µ60	-	50Tr01Tr1	0.901	13.438	-3.409	-6.589	-0.489
R150	-	HSVisc60	-	µ100	+	Trac20SR	0.884	9.518	-2.398	-4.619	0.45
R150	-	HSVisc60	-	µ100	+	Trac50SR	0.881	9.593	-2.541	-4.641	0.54
R150	+	HSVisc80	-	KVisc40	-	20Tr01Tr1	0.914	4.298	5.499	-6.168	-0.678
R150	+	HSVisc80	-	KVisc40	-	50Tr01Tr1	0.941	4.507	5.54	-6.324	-0.772
R150	-	HSVisc80	+	µ40	-	µ60	0.922	8.989	-3.24	14.189	-16.987
R150	-	HSVisc80	-	µ60	-	20Tr01Tr1	0.889	14.262	-3.648	-7.121	-0.542
R150	-	HTHS100	+	HTHS150	-	KVisc100	0.9	1.077	-19.002	32.312	-11.436
R150	-	HTHS100	+	HTHS150	-	KVisc120	0.923	1.839	-21.998	35.445	-12.335
R150	-	HTHS100	+	HTHS150	-	KVisc150	0.96	3.347	-24.894	38.307	-13.809
R150	-	HTHS100	+	HTHS150	-	µ60	0.91	10.701	-11.065	9.414	-6.099
R150	-	HTHS100	+	HTHS150	+	HTHSK60	0.886	-4.757	-21.91	23.277	6.341
R150	-	HTHS100	+	HTHS150	+	HTHSK150	0.943	-9.683	-25.583	25.19	13.027
R150	-	HTHS100	+	µ40	-	µ60	0.921	8.617	-3.197	11.234	-13.704
R150	-	HTHS100	-	µ60	+	Trac20SR	0.888	11.253	-2.55	-6.154	0.402
R150	-	HTHS100	-	µ60	+	Trac50SR	0.882	11.295	-2.677	-6.131	0.464
R150	-	HTHS100	-	µ60	+	Trac70SR	0.89	11.21	-2.722	-6.09	0.553
R150	-	HTHS100	-	µ60	-	20Tr01Tr1	0.903	12.757	-3.635	-5.74	-0.431
R150	-	HTHS100	-	µ60	-	50Tr01Tr1	0.883	12.541	-3.634	-5.561	-0.394
R150	-	HTHS100	-	µ100	+	Trac20SR	0.881	9.399	-2.767	-4.089	0.408
R150	+	HTHS150	-	KVisc40	-	50Tr01Tr1	0.933	2.515	10.195	-8.849	-0.91
R150	+	HTHS150	-	KVisc60	-	50Tr01Tr1	0.908	3.244	10.565	-9.974	-0.885
R150	-	HTHS150	+	µ40	-	µ60	0.914	7.941	-3.697	14.881	-16.174
R150	-	KVisc40	+	µ40	-	µ60	0.947	5.414	-2.17	14.692	-14.985
R150	-	KVisc40	-	µ40	-	20Tr01Tr1	0.905	12.204	-2.818	-5.581	-0.854
R150	-	KVisc40	-	µ60	-	HTHSK60	0.888	18.062	-2.509	-8.37	-4.232
R150	-	KVisc40	-	µ60	-	HTHSK100	0.881	15.361	-2.15	-6.563	-3.697
R150	-	KVisc40	-	µ60	+	Trac20SR	0.88	9.469	-1.481	-5.493	0.456
R150	-	KVisc40	-	µ60	+	Trac70SR	0.888	9.274	-1.637	-5.336	0.651
R150	-	KVisc40	-	µ60	-	20Tr01Tr1	0.931	10.523	-2.593	-4.357	-0.623
R150	-	KVisc40	-	µ60	-	50Tr01Tr1	0.913	10.284	-2.688	-4.015	-0.631
R150	-	KVisc40	-	µ80	+	Trac70SR	0.885	8.384	-1.814	-4.229	0.61
R150	-	KVisc40	-	µ80	-	20Tr01Tr1	0.912	9.586	-2.687	-3.379	-0.569
R150	-	KVisc40	-	µ80	-	50Tr01Tr1	0.895	9.423	-2.765	-3.13	-0.577
R150	-	KVisc40	-	µ100	+	Trac20SR	0.901	7.846	-1.709	-3.654	0.468
R150	-	KVisc40	-	µ100	+	Trac50SR	0.896	7.814	-1.793	-3.627	0.557
R150	-	KVisc40	-	µ100	+	Trac70SR	0.902	7.686	-1.868	-3.508	0.641
R150	-	KVisc40	-	µ100	-	20Tr01Tr1	0.924	9.056	-2.733	-2.798	-0.574
R150	-	KVisc40	-	µ100	-	50Tr01Tr1	0.921	9.059	-2.829	-2.666	-0.613
R150	-	KVisc40	-	µ120	-	07FilmKv40	0.884	11.599	-2.517	-4.214	-1.916
R150	-	KVisc40	-	µ120	-	50Tr01Tr1	0.891	9.009	-2.633	-2.931	-0.493
R150	-	KVisc40	+	HTHSK80	-	20Tr01Tr1	0.883	2.673	-2.55	3.746	-0.918
R150	-	KVisc40	-	HTHSK100	+	HTHSK150	0.913	-1.427	-4.107	-17.986	26.471
R150	-	KVisc60	+	µ40	-	µ60	0.949	5.178	-2.531	16.051	-15.748
R150	-	KVisc60	-	µ40	-	20Tr01Tr1	0.883	12.258	-3.151	-5.293	-0.864
R150	-	KVisc60	-	µ60	-	HTHSK60	0.885	19.45	-2.984	-8.679	-4.836

		Param 1		Param 2		Param 3	R^2	a_0	a_1	a_2	a_3
R150	-	KVisc60	-	μ60	-	20Tr01Tr1	0.915	10.723	-2.898	-4.232	-0.643
R150	-	KVisc60	-	μ60	-	50Tr01Tr1	0.883	10.416	-2.845	-4.02	-0.6
R150	-	KVisc60	-	μ80	-	20Tr01Tr1	0.899	9.841	-3.017	-3.279	-0.594
R150	-	KVisc60	-	μ100	+	Trac20SR	0.892	8.002	-1.854	-3.671	0.474
R150	-	KVisc60	-	μ100	+	Trac50SR	0.886	7.976	-1.939	-3.644	0.558
R150	-	KVisc60	-	μ100	+	Trac70SR	0.892	7.858	-2.032	-3.521	0.646
R150	-	KVisc60	-	μ100	-	20Tr01Tr1	0.919	9.395	-3.086	-2.755	-0.603
R150	-	KVisc60	-	μ100	-	50Tr01Tr1	0.902	9.282	-3.038	-2.706	-0.588
R150	-	KVisc80	+	μ40	-	μ60	0.948	5.039	-2.877	17.174	-16.385
R150	-	KVisc80	-	μ60	-	20Tr01Tr1	0.897	10.919	-3.138	-4.182	-0.648
R150	-	KVisc80	-	μ80	-	20Tr01Tr1	0.883	10.074	-3.283	-3.238	-0.602
R150	-	KVisc80	-	μ100	+	Trac20SR	0.884	8.143	-1.974	-3.696	0.478
R150	-	KVisc80	-	μ100	+	Trac70SR	0.882	8.016	-2.17	-3.544	0.649
R150	-	KVisc80	-	μ100	-	20Tr01Tr1	0.91	9.692	-3.376	-2.75	-0.615
R150	-	KVisc80	-	μ100	-	50Tr01Tr1	0.881	9.461	-3.183	-2.772	-0.556
R150	-	KVisc100	+	μ40	-	μ60	0.946	4.963	-3.209	18.124	-16.927
R150	-	KVisc100	-	μ100	-	20Tr01Tr1	0.898	9.948	-3.614	-2.766	-0.617
R150	-	KVisc120	+	μ40	-	μ60	0.943	4.933	-3.518	18.94	-17.404
R150	-	KVisc120	-	μ100	-	20Tr01Tr1	0.886	10.163	-3.801	-2.798	-0.613
R150	-	KVisc150	+	μ40	-	μ60	0.933	5.203	-3.944	19.203	-17.511
R150	-	TracC60	-	μ140	-	20Tr01Tr1	0.898	22.037	-10.353	-7.699	-1.034

APPENDIX G

Three parameter correlations with R275

		Param 1		Param 2		Param 3	R^2	a_0	a_1	a_2	a_3
R275	+	EHD40	-	EHD100	-	μ60	0.878	63.704	9.112	-41.37	-23.962
R275	+	EHD40	-	EHD100	-	μ80	0.862	54.992	7.277	-35.756	-19.03
R275	+	EHD60	-	EHD100	-	μ60	0.854	57.544	7.914	-36.18	-21.796
R275	-	EHD80	-	μ100	-	Trac20SR	0.858	29.449	-7.149	-13.628	-1.189
R275	-	EHD80	-	μ100	-	Trac50SR	0.865	29.364	-6.813	-13.539	-1.529
R275	-	EHD80	-	μ100	-	Trac70SR	0.869	30.084	-7.12	-13.715	-1.766
R275	-	EHD80	-	μ100	+	07FilmKv60	0.862	20.42	-4.219	-16.45	7.732
R275	-	EHD80	-	μ100	+	07FilmKv80	0.863	24.165	-4.278	-17.075	4.672
R275	-	EHD80	-	μ120	-	Trac20SR	0.866	31.053	-6.687	-15.039	-1.844
R275	-	EHD80	-	μ120	-	Trac50SR	0.878	30.908	-6.118	-14.984	-2.322
R275	-	EHD80	-	μ120	-	Trac70SR	0.883	32	-6.542	-15.307	-2.668
R275	-	EHD80	-	μ140	-	Trac20SR	0.851	36.052	-8.38	-18.164	-2.025
R275	-	EHD80	-	μ140	-	Trac50SR	0.857	35.69	-7.726	-17.992	-2.489
R275	-	EHD80	-	μ140	-	Trac70SR	0.853	36.698	-8.179	-18.259	-2.777
R275	-	EHD100	-	μ80	+	07FilmKv60	0.868	38.713	-20.636	-19.283	8.688
R275	-	EHD100	-	μ80	+	07FilmKv80	0.863	46.299	-24.452	-19.392	5.028
R275	-	EHD100	-	μ100	+	07FilmKv60	0.879	27.638	-12.482	-16.206	8.532
R275	-	EHD100	-	μ100	+	07FilmKv80	0.905	35.225	-16.699	-17.11	6.067
R275	-	EHD100	-	μ100	+	07FilmKv100	0.882	36.689	-17.269	-16.28	4.343
R275	-	EHD100	-	μ120	-	Trac20SR	0.852	36.764	-12.607	-15.136	-1.539
R275	-	EHD100	-	μ120	-	Trac50SR	0.862	35.566	-10.969	-15.128	-1.987
R275	-	EHD100	-	μ120	-	Trac70SR	0.868	37.203	-12.063	-15.382	-2.274
R275	+	HSVisc60	-	μ100	+	07FilmKv60	0.856	11.642	2.704	-17.558	10.695
R275	+	HSVisc80	-	μ100	+	07FilmKv60	0.86	10.155	3.564	-17.463	11.227
R275	+	HTHS100	-	μ100	+	07FilmKv60	0.869	10.081	4.337	-18.588	11.653
R275	+	HTHS100	-	μ100	+	07FilmKv80	0.854	17.469	2.678	-18.677	6.013
R275	+	HTHS150	-	μ100	+	07FilmKv60	0.873	9.233	5.066	-18.603	11.787
R275	+	HTHS150	-	μ100	+	07FilmKv80	0.863	16.051	4.008	-19.055	6.479
R275	+	KVisc40	-	μ100	+	07FilmKv60	0.861	12.901	2.178	-18.966	11.369
R275	+	KVisc40	-	μ100	+	07FilmKv80	0.851	19.001	1.445	-19.049	6.086
R275	+	KVisc60	-	μ100	+	07FilmKv60	0.863	12.739	2.476	-18.982	11.25
R275	+	KVisc60	-	μ100	+	07FilmKv80	0.856	18.591	1.957	-19.353	6.287
R275	+	KVisc80	-	μ100	+	07FilmKv60	0.864	12.629	2.721	-18.953	11.086
R275	+	KVisc80	-	μ100	+	07FilmKv80	0.86	18.198	2.429	-19.571	6.427
R275	+	KVisc100	-	μ100	+	07FilmKv60	0.864	12.569	2.912	-18.895	10.897
R275	+	KVisc100	-	μ100	+	07FilmKv80	0.863	17.833	2.853	-19.723	6.519
R275	+	KVisc120	-	μ100	+	07FilmKv60	0.864	12.507	3.079	-18.837	10.735
R275	+	KVisc120	-	μ100	+	07FilmKv80	0.865	17.501	3.228	-19.825	6.579
R275	+	KVisc150	-	μ100	+	07FilmKv60	0.864	12.312	3.398	-18.801	10.574
R275	+	KVisc150	-	μ100	+	07FilmKv80	0.869	16.949	3.849	-19.984	6.669
R275	+	μ40	-	μ60	-	Trac50SR	0.857	15.145	48.522	-53.475	-2.71
R275	+	μ40	-	μ60	-	Trac70SR	0.874	13.568	56.861	-59.527	-3.42
R275	+	μ40	-	μ100	+	07FilmKv80	0.866	13.656	10.491	-22.754	6.09

		Param 1		Param 2		Param 3	R^2	a_0	a_1	a_2	a_3
R275	+	µ60	-	µ100	+	07FilmKv80	0.87	14.297	14.448	-27.58	6.318
R275	+	µ60	-	µ100	+	07FilmKv100	0.856	13.483	18.696	-29.795	5.099
R275	+	µ80	-	µ100	+	07FilmKv80	0.861	17.149	12.373	-27.875	5.835
R275	-	µ100	+	µ120	+	07FilmKv60	0.852	14.265	-23.663	7.39	9.49
R275	-	µ100	-	HTHSK60	+	07FilmKv60	0.854	20.097	-18.826	-3.002	9.214
R275	-	µ100	-	HTHSK60	+	07FilmKv80	0.871	27.093	-21.087	-4.938	6.415
R275	-	µ100	-	HTHSK80	+	07FilmKv60	0.851	20.076	-18.684	-2.808	8.899
R275	-	µ100	-	HTHSK80	+	07FilmKv80	0.87	27.437	-21.119	-5.054	6.218
R275	-	µ100	-	HTHSK100	+	07FilmKv80	0.857	24.676	-19.084	-3.939	5.83
R275	-	µ100	-	HTHSK150	+	07FilmKv80	0.854	27.061	-19.246	-5.805	5.473
R275	-	µ100	-	Trac20SR	+	07FilmKv60	0.851	16.964	-16.454	-0.513	7.486
R275	-	µ100	-	Trac50SR	+	07FilmKv60	0.856	17.414	-16.244	-0.778	7.09
R275	-	µ100	-	Trac50SR	+	07FilmKv80	0.852	20.786	-16.841	-0.685	4.223
R275	-	µ100	-	Trac70SR	+	07FilmKv60	0.855	17.61	-16.365	-0.841	7.079
R275	-	µ100	-	Trac70SR	+	07FilmKv80	0.851	20.936	-16.96	-0.72	4.227
R275	-	µ100	-	Trac70SR	-	20Tr01Tr1	0.856	25.639	-14.037	-2.807	-1.312
R275	-	µ100	-	07FilmKv40	+	07FilmKv60	0.895	19.62	-22.965	-8.008	18.836
R275	-	µ100	-	07FilmKv40	+	07FilmKv80	0.867	25.162	-21.429	-4.62	8.37
R275	-	µ100	+	07FilmKv60	-	50Tr01Tr1	0.864	15.225	-17.403	10.403	-0.742
R275	-	µ100	+	07FilmKv80	-	07FilmKv100	0.878	18.433	-18.796	20.277	-12.431
R275	-	µ100	+	07FilmKv80	-	50Tr01Tr1	0.853	20.267	-17.941	5.665	-0.508
R275	-	µ120	+	Trac20SR	-	Trac50SR	0.869	26.386	-15.349	6.697	-10.251
R275	-	µ120	-	Trac50SR	-	20Tr01Tr1	0.854	26.445	-15.267	-2.862	-0.833
R275	-	µ120	-	Trac50SR	-	50Tr01Tr1	0.859	26.363	-15.329	-2.706	-0.845
R275	-	µ120	-	Trac70SR	-	20Tr01Tr1	0.863	27.651	-15.617	-3.493	-1.058
R275	-	µ120	-	Trac70SR	-	50Tr01Tr1	0.864	27.315	-15.716	-3.16	-0.957

APPENDIX H

FORTRAN77 Program for discrimination analysis

```
c--- DATA FORMAT
c    current data format is as follows;
c    1. use Microsoft Excel
c       1st row  : Num of Rows and Colums (NUMERICS)
c       2nd row  : The names of each parameter (TEXT)
c       3rd - X  : Oil-index,name(TEXT)
c       X - end  : variables(NUMERICS)
c       all text data should contains 7 characters
c    2. save Excel file with "CSV" data format.
c    3. file name should be given in 7 characters,
c       including '.' and extension.
c
c--- OUTPUT
c    Mahalanobis square distance D^2
c    Discriminant function standardised by D^2
c
c--- USAGE
c    Run and follow the instruction on screen
c
c--- LIST of Variables
c       n    : Num. of oils
c       n1   : Num. of oils in group 1
c       n2   : Num. of oils in group 2
c       m    : Num. of parameters
c       mm   : Num. of parameters reduced in calc.
c       id   : Num. of parameters reduced in calc.
c       index: names of parameters
c       name : names of oils
c       v    : v(n1+n2,m), data normalized
c       v_m1 : avarage of categoty 1 group
c       v_m2 : avarage of category 2 groupe
c       sm   : co-variance matrix without size reduction
c       s    : co-variance matrix reduced
c            s1*w*q : inverse co-variance matrix
c       d    : difference of average between groups
c       dj   : differ. of average between groups(reduced)
c       b    : discriminant coefficient (reduced)
c       dm   : Mahalanobis D^2
c       z    : discriminant function scalled by D^2
c       iz   : grouping indicator
c       imt  : error code of linear equation
c       iq   : parameter number's indicator array
c
c    This program was developed on the Macintosh.
c    However it may work on any platform with Fortran 77.
c
c*************************************************************
```

```
      implicit real (a-h,o-z)
      character*7 infile,outfile
      character*1 yn
      character*7 name(50),index(50),idummy(50)
      dimension s(50,50),b(50),d(50),si(50,50),z(50),id0(50)
      dimension v(50,50),v_m1(50),v_m2(50),iz(50),izero(50)
      dimension id(50),sm(50,50),dj(50),q(50,50),w(50),iq(50)
c
c                     clear vectors and matrices
c                              &   read data
c
      do 10 j=1,50
      v_m1(j)=0.0
      v_m2(j)=0.0
      d(j)  =0.0
      b(j)  =0.0
      do 10 i=1,50
      v(i,j) =0.0
   10 sm(i,j)=0.0
      dmmax  =0.
c
      write(6,*) '%%%%%%%%%%%%%%%%%%%%%%%%%%%%%%%%%%%%%%%%%%%%%%%%%%%%%%%%%%%%'
      write(6,*) '%%%%                       %%%%'
      write(6,*) '%%%%   DISCRIMINANT ANALYSIS    %%%%'
      write(6,*) '%%%%        Version 1.1        %%%%'
      write(6,*) '%%%%                       %%%%'
      write(6,*) '%%%%      Copyright:1997      %%%%'
      write(6,*) '%%%%      Valeria Anghel      %%%%'
      write(6,*) '%%%%      Imperial College    %%%%'
      write(6,*) '%%%%                       %%%%'
      write(6,*) '%%%%   This program includes   %%%%'
      write(6,*) '%%%%      subroutines from     %%%%'
      write(6,*) '%%%%   "Numerical Recepies   %%%%'
      write(6,*) '%%%%       in Fortran"       %%%%'
      write(6,*) '%%%%   with modification by   %%%%'
      write(6,*) '%%%%         T Makino        %%%%'
      write(6,*) '%%%%    Copyright:1986,1992    %%%%'
      write(6,*) '%%%%  Cambridge University Press %%%%'
      write(6,*) '%%%%     All right reserved    %%%%'
      write(6,*) '%%%%                       %%%%'
      write(6,*) '%%%%%%%%%%%%%%%%%%%%%%%%%%%%%%%%%%%%%%%%%%%%%%%%%%%%%%%%%%%%'
      write(6,*)
      write(6,*)
      write(6,*) 'ENTER INPUT  FILE NAME in full : '
      read(5,1100)   infile
      write(6,*)
      write(6,*) 'ENTER OUTPUT FILE NAME in full : '
      read(5,1100)   outfile
      open(7,file=infile,status='old')
      open(8,file=outfile,status='unknown')
      write(8,*) 'INPUT FILE NAME : ',infile
      read(7,*) n,m
      read(7,2) idummy(1),idummy(2),(index(j),j=1,m)
    2 format(46(A7,1x),A7)
      do 20 i=1,n
      read(7,3)name(i),idummy(1)
   20 continue
    3 format(A7,1x,A7)
```

```
      do 22 i=1,n
      read(7,*) (v(i,j),j=1,m)
   22 continue
      do 23 j=1,m-7
            izero(j)=0
      do 24 i=1,n
      if(v(i,j).eq.0.0) izero(j)=1
   24 continue
   23 continue
c
c                                    normalization
c
      write(6,*)
      write(6,*) 'ENTER [y/n] for NORMALIZATION by STD. :'
      read(5,4) yn
    4 format(a1)
      if(yn.eq.'n') goto 41
      do 40 j=1,m
      v_ave=0.0
      v_var=0.0
      do 42 i=1,n
   42 v_ave=v_ave+v(i,j)/float(n)
      do 44 i=1,n
   44 v_var=v_var+(v(i,j)-v_ave)**2.0/float(n-1)
      v_std=sqrt(v_var)
      do 46 i=1,n
   46 v(i,j)=(v(i,j)-v_ave)/v_std
   40 continue
   41 continue
c
c                              arrange difference vector
c
      do 57 i=1,n
      iz(i)=1
            iq(i)=0
   57 continue
   54 write(6,*)' '
      write(6,1300)
      write(6,*) 'OIL LIST:'
      write(6,1000) ((j,name(j)),j=1,n)
      write(6,1300)
      write(6,*)' '
      write(6,*) 'HOW MANY THE HIGH EFFICIENT OILS ?'
            read(5,*) kk
      write(6,*)' '
      write(6,*) 'CHOOSE THE CANDIDATES by NUMBER'
      write(6,*) 'like 1,4,10,20,..... '
      read(5,*)  (iq(j),j=1,kk)
      do 55 j=1,n
      do 56 i=1,n
        if(iq(i).eq.j) then
          iz(j)=2
        end if
   56 continue
   55 continue
      write(6,*)
      write(6,*) '*********************************'
      do 53 i=1,n,2
```

```
      write(6,5) name(i),iz(i),name(i+1),iz(i+1)
    5 format(3x,a7,':[',i1,']    ',a7,':[',i1,']')
   53 continue
      write(6,*) '*********************************'
      write(6,*)' '
      write(6,*) 'ARE YOU SURE ?'
      write(6,*) '  1:TERMINATE'
      write(6,*) '  2:Yes. GO AHEAD !'
      write(6,*) '  3:CHANGE SELECTION'
      write(6,*) 'ENTER [1/2/3] :'
      read(5,*)   iselec
      if(iselec.eq.1) goto 300
      if(iselec.eq.3) goto 54
c
      do 51 j=1,m
      n1=0
      n2=0
      do 52 i=1,n
      if(iz(i).eq.1) then
      v_m1(j)=v_m1(j)+v(i,j)
      n1=n1+1
      else
      v_m2(j)=v_m2(j)+v(i,j)
      n2=n2+1
      end if
   52 continue
      v_m1(j)=v_m1(j)/float(n1)
      v_m2(j)=v_m2(j)/float(n2)
   51 d(j)=v_m1(j)-v_m2(j)
c
c                        arrange co-variance matrix
c
      df=1./float(n1+n2-2)
      do 60 j=1,m
      do 62 k=1,m
      do 64 i=1,n
      if(iz(i).eq.1) then
      sm(j,k)=sm(j,k)+(v(i,k)-v_m1(k))*(v(i,j)-v_m1(j))*df
      else
      sm(j,k)=sm(j,k)+(v(i,k)-v_m2(k))*(v(i,j)-v_m2(j))*df
      end if
   64 continue
   62 continue
   60 continue
c
c         (trial and error to find appropriate parameters)
c
  200 write(6,*)' '
      write(6,*) 'SELECT PROCESS 1-3'
      write(6,*) '  1:TERMINATE'
      write(6,*) '  2:SEARCH THE BEST COMBINATION'
      write(6,*) '  3:TRY WITH YOUR BEST SELECTION'
      write(6,*) 'ENTER [1/2/3] :'
      read(5,*)   iselec
c
      if(iselec.eq.1) goto 300
      do 70 j=1,50
      id0(j) = 0
```

```
      iq(j)  = 0
      id(j)  = 0
      z(j)   = 0.0
      w(j)   = 0.0
      b(j)   = 0.0
      dj(j)  = 0.0
      do 70 i=1,50
      s(i,j) = 0.0
      q(i,j) = 0.0
   70 si(i,j)= 0.0
c
      if(iselec.eq.3) then
      write(6,*)' '
      write(6,1300)
      write(6,*) 'NOMINEES ARE AS FOLLOWS:'
      write(6,1000) ((j,index(j)),j=1,m)
      write(6,1300)
      m0=0
      write(6,*)' '
      write(6,*) 'HOW MANY PARAMETERS DO YOU USE?'
            read(5,*) mm
      write(6,*)' '
      write(6,*) 'CHOOSE THE CANDIDATES by NUMBER'
      write(6,*) 'like 1,4,10,20,..... '
      read(5,*)  (iq(j),j=1,mm)
      do 71 j=1,m
      do 72 i=1,m
        if(iq(i).eq.j) then
          m0=m0+1
          id0(j)=1
        end if
   72 continue
   71 continue
      end if
c
      if(iselec.ne.2) then
        iter=1
        do 73 j=1,m
   73   id(j)=id0(j)
        goto 444
      else
   74   write(5,*) 'ENTER NUMBER OF PARAMETERS'
        read(5,*) m1
        if(m1.ne.3) then
          write(6,*) '  PARAMETERS should be 3 (I am sorry)'
          goto 74
        end if
      end if
c
c     (iselec.eq.2)-->make id(i) sets of (m)C(m1)
      num=0
      do 400 l1=  1, m-9
      do 410 l2= l1+1, m-8
            do 420 l3= l2+1, m-7
            do 430 j=1,m
  430 id(j)=0
      do 440 j=1,m
            if(j.eq.l1.or.j.eq.l2.or.j.eq.l3) id(j)=1
```

```
 440 continue
c
 444 jj=0
     do 76 j=1,m
     if(id(j).eq.0) goto 76
     jj=jj+1
     dj(jj)=d(j)
     ii=0
     do 77 i=1,m
     if(id(i).eq.0) goto 77
     ii=ii+1
     s(ii,jj)=sm(i,j)
  77 continue
  76 continue
     mm=ii
c                    (rearranging for accurate symmetry)
     do 79 i=1,mm
     do 79 j=i,mm
     s(i,j)=s(j,i)
  79 continue
     do 78 i=1,mm
     do 78 j=1,mm
  78 si(i,j)=s(i,j)
c                         calculate discriminat coefficient
     call svdcmp(si,mm,mm,50,50,w,q,imt)
          if(imt.eq.1) goto 140
     do 81 i=1,mm
      if(w(i).gt.wmax) wmax=w(i)
  81 continue
     wmin=wmax*1.0e-4
     do 82 i=1,mm
      if(w(i).lt.wmin) w(i)=0
  82 continue
     call svbksb(si,w,q,mm,mm,50,50,dj,b)
     imt=0
     do 83 i=1,mm
     x=0.0
     do 85 j=1,mm
  85 x=x+s(i,j)*b(j)
     if(abs(dj(i)-x).gt.0.05) imt=1
  83 continue
c                                   Maharanobis distance
c     f=0.0
c     g=0.0
c     h=0.0
     dm=0.0
c     do 90 i=1,mm
c     do 92 j=1,mm
c     f=f+b(i)*b(j)*dj(i)*dj(j)
c  92 g=g+b(i)*b(j)*s(i,j)
c  90 h=h+b(i)*dj(i)
c     do 94 i=1,mm
c  94 b(i)=b(i)/(h*g/f)
     do 96 i=1,mm
  96 dm=dm+dj(i)*b(i)
c                         calculate discriminat functions
     if(iselec.eq.3) then
     do 100 i=1,n
```

```
      jj=0
      do 100 j=1,m
      if(id(j).eq.0) goto 100
      jj=jj+1
      z(i)=z(i)+v(i,j)*b(jj)
  100 continue
      end if
c                                   write out results
  140 if(iselec.eq.3) then
      write(6,*)' '
      write(6,*)' '
      write(6,*)' '
      write(6,*)' '
      write(6,1300)
      write(6,2000)
      write(6,2100)
      write(8,2000)
      write(8,2100)
      do 110 j=1,m
      if(id0(j).eq.0) goto 110
      write(6,2200) j,index(j),id0(j)
      write(8,2200) j,index(j),id0(j)
  110 continue
      if(dm.gt.0.0.and.imt.eq.0) then
      write(6,3100) dm
      write(6,3200)
      write(8,3100) dm
      write(8,3200)
      do 120 i=1,n
      if(iz(i).eq.1) write(6,3300) i,name(i),iz(i),z(i)/dm
      if(iz(i).eq.1) write(8,3301) i,name(i),iz(i),z(i)/dm
  120 continue
      do 130 i=1,n
      if(iz(i).eq.2) write(6,3300) i,name(i),iz(i),z(i)/dm
      if(iz(i).eq.2) write(8,3301) i,name(i),iz(i),z(i)/dm
  130 continue
      else
      write(6,4000)
      write(8,4000)
      end if
c
      write(6,1300)
      write(6,*)' '
      write(6,*)' '
      write(6,*)' '
      goto 200
            else
            num=num+1
            if(num.eq.2000) write(6,*) ' calculation progressing :',num
            if(num.eq.4000) write(6,*) ' calculation progressing :',num
            if(num.eq.6000) write(6,*) ' calculation progressing :',num
            if(num.eq.8000) write(6,*) ' calculation progressing :',num
            if(izero(l1).eq.1.or.izero(l2).eq.1.or.izero(l3).eq.1) dm=0.0
            if(imt.eq.1.or.dm.le.0.) dm=0.0
            if(dm.ne.0.) write(8,5001) num,l1,l2,l3,dm
            if(dm.gt.dmmax) then
              dmmax=dm
                    lm1=l1
```

```
                lm2=l2
                lm3=l3
                numx=num
            end if
        end if
c
 420 continue
 410 continue
 400 continue
    write(6,*)' '
            write(6,*)' **** Max.result ****'
            write(6,5000) numx,lm1,lm2,lm3,dmmax
            goto 200
c
 300 continue
    close(7)
    close(8)
c
 1000 format(6(i3,1x,A7,2x))
 1100 format(A7)
 1200 format(10(1x,A7))
 1300 format(80('*'))
 2000 format(/' **** RESULTS ****')
 2100 format(/' PARAMETERS USED: ')
 2200 format(4x,i2,2x,A7,i3)
 3100 format( ' MAHALANOBIS DISTANCE : ',e12.5)
 3200 format( ' DISCRIMINANT FUNCTIONS:')
 3300 format( '  No.',i2,2x,A7,' GROUP:',i1,'  DFs:',e12.5)
 3301 format(i2,',',A7,',',i1,',',e12.5)
 4000 format(/'  **** DISCRIMINATION FAILED !!!! ****'/)
 5000 format(' #',i5,'  combination(',i2,',',i2,',',i2,')'
   *     ,2x,'dm=',e12.5)
 5001 format(i5,',',i2,',',i2,',',i2,',',i2,',',e12.5)
    stop
    end
c
c
c
c
ccccccccccccccccccccccccccccccccccccccccccccccccccccccccccccccc
c                                       c
c       Solver of linear matrix equation        c
c       from "Numerial Recepies in Fortran"         c
c                                       c
c                                       c
c                                       c
c       checked by T.Makino (MHI/IC) in 1996        c
c                                       c
ccccccccccccccccccccccccccccccccccccccccccccccccccccccccccccccc
    subroutine svdcmp(a,m,n,mp,np,w,v,ig)
    integer m,mp,n,np,NMAX
    real a(mp,np),v(np,np),w(np)
    parameter (NMAX=500)
c
    integer i,its,j,jj,k,l,nm
    real anorm,c,f,g,h,s,scale,x,y,z,rv1(NMAX),pythag
c
    ig=0
```

```
          g=0.0
      scale=0.0
      anorm=0.0
c
      do 25 i=1,n
       l=i+1
       rv1(i)=scale*g
       g=0.0
       s=0.0
       scale=0.0
       if(i.le.m) then
        do 11 k=i,m
         scale=scale+abs(a(k,i))
   11    continue
        if(scale.ne.0.0)then
         do 12 k=i,m
          a(k,i)=a(k,i)/scale
          s=s+a(k,i)*a(k,i)
   12     continue
         f=a(i,i)
         g=-sign(sqrt(s),f)
         h=f*g-s
         a(i,i)=f-g
         do 15 j=l,n
          s=0.0
          do 13 k=i,m
           s=s+a(k,i)*a(k,j)
   13      continue
          f=s/h
          do 14 k=i,m
           a(k,j)=a(k,j)+f*a(k,i)
   14      continue
   15     continue
         do 16 k=i,m
           a(k,i)=scale*a(k,i)
   16     continue
        end if
       end if
       w(i)=scale*g
       g=0.0
       s=0.0
       scale=0.0
       if((i.le.m).and.(i.ne.n)) then
        do 17 k=l,n
         scale=scale+abs(a(i,k))
   17    continue
        if(scale.ne.0.0)then
         do 18 k=l,n
          a(i,k)=a(i,k)/scale
          s=s+a(i,k)*a(i,k)
   18     continue
         f=a(i,l)
         g=-sign(sqrt(s),f)
         h=f*g-s
         a(i,l)=f-g
         do 19 k=l,n
          rv1(k)=a(i,k)/h
   19     continue
```

```
        do 23 j=l,m
          s=0.0
          do 21 k=l,n
            s=s+a(j,k)*a(i,k)
 21       continue
          do 22 k=l,n
            a(j,k)=a(j,k)+s*rv1(k)
 22       continue
 23       continue
          do 24 k=l,n
            a(i,k)=scale*a(i,k)
 24       continue
        end if
      end if
      anorm=max(anorm,(abs(w(i))+abs(rv1(i))))
 25 continue
c
    do 32 i=n,1,-1
      if(i.lt.n) then
        if(g.ne.0.0) then
          do 26 j=l,n
            v(j,i)=(a(i,j)/a(i,l))/g
 26       continue
          do 29 j=l,n
            s=0.0
            do 27 k=l,n
              s=s+a(i,k)*v(k,j)
 27         continue
            do 28 k=l,n
              v(k,j)=v(k,j)+s*v(k,i)
 28         continue
 29       continue
        end if
        do 31 j=l,n
          v(i,j)=0.0
          v(j,i)=0.0
 31     continue
      end if
      v(i,i)=1.0
      g=rv1(i)
      l=i
 32 continue
c
    do 39 i=min(m,n),1,-1
      l=i+1
      g=w(i)
      do 33 j=l,n
        a(i,j)=0.0
 33   continue
      if(g.ne.0.0) then
        g=1.0/g
        do 36 j=l,n
          s=0.0
          do 34 k=l,m
            s=s+a(k,i)*a(k,j)
 34       continue
          f=(s/a(i,i))*g
          do 35 k=i,m
```

```
          a(k,j)=a(k,j)+f*a(k,i)
 35       continue
 36     continue
        do 37 j=i,m
          a(j,i)=a(j,i)*g
 37     continue
      else
        do 38 j=i,m
          a(j,i)=0.0
 38     continue
      end if
      a(i,i)=a(i,i)+1.0
 39 continue
c
    do 49 k=n,1,-1
      do 48 its=1,30
        do 41 l=k,1,-1
          nm=l-1
          if((abs(rv1(l))+anorm).eq.anorm) goto 2
          if((abs(w(nm))+anorm).eq.anorm) goto 1
 41     continue
  1     c=0.0
        s=1.0
        do 43 i=l,k
          f=s*rv1(i)
          rv1(i)=c*rv1(i)
          if((abs(f)+anorm).eq.anorm) goto 2
          g=w(i)
          h=pythag(f,g)
          w(i)=h
          h=1.0/h
          c=(g*h)
          s=-(f*h)
          do 42 j=1,m
            y=a(j,nm)
            z=a(j,i)
            a(j,nm)=(y*c)+(z*s)
            a(j,i)=-(y*s)+(z*c)
 42       continue
 43     continue
  2     z=w(k)
        if(l.eq.k) then
          if(z.lt.0.0) then
            w(k)=-z
            do 44 j=1,n
              v(j,k)=-v(j,k)
 44         continue
          end if
          goto 3
        end if
        if(its.eq.30) then
c         write(6,*) ' no convergence in svdcmp !!!'
                    ig=1
                    return
        end if
        x=w(l)
        nm=k-1
        y=w(nm)
```

```
        g=rv1(nm)
        h=rv1(k)
        f=((y-z)*(y+z)+(g-h)*(g+h))/(2.0*h*y)
        g=pythag(f,1.0)
        f=((x-z)*(x+z)+h*((y/(f+sign(g,f)))-h))/x
        c=1.0
        s=1.0
        do 47 j=1,nm
         i=j+1
         g=rv1(i)
         y=w(i)
         h=s*g
         g=c*g
         z=pythag(f,h)
         rv1(j)=z
         c=f/z
         s=h/z
         f=(x*c)+(g*s)
         g=-(x*s)+(g*c)
         h=y*s
         y=y*c
         do 45 jj=1,n
          x=v(jj,j)
          z=v(jj,i)
          v(jj,j)=(x*c)+(z*s)
          v(jj,i)=-(x*s)+(z*c)
45       continue
        z=pythag(f,h)
        w(j)=z
        if(z.ne.0.0) then
         z=1.0/z
         c=f*z
         s=h*z
        end if
        f=(c*g)+(s*y)
        x=-(s*g)+(c*y)
        do 46 jj=1,m
         y=a(jj,j)
         z=a(jj,i)
         a(jj,j)=(y*c)+(z*s)
         a(jj,i)=-(y*s)+(z*c)
46       continue
47      continue
       rv1(l)=0.0
       rv1(k)=f
       w(k)=x
48     continue
 3    continue
49    continue
      return
      end
c
c
c
      function pythag(a,b)
      real a,b,pythag
      real absa,absb
      absa=abs(a)
```

```
      absb=abs(b)
      if(absa.gt.absb) then
        pythag=absa*sqrt(1.+(absb/absa)**2)
      else
        if(absb.eq.0.)then
          pythag=0.0
        else
          pythag=absb*sqrt(1.+(absa/absb)**2)
        end if
      end if
      return
      end
c
c
c
      subroutine svbksb(u,w,v,m,n,mp,np,b,x)
      integer m,mp,n,np,NMAX
      real b(mp),u(mp,np),v(np,np),w(np),x(np)
      parameter (NMAX=500)
      integer i,j,jj
      real s,tmp(NMAX)
c
      do 12 j=1,n
        s=0.0
        if(w(j).ne.0.0) then
          do 11 i=1,m
            s=s+u(i,j)*b(i)
 11       continue
          s=s/w(j)
        end if
        tmp(j)=s
 12   continue
      do 14 j=1,n
        s=0.0
        do 13 jj=1,n
          s=s+v(j,jj)*tmp(jj)
 13     continue
        x(j)=s
 14   continue
      return
      end
```

BIBL
LONDI
UNI